

The impact of climate variability and land cover change on  
land surface conditions in North-eastern Nigeria

Thesis submitted for the degree of  
Doctor of Philosophy  
at the University of Leicester

by

Bibi, Umar Muhammed  
Department of Geography

March, 2013

## **Abstract**

Recent droughts in the West African Sahel have been the most catastrophic since modern records began posing a threat to the economy and security of the region. Two contending views have evolved in the scientific community to explain the causes of re-occurring droughts in the West African Sahel Region. These themes are “the regional land-atmosphere feedback” mechanism and “ocean-atmosphere interaction”. This study is specific to a part of West Africa the North-eastern part of Nigeria and attempts to examine the impact of climate variability and land cover change on land surface conditions of fluxes in energy and momentum in the past (1980-2000) and in the future (2046-2065) based on the IPCC A2 emission scenario. The level of recovery of the region from previous droughts in the 1980s was evaluated using the Standardised Precipitation Index (SPI) and linear regression to identify trends in monthly rainfall and number of rainy days in a month using monthly rainfall time series data between 1980 and 2006. The study further applies a range of stochastic linear models (ARIMA) to predict monthly rainfall time series over a 24 month period, a Cellular Automata –Markov model to project land cover for the year 2046, and a more dynamic land surface scheme the Joint UK Land Environment Simulator (JULES) for simulating past (1980-2000) and future (2046-2065) land surface conditions of soil moisture, soil temperature, surface runoff, Gross Primary Productivity (GPP), latent and sensible heat fluxes. GIS techniques are used to assemble data on soil texture and fractional land cover types used as boundary conditions required by JULES in

some of the simulations. As part of the model evaluation process the JULES land surface model output of surface soil moisture is evaluated with an European Remote Sensing (ERS) satellite product. The sensitivity of the model to input data is examined through changes in scale and non-linearity in the calculation of soil hydraulic parameters. Results suggest that despite a recovery in rainfall in the 1990s from the previous droughts there is no significant recovery in monthly rainfall in the months following the onset of the wet season. The JULES model is more sensitive to scale than non-linearity in the calculation of soil hydraulic parameters. A strong correlation between the model's near surface soil moisture and the ERS satellite near surface soil moisture product in areas where the satellite is believed to perform well, the RMSE and the similarities in the pattern of anomalies between the model and ERS satellite surface soil moisture is an indication of the ability of the model to successfully simulate land surface conditions in the study area. Simulations into the future (2046-2065) using the IPCC A2 emission scenario suggest a significant change in the land surface conditions due to changes in climatic conditions rather than changes in land cover fraction, despite a projected change in land cover based on previous trends from a predominantly broadleaf trees to a dominance of C4 grass (mostly croplands).

## **Dedication**

This Thesis is dedicated to my late parents. How could I ever be grateful to you?

## **Acknowledgements**

I am grateful to the ever living God and the self-subsisting by whom all subsist for guiding me through this process. All grace goes to the creator the lord of majesty and bounty.

I am thankful to my supervisors Dr Jörg Kaduk and Professor Heiko Balzter for their immense effort in making the study a reality. The three and half years spent in carrying out this study have been a very trying moment for me and my family. I therefore wish to thank my wife Jamila B. Mohammed for her courage and endurance during this period. I am also very grateful to Mustafa and Ahmed Galadima Aminu for their assistance and effort in making my journey to the UK a reality. Indeed I acknowledge the funding provided by the Petroleum Technology Fund (PTDF) Nigeria without which this thesis would not have been possible. I also wish to thank my employer the Adamawa State University (ADSU) Mubi for maintaining a basic salary and providing further bursary when my fellowship elapsed.

I appreciate the assistance by Richard Kidd (TU Wien) and Nicholas Viovy ([Nicolas.viovy@lsce.ipsl.fr](mailto:Nicolas.viovy@lsce.ipsl.fr)) for providing access to the ERS satellite soil moisture data and CRU-NCEP climate data.

I wish to thank Dr Kabiru Waziri, Professor Mala Galtima and Professor Abubakar Gundiri for their support. I am also thankful to the Vice Chancellor ADSU Mubi (Professor Alkasum Abba), the Deputy Vice Chancellor (Dr Ibrahim Saidu) and Registrar (Mrs J. M. Garnvwa) for their kindness.

I acknowledge the support given to me by my friends and colleagues such as Ibrahim Muhammed, Yunusa Buba Mubi, Aliyu Inuwa, Abubakar Aliyu Song, Idris M. Jega, Bashir Adamu, and many others I have not mentioned in this article.

I am deeply humbled by the support given to me by members of my family such as my sister Maimuna, brother Abdulrahman, and Nephew Muhammad (Babagari). I am thankful to my late brother Usman for his initial support and advice who was not able to see the end of this project. Usman may your soul rest in perfect peace.

## Contents

Abstract	i
Dedication	iii
Acknowledgements.....	iv
Chapter 1.	Introduction ..... 1
1.1	Introduction ..... 1
1.1.1	Background and rationale of the study ..... 4
1.1.2	Aim and objectives of the study ..... 13
1.1.3	Limitations..... 13
1.2	The Study Area..... 14
1.2.1	Climate ..... 15
1.2.2	Vegetation..... 16
1.2.3	Topography and Geology ..... 17
1.3	Environmental modelling and simulation ..... 19
1.4	The role of greenhouse gasses in global warming..... 21
1.5	Thesis Structure ..... 23
Chapter 2.	Spatial and Temporal variation of rainfall in North-eastern Nigeria 1980-2006..... 27
2.1	Introduction ..... 27
2.1.1	Objectives ..... 30
2.2	Methods ..... 31
2.2.1	Data source ..... 31
2.2.2	Analysis technique..... 31

2.2.3	Software.....	34
2.3	Results .....	34
2.3.1	Spatial and temporal variation in rainfall .....	34
2.3.2	Periods of moisture deficit, excess and the relationship with ENSO events .....	51
2.3.3	Rainfall Prediction using ARIMA.....	56
2.4	Discussion.....	58
2.4.1	Trends in Rainfall 1980-2006 and relationship with ENSO events.....	59
2.4.2	Predicting Rainfall in the study area .....	62
2.5	Summary.....	63
2.6	Acknowledgement.....	66
Chapter 3.	Modelling land surface processes in North-eastern Region of Nigeria from 1980-2000 using the UK met office land surface energy exchange scheme JULES .....	67
3.1	Introduction .....	67
3.1.1	Land-atmosphere interaction .....	69
3.1.2	Soil moisture and satellite data retrieval methods.....	75
3.2	Methodology.....	78
3.2.1	Methods .....	78
3.2.2	Data Types.....	84
3.2.3	Analysis techniques .....	85
3.3	Results .....	86

3.3.1	Data Processing and integration .....	86
3.3.2	Relationship between the five case experiments .....	95
3.3.3	Evaluating experiments with ERS SSM data and precipitation	105
3.3.4	Land-surface conditions in the study area .....	117
3.4	Summary.....	121
3.5	Discussions on modelling past land surface conditions .....	124
3.5.1	Testing the Land models sensitivity to changes in scale and non-linearity in the calculation of soil input parameters .....	124
3.5.2	Comparing model output of surface soil moisture with ERS satellite product .....	125
3.5.3	Trends in Land-Surface conditions in the study area 1980- 2000 .....	126
Chapter 4.	Modelling land cover change in North-eastern Nigeria .....	128
4.1	Introduction .....	128
4.1.1	Limitations.....	130
4.2	Methodology.....	131
4.2.1	Data Acquisition.....	132
4.2.2	Data Analysis Techniques .....	133
4.3	Results .....	134
4.4	Summary.....	148
4.5	Discussion on modelling land cover change .....	150

Chapter 5.	Modelling future land surface conditions in North-eastern Nigeria from 2046-2065 based on the IPCC special report on emission scenario (SRES) A2 .....	153
5.1	Introduction .....	153
5.1.1	Climate scenarios.....	155
5.1.2	The impact of Land use and land cover change on the global and regional climate .....	158
5.2	<i>Materials and Methods</i> .....	160
5.2.1	<i>Data types</i> .....	161
5.2.2	Experiments and analysis techniques .....	161
5.3	Results .....	163
5.4	Differences in past (1980-2000) and future (2046-2065) land surface condition.....	174
5.5	Summary.....	178
5.6	Discussions .....	179
5.7	Acknowledgment.....	183
Chapter 6.	General Discussion.....	184
6.1	Introduction .....	184
6.2	Overview and general discussion .....	184
Chapter 7.	Conclusions .....	190
7.1	Further work .....	192
Bibliography	194	
Appendix	224	

## List of Figures

Figure 1-1: Anomalies in earth surface temperature from 1880 to 2012.....	3
Figure 1-2: Total annual rainfall in the Sub-humid (Longitude 8.5-15 <sup>0</sup> E, Latitude 6.5-9.9 <sup>0</sup> N) and Semi-arid (Longitude 8.5-15 <sup>0</sup> E, Latitude 10.0-14 <sup>0</sup> N) parts of North-eastern Nigeria from 1901 to 2011.....	9
Figure 1-3: Regions of strong coupling between soil moisture and precipitation for the months of June through August averaged from 12 models. ....	12
Figure 1-4: Map of the study area, North-eastern Nigeria.....	14
Figure 1-5 Elevation map of the study area reproduced from Hastings <i>et al.</i> (1999).....	18
Figure 1-6: The model development procedure.....	20
Figure 1-7: A schematic of the thesis work outlining the 4 stages involved in accomplishing each of the 4 objectives and the relevance of each stage. ....	25
Figure 2-1: The mean annual rainfall in mm for the study area (top) and Percentage coefficient of variation of rainfall (bottom) in North- eastern Nigeria 1980-2006 derived from the CRU-NCEP data.....	36
Figure 2-2: Standard deviation of annual rainfall 1980-2006 in mm North- eastern Nigeria derived from CRU-NCEP data. ....	37

Figure 2-3: The mean annual number of days with rainfall in the study area (top) and Percentage coefficient of variation (bottom) derived from CRU-NCEP data .....	38
Figure 2-4: Pixel averaged monthly rainfall anomalies in mm for the sub- humid (top) and semi-arid parts (bottom) of North-eastern Nigeria derived from CRU-NCEP data .....	40
Figure 2-5: Annual rainfall amounts in semi-arid part (top) and sub-humid part (bottom) of North-eastern Nigeria each plotted against a least square regression line (red) derived from CRU-NCEP data.....	41
Figure 2-6: Temporal variation of rainfall amounts for each month in the semi- arid part of North-eastern Nigeria plotted against a regression line ...	43
Figure 2-7: Temporal variation of rainfall amounts (1980-2006) for each month in the sub-humid part of North-eastern Nigeria plotted against a regression line .....	46
Figure 2-8: Temporal variation in number of rainy days (1980-2006) for each month in the sub-humid part of North-eastern Nigeria plotted against a regression line. ....	47
Figure 2-9: Temporal variation number of rainy days (1980-2006) for each month in the semi-arid part of North-eastern Nigeria plotted against a regression line. ....	49
Figure 2-10: Hovmuller Diagram; Longitudinal averaged SPI of the study area 1980-2006 .....	53

Figure 2-11: SPI of annual rainfall 1980-2006 plotted against ENSO SST anomaly in the Tropical Pacific, semi-arid (top) and sub-humid (bottom) parts of North-eastern Nigeria .....	54
Figure 2-12: Predicted monthly rainfall using the ARIMA model plotted against observation data for the semi-arid (top) and sub-humid (bottom) North-east Nigeria.....	57
Figure 3-1: Diagrammatical representation of some important processes in the land-atmosphere interactions at varying time scales (Betts <i>et al.</i> , 1996; Betts and Silva Dias, 2010).....	72
Figure 3-2: The land-surface processes represented in JULES .....	80
Figure 3-3: The percentage sand (top) and clay (bottom) content of the 16 dominant soil types of North-east Nigeria from Sonneveld (1997) based on the 1990 revised FAO-UNESCO soil units .....	89
Figure 3-4: Correlation coefficient of SSM between Experiment 2 and the four other experiments.....	95
Figure 3-5: Correlation coefficients for soil temperature between Experiment 2 and the other four experiments. ....	96
Figure 3-6: Percentage error of SSM between Experiment 2 and the other 4 experiments (* the black line on the map is the border line of the study area).....	97
Figure 3-7: Percentage error of soil temperature between Experiment 2 and the other 4 experiments. ....	98

Figure 3-8: Pixel averaged percentage error of SSM and soil temperature (January-December 1980) between Experiments 2 and 1 (black line), 2 and 3 (red line), 2 and 4 (green line), and 2 and 5 (blue line). .....	99
Figure 3-9 Pixel and time averaged (1980-2000) predicted soil moisture (top) and soil temperature (below) at different depth for all five experiments .....	104
Figure 3-10: Grid box correlation between satellite product SSM and the 5 experiments. ....	106
Figure 3-11 Satellite SSM observations (black dots) plotted against simulation from experiment 2 in an area of lowest correlation in the Sahel part (Latitude 13-13.5° North, Longitude 10.5-11° East).....	107
Figure 3-12: Scatter plot of ERS scat and predicted SSM for Experiments 1 to Experiment 5 .....	112
Figure 3-13: The ECDF of SSM for ERS scat (black) Experiment 2 (red) and Experiment 5 (blue). ....	113
Figure 3-14: Anomalies of SSM from ERS satellite (black line) and predicted Experiment 5 (green line) SSM .....	115
Figure 3-15 Monthly averaged anomaly indices between ERS satellite product and predicted Experiment 5 SSM for five months (June-October) from 1992-2000 (top) and monthly averaged anomaly indices between ERS satellite product and precipitation data (bottom).....	116

Figure 3-16: Correlation coefficients between precipitation and predicted SSM for all 5 experiments .....	117
Figure 3-17: Pixel averaged least squares regression line of predicted sensible heat, latent heat flux, Bowen's ratio and Evaporative Fraction for Experiment 5 plotted over a regression line .....	119
Figure 3-18: Pixel averaged least squares regression for predicted Experiment 5 SSM plotted over a 21 year period .....	120
Figure 3-19: Pixel averaged annual predicted GPP in $\text{kg C m}^{-2} \text{yr}^{-1}$ from Experiment 5 .....	121
Figure 4-1: Research flow chart for Chapter 4 .....	132
Figure 4-2: Reclassified LC for 1977, 1994, 2005 and 2009 using the JULES LC classification scheme .....	138
Figure 4-3: Changes in LC 1977 to 1994 gains and losses for each class in $\text{km}^2$	139
Figure 4-4: Changes in LC 1994 to 2005 gains and losses for each class in $\text{km}^2$	139
Figure 4-5: Changes in LC 2005 to 2009 gains and losses for each class in $\text{km}^2$	142
Figure 4-6: Bar chart of LC conversion from 1977 to 1994 .....	143
Figure 4-7: Bar chart of LC conversion from 2005 to 2009 .....	144
Figure 4-8: Markov chain analysis conditional probability of being one the seven LC classes .....	145
Figure 4-9: Markov chain analysis conditional probability of being one the seven LC classes .....	146
Figure 4-10: LC Projection 2046 .....	147

Figure 4-11: comparison between LC 2009 and predicted LC for 2009 using the CA-Markov model .....	147
Figure 5-1: General description of the IPCC SRES highlighting how they are related and their differences based on environmental issues and the level of global integration .....	156
Figure 5-2: Global carbon dioxide emissions from the six IPCC special emission scenarios for the years 1990 to 2100 .....	158
Figure 5-3: A schematic of the two experiments. In both cases the IPCC SRES A2 was used as forcing data.....	162
Figure 5-4: Percentage difference in the four vegetative fractional land cover types in the area represented by acronyms BT (Broad leaf trees), C3G (C3 grass), and C4G (C4 grass).....	164
Figure 5-5: Temporally averaged percentage differences of Evaporative Fraction (EF), surface runoff (top right), soil moisture as a fraction of saturation, and GPP (expressed in $\text{kg C m}^{-2}$ ) averaged for the period 2046-2065. ....	166
Figure 5-6: Temporally averaged differences in predicted land surface temperature in $^{\circ}\text{C}$ between Experiment 2 and Experiment 1 .....	167
Figure 5-7: Pixel averaged percentage differences in Evaporative Fraction, predicted surface run off, surface soil moisture, and GPP obtained between the two experiments.....	169

Figure 5-8: Predicted soil moisture content (left) and soil moisture content as a fraction of saturation (right) at different depth plotted for Experiment 1 and Experiment 2 .....	170
Figure 5-9: Box plots of Evaporative Fraction, predicted surface soil moisture, surface runoff and GPP (Latitude 10-10.5 North, Longitude 11-11.5 East). The first (white) box represents Experiment 1 while the second (grey) box represents Experiment 2.....	172
Figure 5-10: Box plots of Evaporative Fraction, predicted surface soil moisture, surface runoff and GPP (Latitude 8-8.5 North, Longitude 12-12.5 East) .....	173
Figure 5-11: Pixel averaged trends in the Bowen ratio (upper left), predicted Evaporative Fraction (upper right), top surface soil moisture (lower left), and GPP (lower right) from Experiment 2.....	174
Figure 5-12: Mean monthly rainfall (RF) and temperature (Temp) used in driving the model to simulate past and future land surface conditions.....	175
Figure 5-13: Mean monthly differences in simulated past (1980-2000) and future (2046-2065) land surface conditions.....	176

# Chapter 1. Introduction

## 1.1 Introduction

The land surface covers only about 30% of the total earth surface area yet it is a host to many of the bio-geochemical and bio-geophysical processes taking place on the planet strongly determining the state of the climate system. Unlike the oceans the land consists of vegetation, mountains, soils, ice and inland water bodies providing a distinctive heterogeneity on the surface. The land is also the living space for man with scattered human landscapes of various kinds, such as agriculture, forestry, towns, and infrastructure, which contribute to the heterogeneity of the land surface. The land surface absorbs incoming solar radiation and is influenced by atmospheric conditions. On the other hand, the land surface redistributes this influx in the form of energy, moisture and carbon fluxes. Differential warming caused by this heterogeneity influences atmospheric circulation and variability in the climate (Yang, 2003) creating spatial, diurnal and seasonal variation in temperature on the land surface and atmosphere. It is thus, very important in determining changes in the climatic and weather conditions at different spatial and temporal scales.

The impact of human activities on the environment has been increasing in recent years with increasing demands for resources to satisfy the growing human population. This has increased global greenhouse gas concentrations in the atmosphere through industrial emission and land use/ land cover change (LUCC).

The IPCC 2007 reports that the global increase in temperature of  $0.13^{\circ}\text{C}$  per

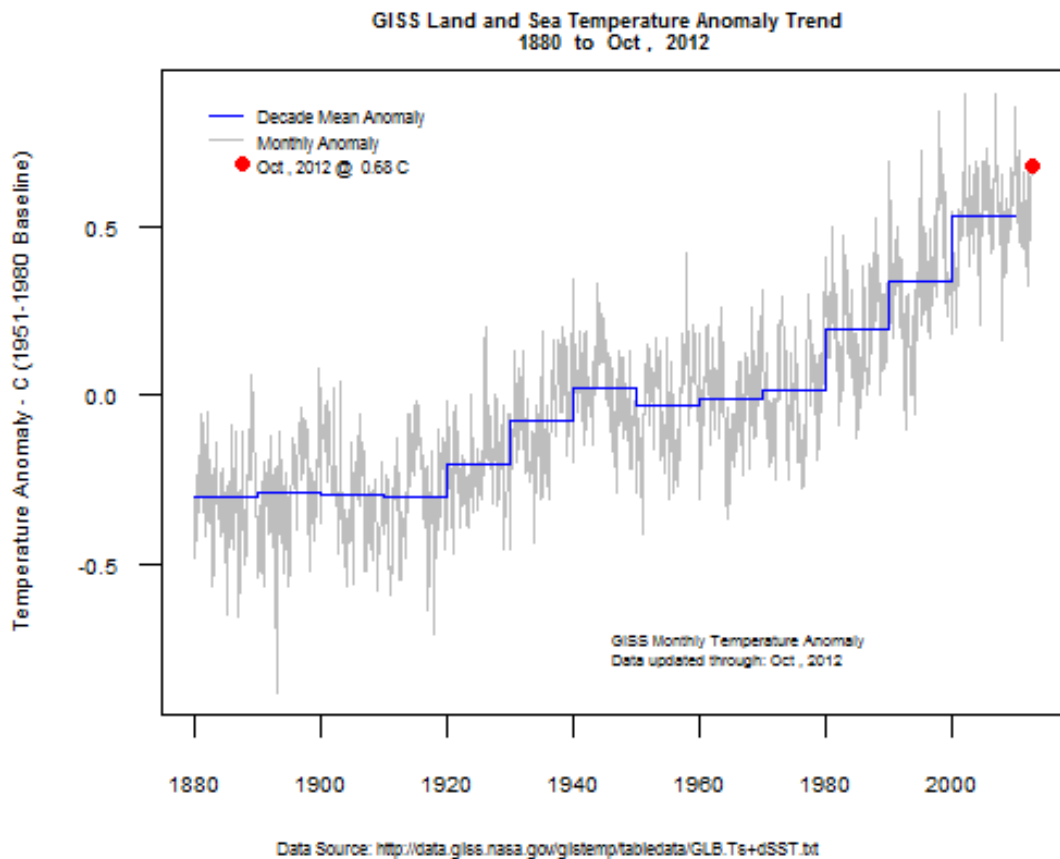
decade in the last 50 years is the highest ever recorded (IPCC, 2007). Increase in global temperatures is attributed to increasing radiative forcing from increasing atmospheric concentration of greenhouse gasses such as carbon dioxide, methane and nitrous oxide. Global atmospheric concentration of carbon dioxide increased from a pre-industrial era level of ~279 ppm to 390 ppm in 2011 (Global Carbon Project, 2012).

There is also a significant increase in global atmospheric concentration of methane and nitrous oxides (IPCC, 2007). At present the average temperature from all global surfaces of land and oceans has increased by 0.68 °C (Figure 1-1) since the 1880s at the early stages of the industrial revolution (Global Carbon Project, 2012). Changes in the net radiation budget of the earth have an effect on land surface processes and land-atmosphere feedbacks with overall impact on how moisture and vegetation is distributed across the land surface.

Pre-industrial causes of global climate variability are mainly from natural causes. Main causes of natural variability in global climatic conditions since pre-historic times are volcanic eruptions and solar variability (Bengtsson *et al.*, 2006).

However, reconstructed records of volcanic eruptions and incoming solar radiation since the pre-industrial era does not explain extreme climatic conditions and variability experienced in the 20<sup>th</sup> Century and onwards (Bengtsson *et al.*, 2006). For instance the 1990s is reported to be the warmest decade in the northern hemisphere and 1998 as the warmest year (IPCC, 2001). In West Africa there has

been a decreasing trend in the amounts of rainfall with increasing variability in the last 50 years (Jury *et al.*, 2002; Anyamba and Tucker, 2005).



D Kelly O'Day - <http://chartgraphs.wordpress.com>

11/20/2012

### Figure 1-1: Anomalies in earth surface temperature from 1880 to 2012

This study primarily focusses on changes in land surface processes in an increasingly human dominated world. Changes in climatic conditions due to anthropogenic greenhouse gas emissions and land use land cover change. The subsequent sections of this chapter will provide the background to the study with the aim and objectives. The Chapter also provides a brief description of the study

where the climate, vegetation and topography are highlighted. Furthermore, there is a brief discussion on modelling as a means of studying complex environmental systems. There is a discussion on the role anthropogenic greenhouse gas emissions on global warming and climate change. Finally, the last section explains how the thesis is structured in terms of the methodology and what objectives the remaining chapters intend to fulfil.

### **1.1.1 Background and rationale of the study**

The West African droughts of 1960-1970s and 1980s are among the catastrophic in modern times with a loss of several thousands of livestock, led to human displacement and raised threats to security in the region (Wittig *et al.*, 2007). In response, the global community attempted to identify the root causes of this natural disaster. Two contrasting views developed in the scientific community to explain the mechanisms associated with the West African Sahel rainfall variability. These two views attempting to explain the root causes of re-occurring droughts in the region are generally summarised by Hulme (2001) as the “the regional land-atmosphere feedback” and “ocean-atmosphere interaction”. The first attempt to explain the Sahel droughts in recent decades stresses on the land-atmosphere feedback mechanism. This premise has evolved over the years from the idea that human activities and changes in the pattern of land use is significantly altering the land cover and leading to desiccation. There were reports of the encroaching desert as early as the first quarter of the 20<sup>th</sup> Century with the papers presented by Hubert (1917) and Bovill (1921) reporting of dry valleys and river beds in the West African Sahel at the fringes of the Sahara with remnants of

settlements perceived to be abundant because of the encroaching Sahara. These arguments were supported by the works of Lamprey (1975), Otterman (1974) and Charney (1975). Evidences that the desert has encroached by 90-100 Km from 1958 to 1975 was put forward by Lamprey (1975) after mapping the desert boundary in Sudan. But his conclusion was realised to be misleading (Hellden, 1988). Otterman (1975) using satellite imagery identified a change in surface albedo caused by overgrazing and removal of the vegetation in the Sinai and this has led to a temperature decrease of 5-3.5 °C relative to the adjacent protected area of Negev. This decrease in temperature he argued reduces the chances of cloud formation and rainfall. Similarly, Charney (1975) using a General Circulation Model (GCM) concluded that removal of vegetation cover in the semi-arid regions increases the surface albedo causing atmospheric subsidence, weakening of convection currents responsible for cloud formation and rainfall further enhancing the drying effect. Ripley (1976) was very critical of the conclusions drawn by Charney since his model did not take into account surface energy fluxes of sensible and latent heat. This inconclusive premise of the relationship between climate variability and human induced land cover change has promoted further research into the issue and also a focus towards other mechanisms that could be responsible for climate variability.

Analysis of rainfall time series using standardised rainfall departures was undertaken from rainfall data collated for the first time across a wider range of observation stations in Sub-Saharan Africa since the beginning of record keeping in 1900 (Nicholson 1979). Prior to the dry years of the 1980s this study by

Nicholson (1979) provided an insight to reoccurring droughts in West Africa identifying drought periods of 1910-1920, 1968-1973 and of a lesser intensity in the 1940s. Furthermore, the study noted a similar pattern in rainfall variation across the Sub-humid and Sudano-Sahelian belts. Annual rainfall in North-eastern Nigeria for a 111 year period (1901-2011) suggests that most years in the 1980s were below the long term mean (Figure 1-2). Annual rainfall from the 1990s onwards is hovering along the long term mean in the sub-humid parts of the region. While, annual rainfall in the semi-arid part is slightly above the long term mean from the 1990s onwards.

In an attempt to understand the mechanism controlling the West African Monsoon (WAM) that seasonally modulates the availability of moisture within the sub-region from the Guinean coast to the Sahel a number of studies in the 1980s focussed on the ocean-atmosphere interaction. Part of these researches investigated the relationship between rainfall variability and sea surface temperature (SST) anomalies (Lamb, 1978). Folland *et al.*, (1986) identified that dry and wet events in the Sahel Region are linked to a wider global SST anomalies not only restricted to the Atlantic but also SST variations in the pacific and resultant El-Nino effects. The strength and depth of the WAM has been noticed to correspond with seasonal rainfall patterns in the region (Lamb, 1983) and the northward displacement of the Inter-tropical Convergence Zone (ITCZ). The role of the African Easterly Jet (AEJ) in the formation of convective currents has been investigated by Cook (1999) and (Fontaine *et al.*, 1995).

The contribution of Sahelian dust in the global atmospheric aerosol concentrations is receiving more interest in recent years. Not only because there is an increase in aerosol production as a result of the prolonged droughts of the 1960s and 1980s (Mbourou-N'Tchayi, 1997) but also the effect it may have on regional and global climate variability. The African Sahelian dust is transported to a wide region and large traces are recorded as far as the Caribbean (Carlson and Prospero, 1972). Aerosols are important atmospheric forcing either scattering or absorbing solar radiation and may have a cooling or warming effect (Nicholson, 2013). The positive role of Sahelian dust in cloud formation and the concentration of ice nuclei on dust particles has been investigated by DeMott *et al.* (2003). However there is a majority view that Sahelian aerosol reduces rainfall (Nicholson 2013) through the suppression of deep convective currents (Huang *et al.*, 2009). Yoshioka *et al.*, (2007) used climate models to conduct several experiments to study the effect of large size dust particles on climate variability and noted that a 36% increase in optical depth of dust in the Sahelian atmosphere may have contributed to 15% reduction in precipitation in the region. In this study Yoshika *et al.* also noted a greater contribution of changes in SST and vegetation on changes in precipitation.

In the 1990s there was a sign of recovery (Nicholson, 1997) and studies using satellite observation suggest that the Sahara is not expanding as previously thought but rather the boundaries of the Sahel and the Sahara fluctuates in response to seasonal rainfall regimes. Prince (1998) analysed Rain Use efficiency (RUE) of the Sahel derived from 8 years (1982-1990) of remotely sensed

vegetation index and rainfall data and concluded that there is no evidence of wide scale desertification in the Sahel. Except for a few areas in the Sahel, Prince noted a slight increase in RUE suggesting that the increase is either a response to a slight increase in rainfall after 1984 or a change in land cover from woodlands to grasslands. Similarly, Anyamba and Tucker (2005) analysed 23 years (1981-2003) Normalized Difference Vegetation Index (NDVI) generated from monthly satellite observations and rainfall time series data and noticed a strong relationship between the NDVI and rainfall anomalies. The study by Anyamba and Tucker identified two distinct periods of below average NDVI (1982-1993) and above average (1994-2003) where the years with the highest NDVI 1994 and 1999 corresponds with years of higher rainfall.

Progressively models are used in both the traditional fields of ocean-atmosphere interaction and land-atmosphere feedback for studying climate variability in Sub-Saharan Africa. Also of similar interest is the study of the Sahel under future climate change scenarios. Studies by Rowell *et al.* (1995) and Giannini *et al.* (2003) used climate model to reiterate the influence of SST on the rainfall variability in the Sahel. Rowell *et al.* (1995) carried out a number of experiments using a climate model forced by only SST anomalies to simulate previous climatic conditions (1902-1992) in West and North Africa and compared results with observations during the same period. Giannini *et al.* (2003) conducted a similar experiment with observed SST temperature forcing from the year 1930 to 2000 and concluded that rainfall in the Sahel is sensitive to all tropical oceanic SST anomalies including the tropical Atlantic, the Indian and the Pacific Ocean. The

study by Giannini *et al.* further suggested that the Sahel droughts from the 1960s to the 1980s are caused by a warmer than average SST in the Indian and Atlantic Oceans thereby is reducing the effect of the warm continent and cooler ocean temperature gradient supporting the WAM during the boreal summer. However, both studies by Rowell *et al.* and Giannini *et al.* acknowledged that rainfall variability in the Sahel is amplified by land surface conditions through land-atmosphere interaction.

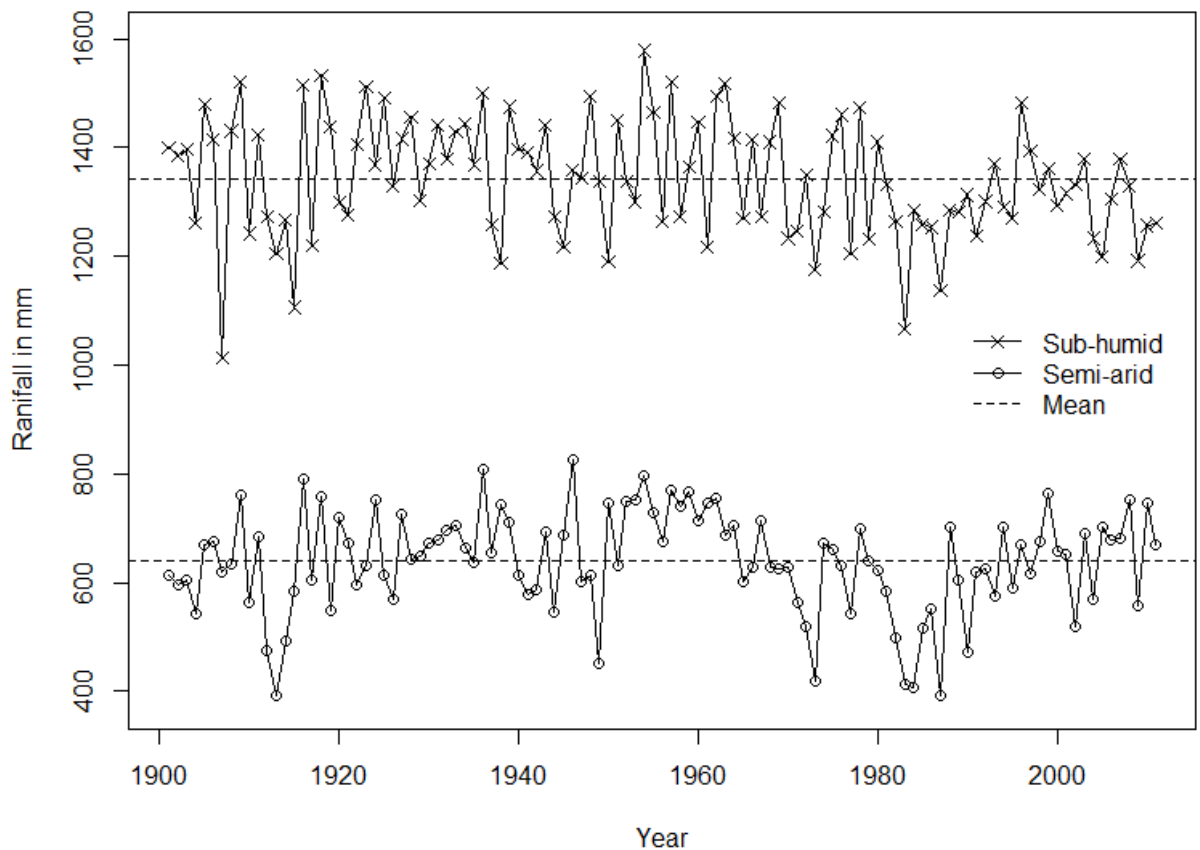


**Figure 1-2: Total annual rainfall in the Sub-humid (Longitude 8.5-15 °E, Latitude 6.5-9.9 °N) and Semi-arid (Longitude 8.5-15 °E, Latitude 10.0-14 °N) parts of North-eastern Nigeria from 1901 to 2011**

\*Source: CRU 3.2 precipitation data set.

Various studies supporting the land-atmosphere paradigm reiterate the importance of soil moisture and vegetation in influencing the fluxes of energy and momentum from the land surface into the lower atmosphere. While the study by Charney (1975) used a simple land surface-atmosphere scheme to examine the effect of changes to surface albedo on land surface properties recent studies have used a more sophisticated land surface scheme that incorporates vegetation, soil and other surface parameters. Xue and Shukla (1993) conducted an experiment using a climate model. They obtained a similar pattern of rainfall reduction experienced in the drought years by replacing the savanna vegetation in West Africa with bare soils and grasslands. A similar experiment was repeated by Taylor *et al.* (2002) incorporating a more realistic land use model.

West Africa is among the regions identified by Koster *et al.* (2004) having a strong coupling between soil moisture and precipitation. Those regions they referred to as “hot spots” are areas where soil moisture anomalies have a strong influence on precipitation. Their study was centred on the Global Land Atmosphere Coupling Experiment (GLACE) with 12 climate models incorporated in the project. Areas where the climate models indicate a strong coupling between the models and regions of strong soil moisture-atmosphere feedback is presented in Figure 1-3.

Soil moisture is responsible for the partitioning of incoming energy into latent heat and sensible heat fluxes; the distribution of precipitation into vertical

infiltration and horizontal surface run off; and the albedo characteristics of the surface since wet soils are darker than dry soils. All of this leads to significant feedbacks (Taylor *et al.*, 2002). Improved representation of the land surface processes will therefore improve predictions of the atmospheric boundary conditions in climate models and climate predictions.

The land surface stores a large pool of carbon (Yang, 2003) and is also very vulnerable to various forms of degradation with potentials of turning this pool into a large source of carbon for the atmosphere. Williams *et al.* (2007) identified Africa as the “weakest link” in the study of the global carbon cycle because of the scarcity of observation stations despite the contributions of the continent in the inter annual variability of the global carbon balance. The West African Savanna is one of the significant regions for this yearly variability in the continents carbon stock which is primarily driven by climatic perturbations and bush fires.

Moreover, the Savanna covers half of the African continent contributing a larger proportion of its carbon emissions through fires and large proportion of emissions through LUCC (Cias *et al.*, 2011). The West African open Savanna has potentials for carbon stoking through afforestation and re-afforestation but is very vulnerable to land degradation from increasing poor land management practices (Lykke *et al.*, 2009). Generally, little is known about the carbon dynamics of the Savanna ecosystem and whether it is a source of carbon or a sink (Cias *et al.*, 2011). Most studies on the carbon dynamics of the African Savanna are more general and do not take into account the complexity of the ecosystem and regional or local variations existing across the continent (Cias *et al.*, 2011).

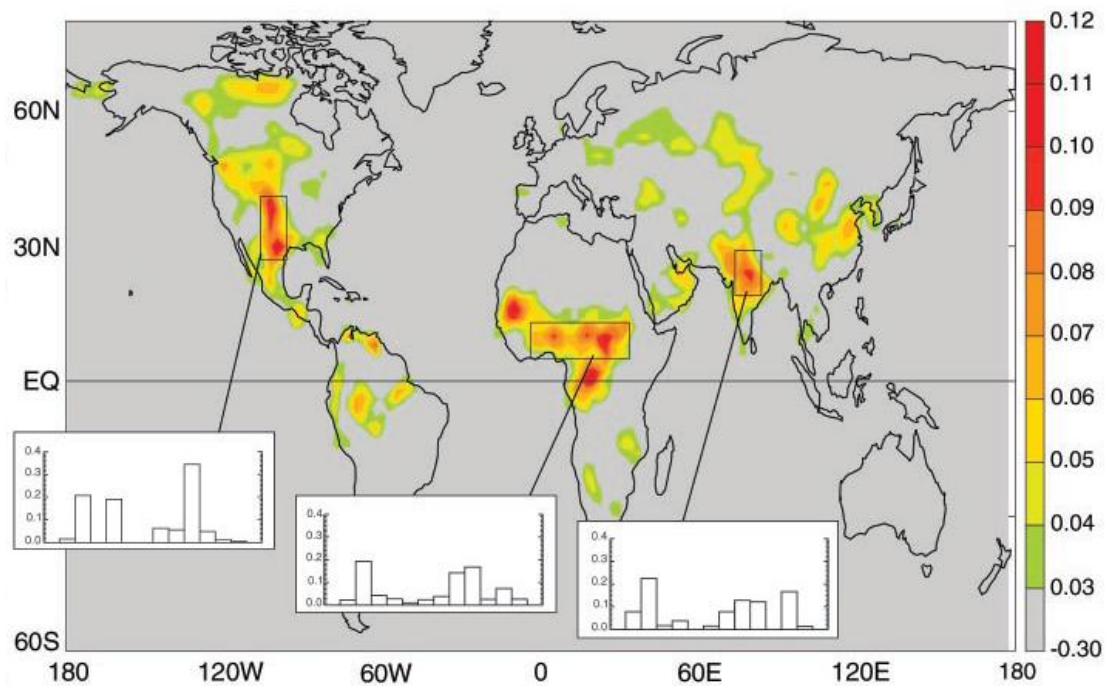


**Figure 1-3: Regions of strong coupling between soil moisture and precipitation for the months of June through August averaged from 12 models.**

\*West Africa is among those regions. The colour bar represents the strength of the coupling between soil moisture and precipitation averaged for the 12 climate models that participated in the GLACE experiment. The three histogram plots show the strength of the coupling for each of the 12 climate models. From Koster *et al.* (2004)

Finally, the economies of the West African countries are mostly agrarian and subject to climatic perturbations; additionally the poor nature of land management systems within the region is also a major cause of deforestation and land degradation with likely effects on the climate through the changes in surface

albedo, and fluxes of energy carbon and moisture. An improved understanding of the local and regional land surface processes in relation to climatic changes and LUCC will strengthen the existing knowledge of the land-atmosphere interaction furthermore assisting in future decision making and policy.

### **1.1.2 Aim and objectives of the study**

The aim of this Thesis is to study the impact of climate variability and land cover change in North-eastern Nigeria on land surface conditions. The specific objectives are:

- I. To analyse and predict rainfall trends in the North-eastern region of Nigeria 1980-2006.
- II. To evaluate the Joint UK Land Environment Simulator (JULES) land surface model and undertake sensitivity analysis of the model to changes in scale and non-linearity in the calculation of soil input data.
- III. To Model past land surface processes in the study area from 1980 to 2000.
- IV. To analyse past changes in land cover and predicting future changes.
- V. To Model future land surface conditions in the area using the IPCC climatic scenarios A2 and a projected land cover.

### **1.1.3 Limitations**

A major limitation to this study is the availability of higher resolution data. One of these problems is the availability of forcing data such as atmospheric conditions and fractional land cover required for running land surface models. Most of the available forcing data are used in global general circulation models that cover the

entire globe and are produced with intention for higher coverage rather than greater detail. This problem has limited the running of the land surface model on  $1^0 \times 1^0$  and  $\frac{1}{2}^0 \times \frac{1}{2}^0$  resolutions.

## 1.2 The Study Area

The study area lies between Latitude  $6^0$  and  $14^0$  North, and Longitude  $8^0$  and  $15^0$  East (Figure 1-4). The area known as the North-eastern Region of Nigeria is a political amalgamation of various peoples previously living under separate entities before the creation of Nigeria. It was only in 1966 that a state was created covering the whole region from the former northern region for easier administration, grass root development and to reduce the sphere of influence of the three major contending tribes in Nigeria at that time (Barbour, 1971).

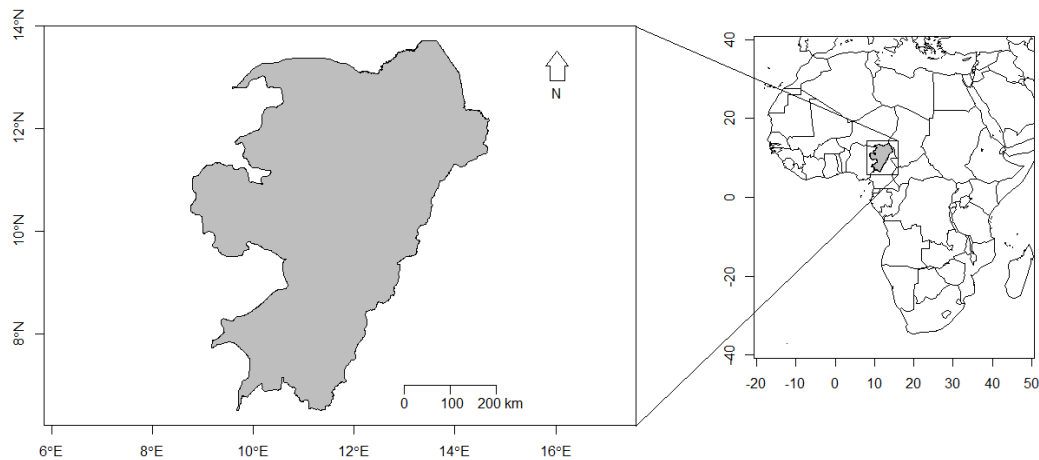


**Figure 1-4: Map of the study area, North-eastern Nigeria**

Subsequently the region was further subdivided into six states Adamawa, Bauchi, Borno, Gombe, Taraba, and Yobe. The significance of the region is that it is part of two major hydrological basins; the Lake Chad and the Upper Benue River

Basins. Both basins support a large ecology and are an important component of the West African hydrological system supporting millions of people. Furthermore the geology of the basins indicates potentials for hydrocarbon reserves (Obaje *et al.*, 2006).

### **1.2.1 Climate**

The study area has a tropical continental climate marked by a dry and wet season. In the updated Köppen's climatic classification most parts of the area fall under the Aw (Tropical wet and dry) climate type while a much smaller part in the northern end of the study area falls under the BSh (sub-tropical steppe) climate (Peel *et al.*, 2007). Generally, the area is under the influence of the West African Monsoon (WAM) where the availability of moisture varies seasonally with the movement of the inter-tropical convergence zone (ITCZ). The wet season coincides with the high angle of the sun and the tropical low pressure belt created in North Africa and a parallel low pressure belt in the Gulf of Guinea. These parallel pressure belts are reversed with the movement of the sun towards the Tropics of Capricorn. The resulting dry season created by this shift is much related to the existence of a subtropical high zone and the stable air associated with its presence (Pidwirny, 2006). Rainfall is mostly a product of convection and instability in the lower atmosphere caused by heating of the land surface. The nature and characteristics of the land surface to a great extent determines the creation of these convectional currents. Rainfall amounts and frequency decreases northwards with the period of precipitation varying between 7 months in the south

to less than 3 month in the north with a few exceptions as a result of orographic influences.

### **1.2.2 Vegetation**

The study area is within a Savanna region with a small Sahel vegetation belt in the north, and also small forest and mountain vegetation areas in the south. The Savanna is a grassland area characterized by a varying degree of woody cover. Plant productivity and respiration in this vegetation type is a function of numerous factors including water availability, soil type, nutrients, animal and human influence (Sankaran *et al.*, 2005). Most significant is the availability of water in the form of precipitation which controls soil moisture, moderates temperature and stimulates microbial activity (Sankaran *et al.*, 2005 and Williams *et al.*, 2009). Availability of moisture has also delimited the Savannah region into a wet and dry season where the dry season is a period of inactivity or limited terrestrial productivity due to high deficiency in moisture. The seasonal changes in the ecosystem production and the distribution of woody and grass biomass over the land reflect the spatial and temporal variability of the ITCZ. In addition, there is a carry-over effect of moisture conditions from year to year; according to Los *et al.* (2006) moisture conditions of a previous wet season aids plant investment in stems and seeds which boost productivity in the following wet season. The region is also very sensitive and vulnerable to climatic variability. In the past few decades the region experienced droughts that led to the encroachment of the Sahara desert from the north (Oladipo, 1993). The Savanna is equally a very

important ecological region in Africa supporting varying groups of wildlife and people.

### **1.2.3 Topography and Geology**

The topography of the study area (Figure 1-5) is a function of the underlying geology and previous processes of tectonics and denudation. The area is part of two basins: the Chad Basin and the Benue River basin. The Benue-Chad Trough are part of the central West African Rift system formed in the Cretaceous period as a result of the separation of the African and South American Continents and subsequent opening of the South Atlantic (Olugbemi *et al.*, 1997). The Chad Basin is the largest intracratonic basin in Africa covering an area of 2,334,000 km<sup>2</sup> with about one tenth of the basin area in Nigeria (Obaje, 2009). After the formation of the Benue-Chad Trough there has been subsequent deposition of continental and marine sediments on the basement complex at various periods and later intrusions of tertiary volcanic rocks. Notable marine sediments studied at present for hydrocarbon potentials include the Gongila and Fika formations in the Chad Basin, and the Dukkul, Jessu, and Lamja shale in the Benue Rift System. The Chad Basin is bordered by the basement complex rock to the west and the east, the Biu Basalt Plateau and the Benue Basin in the south. The Benue basin is bounded by the Basement rocks to the east and west. This arrangement provides the area with a unique topography with rivers rising from the granite and Basalt Mountains and emptying into the Lake Chad in the north east or the Benue River flowing in a south west direction and emptying into the Niger River. The topography could be classified into highlands, plains and lowlands. The highest

points in the area are on the Adamawa highlands, a mountain range bordering the study area with Cameroun Republic from the southeast and stretching northwards. Chappal Waddi (2419 meters above sea level) is the highest Peak in this mountain range and in the entire study area (Borokini *et al.*, 2012).

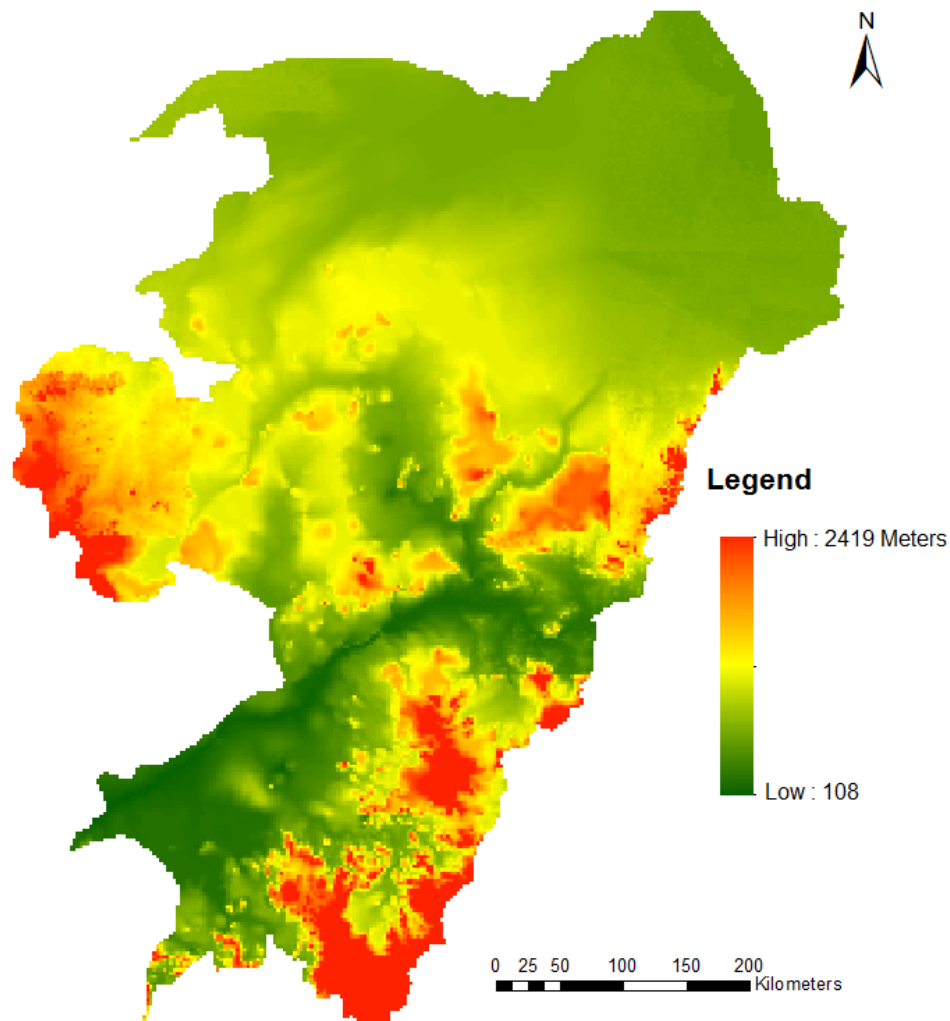


**Figure 1-5 Elevation map of the study area reproduced from Hastings *et al.* (1999)**

### **1.3 Environmental modelling and simulation**

The environment is composed of several systems operating at varying spatial scales. A system here refers to a unit comprising of a set of interrelated components (Hardisty *et al.*, 1993). There are inputs and outputs from the system and the level of these depends on the permeability of the boundaries of the unit and openness. An example of an environmental system given by Hardisty *et al.* (1993) is the climate: in this case the inputs and outputs are energy and matter; the system components include the water bodies; and the system boundaries are the earth surface and the atmosphere. The need to study and understand environmental systems is necessary for obvious reasons. Traditionally these reasons are to advance the utilization of the Earth Resources, to explain the origin of nature, improve on techniques of warfare, foster industrialisation, prevent or treat diseases, or even just to satisfy human curiosity (Oreskes, 2003).

Environmental systems in most cases are too vast and complex to easily study and comprehend. For this reason, in order to simplify the study of such systems scientists employ models. Models are idealized simplifications of some phenomenon or system (Perry, 2009). Models are therefore used in the study of the natural environment for understanding both processes and products of the environment and how they interact (Oreskes, 2003). Advances in modelling in recent years have been achieved by the increasing computational powers of computers.

Environmental models can be classified into three groups (Hardisty *et al.*, 1993): descriptive models are a narrative of how the components of a system are

organised and how they work presented graphically, or in the form of sentences; empirical models uses two or more data sets to develop a statistical relationship between the parameters of interest; thirdly theoretical models develop a proposal of the operative process of a system, and then construct some mathematical equations based on these processes. The basic procedure for developing and operating a model is provided in Figure 1- 6. Model development starts with observing how a system works through experimentation and analysis. The most important features controlling the processes within the system are identified and this can be represented diagrammatically or using mathematical equations to express those functions. Based on the findings a conceptual, mathematical or computer based model can be developed.

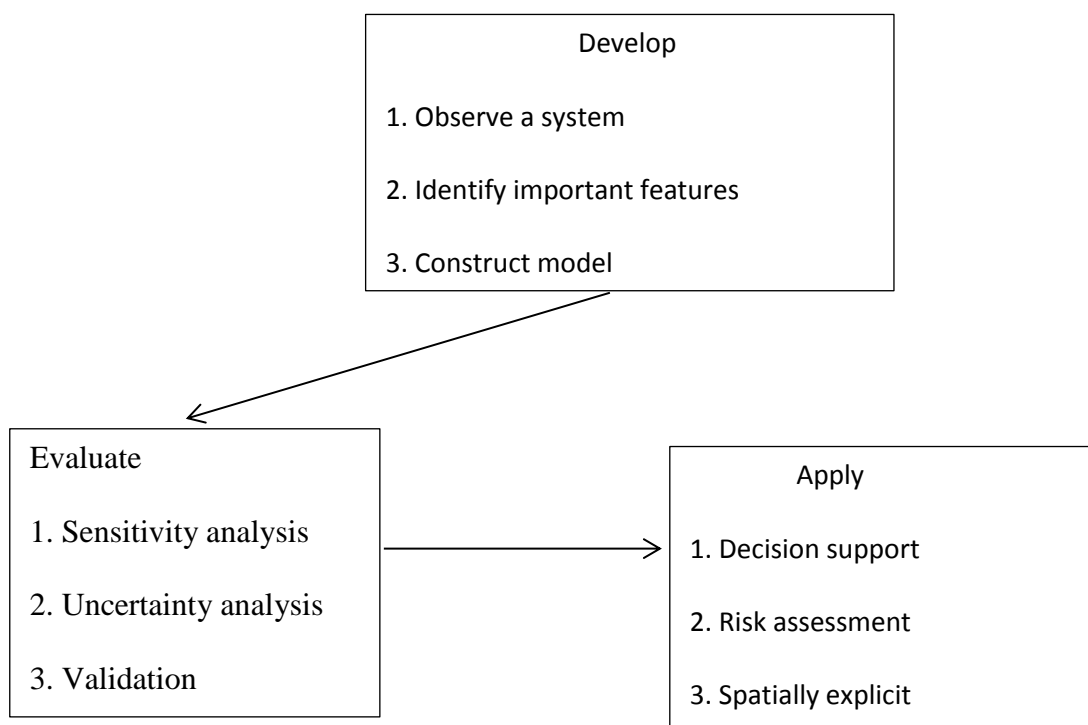


**Figure 1-6: The model development procedure**

Models need to be evaluated to know whether they are reproducing the processes in reality or doing something different. This can be done by comparing the model output to the results of a given experiment. As part of the model evaluation sensitivity and uncertainty analysis are undertaken for a number of reasons as identified by Hamby (1994) primarily to identify: model parameters that are strongly correlated with the output and those that are insignificant and can be eliminated; parameters that require additional research thereby reducing uncertainty; inputs that contributes highest to output variability.

#### **1.4 The role of greenhouse gasses in global warming**

Earth is habitable because of the distance of the planet to the sun and the existence of greenhouse gasses like water vapour, carbon dioxide, ozone and trace gasses like methane naturally occurring in the atmosphere (Karl and Trenberth, 2003). Without these, the earth's surface would be much cooler than it is at present. Much of the solar energy received by the earth surface (land and oceans) is radiated back into the atmosphere and a part of this is absorbed by greenhouse gasses then released upwards and downwards into the lower atmosphere (at a longer wavelengths). This mechanism raises the temperature of the atmosphere and the surface compared to an atmosphere without greenhouse gasses. The major sources of anthropogenic carbon dioxide emission are through the burning of fuel and LUCC. The radiative forcing of the various greenhouse gasses differ including lifespan in the atmosphere in Table (1-1).

Recent increases in the emission of greenhouse gasses from anthropogenic sources have raised the concentrations of these gasses which has increased its

effect. Since the industrial revolution the concentration of greenhouse gases have steadily increased. Carbon dioxide concentrations rose from pre-industrial levels of 280ppm to over 380ppm at present (Van Minnen *et al.*, 2009). A sharp increase in atmospheric carbon concentrations started in the 1950s, a trend that has been sustained as the world economy grows and become more energy dependent. The increasing rate in atmospheric carbon dioxide accumulation is highest from 1995 onwards at 1.9 ppm per year (IPCC 2007). Increases in carbon dioxide emissions are related to three major anthropogenic sources; fossil fuel combustion, cement production and land use changes. Most of the emissions are absorbed by sinks on land and sea but with increasing emissions these sinks become less efficient. Estimates indicate that only 44% of all emissions have remained in the atmosphere the rest being absorbed by sinks (Van Minnen *et al.*, 2009). There is an expectation that emissions due to changes in land use will reduce gradually as a result of improved management systems and re-forestation schemes, thereby reducing land carbon dioxide emissions and possibly enhancing land sinks. However, fossil fuel combustion and cement production is also expected to rise (IPCC 2007). Such sources are already responsible for two third of all anthropogenic carbon dioxide emissions (Raupach, 2007). Central to this issue is the problem of global warming. Carbon dioxide though having a less global warming potential (GWP) than other substances such as methane or nitrous oxides is relevant because of the quantity and rate at which it is emitted into the atmosphere. It accounts for 63% of radiative forcing from gasses and it is a major contributor to anthropogenic causes of climate change (Raupach, 2007). Global

temperature averages have increased by over 0.6 °C since the beginning of the industrial age and this increase could be sustained unless controlled due to the current global emission of greenhouse gasses related to global energy demands and economic growth.

**Table 1-1: Three main greenhouse gasses and their potential for global warming**

Greenhouse gasses	Concentration in 2005	Radiative forcing (W m <sup>-2</sup> )	Radiative Efficiency (W m <sup>-2</sup> ppb <sup>-1</sup> )	Lifetime (Years)	Global warming potential		
					20-yr	100-yr	500-yr
CO <sub>2</sub>	379 ±0.65 ppm	1.66	1.4x10 <sup>-5</sup>	*	1	1	1
CH <sub>4</sub>	1,774±1.8 ppb	0.48	3.7x10 <sup>-4</sup>	12	72	25	7.6
N <sub>2</sub> O	319±0.12 ppb	0.16	3.03x10 <sup>-3</sup>	114	310	298	153

Source: Forster *et al.* (2007)

## 1.5 Thesis Structure

The thesis comprises of seven chapters beginning with an introductory chapter, a general discussion chapter and a remarks and conclusion chapter at the end. It is intended that a separate chapter will be used to accommodate each of the 4 major objectives (Figure 1- 7). Chapter 2 highlights the importance of rainfall as a major driver of ecosystem productivity in areas under the influence of the West African Monsoon. There has been a decreasing trend in rainfall amounts in the area with increasing variability in the past 60 years with droughts occurring in the 1960s, 70s and 80s. These droughts had an ecological, economic and societal impact on

the region (Wittig *et al.*, 2007). However, there has been an indication of a recovery in the 1990s with overall annual rainfall recorded slightly higher than the long term average. In Chapter 2 this recovery is analysed using medium term rainfall records from 1980 to 2006 derived from station data and model reanalysis. There is also an attempt to predict monthly rainfall over a 24 month period using the Auto regressive integrated moving average (ARIMA) model. The strength of this prediction is further evaluated using existing records.

In Chapter 3 a description is given of the response of land surface conditions of soil moisture, GPP, latent and sensible heat flux to climate variability during the drought years of the 1980s to the period of rainfall recovery in the 1990s in an experiment carried out using a “stand alone” mode of the Met office Joint UK Land Environment Simulator (JULES) forced by CRU-NCEP atmospheric forcing data. The sensitivity of the model to input parameters such as the non-linearity in the calculation of soil hydraulic parameters and spatial resolution is examined in this Chapter 3. The top 5 cm of the soil referred to in this Thesis as the surface soil moisture (SSM) produced by the model is evaluated using a satellite product SSM in order to determine the ability of the model to simulate land surface processes in the study area.

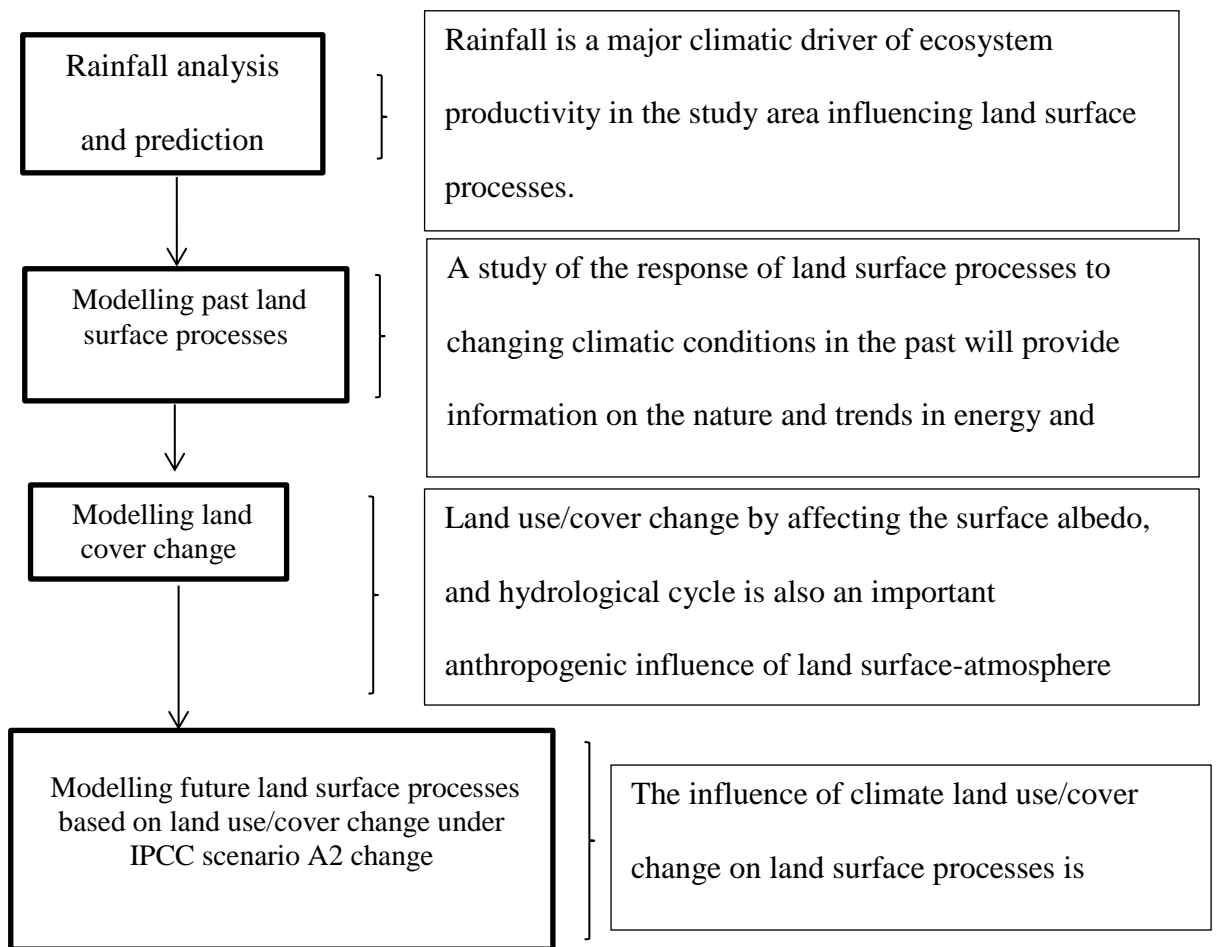


**Figure 1-7: A schematic of the thesis work outlining the 4 stages involved in accomplishing each of the 4 objectives and the relevance of each stage.**

Chapter 4 reflects on the importance of LUCC in the study area. There is an analysis of LUCC in the last 4 decades and an attempt is made to predict land cover for 2046 using a Cellular-Automata Markov Chain model based on previous trends in land cover change (LCC).

Finally, in Chapter 5 the significance of climate change and LUCC on future land surface processes is highlighted. Also in Chapter 5 an attempt is made to identify the degree of influence of LUCC and variability in atmospheric conditions on land surface conditions of energy, soil moisture, soil temperature, runoff and GPP. A

fractional land cover is derived from the projected land cover for 2046 described in Chapter 4 and is used as forcing data for one of two experiments using the JULES model. The first numerical experiment uses the IPCC climate change scenario A2 as atmospheric forcing data and present land cover fraction. While in the second experiment the IPCC A2 atmospheric forcing is used together with a projected fractional land cover for 2046. The outputs of the two experiments are compared in order to assess their level of differences.

## Chapter 2. **Spatial and Temporal variation of rainfall in North-eastern Nigeria 1980-2006**

### **2.1 Introduction**

Rainfall in North-eastern Nigeria is under the influence of the West African Monsoon (WAM). In the last 50 years there has been a decreasing trend in the amount of rainfall received in West Africa (Jury *et al.*, 2002) and large annual variations and severe droughts have been recorded (Anyamba and Tucker, 2005) in 1967-1973, and 1983-1987 (Amissar-Arthur and Jagtap 1999; ). These changes have a large impact on the region's agricultural output and economy where majority of the people depend on subsistence agriculture (Jalloh *et al.*, 2011). In the 1990s there was a sign of a recovery with higher annual averages compared to the 1961-1990 period but annual rainfall amounts were near or slightly above the long term mean for the century (Nicholson *et al.*, 1998; Ati *et al.*, 2009; Oguntunde *et al.*, 2011). Mortimore and Adam (1999) described the prevailing rainfall characteristics of the region as follows:

1. The amount and frequency of rainfall varies in space generally decreasing from Southwest to Northeast.
2. Variations in rainfall could be over a short distance.
3. Total annual rainfall may vary considerable from year to year with considerable impact on agricultural production.
4. Rainfall is un-evenly distributed within a single season

Several publications have looked at the rainfall trends of the region with several more attempting to explain the causes of these changes. Tarhule and Woo (1998) analysed rainfall characteristics recorded from 1931 to 1996 in 25 locations across Northern Nigeria for abrupt changes and trends using the Pettitt and the Mann-Kendall tests. Six of those stations were in the North-eastern region. The rainfall characteristics analysed include total annual rainfall, intensity, and number of rainy days, onset and cessation of the wet season. Results of their study indicate an abrupt change in the seasonal amount of rainfall and the number of rainy days between the years of 1964 to 1972 mainly caused by a reduction in the frequency of high intensity rainfall ( $\geq 25$ mm of rainfall per day) in the month of August and September. The fact that most of the reduction in rainfall was at the peak of the rainy season reduces the impact that this may have on agricultural production. Ati *et al.* (2009) analysed 50 years of rainfall data from 9 stations in Northern Nigeria where 2 of the stations are in the North-east. The study compared 5 year means with the long term mean and concluded that there was a significant increase in annual rainfall during the last decade of the study which is a sign of recovery. Amissar-Arthur and Jagtap (1999) identified a significant negative trend in yearly rainfall of four stations in the Northeast region of Nigeria over a 30 year period (1961-1990) with a gradual reduction in the amount of rainfall for all the months of the wet season. A similar pattern was obtained by Hess *et al.* (1995) after analysing daily rainfall of three stations in the semi-arid region of North-east Nigeria using the same period of rainfall records (1961-1990). Their findings indicate a consistent decrease in rainfall of 8mm per year. Most of the reduction is

in the months of August and September with an increase in the length of dry spells by 1.5 days as a result of the reduction. In terms of overall annual rainfall amounts the 1950s was the wettest period while the 1980s was the driest (Oguntunde *et al.*, 2011).

Several studies on the variability of rainfall in the region associate the causes to a combination of factors prevailing both within and outside the West African sub region which includes the movement of the ITCZ, the Easterly Air Jet (EAJ), El Niño Southern Oscillation (ENSO), Sea Surface Temperature (SST) anomaly, and the bio-geophysical feedback mechanism. The ITCZ is the region of convergence of the warm moist south westerly air jets from the Gulf of Guinea and the dry north easterly air jet from North Africa. There is a continuous displacement of this area northwards or southwards according to the movement of the angle of incidence of solar radiation and the location of high and low pressure belts created in response to this movement in the Gulf of Guinea and in North Africa. When a high pressure belt is established over the Gulf of Guinea the oceans provide the moisture for the south westerly winds providing rainfall for the West African sub region. Previous studies have obtained a strong correlation between the SST anomaly and precipitation over West Africa Sudano-Sahelian region (Jury *et al.*, 2002) while Lamb (1983) identified a corresponding shallow and much weaker monsoon during years of severe drought therefore concluding that the thickness and strength of the West African Monsoon (WAM) determines the precipitation regime of West African Sahel. The African Easterly Jet (AEJ) is known to be a source of tropical cyclone activity and may play a role in the distribution of

precipitation in the region (Cook, 1999). The impact of the El Niño Southern Oscillation (ENSO) events is very much obvious in East Africa because of the adjacent Indian Ocean although according to Jury *et al.* (2002) sea surface pressure in the Indian Ocean has an effect on the West African climate after a six month lag. ENSO events influence rainfall in the Sahel directly through the convergence over the continent of Africa anomalous Rossby Waves originating from the Indian Ocean in response to an El Niño event in the Pacific and Kelvin waves from the Atlantic Ocean subsequently intensifying large scale atmospheric subsidence over the Sahel and reducing rainfall (Rowell, 2001). In this study we analyse medium term (1980-2006) rainfall of North-east Nigeria for spatial and temporal changes while relating these changes to remote El Niño events.

### **2.1.1 Objectives**

- To examine the spatial and temporal changes in rainfall.
- To identify extreme periods of rainfall excess and deficit and to compare these with ENSO events.
- To predict monthly rainfall over a 24 month period using the ARIMA model.

## **2.2 Methods**

### **2.2.1 Data source**

Six hourly half degree rainfall data was obtained from Climate Research Unit-National Centre for Environmental Prediction (CRU-NCEP) six-hourly global climate data (N. Viovy pers. comm., [Nicolas.viovy@lsce.ipsl.fr](mailto:Nicolas.viovy@lsce.ipsl.fr)). The CRU-NCEP data set was produced by reanalysing and partly modelling daily climate records of the CRU obtained from meteorological observation stations across the globe since 1901. And SST anomalies in the tropical pacific from 1979 to 2006 data obtained from the Climate prediction centre (CPC) of the National Ocean and Atmospheric Administration (NOAA) web site.

### **2.2.2 Analysis technique**

Statistical analysis techniques used include the mean, percentage coefficient of variation, least squares regression, climate anomalies, standardized precipitation index (SPI), Pearson correlation, and Autoregressive integrated moving average (ARIMA).

First of all the rainfall data for the study area consisting of 16x17 grid box pixels was extracted from the CRUNCEP six hourly half degree global precipitation data set. The single time series of the data was derived by joining the yearly rainfall data from 1980 to 2006 firstly by producing a six hourly time series, then transforming the data into daily, monthly, and yearly time series. A record of the number of days with rainfall is also produced using the daily rainfall. 1 mm of precipitation was taken to be the minimum value for recording a rainy day

(Odekunle, 2006; Schmidli and Frei, 2005) and all daily records of less than 1 mm are regarded as insufficient and discarded. The percentage coefficient of variation is used to determine the level of temporal variation in the rainfall for each pixel using the equation below.

$$cv\% = \frac{\sigma}{\mu} \times 100 \quad \text{Eq. [2-1]}$$

where the percentage coefficient of variation is  $cv\%$ ,  $\sigma$  is the standard deviation, and  $\mu$  is the mean.

The standardized precipitation index was used to determine the periods with extreme rainfall conditions that are either very dry or extremely wet. SPI is used as a drought index and is generated from rainfall data only based on a time series indicating the lack or surplus of rainfall in given periods (Khan *et al.*, 2008; Kurnik *et al.*, 2011).

$$SPI_j = \frac{(x_{ij} - \mu_{im})}{\sigma} \quad \text{Eq. [2-2]}$$

where  $SPI_j$  is the standardised precipitation index calculated for each month,  $x_{ij}$  is the  $j^{\text{th}}$  monthly rainfall amount at point  $i$ .  $\mu_{im}$  is the long term mean at point  $i$  and  $\sigma$  is the standard deviation.

To determine the overall increasing or decreasing trend in the yearly rainfall a least squares regression line was plotted against the time series of yearly rainfall. The same process was also applied to a time series of rainfall in each of the individual months of the year during the wet season and some months that also receives a sizable amount of rainfall before and after the wet season. A monthly rainfall anomaly was obtained.

The ARIMA model is used to predict monthly rainfall over a 24 month period.

ARIMA is a linear stochastic model for time series analysis widely publicised by Box and Jenkins (1976). The ARIMA model is provided below Yurekli and Kurunc (2006):

$$\phi(B)\Phi(B^s)(w_i - \mu) = C + \theta(B)\theta(B^s)a_i \quad \text{Eq. [2-3]}$$

$$w_i = (1 - B)^d(1 - B^s)^D x_i \quad \text{Eq. [2-4]}$$

Where,

$a_i$ = white noise

$B$ = backward shift operator

$C$ =constant term

$d$ =order of the non-seasonal differencing operator

$D$ = order of the seasonal differencing operator

$s$ = seasonal length

$x_i$ = discrete time series value at time  $i$

$w_i$ = Stationary series formed by differencing the  $x_i$

$z_i$ = transformation of the  $x_i$  series

$\mu$ = mean level of the  $w_i$  series

$\phi(B)$ = non-seasonal AR operator of order  $p$

$\theta(B)$ = non-seasonal MA operator of order  $q$

$\Phi(B)$ = seasonal AR parameter of order  $P$

$\Theta(B)$ = seasonal MA parameter of order  $Q$

$w_i = z_i$  and either can be used depending on the non-stationarity of the time series

The ARIMA (p,d,q) model includes the AR (p), I (d) and MA (q) components and is normally fitted to a time series for better interpretation of the data or can be used to predict future points. The p,d, and q components are normally represented

by a non-negative integer. Part of the ARIMA model development includes identifying the p, d, and q components that best fit the time series, estimating points ahead and diagnostic check (Yurekli and Kurunc 2006):.

The level of deviation between the predicted and observed monthly rainfall is obtained using the root mean square error (RMSE).

### **2.2.3 Software**

Ferret NOAA/PMEL (Hankin *et al.*, 2007) and R (Venables *et al.*, 2013) were used for data analysis and visualisation of monthly rainfall amounts, number of days with rainfall in a month, rainfall anomalies, percentage coefficient of variance, and standard deviation are derived using Ferret NOAA. While, R was used for obtaining linear trends in the time series and the ARIMA model for predicting monthly rainfall over a 24 month period.

## **2.3 Results**

### **2.3.1 Spatial and temporal variation in rainfall**

The mean annual rainfall in the study area for 27 years is provided in Figure 2-1. Mean annual rainfall varies from 1800 mm in the far southern tip to less than 300 mm at the northern end of the area with a standard deviation of 130 mm to less than 40 mm (Figure 2-2). Rainfall amounts successively reduce northwards and with increasing latitude. However the isohyets are not parallel to the lines of latitude instead from latitude 10° north the lines run in a northwest to southeast

direction. Therefore rainfall decreases in space from the south-west to north-east. The level of variation in rainfall for each location is determined by calculating the percentage coefficient of variation (Figure 2-1). Values of the percentage coefficient of variation increases northwards with the increase distinctively marked by the 10° line of latitude. South of this line the percentage coefficient of variation ranges between 10% to less than 15%; north of this line the variation in rainfall rapidly increases with increase in latitude reaching 35% at the northern end of the study area.

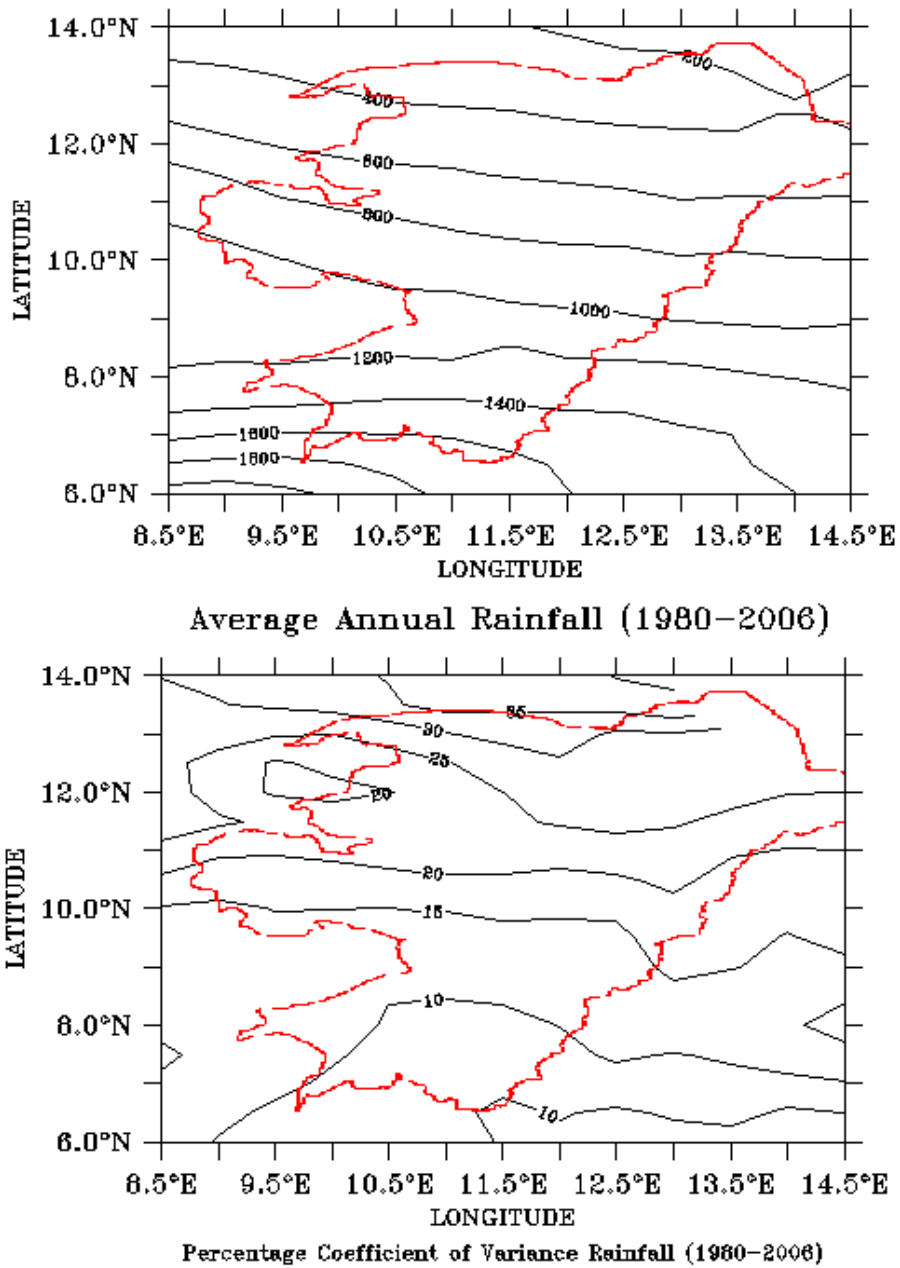


**Figure 2-1: The mean annual rainfall in mm for the study area (top) and Percentage coefficient of variation of rainfall (bottom) in North-eastern Nigeria 1980-2006 derived from the CRU-NCEP data**

\*Note: boundary line of the study area in red

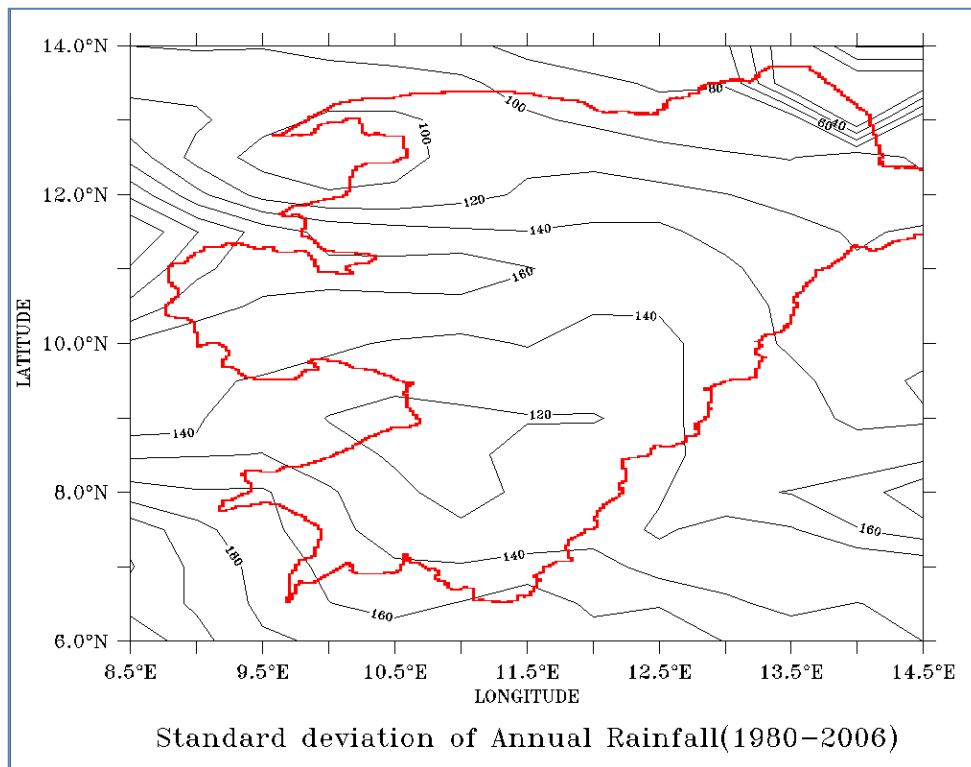


**Figure 2-2: Standard deviation of annual rainfall 1980-2006 in mm North-eastern Nigeria derived from CRU-NCEP data.**

\*Note: boundary line of the study area in red

The mean number of days with rainfall and percentage coefficient of variation is plotted in Figure 2-3. The average number of rainfall days reduces northward from over 220 days of rainfall in a year to less than 40 days. Large variation in the number of days with rainfall is also more evident north of the 10° line of latitude (10-50%). South of the line the percentage coefficient of variation is more uniform and lower than 10%.

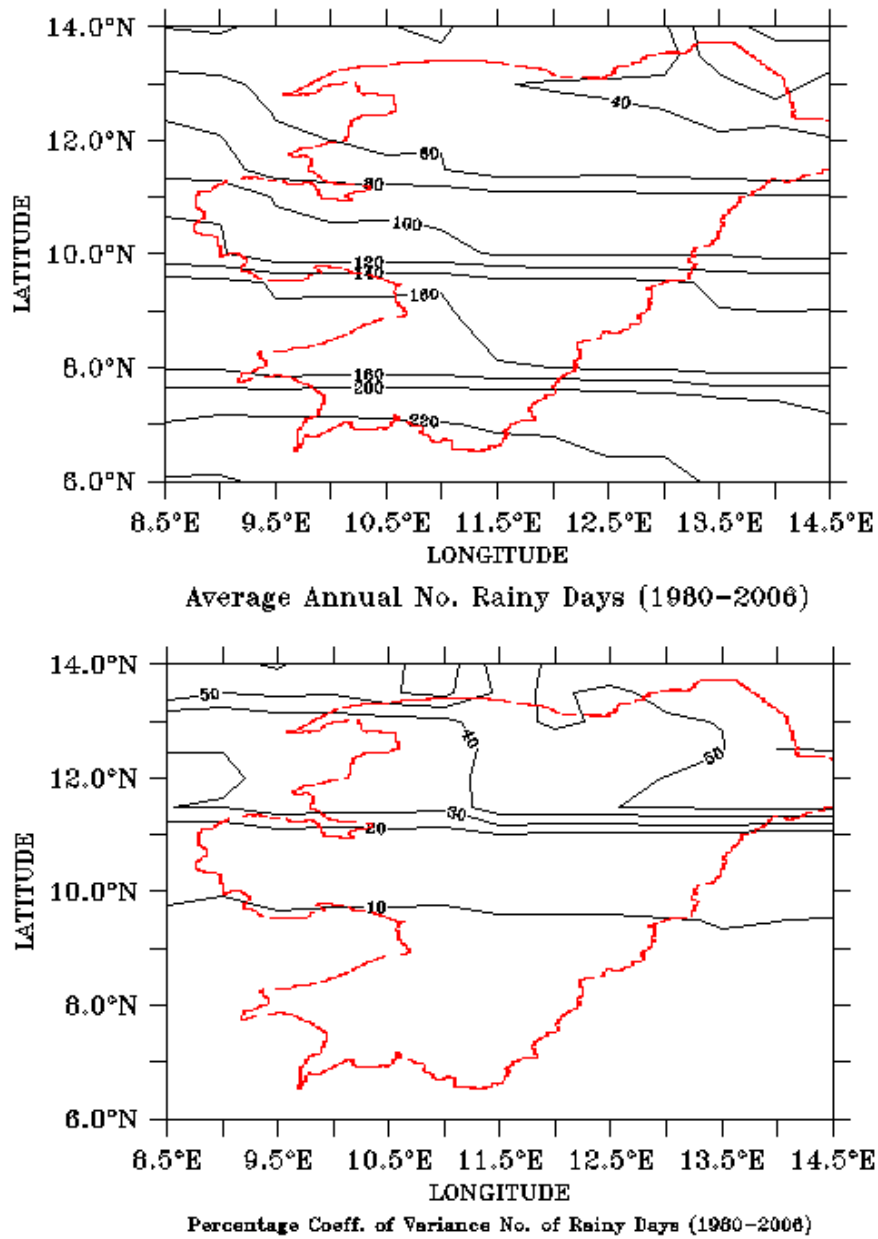


**Figure 2-3: The mean annual number of days with rainfall in the study area (top) and Percentage coefficient of variation (bottom) derived from CRU-NCEP data**

\*Note: boundary line of the study area in red

The 10° line of latitude is considered as the line demarcating the sub humid region of West Africa and the semi-arid region of transition (Lamb, 1983). Because of this and the clear differences north and south of the line identified in this study this line of latitude was used to divide the study area into two separate parts; the sub-humid south and the semi-arid north. Rainfall anomalies for these two parts are plotted in Figure 2-4. During the 1980s negative anomalies prevailed in both of the areas but by the 1990s rainfall conditions changed and positive anomalies were recorded for both regions. These conditions persist well into the new millennium in the semi-arid part. In the sub-humid region, positive anomalies prevailing in the 1990s are sandwiched by fewer negative anomalies. A least square regression indicates an increasing trend in the total amounts of annual rainfall (significance  $p < 0.05$ ) from 1980 to 2006 in both parts (Figure 2-5).

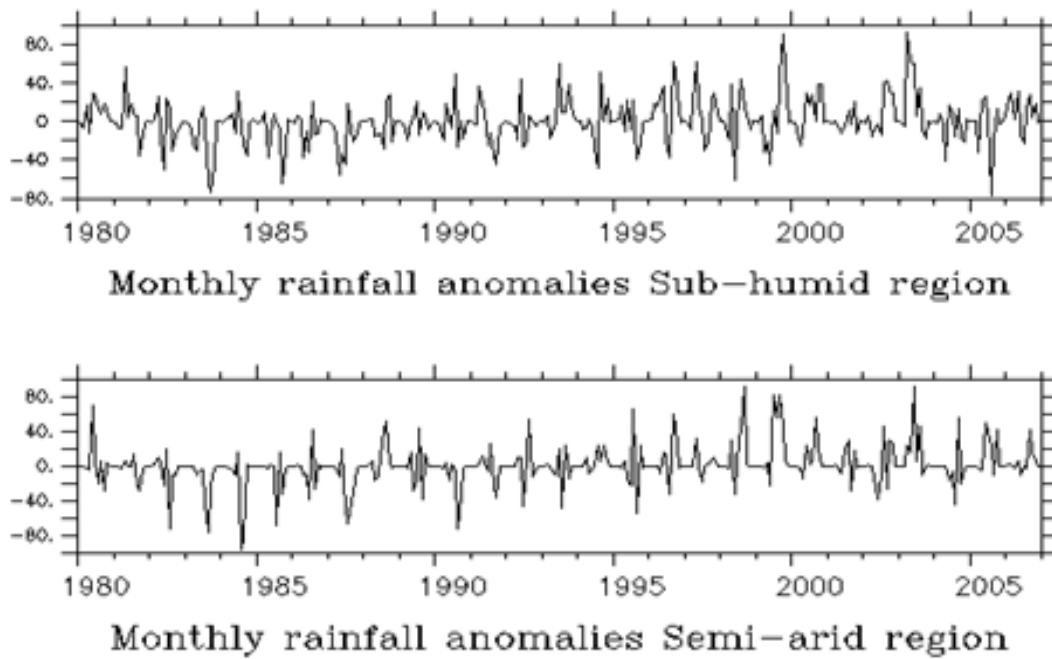


**Figure 2-4: Pixel averaged monthly rainfall anomalies in mm for the sub-humid (top) and semi-arid parts (bottom) of North-eastern Nigeria derived from CRU-NCEP data**

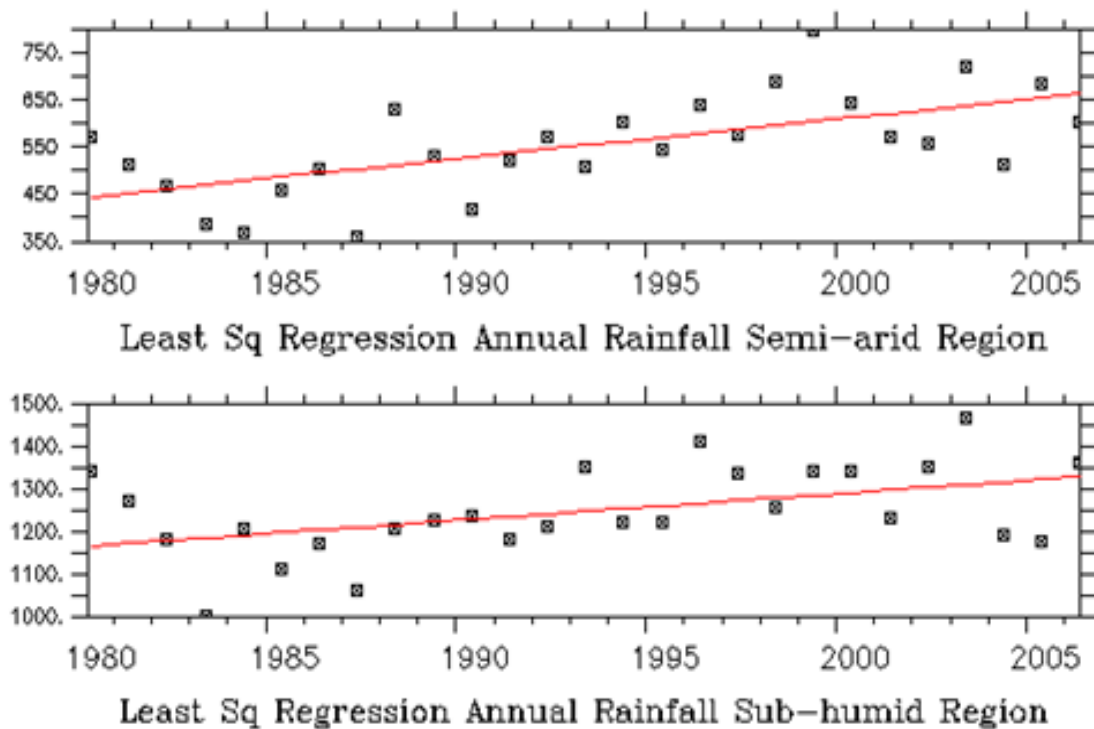


**Figure 2-5: Annual rainfall amounts in semi-arid part (top) and sub-humid part (bottom) of North-eastern Nigeria each plotted against a least square regression line (red) derived from CRU-NCEP data**

The study also focussed on the monthly rainfall pattern of the two parts of the study area with emphasis on the variation in the amounts of rainfall for each month and the number of days with rainfall for each month over the period under study. The length and duration of the wet season varies spatially and progressively decreases northwards for this reason the study selected 9 months each year in the sub-humid part and 8 months in the semi-arid part. The periods cover the length of the wet season and the onset and cessation of rainfall taking into account occasional rainfall during the dry season. There is a positive trend in rainfall in the

semi-arid part from the month of March to October but the increasing trend is only significant at 95% degree of confidence for the months of July to October (p-values of 0.03, 0.02, 0.003, and 0.03) (Figure 2-6). July, August and September are the wettest months and the most agriculturally productive in the semi-arid region (Table 2-1). Rainfall in the southern sub-humid region is characterised by an increasing trend in the months between February and May with no significant trend in the increase (Table 2-2). The month of June and July are marked by a decreasing trend but this is also not statistically significant with p-values of 0.50 and 0.81 (Figure 2-7). This trend changes in the month of August and continues until the month October. The positive trend for the month of August is significant at 95% level of confidence while for the month of September and October the significance increases to 99%.

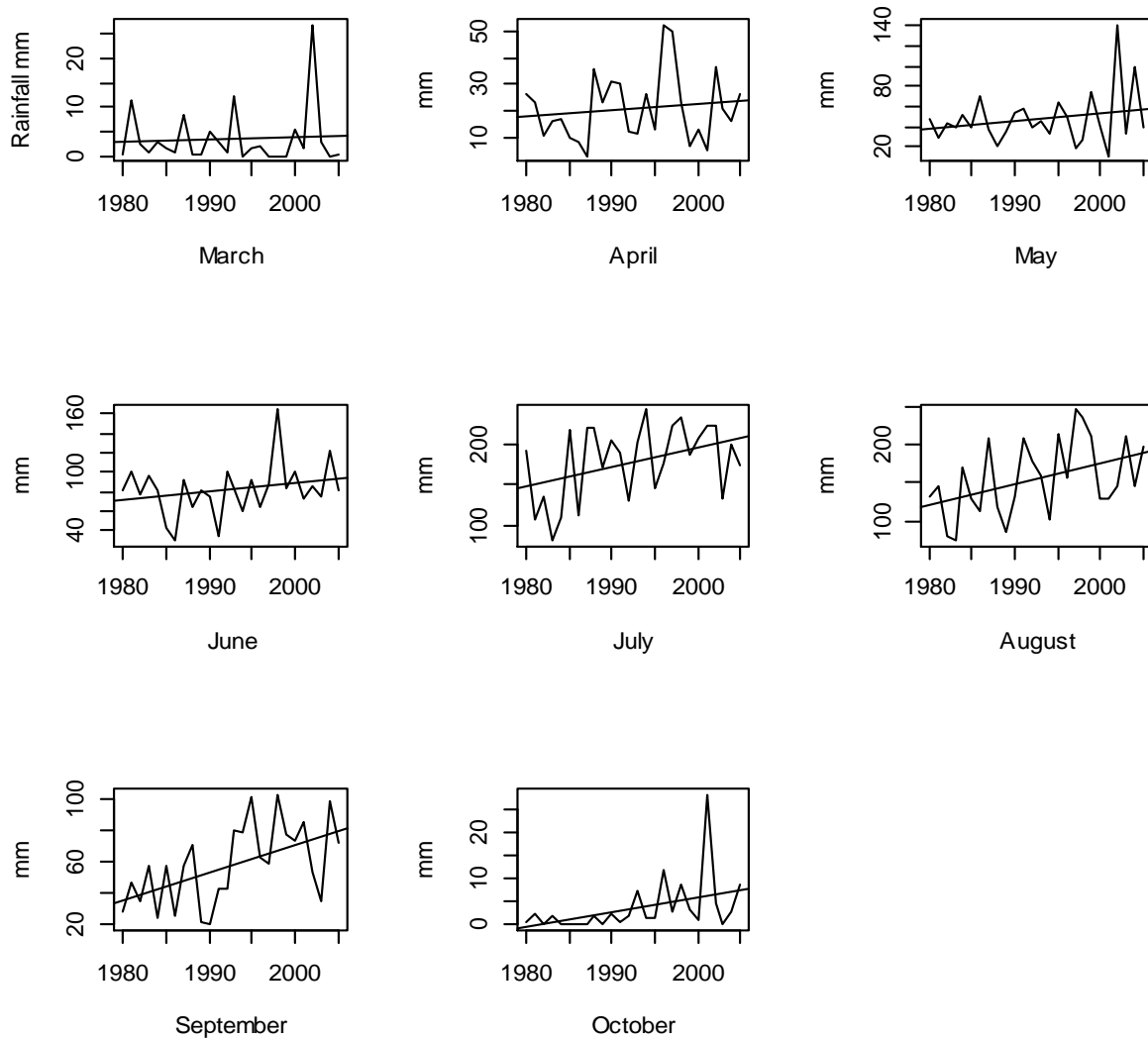


**Figure 2-6: Temporal variation of rainfall amounts for each month in the semi-arid part of North-eastern Nigeria plotted against a regression line**

**Table 2-1: Results of a linear regression of the amount of rainfall for each month in the semi-arid part of North-eastern Nigeria**

	<b>Mar</b>	<b>Apr</b>	<b>May</b>	<b>Jun</b>	<b>Jul</b>	<b>Aug</b>	<b>Sep</b>	<b>Oct</b>
<b>P-value</b>	0.74	0.48	0.24	0.20	0.03*	0.023*	3e-03*	0.03*
<b>F-stat</b>	0.12	0.51	1.46	1.72	5.1	5.91	11.08	5.64
<b>R<sup>2</sup></b>	5e-03	0.02	0.06	0.07	0.17	0.19	0.32	0.19
<b>Intercept</b>	-97.36	-438.6	-1550.9	-1641.2	-4614.1	-5337.2	-3461.5	-638.8
<b>slope</b>	0.05	0.23	0.80	0.86	2.41	2.76	1.77	0.32

\*p-values that are statistically significant at 95% confidence level

**Table 2-2: Results of a linear regression of monthly rainfall in the sub-humid part of North-eastern Nigeria**

	<b>Feb</b>	<b>Mar</b>	<b>Apr</b>	<b>May</b>	<b>Jun</b>	<b>Jul</b>	<b>Aug</b>	<b>Sep</b>	<b>Oct</b>
<b>P-value</b>	0.12	0.87	0.19	0.14	0.50	0.82	0.05**	6e-03**	7e-03**
<b>F-stat</b>	2.57	0.03	1.79	2.29	0.46	0.06	4.39	8.95	8.46
<b>R<sup>2</sup></b>	0.0978	1e-03	0.07	0.09	0.02	2e-03	0.15	0.27	0.26
<b>Intercept</b>	-684.32	-182.22	-2004.3	-1937	969.7	608.4	-2707.9	-4535.87	-2796.1
<b>slope</b>	0.35	0.11	1.06	1.05	-0.39	-0.18	1.49	2.36	1.43

(the asterisk \* represents the level of significance for  $p < 0.1$  having a single asterisk and  $p < 0.05$  having a double asterisk)

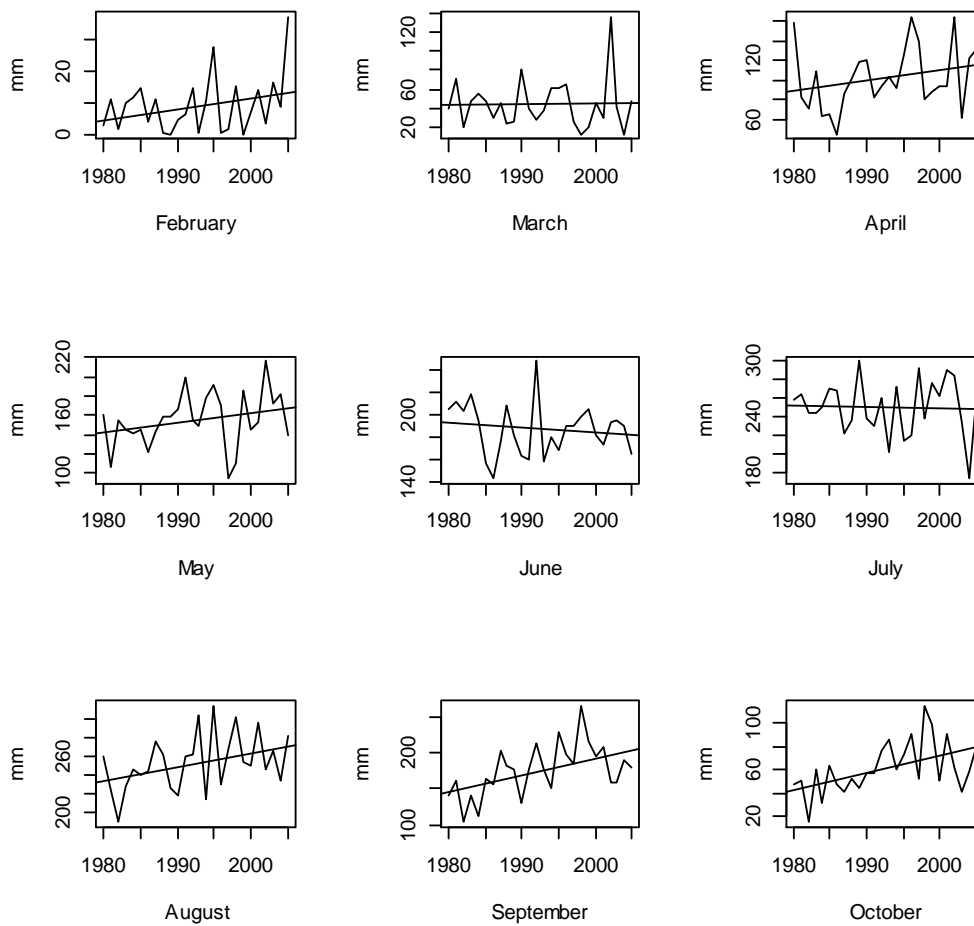


**Figure 2-7: Temporal variation of rainfall amounts (1980-2006) for each month in the sub-humid part of North-eastern Nigeria plotted against a regression line**

In the sub-humid part in the month of March, May and June there is a reduction in the number of days with rainfall (Figure 2-8). The decreasing trend is statistically significant at 95% for the month of May ( $p$ -value= 0.01) and at 90% for the month of March ( $p$ -value=0.06). All other months have experienced an increase in the number of rainy days which is statistically significant (Table 2.3) at 95% for the

month of August (p-value=0.06) and October (p-value=0.05), and 99% for the month of September (p-value=5.6e-05).

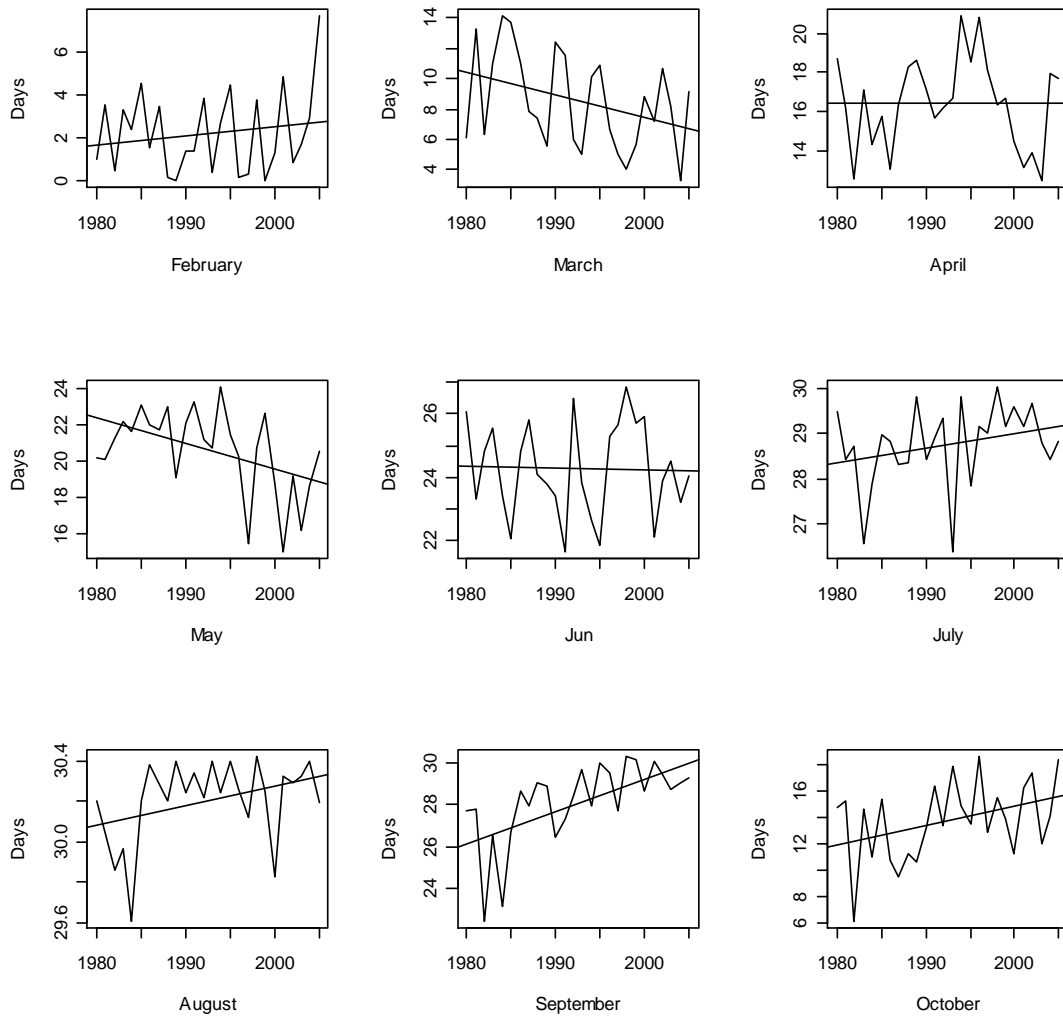


**Figure 2-8: Temporal variation in number of rainy days (1980-2006) for each month in the sub-humid part of North-eastern Nigeria plotted against a regression line.**

**Table 2-3: Results of a linear regression of the monthly number of rainy days in the sub-humid part of North-eastern Nigeria**

	<b>Feb</b>	<b>Mar</b>	<b>Apr</b>	<b>May</b>	<b>Jun</b>	<b>Jul</b>	<b>Aug</b>	<b>Sep</b>	<b>Oct</b>
<b>P-vaule</b>	0.4	0.06*	0.99	0.012*	0.89	0.16	0.06*	5e-05**	0.05**
<b>F-stat</b>	0.73	4.03	2.9e-06	7.3	0.02	2.13	4.02	15.8	4.41
<b>R<sup>2</sup></b>	0.03	0.15	1.2e-05	0.23	6.9e-05	0.08	0.19	0.4	0.16
<b>Intercept</b>	-80.12	304.8	18.5	300	34.1	-34.4	11.27	-277.1	-280.5
<b>slope</b>	0.04	-0.14	-1e-03	-0.14	-5e-03	0.0317	9e-03	0.15	0.145

(the asterisk \* represents the level of significance for  $p < 0.1$  having a single asterisk and  $p < 0.05$  having a double asterisk)

In the semi-arid part of the study area there is a decreasing trend (Figure 2-9) in the number of days with rainfall for the month of March (p-value=0.328) and June (p-value=0.85) with no statistical significance (Table 2-4). For the rest of the 6 month there is an increasing trend. However, only the month of August (p-value<0.05) and October (p-value<0.05) is significant at 95% significant level while September (p-value<0.01) has a significance level of 99%.

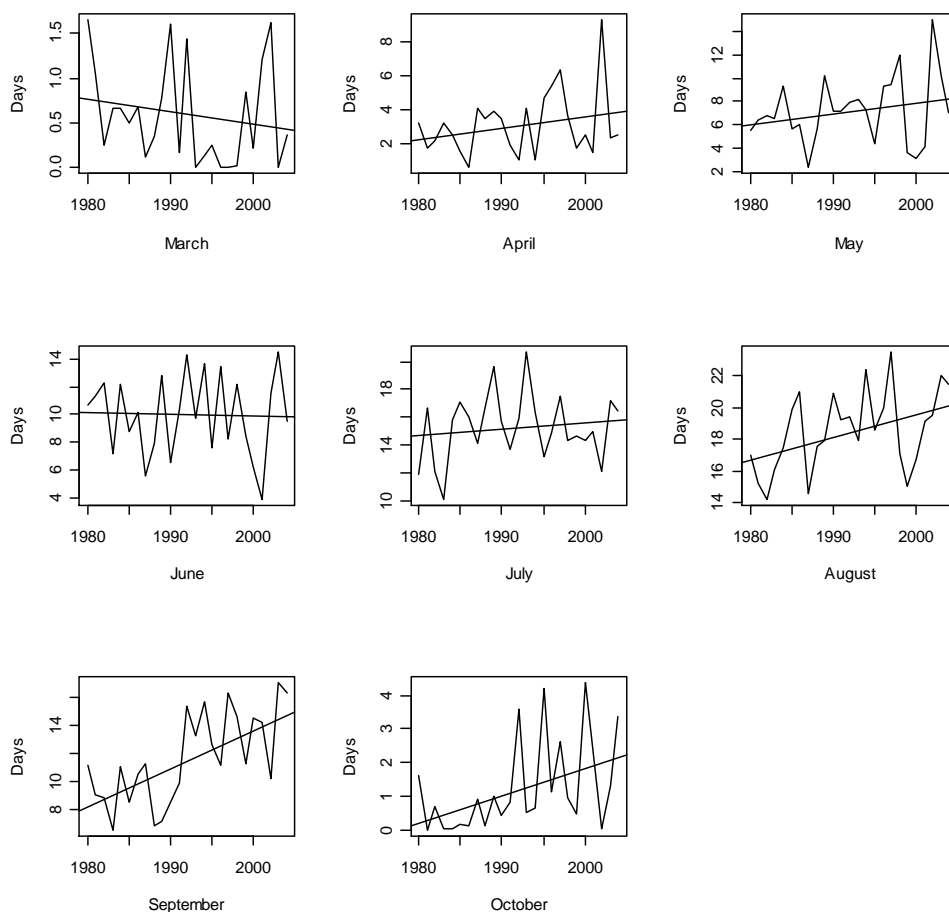


**Figure 2-9: Temporal variation number of rainy days (1980-2006) for each month in the semi-arid part of North-eastern Nigeria plotted against a regression line.**

**Table 2-4: Results of a linear regression of the monthly number of rainy days in the semi-arid part of North-eastern Nigeria**

	<b>Mar</b>	<b>Apr</b>	<b>May</b>	<b>Jun</b>	<b>Jul</b>	<b>Aug</b>	<b>Sep</b>	<b>Oct</b>
<b>P-vaule</b>	0.33	0.19	0.23	0.85	0.47	0.02*	1.8e-06**	0.01*
<b>F-stat</b>	0.99	1.83	1.51	0.04	0.54	6.09	19.82	6.83
<b>R<sup>2</sup></b>	0.04	0.07	0.06	1.6e-03	0.02	0.21	0.46	0.23
<b>Intercept</b>	28.94	-126.28	-171.38	38.78	-75.68	-268.79	-525	-161.5
<b>slope</b>	-0.01	0.07	0.09	-0.01	0.05	0.14	0.27	0.08

(the asterisk \* represents the level of significance for  $p < 0.1$  having a single asterisk and  $p < 0.05$  having a double asterisk)

### **2.3.2 Periods of moisture deficit, excess and the relationship with ENSO events**

The longitudinal averaged SPI of the study area is provided in Figure 2-10. In the years 1980-81 many parts of the study area have SPI index that are either moderately wet or near normal. In 1983 the SPI index was below -1.2 with areas between longitudes 6 to 7° north having an index of -2. All values ranging from -1.2 to -2 indicate moderately dry to extremely dry conditions. These negative values continued into 1984 and 1985 from latitude 9° to 14° lasting until the first quarter of 1985 between latitude 9 and 10° north. In 1987 a negative index was recorded across the latitudes with very low index of -1.6 to -1.8 recorded between latitude 12 to 14° north. Except for the southern tip of the study area (latitude 6-8° north) all other latitudes recorded a moderate index in 1988 ranging from 0.6 to 1.0 indicating near normal rainfall in that year and apart from a small area these conditions continued until 1995. SPI index values ranging from 1.5 to 1.1 were obtained between longitudes 6° to 9° north in 1996 signifying wet to moderately wet conditions. In 1999 there was a positive SPI index of 1.5 to 2.1 between latitude 10 to 14° north indicating wet conditions in those areas but in contrast a lower index of 0.1 to 1.0 is recorded south of the 10° degree latitude line. Between 2000 and 2006 the index ranged from -1 to 2 indicating moderate to wet rainfall conditions. Wet conditions were recorded between latitudes 8 to 13° north in 2003 and between longitudes 12 to 14° in 2005.

The study area was further divided into two sub-humid and semi-arid parts using the 10° line of latitude and the x and y coordinates for each part were averaged to

obtain a one dimensional time series. This was used to calculate the yearly SPI index for each part for the time period under study (Figure 2-11) and subsequently each year was classified (Table 2-5). In the Semi-arid region 1999 and 2004 were the very wet periods while in the sub-humid region 1996 and 2003 were the wettest. Moderately wet conditions were experienced in 1998 and 2006 in the Semi-arid region but 1993 and 2006 were recorded moderately wet in the sub-humid region. Most of the 1980s fall under near normal or dry conditions in both parts. The SPI index for the two parts were compared with the tropical pacific SST anomalies (Figure 2-11) and all of the drought years except 1984 fall under periods of El Niño events (1982/83, 1986/87). However, not all El Niño events are accompanied by dry periods in the region. 1997/98 for instance was an El Niño period but rainfall conditions were near normal in 1997 in both parts and moderately wet in the semi-arid part. Moreover, during the 2002/03 El Niño years the sub-humid part of the study area experienced very wet conditions. The Pearson Product Moment Correlation was used to assess the association between the SPI index for each part and the tropical pacific SST temperature anomalies for the same period. Correlation coefficients of -0.04 was obtained for the Semi-arid part and a value of -9.0e-03 was obtained for the sub-humid part.

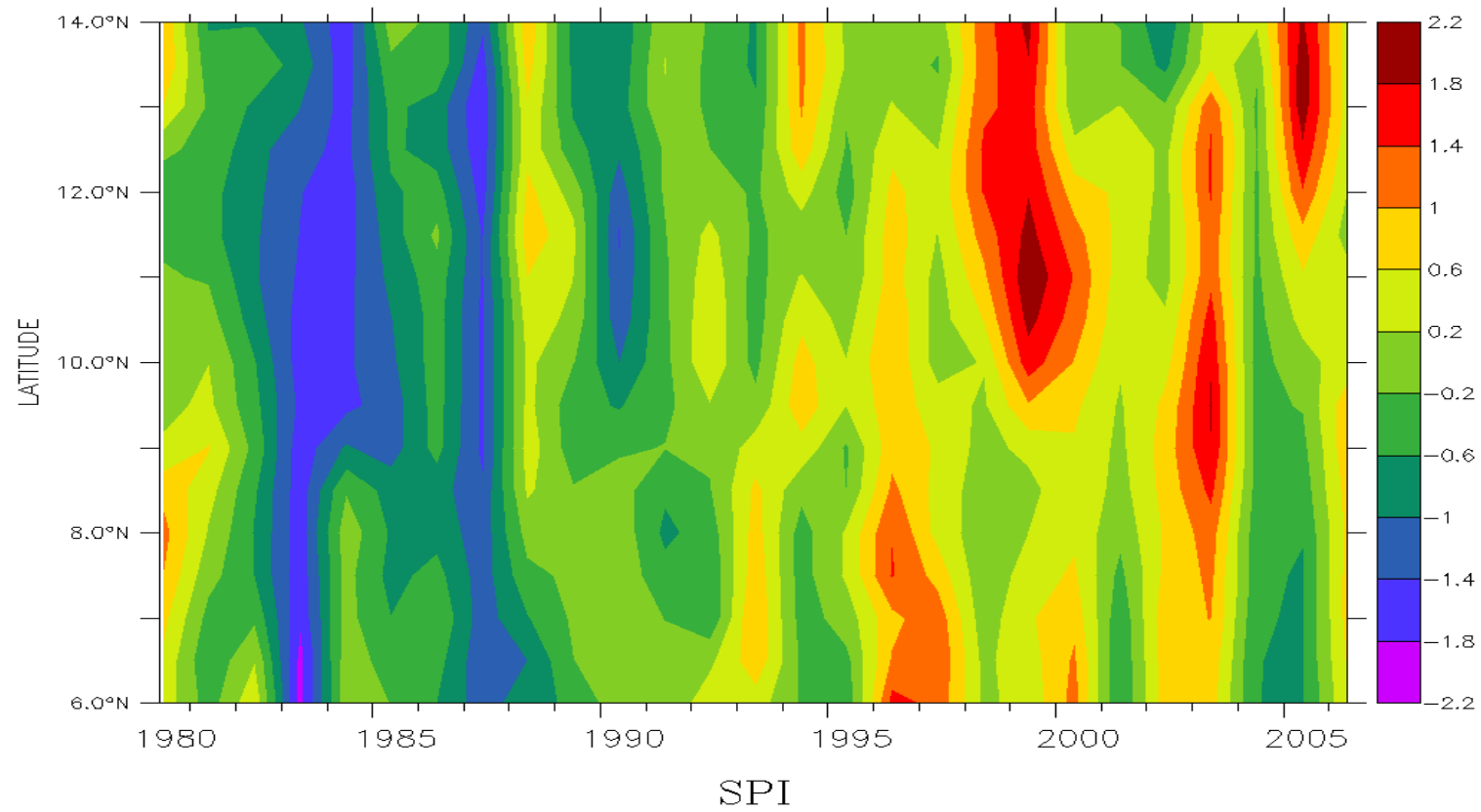


**Figure 2-10: Hovmuller Diagram; Longitudinal averaged SPI of the study area 1980-2006**

\* the colour bar represents the SPI index

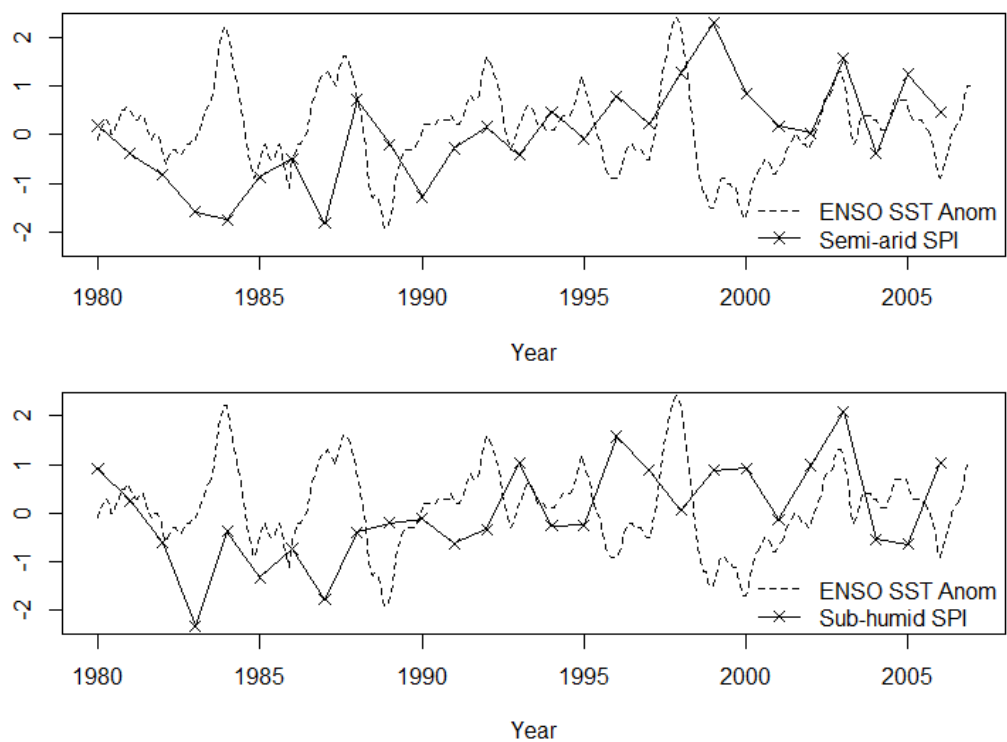


**Figure 2-11: SPI of annual rainfall 1980-2006 plotted against ENSO SST anomaly in the Tropical Pacific, semi-arid (top) and sub-humid (bottom) parts of North-eastern Nigeria**

**Table 2-5: SPI Index and the yearly moisture conditions of the study area**

	<b>Very Wet (SPI≥1.5)</b>	<b>Mod wet (1.0≥SPI≤1.49)</b>	<b>Near normal (-0.99≥SPI≤0.99)</b>	<b>Mod dry (-1.5≥SPI≤-1.0)</b>	<b>Severely dry -1.99≥SPI≤-1.49</b>	<b>Extremely dry SPI≤-2.0</b>
<b>Semi-Arid</b>	1999 2004	1998 2006	1980-1982, 1985-1986 1988-1989, 1991-1997 2000-2002, 2004,2006	1990	1983 1984 1987	
<b>Sub-humid</b>	1996 2003	1993 2006	1980-1982, 1984, 1986 1988-1992,1994-1995 1997-2002, 2004-2005	1985	1987	1983

### **2.3.3 Rainfall Prediction using ARIMA**

An attempt was made to predict the monthly rainfall of the study area over a two year period between 2005 and 2006 using ARIMA based on 25 years monthly rainfall data (1980-2004) for the sub-humid and semi-arid parts of North-eastern Nigeria (Figure 2-12). The ARIMA (1, 1, 0) Box Jenkins method was used in this respect. Results of a correlation between the predicted and observed rainfall gave values of 0.96 and 0.94 for the semi-arid and sub-humid regions respectively. To explore the strength of the relationship, results of a linear regression between the 24 months prediction and 24 months observation yielded an adjusted R-squared value of 0.91 ( $p < 0.01$ ) for the semi-arid part and 0.88 ( $p < 0.01$ ) for the sub-humid region. A root mean square error (RMSE) between the observed and predicted monthly rainfall is 31.73 mm in the sub-humid part and 20.11 mm in the semi-arid part.

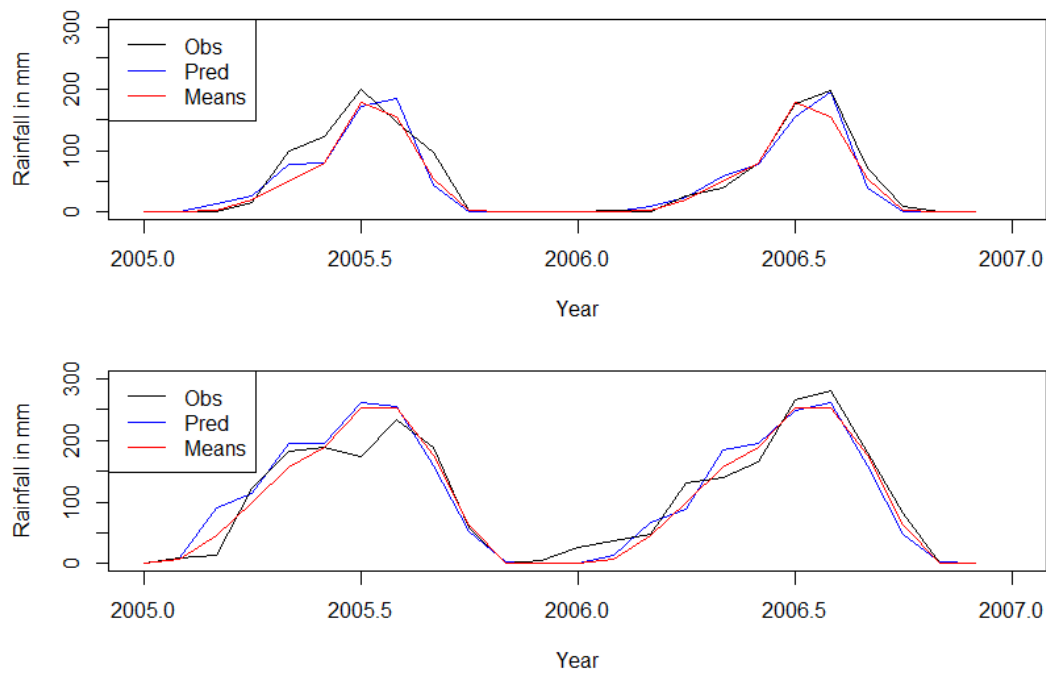


**Figure 2-12: Predicted monthly rainfall using the ARIMA model plotted against observation data for the semi-arid (top) and sub-humid (bottom) North-east Nigeria**

The study further tests the performance of the ARIMA model in order to clarify whether the predictions are better than a repetition of the long term mean monthly rainfall of the 25 years (1980-2004) data used for making the prediction. Figure 2-12 shows that the prediction using the ARIMA model is not the same as the long term mean. A RMSE of 19.25 mm of rainfall between the long term monthly rainfall means and the 24 month rainfall observation in the semi-arid part of the study area was slightly lower than the RMSE of 20.11 mm of rainfall obtained between the 24 month rainfall prediction and 24 month observation data. Similarly, a RMSE of 24.19 mm of rainfall between the long term monthly

rainfall means and the 24 month rainfall observation in the sub-humid part of the study area was lower than the RMSE of 31.73 mm of rainfall obtained between the 24 month rainfall prediction and 24 month observation data.

However, differences between the 25 years (1980-2000) long term mean and the 24 months prediction were tested using the Student's t-test and Kolmogorov-Smirnov test to establish if their differences were statistically significant. But the output of the two statistical tools did not yield any statistical significance. And neither was there any significant difference between the 24 months observation and the 25 years long term monthly means when the two statistical tools were used to test for their differences.

## **2.4 Discussion**

Terrestrial productivity in the Savanna region of Africa is a function of soil type, nutrients, interference from animals and, mostly importantly, the availability of moisture (Sankaran *et al.*, 2005). In West Africa the dominance of the West African Monsoon during the summer determines the availability of moisture through heavy torrential rainfall, mostly initiated by convection currents.

However, since the 1960s the region has been experiencing increased rainfall variability and droughts with an assumed recovery during the 1990<sup>s</sup>. In this Chapter the study analysed this recovery using monthly rainfall amounts and the number of days with rainfall from 1980 to 2006. This monthly data set is also used to predict monthly rainfall for a 24 months period between January 2005 and

December 2006 in advance using the ARIMA Model. Observation data for the same period (2005-2006) was used to validate the model.

#### **2.4.1 Trends in Rainfall 1980-2006 and relationship with ENSO events**

Results from the mean, standard deviation and percentage coefficient of variation of rainfall amounts and the number of rainy days in the study area shows that the two variables vary over space and time (Figure 2-1 and 2-2). Similar to the assertion made by Mortimore and Adam (1999) rainfall generally decreases in space from the south-west and north-east. The mean annual rainfall and number of days with rainfall also decreases northwards with increasing temporal variability. In a similar study Oguntude *et al.* (2011) identified that the coefficient of variation for rainfall increases northwards in Nigeria. Variation in rainfall variables is marked by the 10° line of latitude which has been identified by other studies in the region as the borderline between the sub-humid north and the semi-arid zone of transition (Lamb, 1983). This is an indication that the rainfall regime in the semi-arid areas is subject to fluctuation and wide variability over time.

Linear regressions of rainfall amounts in each month of the year calculated for 9 months in the sub-humid part (Figure 2-6) and 8 months in the semi-arid part (Figure 2-7) of the study area indicate an increasing trend for most of the month except for the month of June and July in the sub-humid part (Table 2-2).

However, the reduction in rainfall in these two months is not statistically significant since the 1980s the area has been recovering from periods of drought. This result may signify that there is no significant recovery in the two months following the onset of the rainy season coupled with the decreasing trend in the

number of rainy days in May and June in the area, this may provide an explanation for the dry spells experienced at the onset of the wet season which can be catastrophic for rainfed agricultural production in the area. In areas of the same latitude across Nigeria planting of crops commences between the beginning and the end of May (Odekunle, 2006) the following days after planting are very significant for crop germination and growth. Prolonged dry periods or dry spells may lead to crop failure. However in the semi-arid part there is an increasing trend in both the number of days with rainfall and the rainfall amount in most months. Most importantly, the increasing trend in the amount of rainfall is statistically significant for the months between July and September. These months are the productive periods for rain fed agriculture in the area (Odekunle, 2006; Hess, 1995). Generally, the results show an increasing trend in monthly rainfall however, statistically significant increases is confined to a fewer months at the later stages of the wet season (between August and September). In a previous study by Tarhule and Woo (1998) reductions of rainfall for 55 years (1931-1996) in the region was in the months of August and September. A similar finding was made by Hess *et al.* (1995) after analysing 30 year (1961-1990) rainfall records from some meteorological stations in North-eastern Nigeria. Also having certain significance is the increasing trend during the dry season such as the statistically significant increase in the number of rainy days and rainfall in the month of October throughout the study area. This may indicate a slight shift in the wet season which may not be productive to rainfed agriculture in the short term but

may be significant to the vegetation in the region that can withstand short term dry periods and will contribute to prolonged greening.

The SPI index was used in this study to determine the periods of moisture stress and availability in the study area over a 27 year period (1980-2006). Results from the SPI analysis are provided in Figures 2-15, 2-16 and Table 2-1. They show how the SPI index varies with time and latitude. Similar to other studies (Nicholson *et al.*, 1998; Oguntude *et al.*, 2011; Amissar-Arthur and Jagtap 1999), SPI index shows the 1980s as predominantly dry in the study area. Based on the SPI, droughts of the 1990s were accompanied by moderate and wet periods in the 1990s as reported by (Nicholson *et al.*, 1998). However, there is variation between the Semi-arid and Sub-humid parts of the study area in terms of wet years. For instance, in the 1990s the wettest years in the sub-humid were 1993 and 1996 in the semi-arid part and 1998 and 1999 in the sub-humid part. Also, in the following decade 2003 was the wettest year in sub-humid parts and 2004 was the wettest year in the semi-arid part of North-eastern Nigeria. The SPI result in this chapter is an indication of the spatial and temporal variability of rainfall in the study area described by Mortimore and Adam (1999) stating that such variation in rainfall could be over short distances. Furthermore, Oguntunde *et al.* (2011) identified three cycles of rainfall variability in Nigeria over a 100 years period (1901-2001). Their study identified short (5-7 years), medium (10-15 years) and long (30 years) term cycles in rainfall variability attributing the causes of these cycles to the influence of ENSO, solar variability and Atlantic multi-decadal sea surface temperature anomalies.

There was no significant correlation between SPI index of the study area and remote El Niño events. However the driest years in the region do coincide with El Niño years or a year following an El Niño event. This is similar to the affirmation made by Nicholson *et al.* (1998) that the 1997/1998 El Niño did not have any affirmative impact on the rainfall regime of West Africa. Instead, as they predicted, 1998 was a moderately wet year in the eastern regions of semi-arid West Africa. Other El Niño years 1991/1992 El Niño and 2002/2003 were near normal rainfall years in both parts of the study area, except 2003 which was a very wet year in the sub-humid part.

#### **2.4.2 Predicting Rainfall in the study area**

The study used the ARIMA model to predict 24 month rainfall (January 2005 to December 2006). The strength of the relationship between the predicted and observed rainfall was tested using the Pearson's product moment correlation coefficient and a linear regression model. A correlation of 0.95 (Adjusted R-squared=0.89,  $p<0.01$ ) and 0.98 (Adjusted R-squared=0.95,  $p<0.01$ ) between the observed and predicted rainfall in the semi-arid and sub-humid respectively, suggests a strong relationship and the strength of the prediction. Furthermore a RMSE of 31.73 mm (sub-humid) and 20.11 mm (semi-arid) of monthly rainfall between the 24 months prediction and the 24 months observation is within a reasonable margin of error since in the sub-humid part the month with the least rainfall during the wet season (May-October) during the 24 months rainfall observation (January 2005- December 2006) received 59.2 mm of rainfall. While, in the semi-arid part the month with the least rainfall in the wet season (June-

September) during the 24 months of rainfall observation received 71.1 mm of rainfall.

The differences shown in Figure 2-12 between the 24 months prediction, the long term 25 years (1980-2006) rainfall monthly means (January-December) and the 24 months rainfall observation was an indication that the model is not repeating the long means of the rainfall observation used in the prediction. However, the lower RMSE obtained between the long term monthly means and the 24 months observation compared to the RMSE between the long term monthly means and the 24 months prediction raises some uncertainties on the ARIMA model predictions. Despite these uncertainties the strength of the relationships between the observed and predicted rainfall in both parts of the study area suggests that the model can satisfactorily predict monthly rainfall over a short time period.

## **2.5 Summary**

In view of the changing rainfall conditions in North-east Nigeria the study examined the spatial and temporal variation of rainfall in the region from 1980 to 2006 having set three objectives for achieving this aim. These objectives were to examine the spatial and temporal changes in rainfall, identify and compare periods of excess rainfall and deficits with remote ENSO events, and predict monthly rainfall over a 24 months period. Results show that the mean value and standard deviation of the two rainfall indices of monthly rainfall and number of rainy days in a month reduces in a south-west to north-east direction while the percentage coefficient of variation increases northwards. The 10° line of latitude is identified as the demarcation between a moderate variation in rainfall conditions south of

the line and an extreme variation north of the line. Results of a least squares regression of annual rainfall amounts indicate an increasing trend in the area of study during the period 1980-2006. These findings prompted a further study on the monthly time series data with the aim of identifying the trends associated with the increase. Significant increase in the amount of monthly rainfall in the region is mostly between the months of August and October in the sub-humid (August has  $p\text{-value} < 0.05$ , September has a  $p\text{-value} < 0.01$ , and October has  $p\text{-value} < 0.01$ ) and the semi-arid part (August has  $p\text{-value} < 0.05$ , September has a  $p\text{-value} < 0.01$ , and October has  $p\text{-value} < 0.05$ ). There is also a significant increasing trend in the month of July ( $p\text{-value} < 0.05$ ) in the semi-arid part giving an indication of favourable rain fed agriculture in that part of the study area. Also, there is a decreasing trend in the monthly rainfall amounts in the months of June and July in the sub-humid part of the study area but with no statistical significance. There is an increasing trend in the monthly number of rainfall days in the months between July and October in the region but the increase is only statistically significant for the months of August, September, and October in the sub-humid part ( $p\text{-value} < 0.1$ ,  $p\text{-value} < 0.01$  and  $p\text{-value} < 0.05$ ) and in the semi-arid part ( $p\text{-value} < 0.05$ ,  $p\text{-value} < 0.01$  and  $p\text{-value} < 0.05$ ). A decreasing trend in the months between March and June in the sub-humid region is significant for the months between March (at 90% significance level with a  $p < 0.1$ ) and May ( $p\text{-value} < 0.05$ ). Number of days with rainfall for the month of June in the semi-arid part has a decreasing trend but with no statistical significance.

In determining the period of moisture availability and stress the study produced a longitudinal averaged and annual SPI of the study area. Results of the SPI show that droughts occurring in the region occur almost simultaneously but with slight variations both in time and space. The droughts of the 1980s started in the sub-humid part in 1983 and reached the northern semi-arid part later in 1984. The area most widely affected is in the central part of the study area where the severe drought lasted until the first quarter of 1985. Generally dry conditions prevailed for most of the decade with a return of severe droughts in 1987. It is only in 1988 that rainfall conditions changed to near normal and this continued into the 1990s. At least two years in the 1990s were either very wet or moderately wet in the sub-humid (1996 and 1993) and in the semi-arid (1999 and 1998) parts. This signals the end of the drought period and moderate to wet conditions continued well into the new millennium with 2004 and 2003 being the very wet years in the sub-humid and semi-arid parts. 2006 was a moderately wet year in all areas of the region. The study attempted to identify the relationship between rainfall conditions and remote El Niño events and therefore compared years of drought with El Niño years. All drought years except 1984 coincided with an El Niño year but not all El Niño events were accompanied by drought in the region. The yearly SPI was correlated with SST anomalies in the Tropical Pacific (the Niño 3.4 sector, Latitudes 5° North-5° South, Longitudes 120°-170° West) in order to determine the relationship between rainfall and remote El Niño events but a negatively weak correlation was obtained for both parts of the study area ( sub-humid  $r=-9.0e-03$ , semi-arid  $r=-0.04$ ). El Niño years of 2002/2003 and 2004/2005

corresponded with very wet years in the sub-humid part (2003) and in the semi-arid part (2004).

Finally, the study used an ARIMA model to predict monthly rainfall over a 24 month period (February 2004-December 2006) separately in the semi-arid and sub-humid parts of the study area. A correlation of 0.96 (Adjusted R-squared=0.91,  $p<0.01$ ) was obtained for the semi-arid part and 0.94 (Adjusted R-squared=0.88,  $p<0.01$ ) was obtained for the southern sub-humid part. The RMSE between the observed and predicted monthly rainfall was 31.73 mm of monthly rainfall in the sub-humid part of the study area and 20.11 mm in the semi-arid region. Similarity between the values of monthly rainfall predicted by the model and the monthly means of the 25 year monthly observation varies and the differences increases in the wet months while diminishing during dry months when there is no rainfall.

## **2.6 Acknowledgement**

The author is grateful and wish to acknowledge the use of CRUNCEP data received from N. Viovy pers. comm., [Nicolas.viovy@lsce.ipsl.fr](mailto:Nicolas.viovy@lsce.ipsl.fr) and the SST anomalies in the tropical pacific from the climate prediction centre (CPC): [http://www.cpc.ncep.noaa.gov/products/analysis\\_monitoring/ensostuff/ensoyears.shtml](http://www.cpc.ncep.noaa.gov/products/analysis_monitoring/ensostuff/ensoyears.shtml)

**Chapter 3. Modelling land surface processes in North-eastern Region of Nigeria from 1980-2000 using the UK met office land surface energy exchange scheme JULES**

**3.1 Introduction**

The aim of this chapter is to simulate past land surface conditions of soil moisture and energy flux in the study area from 1980-2000. An understanding of previous surface conditions is important for this study in achieving some of its objectives (listed below) and will form the basis for further modelling. Land surface conditions represent the lower boundary conditions in global circulation models (GCMs) and are known to influence atmospheric conditions. Moisture and solar energy from the atmosphere on reaching the land surface can be released back into the atmosphere in the form of sensible and latent heat flux. These fluxes in moisture and energy have an effect on the lower atmosphere. Studies using GCMs are mainly focussed in improving the representation of the surface boundary conditions. Soil moisture is an important variable in this aspect and is responsible for surface hydrology, vegetation growth through the available water in the root zone, and the partitioning of surface energy fluxes into latent and sensible heat. Soil moisture content is important in ecosystem productivity through direct effects on plant metabolism and enhancing soil microbe activity (Flanagan and Johnson, 2005). This is more important in the monsoon conditions prevailing over West

Africa where moisture availability is greatly dependent on the seasonal rainfall (Schüttemeyer, 2005). Several methods are used in measuring *in situ* soil moisture but these methods are mostly expensive and time consuming (Brocca *et al.*, 2010; Li *et al.*, 2007; Tietje and Hennings, 1996). This problem has inhibited the availability of data in many parts of the world especially in developing countries. This study uses a standalone version of the Joint UK Land Environment Simulator (JULES) version 3.0 to study past surface conditions. The model is used to conduct five experiments to test the model's sensitivity to scale and non-linearity in the calculation of soil input data. Results from the model are evaluated using the European remote sensing satellite (ERS) surface soil moisture data. A description of land surface models especially the type used for the study, the satellite SSM product and retrieval method and the study area is presented in the following part of this section. The remaining sections provide a description of the methodology used for the study, results, discussion, and final summary.

This chapter attempts to accomplish the following objectives:

1. Study the effect of scale and non-linearity in the calculation of soil hydraulic parameters on the heterogeneity of some model output.
2. Evaluate model performance with satellite observation of soil moisture.
3. Examine changes in land-surface conditions 1980-2000.

The research intended to answer the following questions from this chapter:

- Can we increase heterogeneity in model output of surface soil moisture, soil temperature and surface runoff by increasing variability in soil data input?
- Have there been any significant changes in the land surface fluxes of latent and sensible heat energy over the 21 year period (1980-2000)?
- What is the strength of the relationship between precipitation and soil moisture in the study area?
- What are the trends in carbon fluxes in the study area over the 21 year period (1980-2000)?
- Is there a significant relationship between modelled and ERS satellite soil moisture product over North-east Nigeria?

### **3.1.1 Land-atmosphere interaction**

The thin envelope of mostly gasses making up the atmosphere has a strong influence on the earth surface. Most of the energy from the sun passes through the atmosphere where it is moderated before reaching the earth's surface. Part of this energy is either reflected, transmitted or absorbed (Karl and Trenberth, 2003). The atmosphere not only serves as a medium by which solar radiation is transmitted onto the earth's surface but also provides a direct influence through the changing atmospheric conditions such as temperature and precipitation. The energy and momentum received by the earth's surface is represented by three fundamental equations as presented by Pitman (2003). Two of these represent the net surface radiation budget and the third represents the surface water budget

$$Rn = S \downarrow (1 - \alpha) + L \downarrow - L \uparrow \quad \text{Eq. [3-1]}$$

Where,  $Rn$  is the net surface radiation,  $S \downarrow$  represents the total short wave radiation reaching the surface, part of which is reflected back into the atmosphere depending on the reflectance (albedo) of the earth surface  $\alpha$ ,  $L \downarrow$  is long wave radiation received and  $L \uparrow$  is long wave radiation emitted back into the atmosphere.

Part of the energy received warms up the surface and is transmitted back to the atmosphere as sensible heat and latent heat. The remaining energy is absorbed by the surface or used by plants in the process of photosynthesis. This is described by the equation below (Ellis and Mellor, 1995).

$$Rn = SH + LH + G \quad \text{Eq. [3-2]}$$

where  $SH$  is the sensible heat flux,  $LH$  is the latent heat flux and  $G$  is the energy absorbed by the surface (including the soil and vegetation).

Precipitation in whatever form either rainfall or snow is a major atmospheric phenomenon influencing the surface water balance. During and after a rainfall or snow melt runoff, infiltration and evapotranspiration takes place. The water balance is represented by the following equation (Pitman, 2003).

$$P = E + R_{\text{drain}} + R_{\text{surf}} + \Delta S \quad \text{Eq. [3-3]}$$

where  $P$  is the precipitation,  $E$  evapotranspiration,  $R_{\text{drain}}$  is the slow component of a runoff,  $R_{\text{surf}}$  is the fast component of a runoff, and  $\Delta S$  is the change in soil moisture storage.

The interrelationship between land surface properties of soil moisture, vegetation, and land cover on atmospheric conditions through their influences on surface albedo, and energy fluxes and aerosols on the boundary layer and the atmospheric radiation budget at diurnal, seasonal and multi-decadal time scales is summarised in figure 3-1 based on Betts *et al.* (1996) and Betts and Silvia Dias (2010).

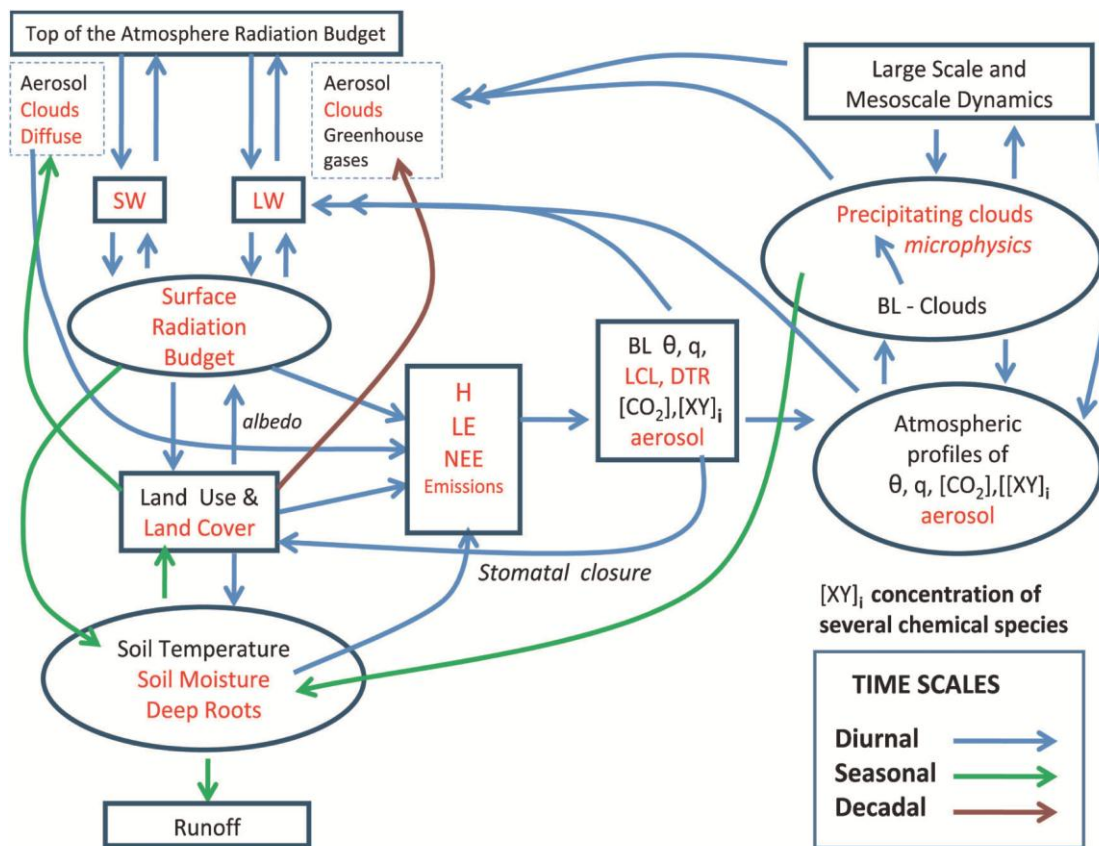


**Figure 3-1: Diagrammatical representation of some important processes in the land-atmosphere interactions at varying time scales (Betts *et al.*, 1996; Betts and Silva Dias, 2010).**

\*Where SRB is the surface radiation budget, BL is the boundary layer, SH is the sensible heat flux, and LH is the latent heat flux.

In West Africa climatic conditions are controlled by a number of factors. Most important is the movement of a squall line and sea surface temperature both related with the West African Monsoon. There also seems to be a strong feedback mechanism existing between the land surface and the atmosphere. Several

studies in the region indicate a strong correlation between soil moisture and precipitation (Wagner and Scipal, 2000; Koster *et al.*, 2009; Zribi *et al.*, 2008).

When studying land atmosphere interaction the influence of the atmosphere on the earth surface is more obvious but studying the feedback between the land and the atmosphere is much more complex and challenging. Numerical models have been used to accomplish this task, with a certain degree of success. For instance understanding the extent by which certain surface conditions such as soil moisture influences precipitation. This is because measurement of land surface processes such as soil moisture content is less frequent. Modelling of the processes require the correct understanding of the various mechanisms involved.

### **Land surface Models**

Land surface models (LSMs) are mathematical representations of the numerous land surface processes which include radiative fluxes, evaporation, transpiration, soil moisture and temperature (Tischler *et al.*, 2007). A growing understanding of the importance of land surface processes for the climate in the 1970s and the influence of these processes on the lower atmospheric circulation encouraged the use of land surface models in climate models for a more accurate representation of the lower boundary layer (Decharne *et al.*, 2011). Since then models have evolved from a simple bucket system having a single soil layer with a fixed threshold of water retention beyond which runoff is generated (Manabe, 1969) into complex schemes representing the various biogeochemical and geophysical processes

through which the land surface provides feedback in climate models (Pitman, 2003).

As a result of the growing importance of LSMs in providing near realistic estimate of surface processes for improved climate prediction the accuracy of such models have been under frequent study under two major focusses; the variations between models as a result of different parameterization methods, and improving model output to reflect the heterogeneity of the land surface (Viterbo, 2002; Zhang and Shihua, 2001). An accurate estimate of land surface parameterization requires a model to address the following key issues: effectively simulate the function of vegetation in intercepting rainfall and evapotranspiration; heat and water transfer in the soil; exchange of energy and water on ice and snow covered surfaces; account for the carbon flux from the soil and plant respiration (Viterbo, 2002; Pitman, 2003).

LSMs coupled to climate models have been used to study precipitation-soil moisture feedback mechanisms, and the influence of soil moisture “memory” on the climate (Dirmeyer *et al.*, 2009; Koster *et al.*, 2004; Guo *et al.*, 2006). This has improved the study of the climate over West Africa and studies like Steiner *et al.* (2009) have shown the ability of land-surface feedbacks to have an impact over regional circulations where a strong hydro-climatic gradient exist.

For this study we used the Joint UK Land Environment Simulator (JULES). This LSM has been used to study the land surface conditions over Africa. Ghent *et al.* (2010) assimilated soil satellite temperature observations into JULES noticing

improved model output of soil moisture, surface temperature, latent and sensible heat fluxes over the continent. The sensitivity of JULES to sub grid heterogeneity when coupled to a climate model was shown by Gedney and Cox (2003) and on a “standalone mode” by Clark and Gedney (2008). This study also attempts to introduce heterogeneity in JULES in order to study the response of the model to surface conditions in the study area by making changes to soil parameters used as input data. Further detail of the model is provided in the methodology section.

### **3.1.2 Soil moisture and satellite data retrieval methods**

Soil moisture is the liquid water stored in the pores of a soil (Wagner *et al.*, 2003). Thus, soil moisture is a reservoir in the hydrologic cycle influencing stream flow, ground water, and evapotranspiration (Western *et al.*, 2002). Soil is the thin top layer of the earth surface providing support to plants and first point of contact of the changing atmospheric conditions above. Soil moisture with other land surface characteristics is responsible for the partitioning of incoming solar energy into latent heat and sensible heat flux (Li *et al.*, 2007). In terms of horizontal and vertical flow of water it determines the rate of infiltration into the vadose zone and the rate of runoff. Therefore, soil moisture is important in a number of fields of research ranging from meteorology, climate change, agronomy and hydrology (Wagner, 1998).

In weather processes soil moisture influences the air temperature above through convection. Differential heating normally develops in the lower atmospheric boundary because of the uneven surface roughness and variations in soil moisture

and areas where conditions are favourable may experience thermal uplift, cause convectional circulation cells to develop, mixing the air, and could lead to the formation of clouds and condensation (Ellis and Mellor, 1995). This process is most prevalent in tropical areas where surface heating during the day causes convectional cells to develop and the formation of large vertical cumulonimbus clouds and subsequent heavy rainfall in the late afternoons.

The relationship between precipitation and soil moisture may be described in three stages: wetting of the soil by precipitation; increase in evapotranspiration, higher latent and lower sensible heat flux; a strengthening in precipitation potentials (Koster *et al.*, 2003). Recent studies in the fields of climate change and meteorology are focussed on the impact of soil moisture on precipitation (Mahmood *et al.*, 2011; Meng and Quiring, 2010; Guo *et al.*, 2006). Establishing the level of feedback existing between soil moisture and precipitation may improve forecasts in meteorology and predictions in future climate change. Despite the importance of soil moisture to various fields, there are only a few countries that maintain a number of stations for *in situ* soil moisture measurements and therefore data at the global scale is lacking. These field measurements provide useful information but lack spatial coverage (Njoku, 2003). The reason for this is *in situ* measurements are mostly expensive (Brocca *et al.*, 2010) and, therefore, it is difficult to establish a sufficient number of stations to reflect the average soil moisture conditions in a given river basin. Soil moisture varies in both space and time (Mahmood *et al.*, 2012) and varies within short distances in response to changes in soil types, topography, land cover and

prevailing atmospheric conditions. Therefore, *in situ* observations are unable to provide the wider coverage required for regional and global studies.

The absence of regional and global data on soil moisture has encouraged the use of numerical models and of recent satellite data. In the field of remote sensing both active and passive microwave sensors are used to estimate soil moisture. The L-band (1-2 GHz, Wavelength 30-15cm), C-band (Frequency=4-8 GHz, Wavelength=7.5-3.8cm), and X-band (frequency=8-12 GHz, wavelength=3.8-2.5 cm) spectra of the microwave are favourable for measuring SSM (Wagner *et al.*, 2007). These spectra of the microwave radar are sensitive to the dielectric properties of moisture in the soil and the effects of vegetation and surface roughness is minimised (Njoku *et al.*, 2003). Passive sensors (radiometers) record the signals emitted from surfaces while active (scatterometers) sensors sends signals and records the backscatter reflected from surfaces. The advantage of using radar techniques compared to those using visible and infrared images is the ability to penetrate through clouds and to obtain data that are free from the influence of solar radiation (Brocca *et al.*, 2010; Western *et al.*, 2002). However, interpretation of signals from sensors is difficult and may require complex algorithms for SSM retrieval in order to account for the effects of vegetation and surface roughness which may still exist (Brocca *et al.*, 2010). It should also be noted that microwave signals can only penetrate a few centimetres of the top soil. The exact depth depends on the moisture stress and could be 5 cm when the soil is wet or 2 meters when the soil is dry (Wagner 1998, Wagner *et al.*, 1999, Njoku *et al.*, 2003).

## **3.2 Methodology**

This section describes in detail the methods, the types and sources of data, and the analytical techniques used for the study.

### **3.2.1 Methods**

The main tool used in this study is the JULES land surface model. JULES was used to conduct five experiments differing by the resolution and method used for interpolating soil hydraulic parameters. Soil properties required for some of the simulations in JULES were obtained by digitizing a soil map of the study area in a GIS platform.

#### **GIS and Ferret for producing soil hydraulic parameters, data analysis and visualisation**

The GIS software package Arc Info 9.3.1 was used to process part of the soil data required for the study. Arc map was used to import a soil map of the area, geo-referencing and digitizing. A shape file of the new soil data was created using Arc catalogue. The clip feature in the analysis tool box and the convert features in the conversion tool box in Arc map were then used in delineating and converting the shape file into raster and then into an ASCII file for further export into Ferret.

Ferret is a software application for visualisation and analysis of large and complex gridded data developed by the thermal modelling analysis project (TMAP) of the National Ocean and Atmosphere Administrations (NOAA) Pacific Marine Environmental Laboratory PMEL (Hankin *et al.*, 2007). The software is designed to satisfy the needs of researchers in the field of oceanography, meteorology and climate studies. Ferret was used for most of the analysis and visualisation in this study.

## **JULES**

JULES is based on the UK Meteorological Office surface exchange scheme (MOSES) used to provide land-surface conditions for General Circulation Models (GCMs) but is often used in “stand-alone mode”, not coupled to a GCM for studying hydrological processes and impacts of food supply, water availability and health risk (references from BEST and Clarke in GMD, JULES website, 2010; Betts, 2006). In stand-alone mode it can be driven by externally supplied meteorology. In addition to the energy flux processes, JULES has an inbuilt plant respiration and soil dynamics schemes (TRIFFD). Thus JULES can provide simulations of evapotranspiration, surface run-off, heat and carbon dioxide transfer. Figure 3-2 shows an overview of the process structure of JULES.

Simulations can be run on grids of different sizes and resolutions or single points. The heterogeneity of the land surface is accounted for by nine “tiles” in each grid box representing five vegetation and four non-vegetated cover types. The energy balance of each tile is modelled separately and except for ice covered surfaces the

grid box value is taken as the average weighting of all tiles (Clark and Harris, 2007). Vegetation tiles include Broad leaf, needle leaf, C3 and C4 grasses, and Shrubs while non-vegetated cover tiles include urban, inland water, bare soil and ice. As standard JULES, structures the soil in four vertical layers from 0.1, 0.25, 0.65, and 2.0 meters below the surface tiles (Cox *et al.*, 1999), but this can be expanded to six. JULES accepts variable input in ASCII, binary and netCDF file formats.

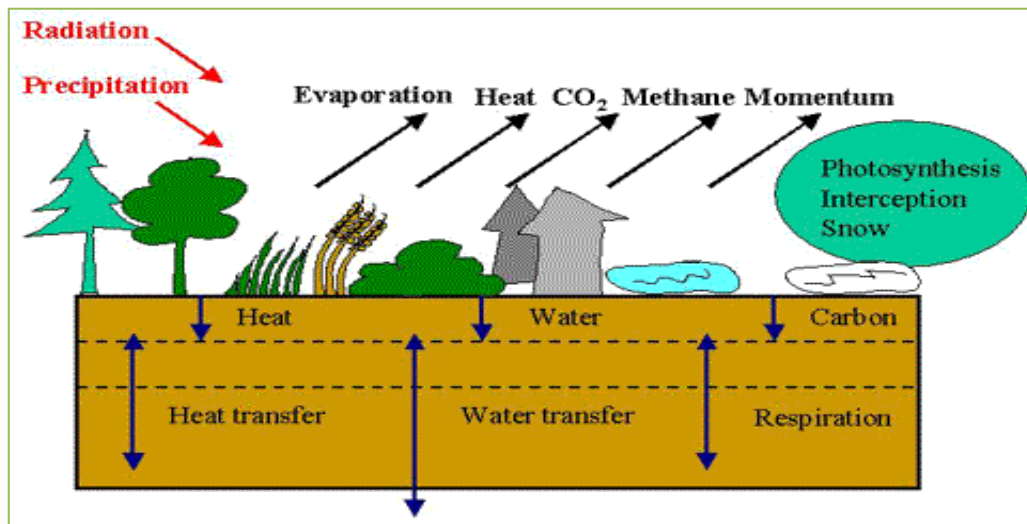


**Figure 3-2: The land-surface processes represented in JULES**

\*source: JULES website (<https://jules.jchmr.org/>)

The fluxes in energy and momentum from each tile are calculated separately and the surface flux of each grid surface is the weighted average of all the tiles. There are two distinctive surfaces in JULES: (1) non-vegetated where fixed albedo and surface roughness values are specified at the beginning of a model run and (2) vegetated whose surface varies with time and is calculated during the run time.

In order to derive the surface energy balance, a vegetation fraction is coupled to the soil using radiative exchange and atmospheric turbulence while other surfaces are coupled through conduction. This is represented below (Best *et al.*, 2011):

$$C \frac{\delta T_*}{\delta t} = (1 - \alpha)Sw_{\downarrow} + \varepsilon Lw_{\downarrow} - \sigma\varepsilon(T_*)^4 - H - L_c E - G \text{ Eq. [3-4]}$$

where:

$C$  =Heat capacity associated with the surface material ( $J K^{-1} m^{-2}$ )

$\alpha$ = surface albedo (-)

$Sw_{\downarrow}$ =downward component of the solar radiation ( $W m^{-2}$ )

$Lw_{\downarrow}$ =downward component of the long wave radiation ( $W m^{-2}$ )

$\varepsilon$ =surface emissivity (-)

$\sigma$ =Stephan Boltzmann constant ( $5.6697 \times 10^{-8} W m^{-2} K^{-4}$ )

$T_*$ =surface temperature (K)

$H$ =heat flux ( $W m^{-2}$ )

$L_c$ =latent heat of condensation of water at 0 °C ( $W m^{-2}$ )

$E$ =Turbulent latent heat ( $W m^{-2}$ )

$G$ =Surface soil heat flux ( $W m^{-2}$ )

The turbulent latent, sensible and surface soil heat fluxes are derived using the following equations:

$$H = \frac{\rho c_p}{r_a} (T_* - T_1) \text{ Eq. [3-5]}$$

$$E = \frac{\rho}{r_a + r_s} (Q_{sat}(T_*) - Q_1) \text{ Eq. [3-6]}$$

$$G = v \left[ \sigma\varepsilon\varepsilon_s(T_*)^4 - \sigma\varepsilon\varepsilon_s(T_{s1})^4 + \frac{\rho c_p}{r_{a\text{can}}} (T_* - T_{s1}) \right] + (1 - v)A_s(T_* - T_{s1})$$

Eq. [3-7]

where;

$\rho$  = the density of air ( $\text{kg m}^{-3}$ )

$c_p$  =the specific heat capacity of air ( $\text{J kg}^{-1} \text{K}^{-1}$ )

$T_1$ =reference level atmospheric temperature (K)

$Q_{sat}(T_*)$ =Saturated specific humidity at the surface temperature (-)

$Q_1$ =specific humidity at the reference atmospheric level (-)

$r_a$  =the aerodynamic resistance ( $\text{S m}^{-1}$ )

$r_s$  = the stomatal or surface moisture resistance ( $\text{S m}^{-1}$ )

$v$ = fraction of vegetation (-)

$\sigma$ = Stefan Boltzmann constant ( $5.6697 \times 10^{-8} \text{ W m}^{-2} \text{ K}^{-4}$ )

$\varepsilon_s$  = the emissivity of the underlying soil surface (-)

$T_{s1}$ =Temperature of the first soil level (K)

$r_{a_{can}}$  = aerodynamic resistance between the surface canopy of vegetation and the underlying soil ( $\text{S m}^{-1}$ )

$A_s$ = Thermal conductivity of the soil ( $\text{W m}^{-1} \text{K}^{-1}$ )

Rainfall is considered to be a through fall depending on the fraction of the vegetation canopy, and then on reaching the surface, rainfall is partitioned into runoff and infiltration. Subsurface flow is derived from the Richard's equation where each layer of soil gains from the top through gravity drainage (Cox *et al.*, 1999). Evapotranspiration is removed through root uptake or in the top layer as a moisture loss from the layer. There are two options in deriving the soil water retention characteristics in JULES either by applying the Brooks and Corey

(1964) equation used in this study, or alternatively the hydraulic relationships of van Genuchten (1980).

The rate of soil respiration is dependent on the soil temperature, volumetric soil moisture content and soil carbon content.

$$R_s = k_s C_s f_\theta f_T \quad \text{Eq. [3-8]}$$

where  $R_s$  is the rate of soil respiration,  $k_s$  is the specific respiration rate at 25<sup>0</sup>C and is equal to  $5 \times 10^{-9} \text{ s}^{-1}$ ,  $C_s$  is the soil carbon content,  $f_\theta$  and  $f_T$  are moisture and temperature dependent functions (Essery *et al.*, 2001).

In JULES the soil thermal characteristic is moisture dependent and is given as:

$$C_a \Delta z_k \frac{dT_k}{dt} = G_{k-1} - G_k - J_k \Delta z_k \quad \text{Eq. [3-9]}$$

where the temperature of the  $k^{\text{th}}$  soil layer changes via diffusive heat fluxes into and out of the layer  $G_k$  and  $G_{k-1}$  and the advective flux from the layer by flowing water  $J_k$  (Best *et al.*, 2011).

The CO<sub>2</sub> diffusion equation is used to link photosynthetic uptake and stomatal conductance.

$$A = \frac{g_s}{1.6(C_c - C_i)} \quad \text{Eq. [3-10]}$$

where  $A$  is the net photosynthetic uptake,  $g_s$  leaf level stomatal conductance,  $C_c$  and  $C_i$  are the leaf surface and internal carbon dioxide concentrations.

In this particular study, JULES version 3.0 was used. The main difference between this versions and other previous version is the inclusion of the IMOGEN

tool which when switched provides simulation of surface flux of energy and momentum based on various climate change scenarios (Clark *et al.*, 2011).

### **3.2.2 Data Types**

JULES requires three types of data; the initial conditions, boundary conditions and parameters, and atmospheric forcing data. The initial conditions are obtained from the initial “spin up” run of the first and second year repeated ten times. Data for the boundary conditions were obtained from the global land cover characteristics data base version 2.0, Ecoclimap 2, and Modis albedo. A soil map of Nigeria (Sonneveld, 1997) was reclassified to 16 textural groups based on the FAO 1973 textural classification and FAO-UNESCO revised classification (Batjes *et al.*, 1997) used to produce a new set of soil hydraulic parameters calculated based on the Clapp and Hornberger (1978) hydraulic functions. Meteorological forcing data was obtained from the CRU-NCEP six hourly data set of: precipitation, pressure, humidity, temperature, downward radiation, wind direction and speed.

The ERS SCAT data SSM data for the period of 1992-2000 was used to evaluate results of soil moisture from the five simulation experiments. The ERS SSM is a product retrieved from a scatterometer on board the European remote sensing satellite ERS 1 and ERS 2. The ERS scatterometer is active C band radar that measures the backscatter coefficients of objects on the Earth’s surface at half degree resolution. ERS radar can only penetrate a few centimetres of the soil upper layer to the depth of 10cm when the soil is dry and 2 cm when saturated

(Wagner, 1998). The data retrieval method uses change detection developed by TU Wien (ESCAT soil moisture product sheet). It uses a harmonised time series of dry and wet events for producing a relative surface soil moisture data using a scale of 0 when the soil is very dry and 100 when fully saturated. The equation for the retrieval from backscatter coefficients is provided below (Wagner *et al.*, 1999).

$$MS(t) = \frac{\sigma^0(40,t) - \sigma_{dry}^0(40,t)}{\sigma_{wet}^0(40,t) - \sigma_{dry}^0(40,t)} \quad \text{Eq. [3-11]}$$

where

$M_s$  = relative soil moisture content in the few centimetres

$t$  = time

$\sigma^0(40)$  = referral angle of incidence for all backscatter coefficients

$\sigma_{dry}^0(40,t)$  = dry events or lowest values of backscatter

$\sigma_{wet}^0(40,t)$  = wet events or periods of high backscatter.

ERS Scat SSM data has been validated in West Africa. Furthermore it is available for the period of interest (1992-2000).

### 3.2.3 Analysis techniques

Output data from the model experiments and ERS scat SSM data were analysed using time series plots, scatter plots, empirical cumulative distribution function (ECDF), percentage error, correlation coefficients, Kendall rank correlation,

Student's t-test, and Kolmogorov-Smirnov test. The objective of using these statistical methods is to study the possible differences between the variables, differences in their distribution, the level of deviation from averages, and temporal changes of land-surface processes.

### **3.3 Results**

#### **3.3.1 Data Processing and integration**

The soil map used as a base map is the dominant soil map of Nigeria 1996 produced by Sonneveld (1997) based on the FAO/UNESCO soil classification consisting of 16 soil types occurring in single units or in association. The new base map was geo-referenced using the GCS-WGS-1984 projection. After digitizing and producing a shape file for the soil map another shape file of North-eastern Nigeria was used to delineate the study area using the clip tool.

It was noticed that some cells in the base map were covered by two or more soil units therefore; the study decided to pick the soil characteristics of the dominant soil type covering that cell. As a result the 66 different cells were reclassified into 16 (Table 3-1). The final shape file was converted to a raster image and then into an ASCII format which can be read into the ferret NOAA software. In the absence of field measurements of soil parameters, soil textural classes (Figure 3-3) were used to calculate the soil hydraulic properties. Sand and clay composition of each of the dominant soil types was obtained using the 1990 revised FAO-UNESCO soil units (Batjes *et al.*, 1997).

**Table 3-1: Soil types in the study area**

<i>ID</i>	<i>Name</i>	<i>Abbreviation</i>	<i>Sand</i>	<i>Silt</i>	<i>Clay</i>	<i>Soil triangle</i>
1	Acrisols	AC	6	53	41	silt loam
2	Alisols	AL	15	28	57	silt loam
3	Arenosols	AR	95	5	0	sands
4	Cambisols	CM	11	70	19	silt loam
5	Fluvisols	FL	5	57	38	silt loam
6	Ferralsols	FR	6	38	56	clay loam
7	Gleysols	GL	9	66	25	silt loam
8	Leptosols	LP	59	28	13	sandy loam
9	Luisols	LV	18	67	15	silt loam
10	Lixisols	LX	63	7	30	sandy clay
11	Nitisols	NT	7	39	54	clay loam
12	Phaezoms	PH	5	67	28	silt loam
13	Plinthosols	PT	64	17	19	sandy loam
14	Regasols	RG	54	41	5	sandy loam
15	Solenetz	SN	17	33	50	clay loam
16	Vertisols	VR	0	2	98	clay

An important property of soils is their texture which is defined by the composition of sand, silt and clay particles in each soil type (Zao *et al.*, 2009). Soil texture can affect pore size distribution which affects the flow of water within the soil and the quantity of moisture that is eventually retained. It also affects the susceptibility to

erosion, nutrient holding capacity and fertility of soils. Thus soil texture determines the availability of soil moisture directly through water retention and flow characteristics (Zao *et al.*, 2009). Soil particles vary in size with sands composed of large particles ranging from 0.05 to 2.0 mm. The size creates large pores between the particles and allows for easy infiltration of water and low retention capacity. Silt has a particle size of 0.002-0.05 mm and creates moderately drained soils with moderate water retention capacity. Clays have a particle size of less than 0.002 mm which creates small pores, higher water retention capacity and poor drainage.

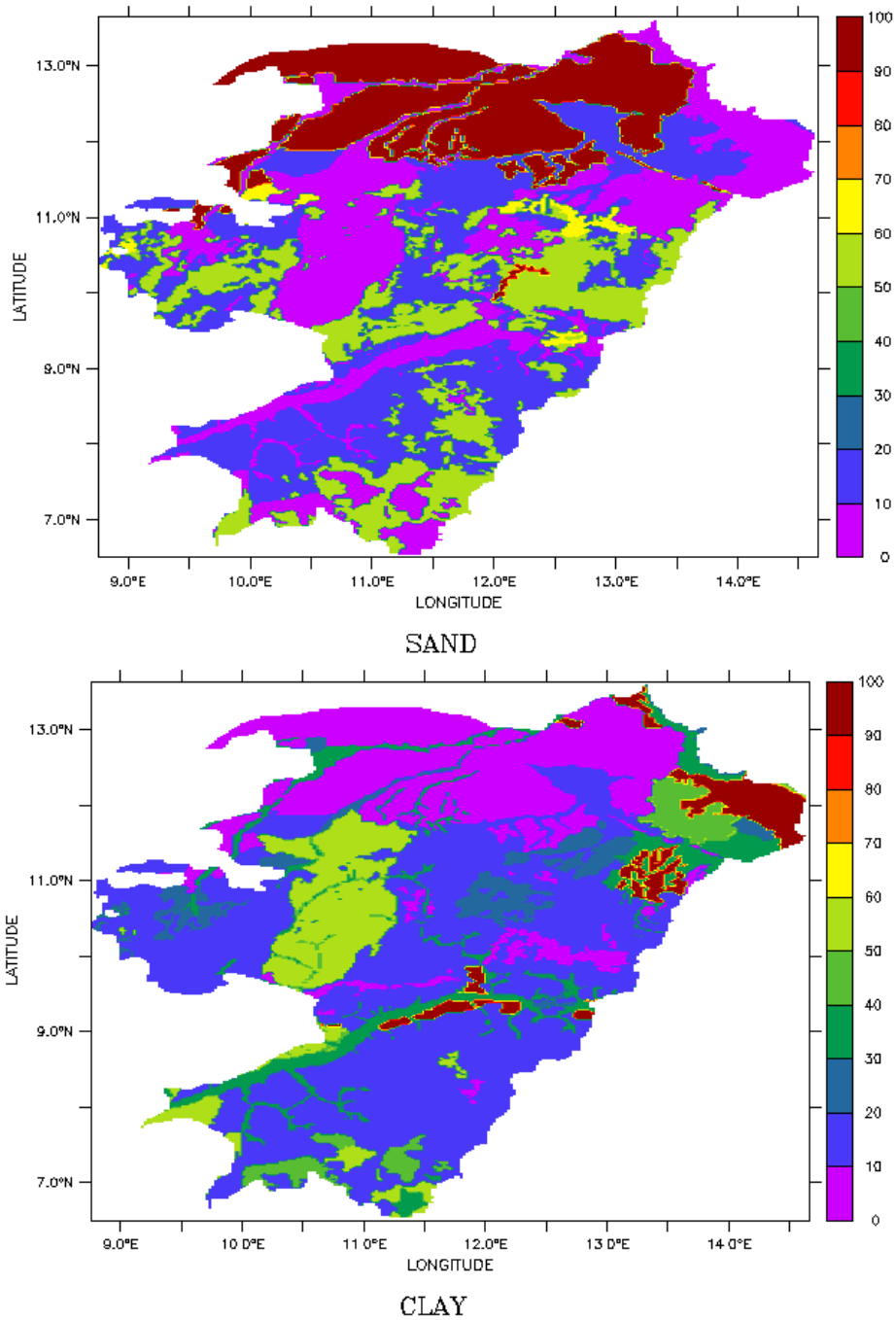


**Figure 3-3: The percentage sand (top) and clay (bottom) content of the 16 dominant soil types of North-east Nigeria from Sonneveld (1997) based on the 1990 revised FAO-UNESCO soil units**

In land surface models, soil texture is often used in producing pedo-transfer functions (PTF) for water movement and retention within soils. This is because direct field measurements are expensive, time consuming and labour intensive (Tietje and Hennings, 1996; Saxton *et al.*, 1986; Rawles *et al.*, 1982). Thus, data on soil textural characteristics are used to estimate soil hydraulic properties such as hydraulic conductivity and water retention curves (Rawles *et al.*, 1982). There are various mathematical equations for the estimation of these two properties but the most frequently used in GCMs is by Clapp and Hornberger (1978) for hydraulic conductivity and water suction as a function of soil moisture content (Cox *et al.*, 1999).

$$\Psi = \Psi_s S_u^{-b} \quad \text{Eq. [3-12]}$$

$$K = K_s S_u^{2b+3} \quad \text{Eq. [3-13]}$$

where,  $\Psi$  is the soil suction;  $K$  is the hydraulic conductivity;  $S_u$  is the mass of unfrozen water in a soil layer as a fraction of liquid water at saturation (Cosby *et al.*, 1999):

$$S_u = \frac{\theta_u}{\theta_s} \quad \text{Eq. [3-14]}$$

where  $\theta_u$  is the volumetric concentration of unfrozen water and  $\theta_s$  is the saturation soil moisture concentration.

$\Psi_s$ ,  $b$  and  $K_s$  are empirical soil dependent constants.

The values of  $b$ ,  $\Psi_s$ ,  $K_s$  and  $\theta_s$  is calculated using the following linear regression model in Cosby *et al.* (1984) and were subsequently used for the Brooks and Corey Model (1964).

$$b = 3.1 + (0.157 \times \text{clay}) - (0.003 \times \text{sand}) \quad \text{Eq. [3-15]}$$

$$\log \Psi_s = 1.54 - (0.0095 \times \text{sand}) + (0.0063 \times \text{silt}) \quad \text{Eq. [3-16]}$$

$$\Psi_s = 10^{\log \Psi_s} \quad \text{Eq. [3-17]}$$

$$\log K_s = -0.6 + (0.0126 \times \text{sand}) - (0.0064 \times \text{clay}) \quad \text{Eq. [3-18]}$$

$$K_s = 10^{\log K_s} \quad \text{Eq. [3-19]}$$

$$\theta_s = 50.5 - (0.142 \times \text{sand}) - (0.037 \times \text{clay}) \quad \text{Eq. [3-20]}$$

Five separate simulations over a twenty year period (1980-2000) were carried out four of which use the same soil parameters but differ based on methods of interpolating and calculating soil hydraulic parameters (Table 3-2). The soil volume was divided into 6 layers at 5 cm, 10 cm, 25 cm, 50 cm, 1 m, and 2 m depths using a thinner top layer than is standard in JULES. This first 5cm layer of the soil was used to analyse predicted SSM and evaluate it with the ERS satellite product. The fraction of saturation was used as a measure for both satellite and predicted SSM ranging from 0 when the soil is absolutely dry and 1 when fully saturated.

Apart from the variation in scale and non-linearity in the calculation of soil hydraulic parameters, all other input parameters and model set up for each of the 5

experiments remain the same. A highlight of the general set-up of the model, soil input parameters and model outputs are given in Table 3-3.

**Table 3-2 Methods employed in producing soil hydraulic parameters used in Experiments 1, 3, 4, and 5**

HIGH RESOLUTION SOIL TEXTURE DATA SET (0.024°)	→	→ RESOLUTION	→	USED AS SOIL PARAMETERS ↓
	Interpolate input data	½°	calculate soil hydraulic	Experiment 1
		1°	parameters with coarse data	Experiment 4
	Calculate soil hydraulic parameters	½°	interpolate outputs	Experiment 5
	with high resolution data	1°		Experiment 3

**Table 3-2: Model set up, some input parameters and model output parameters in each of the 5 experiments carried out**

<b>Spin up (Years)</b>	<b>Time step (minutes)</b>	<b>Soil layers</b>	<b>Soil parameters</b>	<b>Vegetation</b>	<b>Output parameters included in the model run</b>
<b>20</b>	30	6	<ol style="list-style-type: none"> <li>1. Saturated soil water pressure (<math>\text{m}^2</math>) sathh</li> <li>2. Saturated hydraulic conductivity (<math>\text{kg m}^{-2} \text{s}^{-1}</math>) (satcon)</li> <li>3. Volumetric moisture content at saturation (smvcs)</li> <li>4. Volumetric moisture content at critical point (smvcl)</li> <li>5. Volumetric moisture content at wilting (smvcwt)</li> <li>6. Soil heat capacity (<math>\text{J K}^{-1} \text{m}^{-3}</math>) hcap</li> <li>7. Soil thermal conductivity (<math>\text{W m}^{-1} \text{K}^{-1}</math>) hcon</li> <li>8. Brooks-Corey exponent (b-soil)</li> <li>9. soil albedo (albsoil)</li> </ol>	Driven by separate leaf area index (LAI) file	<ol style="list-style-type: none"> <li>1. Latent heat flux (<math>\text{W m}^{-2}</math>)</li> <li>2. Sensible heat flux (<math>\text{W m}^{-2}</math>)</li> <li>3. Evapotranspiration (<math>\text{kg m}^{-2} \text{s}^{-1}</math>)</li> <li>4. Gross primary productivity (<math>\text{kg C m}^{-2} \text{s}^{-1}</math>)</li> <li>5. Net primary productivity (<math>\text{kg C m}^{-2} \text{s}^{-1}</math>)</li> <li>6. Soil moisture as a fraction of saturation</li> <li>7. Soil runoff (<math>\text{kg m}^{-2} \text{s}^{-1}</math>)</li> <li>8. Soil temperature (K)</li> </ol>

### 3.3.2 Relationship between the five case experiments

Results of soil moisture and temperature of Experiments 1, 3, 4, and 5 were compared with experiment 2. This is because different soil data were used for Experiment 2 unlike, the rest of the other four that differ only in the methods of calculating soil hydraulic parameters and interpolation. For this reason, results of SSM for experiments 1, 3, 4, and 5 were correlated with Experiment 2 (Figure 3-4).

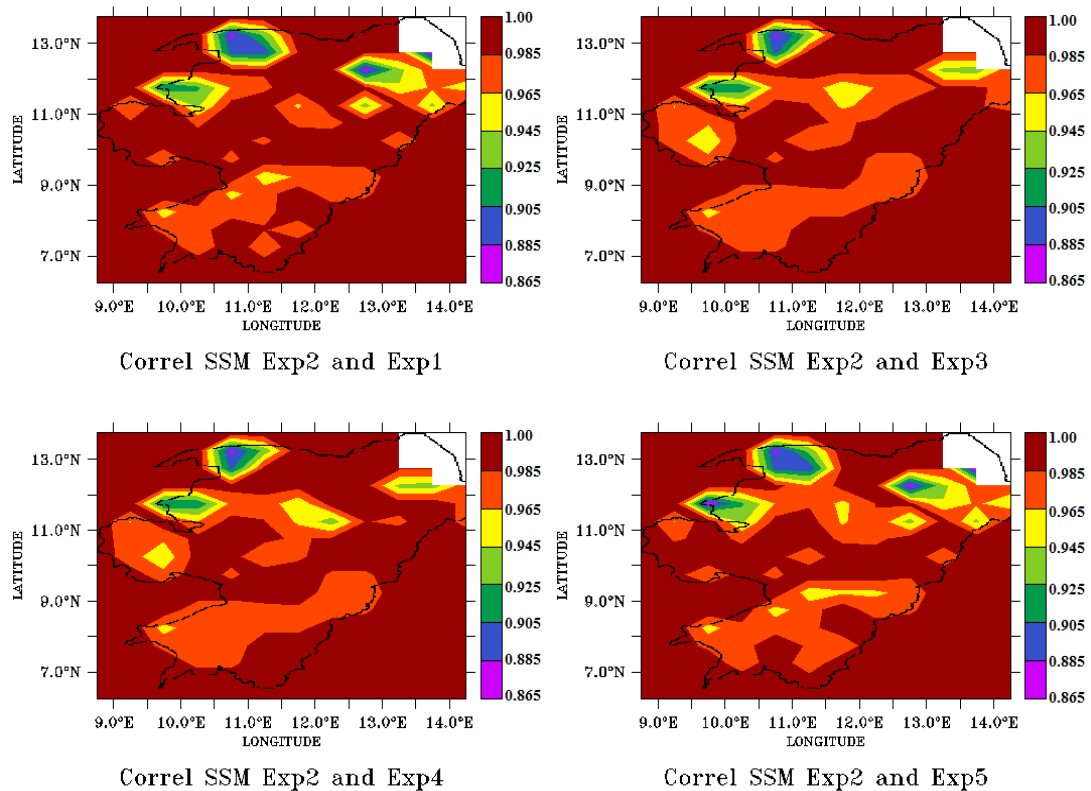


**Figure 3-4: Correlation coefficient of SSM between Experiment 2 and the four other experiments**

\* the black line on the map is the border line of the study area

Correlation coefficients vary from 0.875 to 1.00. The same correlation method was applied to results of soil temperature (Figure 3-5) with correlation coefficient values ranging from 0.985 to 1.00.

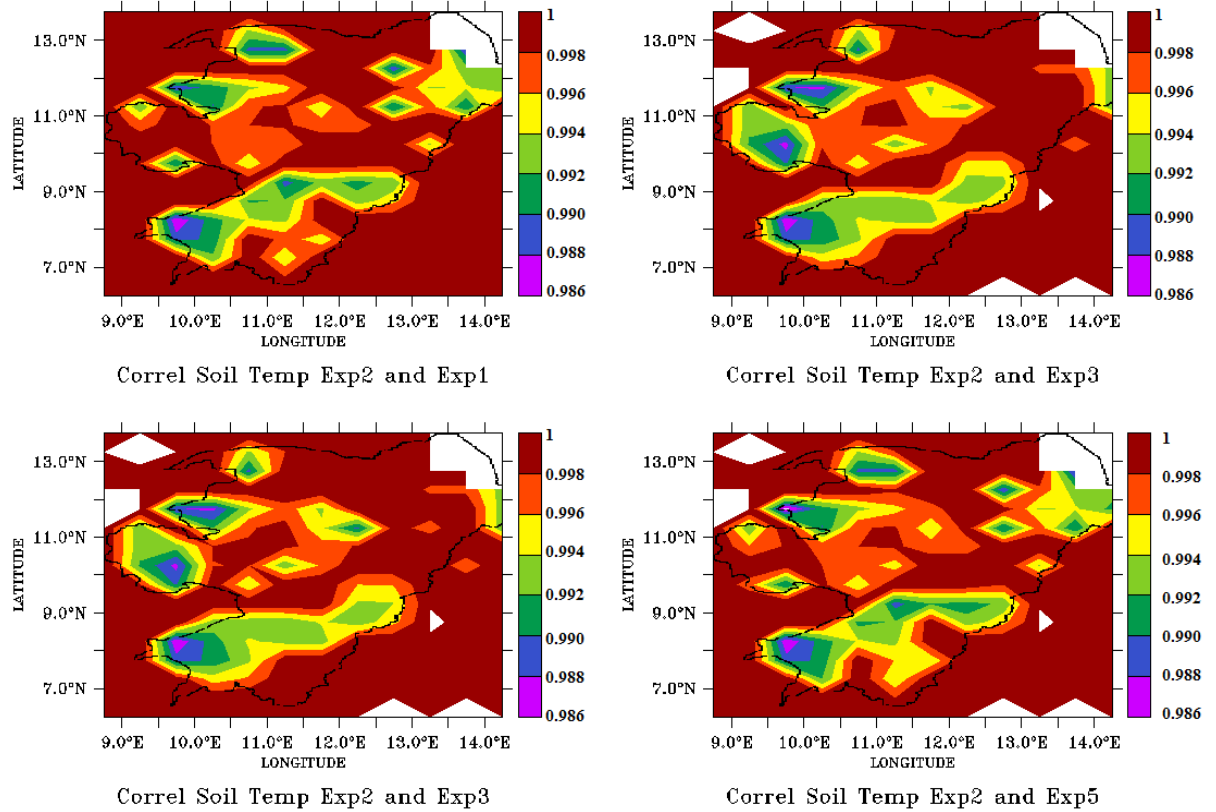


**Figure 3-5: Correlation coefficients for soil temperature between Experiment 2 and the other four experiments.**

\* the black line on the map is the border line of the study area

The study further examined the percentage error between Experiment 2 and the other 4 experiments (Figure 3-6) calculated as the percentage difference between Experiment 2 and any of the four experiments using:

$$\%err = \frac{e2-ex}{e2} \times 100 \quad \text{Eq. [3-21]}$$

where %err is the relative percentage error,  $e_2$  is experiment 2,  $e_x$  is any of the Experiments 1, 3, 4 or 5.

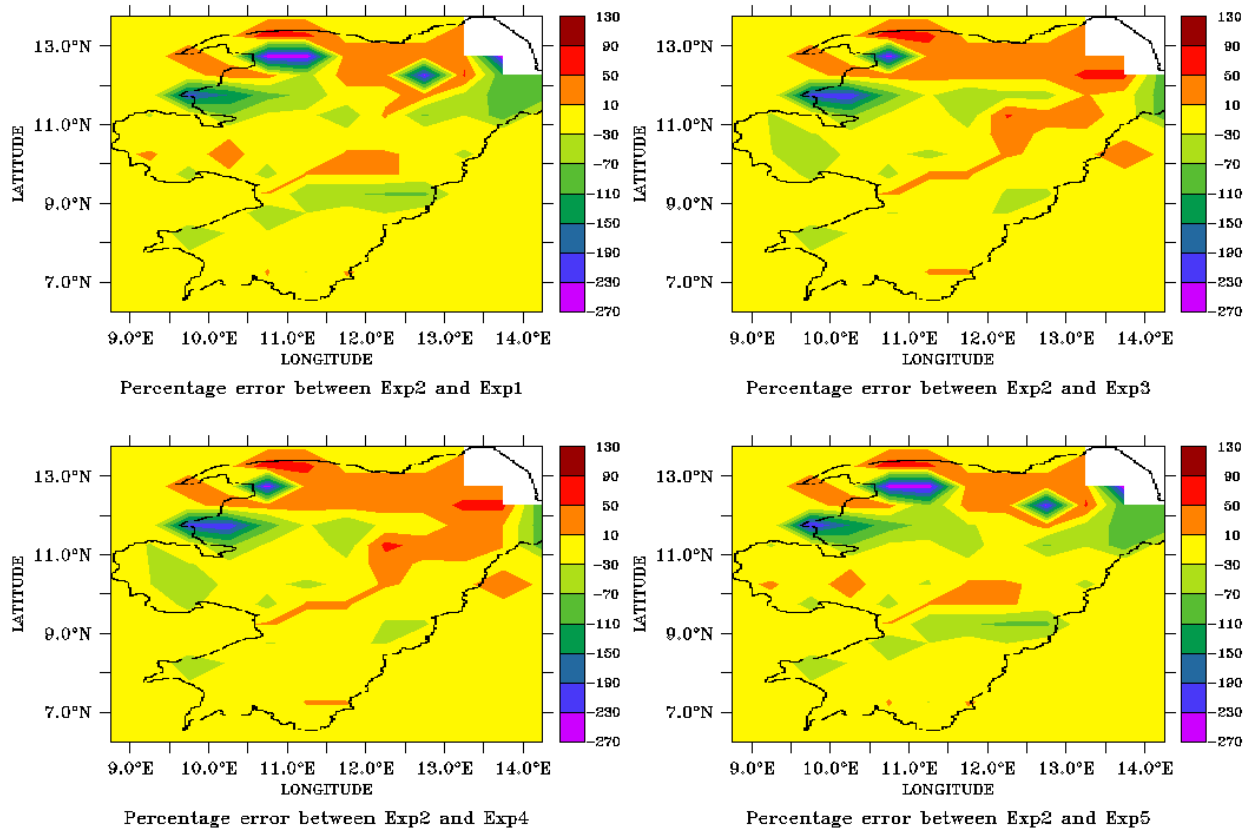


**Figure 3-6: Percentage error of SSM between Experiment 2 and the other 4 experiments (\* the black line on the map is the border line of the study area)**

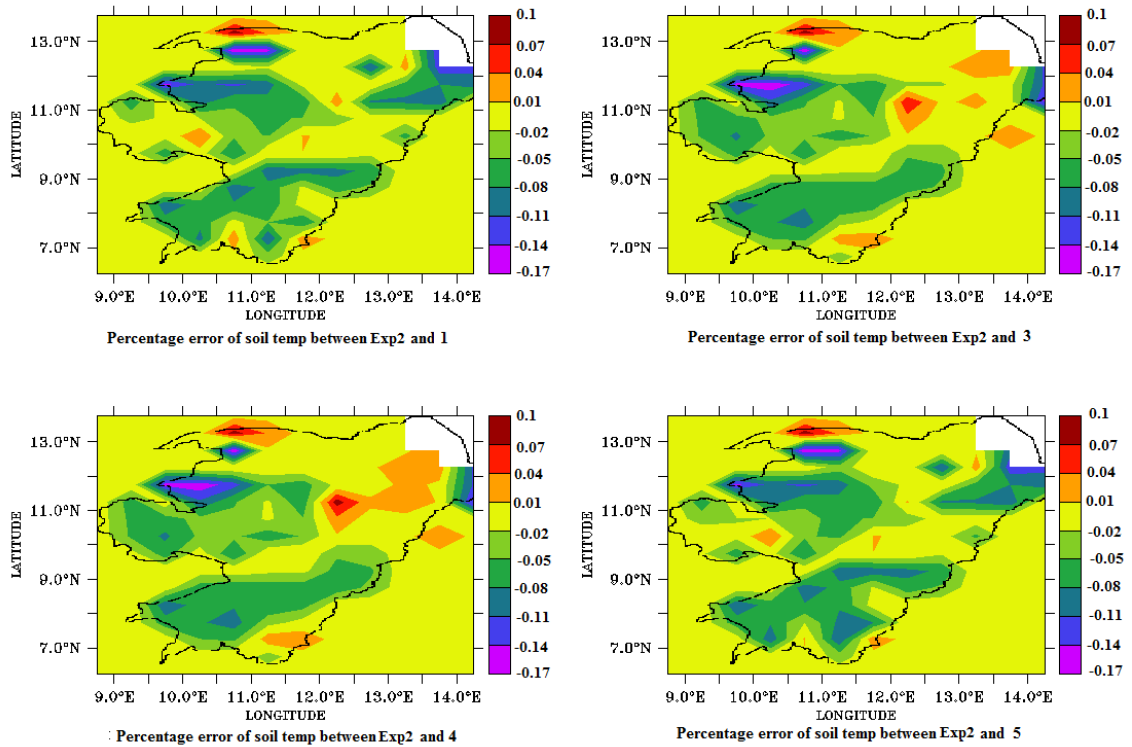


**Figure 3-7: Percentage error of soil temperature between Experiment 2 and the other 4 experiments.**

\* the black line on the map is the border line of the study area

The percentage error for the pixel averaged time series of soil moisture and temperature between Experiment 2 and the other four experiments were plotted for the purpose of identifying the pattern of variation across the seasons. Percentage error of soil moisture and temperature varies between zero during the wet season to between -50 and -20 during the dry season (Figure 3-8).

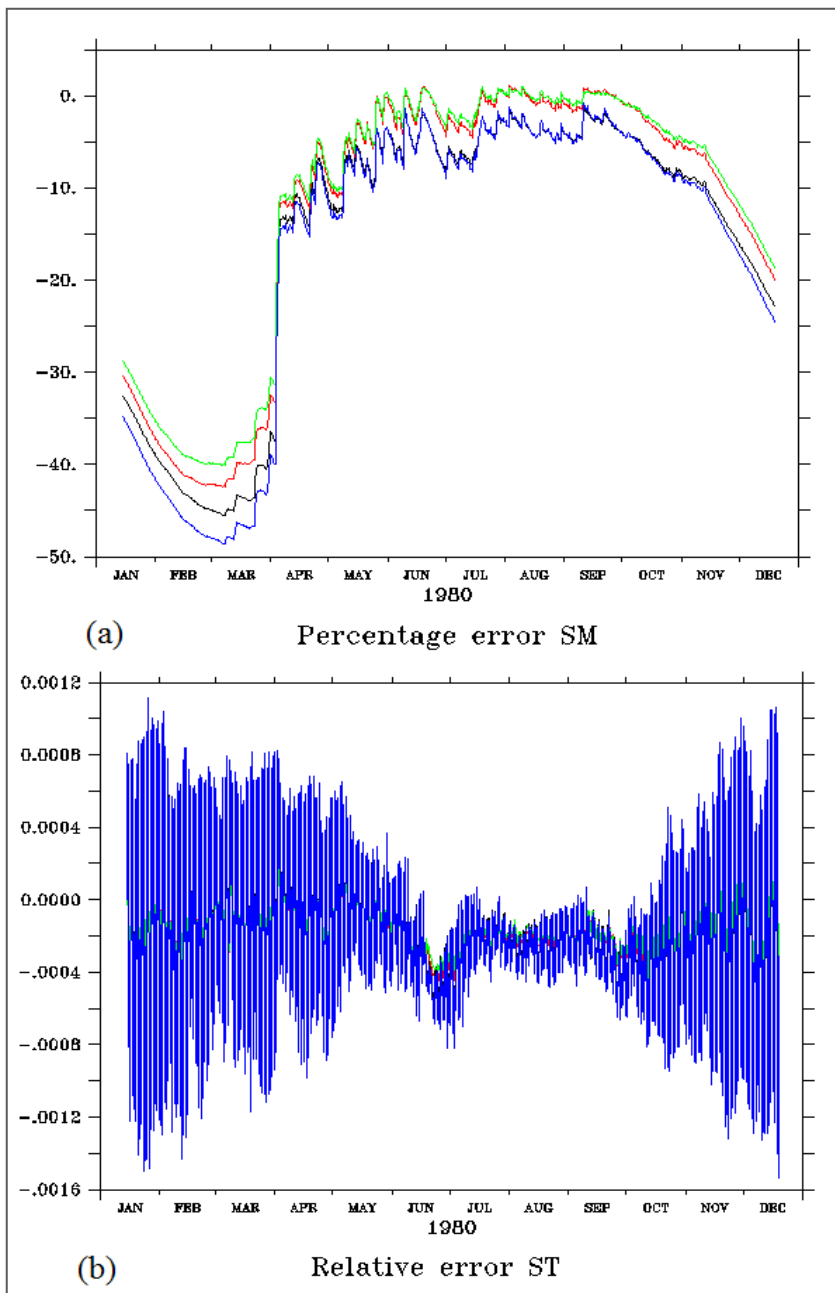


**Figure 3-8: Pixel averaged percentage error of SSM and soil temperature (January-December 1980) between Experiments 2 and 1 (black line), 2 and 3 (red line), 2 and 4 (green line), and 2 and 5 (blue line).**

Differences in SSM are more pronounced during the dry season (November-March) when this can be as much as 50%

The pixel averaged differences for SSM between the experiments were further analysed using Student's t-test to determine the difference in means and the Kolmogorov-Smirnov test for testing the similarities in distribution between two data sets (Table 3-4 and Table 3-5). The null hypothesis was set as: there is no difference between the means of the data sets (for Student's t-test) and there is no difference in their distribution (for the Kolmogorov-Smirnov test). The null-hypothesis will be rejected of the alternative hypothesis if  $p\text{-value} < 0.05$ . Furthermore, the Bonferroni-Holm's test was applied to remove any type 1 error from the statistical test.

**Table 3-3: Output of a Student's t-test for SSM, ST and SR (surface runoff) for testing the differences in the means of SSM, ST, and SR between the 5 experiments**

			<i>Experiment 1</i>	<i>Experiment 2</i>	<i>Experiment 3</i>	<i>Experiment 4</i>	<i>Experiment 5</i>
Experiment 1	SSM	1	<2.2e-16	3.6e-03	8e-04	0.70	
	ST	1	0.49	0.89	0.87	0.99	
	SR	1	6.6e-05	0.73	0.77	0.79	
Experiment 2	SSM		1	8.4-e09	1.16e-07	<2.2e-16	
	ST		1	0.59	0.61	0.88	
	SR		1	2e-04	1e-04	1e-04	
Experiment 3	SSM			1	0.64	1e-04	
	ST			1	0.98	0.88	
	SR			1	0.95	0.94	
Experiment 4	SSM				1	2e-03	
	ST				1	0.87	
	SR				1	0.98	
Experiment 5	SSM					1	
	ST					1	
	SR					1	

**Table 3-4: Output of a Kolmogorov-Smirnov test for testing the differences in the distributions of SSM, ST, and SR between the 5 experiments**

		<i>Experiment 1</i>	<i>Experiment 2</i>	<i>Experiment 3</i>	<i>Experiment 4</i>	<i>Experiment 5</i>	
For the	Experiment 1	SSM	1	<2.2e-16	<2.2e-16	8.8e-06	0.99
		ST	1	0.43	0.99	0.99	1
		SR	1	0.92	1	1	1
	Experiment 2	SSM		1	1.8e-14	5.8e-13	<2.2e-16
		ST		1	0.91	0.95	0.42
		SR		1	0.92	0.92	0.95
	Experiment 3	SSM			1	0.99	2.6e-05
		ST			1	1	0.99
		SR			1	1	1
Experiment 4	SSM				1	9.9e-06	
	ST				1	0.99	
	SR				1	1	
Experiment 5	SSM					1	
	ST					1	
	SR					1	

Student's t-test calculated statistical values higher than the p-values were obtained between Experiment; 1 and 5 (p-value>0.05), 3 and 4 (p-value>0.05).

A similar result was obtained for the Kolmogorov-Smirnov test; 1 and 5 ( $p$ -value $>0.05$ ), 3 and 4 ( $p$ -value $>0.05$ ). Based on these result the null hypothesis was accepted in favour of the alternative hypothesis.

The same statistical test was used to test the differences between other simulated variables of soil temperature (ST) and surface runoff (SR) that are presumed to be related to SSM conditions. Student's t-test and Kolmogorov-Smirnov test for predicted ST between all the experiments yielded values of  $p>0.05$ . Therefore the null hypothesis was accepted indicating that there are no differences between the means of predicted ST between all the experiments and there are no differences in their distribution.

However, the outputs of the Student's t-test for SR between Experiment 2 and the other 4 experiments have  $p<0.05$ . The null hypothesis was rejected suggesting there is a difference in the means of the predicted SR between Experiment 2 and the other 4 experiments. The outputs of the Kolmogorov-Smirnov test gave  $p$ -values  $> 0.05$  for all the experiments. This indicates that despite the difference in the means of SR between Experiment 2 and Experiments 1, 3, 4, and 5, there is no differences in their distribution.

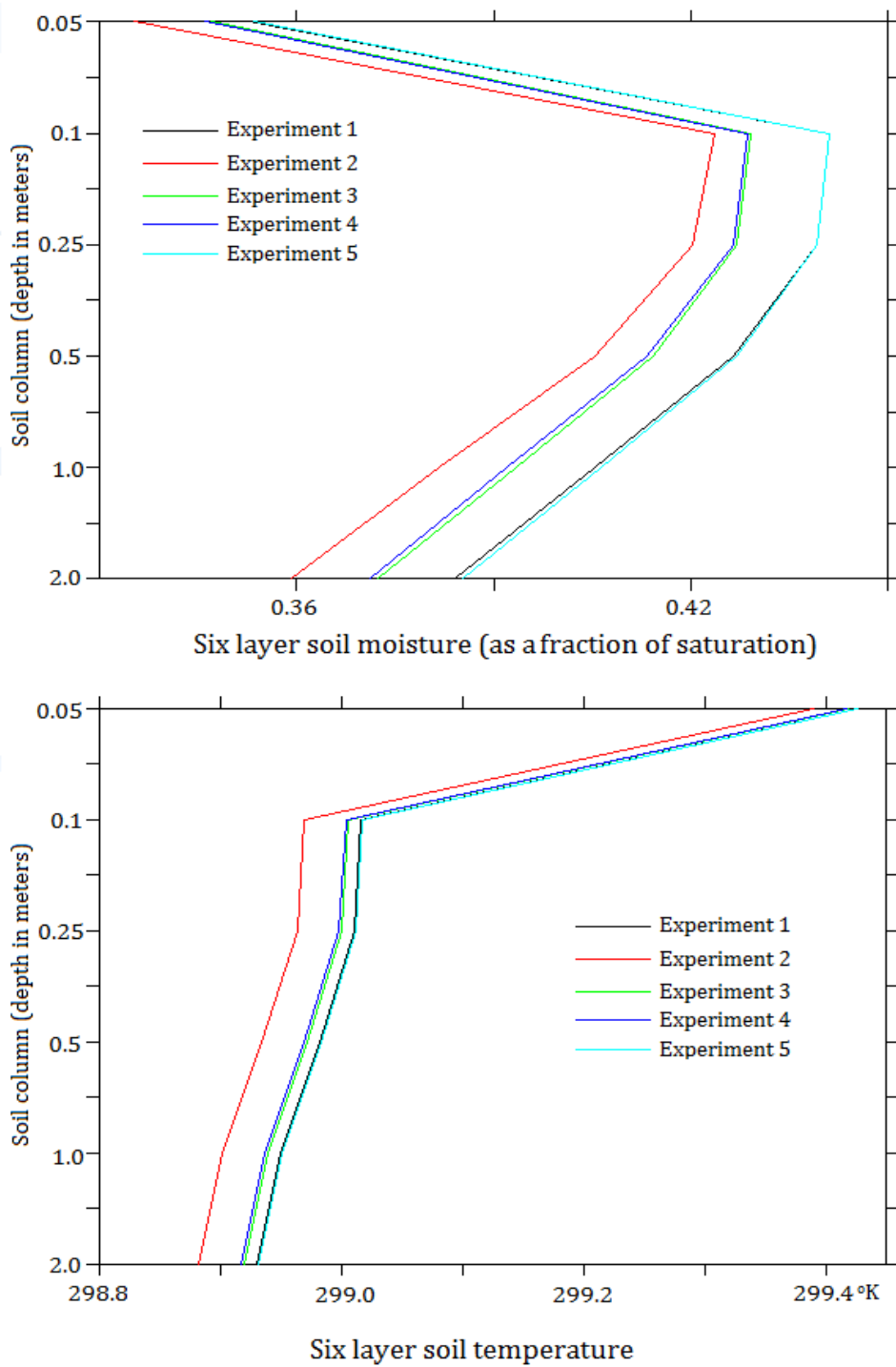


**Figure 3-9 Pixel and time averaged (1980-2000) predicted soil moisture (top) and soil temperature (below) at different depth for all five experiments**

The pixel and time averaged predicted soil moisture and temperature at six different depths is presented in Figure 3-9. Visual observation of the plots in Figure 3-9 suggest that differences in predicted soil moisture and temperature between the 5 experiments increase with an increase in soil depth. The statistical significance of these differences was verified by averaging the pixel values of predicted soil moisture and temperature of the 5 soil layers (10 cm, 25 cm, 50 cm, 1 meter and 2 meters deep) beneath the top soil layer (5 cm deep) and applying the Student's t test and Kolmogorov test between the 5 experiments. Outputs from the two statistical tests (not presented here) suggest that differences between experiments using different scales for soil parameter inputs are more statistically significant than experiments using the same scale.

There are differences in predicted surface energy fluxes of latent and sensible heat between the 5 experiments. Differences in predicted latent heat between Experiment 2 and Experiment 5 varies seasonally by  $3.7 \text{ W m}^{-2}$  and seasonal differences of predicted sensible heat varies by  $3.0 \text{ W m}^{-2}$ .

### **3.3.3 Evaluating experiments with ERS SSM data and precipitation**

ERS Satellite SSM for 1992-2000 and precipitation data (1980-2000) were used for evaluating the results obtained from the five model experiments. Pixel correlation coefficients of simulated soil moisture for the top layer (5cm) of the soil and ERS Scat data is within the range of 0.48-0.88 for Experiments 1, 3, 4 and 5. The values for the correlation between predicted soil moisture in Experiment 2 and the ERS Scat SSM are within the range of 0.48-0.9 (Figure 3-9).

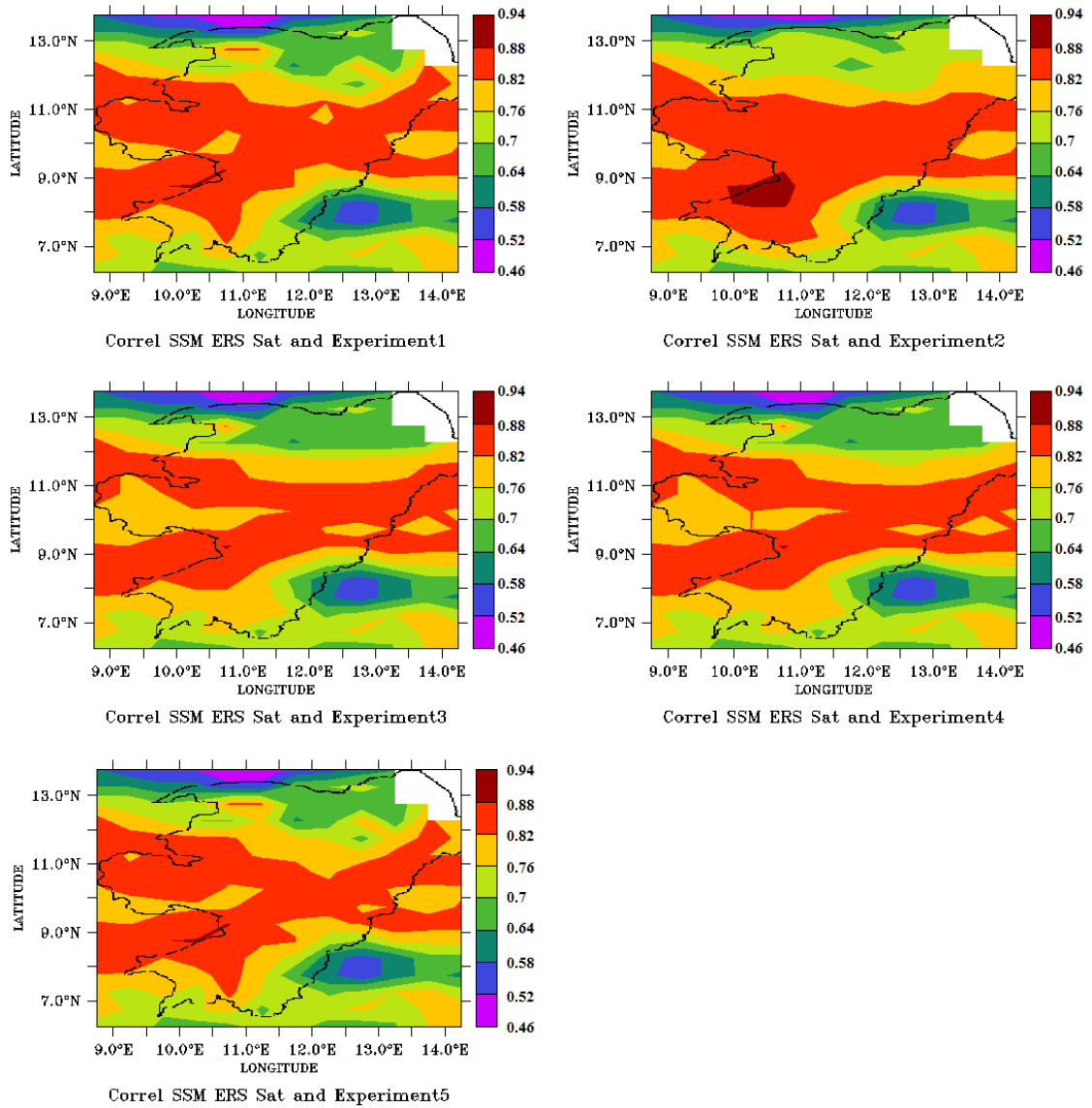


**Figure 3-10: Grid box correlation between satellite product SSM and the 5 experiments.**

\* the black line on the map is the border line of the study area

\*Except for two  $\frac{1}{2}^{\circ} \times \frac{1}{2}^{\circ}$  grid boxes in the North (Latitude  $13.5^{\circ}$  to  $14.0^{\circ}$  North and Longitude  $10^{\circ}$  to  $11^{\circ}$  East) all other grid boxes have correlation coefficients above 0.5.

The lowest correlation between the model and the satellite observation is in the northern Sahel region (latitude 13-14<sup>0</sup> North) (Figure 3-11).

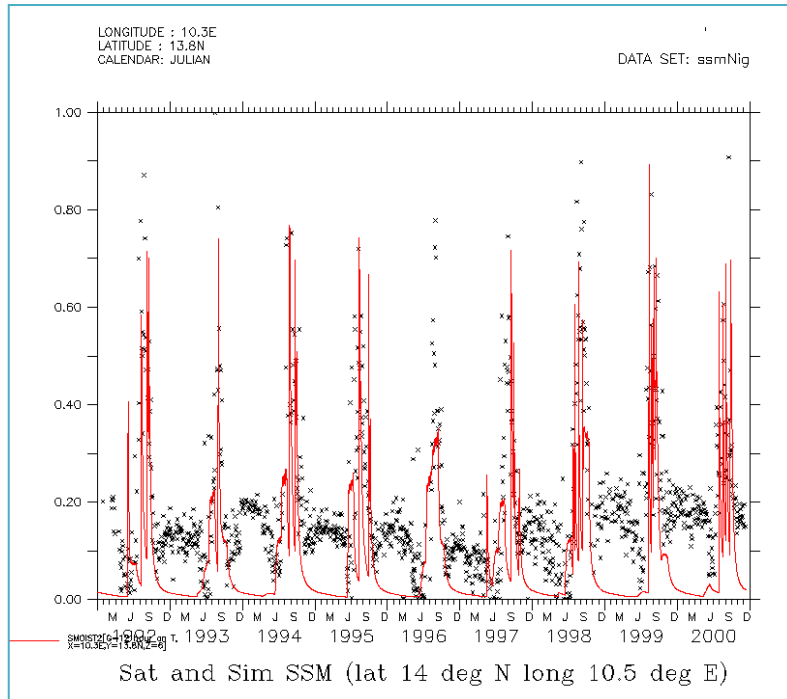


**Figure 3-11 Satellite SSM observations (black dots) plotted against simulation from experiment 2 in an area of lowest correlation in the Sahel part (Latitude 13-13.5<sup>0</sup> North, Longitude 10.5-11<sup>0</sup> East).**

\* In this plot satellite observation register values around 0.1-0.2 for SSM all year round despite the area being dry for most of the months and the soil is replenished with moisture only during short down pours.

Since the whole area normally experiences a strong latitudinal gradient in terms of moisture availability data from the same latitude were averaged and the same correlation procedure was repeated primarily to observe the differences in correlation at different latitudes. At half degree intervals the lowest values for all

correlations is 0.62 obtained in the Sahel region of latitude  $13.75^{\circ}$  North (Table 3-6).

**Table 3-5: Latitudinal correlation of ERS Satellite and predicted SSM from the 5 experiments**

<i>Latitude (degrees North)</i>	<i>Experiment 1</i>	<i>Experiment 2</i>	<i>Experiment 3</i>	<i>Experiment 4</i>	<i>Experiment 5</i>
13.75	0.62	0.62	0.62	0.62	0.62
13.25	0.68	0.71	0.68	0.68	0.68
12.75	0.82	0.78	0.78	0.78	0.82
12.25	0.84	0.82	0.81	0.81	0.84
11.75	0.86	0.85	0.86	0.86	0.86
11.25	0.86	0.86	0.86	0.86	0.86
10.75	0.86	0.87	0.86	0.86	0.86
10.25	0.85	0.85	0.84	0.84	0.85
9.75	0.83	0.83	0.83	0.83	0.83
9.25	0.86	0.87	0.87	0.87	0.86
8.75	0.84	0.85	0.84	0.84	0.84
8.25	0.79	0.80	0.78	0.78	0.79
7.75	0.75	0.77	0.75	0.75	0.75
7.25	0.78	0.8	0.78	0.79	0.78
6.75	0.78	0.79	0.78	0.78	0.78
6.25	0.76	0.76	0.76	0.76	0.76

The Kendall rank correlation is a non-parametric test that evaluates the similarities in order of two sets of measurements (Abdi, 2007). It was used to study the similarities between the ERS SSM product and the five experiments. The results of the pixel averaged Kendall correlation for SSM between the model prediction and the satellite product is provided in Table 3-7 below.

**Table 3-6: Kendall rank correlation of spatially and temporally averaged SSM**

	<i>ERS SSM</i>	<i>Experiment 1</i>	<i>Experiment 2</i>	<i>Experiment 3</i>	<i>Experiment 4</i>	<i>Experiment 5</i>
ERS	p-value<2.2e-16	p-value<2.2e-16	p-value<2.2e-16	p-value<2.2e-16	p-value<2.2e-16	p-value<2.2e-16
SSM	<i>tau=1.0</i>	<i>tau=0.62</i>	<i>tau=0.63</i>	<i>tau=0.62</i>	<i>tau=0.62</i>	<i>tau=0.62</i>

In order to observe the relationship between ERS and simulated SSM a scatter plot of ERS and predicted SSM from Experiment 5 is presented in Figure 3-12. Differences in the distribution of predicted SSM values in Experiment 2 where a separate  $\frac{1}{2}^\circ \times \frac{1}{2}^\circ$  soil data set was used, Experiment 5 which has the least similarities with Experiment 2, and the ERS satellite product SSM was plotted using an empirical distribution function shown in Figure 3-13.

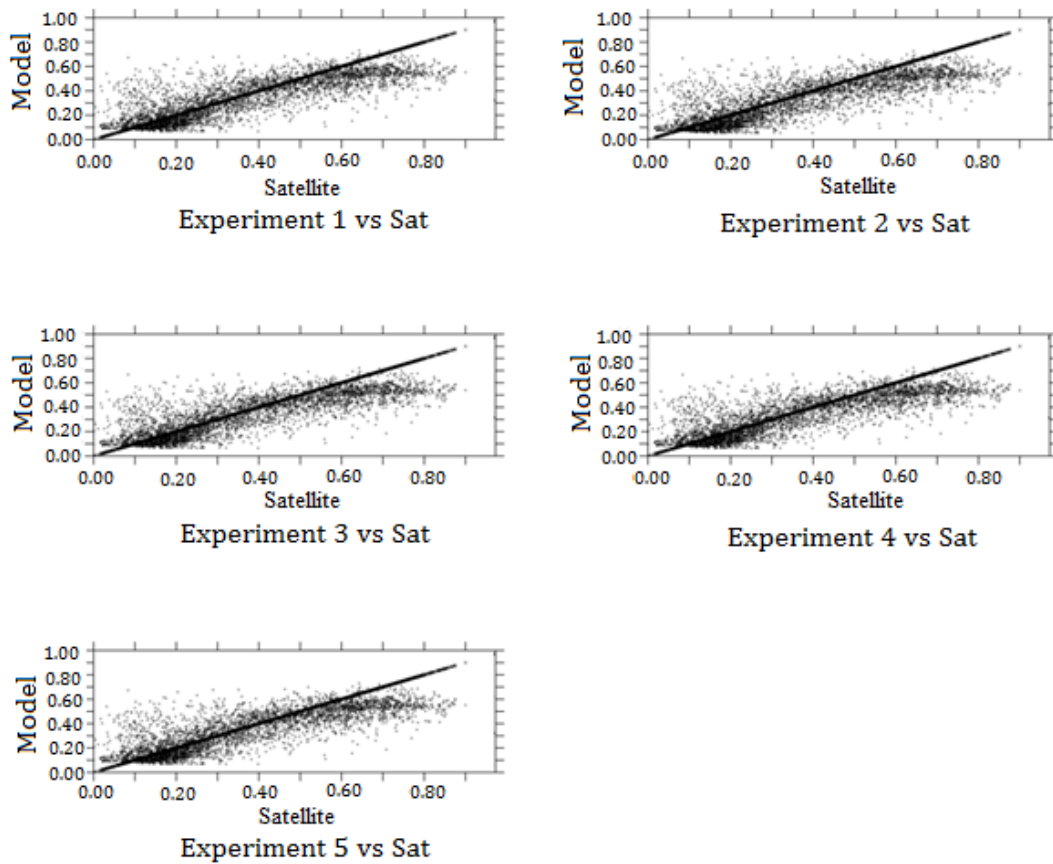


**Figure 3-12: Scatter plot of ERS scat and predicted SSM for Experiments 1 to Experiment 5**

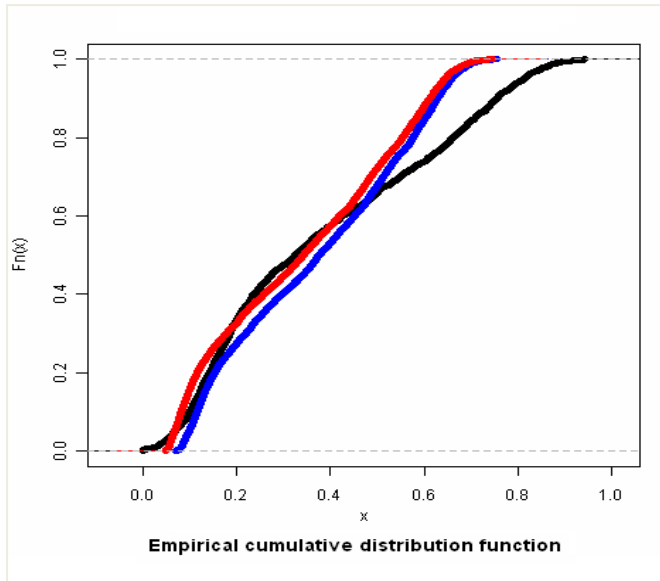


**Figure 3-13: The ECDF of SSM for ERS scat (black) Experiment 2 (red) and Experiment 5 (blue).**

\*ERS SSM has values from absolute 0 for dry soils to 1.0 for completely saturated soils. The experiments start with lower values above 0.

SSM anomalies were computed using the predicted SSM for Experiment 5 and the ERS Satellite product. This was carried out based on the issues raised by Koster *et al.* (2009) relating to the nature of soil moisture indexing and direct comparability between two soil moisture products. They argue that the differences in means and standard deviation of two different soil moisture indices should be recognised when comparing soil moisture products or transferring soil moisture produced from one model into another. And they further suggested correlating the anomaly indices of two soil moisture data. The equation for computing these anomalies is as follows (Koster *et al.*, 2009):

$$w' = (w - w_m)/\sigma_w \quad \text{Eq. [3-22]}$$

where  $w'$  is the anomaly,  $w$  is the time series of soil moisture,  $w_m$  is the mean, and  $\sigma_w$  is the standard deviation

Apart from the arguments made by Koster *et al.* (2009), in this study, the anomaly index is presumed to be a good means of studying periods of extreme deviation from the mean in the predicted SSM time series and useful for comparison with another data set that is thought to have similarities. The study compared the anomaly indices of ERS satellite and the predicted Experiment 5 SSM (Figure 3-14). Correlation coefficient of 0.12 was obtained between the two anomaly indices. However, after interpolating the predicted Experiment 5 and ERS satellite SSM data sets into monthly averages from 1992 to 2000, correlation of monthly anomaly indices between the two yielded much stronger correlation coefficients in the months during and after the wet season especially in the semi-arid part. Correlation coefficients of the anomaly index for 5 months at the onset of the wet season (June) in the semi-arid parts and the end of the wet season (October) in most parts of the study area are presented in Figure 3-15.

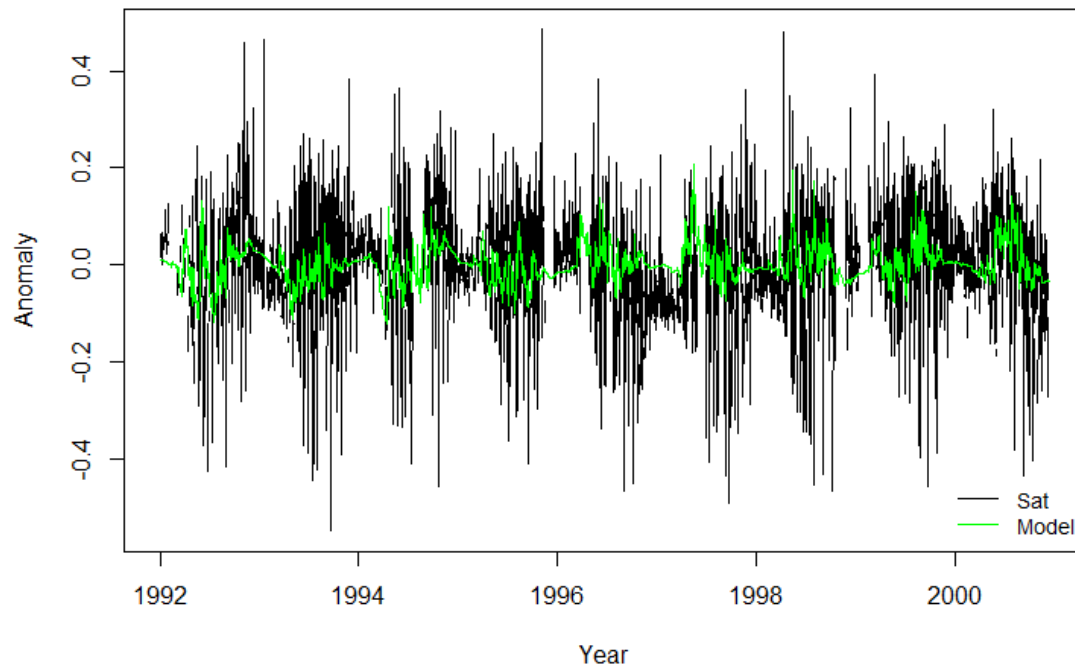


**Figure 3-14: Anomalies of SSM from ERS satellite (black line) and predicted Experiment 5 (green line) SSM**



**Figure 3-15 Monthly averaged anomaly indices between ERS satellite product and predicted Experiment 5 SSM for five months (June-October) from 1992-2000 (top) and monthly averaged anomaly indices between ERS satellite product and precipitation data (bottom).**

The satellite SSM monthly anomaly indices was also correlated with precipitation data used in driving the model also presented in Figure 3-15 (bottom plot).

Precipitation is known to be the major determinant of soil moisture variability in the Sahel. In this study there was an attempt to observe the strength of the relationship between predicted SSM and precipitation. Correlation of simulated soil moisture from the 5 experiments and precipitation produced correlation coefficients values ranging from 0.69 to 0.95 with Experiments 1 and 5, 0.72 to 0.96 for Experiments 3 and 4 and 0.75 to 0.96 for Experiment 2. Higher correlation coefficient values were obtained in some parts of the north of the study area for all the cases (Figure 3-16).

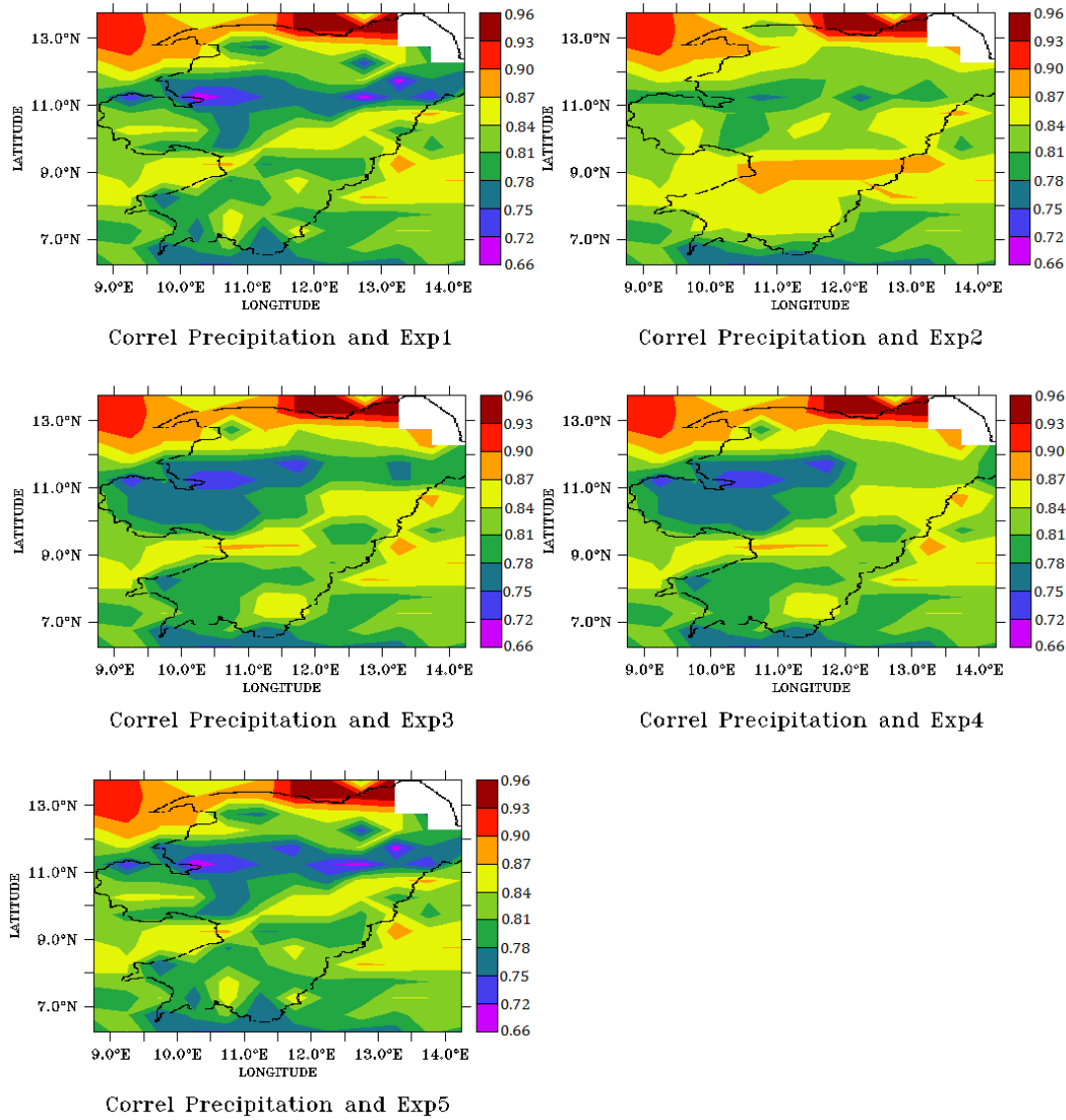


**Figure 3-16: Correlation coefficients between precipitation and predicted SSM for all 5 experiments**

\* the black line on the map is the border line of the study area

### 3.3.4 Land-surface conditions in the study area

Changes in energy, moisture and momentum fluxes on the land surface during the period under study were examined. To achieve this, least square regression of simulated SSM, net primary productivity, latent and sensible heat flux was computed for the two decades (1980-

2000). Plots of these simulated variables are presented (Figures 3-17). The Bowen ratio ( $B$ ) and the evaporative fraction ( $EF$ ) were also calculated from the energy fluxes using:

$$B = \frac{sh}{lh} \quad \text{Eq. [3-23]}$$

where  $sh$  is the sensible heat flux and  $lh$  represents latent heat flux both measured in  $\text{W m}^{-2}$

$$EF = \frac{lh}{lh+sh} \quad \text{Eq. [3-24]}$$

These two ratios give an insight into the energy fluxes from the surface and the contribution of the land surface to the lower atmosphere in the creation of convection currents and instability, mostly responsible for producing clouds and precipitation (Li *et al.*, 2010).

The daily evaporative fraction during the 21 year period (1980-2000) increased by 0.006 per Month (R-squared=0.026, p-value<0.05) while the Bowen's ratio decreased by -0.034 per Month (R-squared=0.02, p-value<0.05).

The 10 degree latitude was used to partition the study area into two regions: one south of the 10 degree line (sub-humid) and one north of the line (semi-arid) based on the prevailing climatic conditions over West Africa described by Lamb (1983). Trends in average grid box SSM are observed in each of the two parts of the study area (Figure 3-18). Daily trends in SSM increased in both the northern Semi-arid by a fraction of 0.003 per Month (R-squared=0.012, p-value<0.01) and southern Sub-humid by 0.03 per Month (R-squared=0.005, p-value<0.01) parts of the study area.

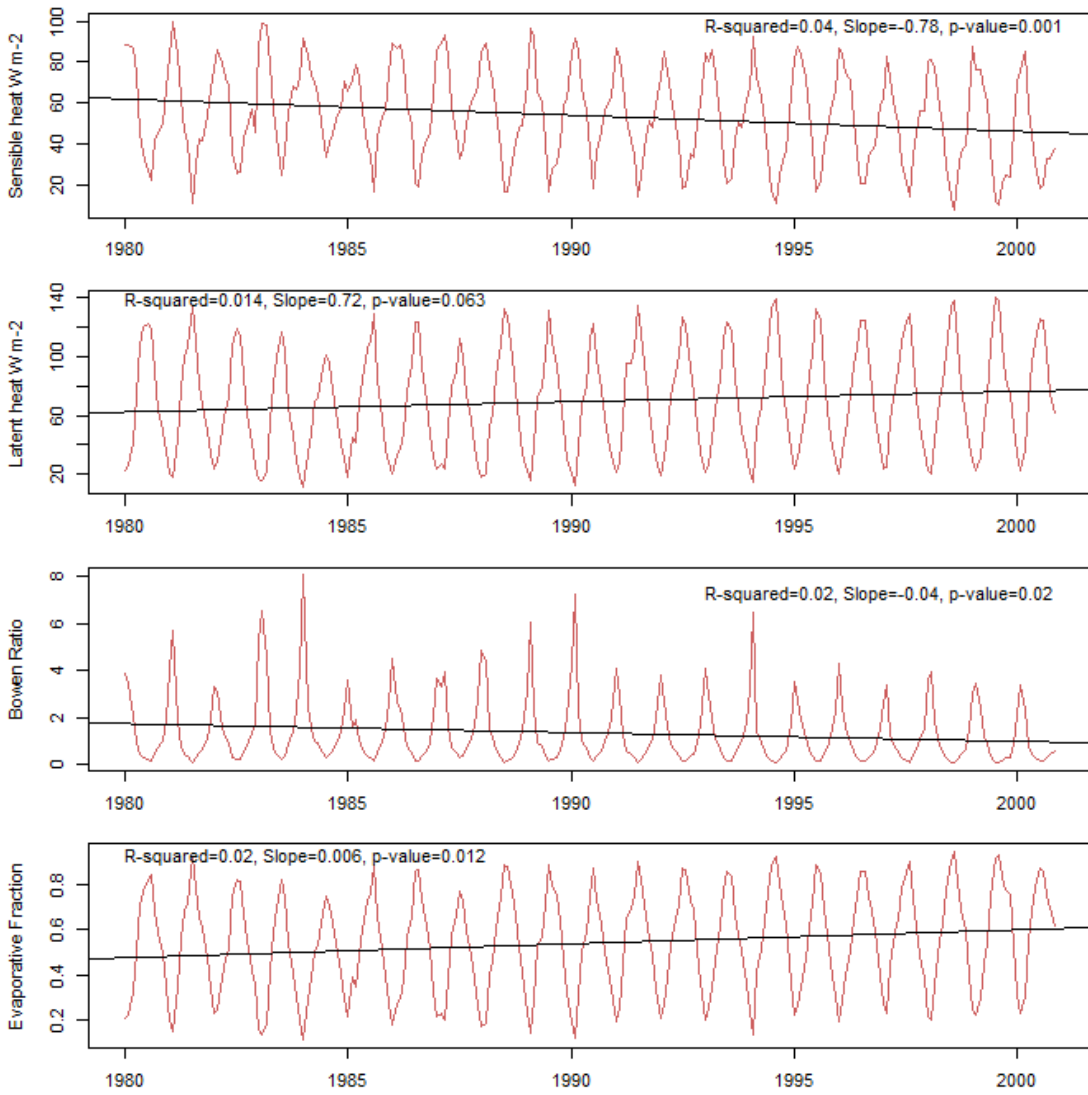


**Figure 3-17: Pixel averaged least squares regression line of predicted sensible heat, latent heat flux, Bowen's ratio and Evaporative Fraction for Experiment 5 plotted over a regression line**

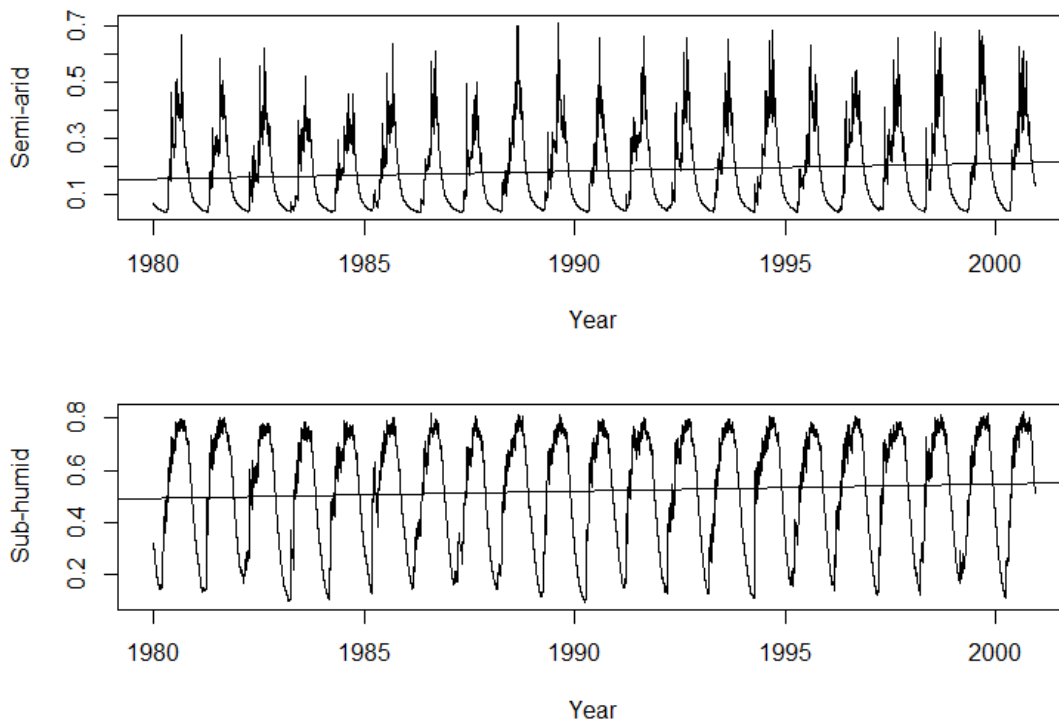


**Figure 3-18: Pixel averaged least squares regression for predicted Experiment 5 SSM plotted over a 21 year period**

Predicted Gross Primary Productivity (GPP) from Experiment 5 was used to assess the carbon status of the area in terms of whether it is a “source” or a “sink” throughout the period under study. There are annual variations in the GPP but it generally increased by 0.019 kg C m<sup>-2</sup> per year (R-squared=0.386, p-value<0.01) from the 1980 into the 1990s (Figure 1-19).

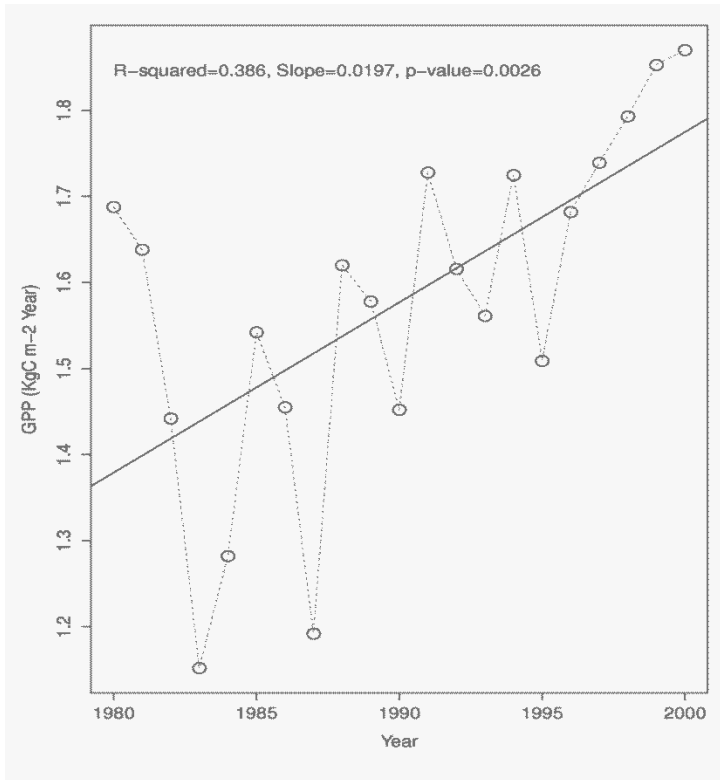


**Figure 3-19: Pixel averaged annual predicted GPP in kg C m<sup>-2</sup> yr<sup>-1</sup> from Experiment 5**

### 3.4 Summary

The aim of this study was to model land surface processes in the North-eastern Region of Nigeria using JULES. Three objectives were set to achieve this aim. The first objective of the study was to use two separate soil maps of the North-eastern Nigeria one of them was introduced into the model with the hope of increasing heterogeneity in model output of predicted soil moisture content. Arc GIS was used to geo-reference and digitize the map of the dominant soils in Nigeria into a 0.024<sup>0</sup> (2.4km) shape file of 16 soil textural classes later used to calculate soil hydrological parameters in Ferret based on four interpolation schemes to conduct four experiments with JULES. In the fifth experiment (referred to as Experiment 2) a separate ½<sup>0</sup> x ½<sup>0</sup> degree soil data set was used. Results of SSM, ST, and SR from each experiment were compared with results from other experiments using the statistical analysis

techniques of correlation, Student's t-test, Kolmogorov-Smirnov test and relative percentage error to determine the relationship between the results, the differences in their mean, the similarities in the distribution of values, and the percentage differences between them.

Despite variations in areas where the soil data was introduced there is a strong correlation for the results of predicted SSM between all experiments. The Student's t-test and Kolmogorov-Smirnov test suggest that differences in predicted soil moisture was significantly influenced by scale of the soil hydraulic input data rather than non-linearity in the interpolation of the hydraulic parameters. However, soil temperature is not significantly affected by these differences in SSM at the top 5cm soil layer. Results from the two statistical tests suggest no differences in soil temperature. Percentage error for soil temperature between the four other experiments and experiment 2 is very low (range of 9% to -17%) unlike for SSM. Variation in SSM and ST between experiments is widest during the dry season when moisture is low and temperature variations are high. The two statistical tests suggest a change in the mean of SR but no significant change in the mean.

The second objective set was to evaluate the five simulations of SSM compared with ERS Satellite SSM and precipitation. Spatial correlation, Kendall rank correlation, a scatter and empirical distribution function plot were used in analysing and presenting the data. A strong correlation between the satellite SSM observations and all five simulations was obtained between latitudes  $8.50^{\circ}$ - $12.75^{\circ}$  North which is an area of low vegetation interference for the satellite observations. A strong correlation of SSM between the model and the observations in this region suggests a good performance. The lowest value of the correlation coefficients between the satellite observations and the five simulations is obtained in the northern Sahel area  $13.75^{\circ}$ - $14.25^{\circ}$  North. The dominant soil type in this area is arenosols with high sand composition (see Table 3-1 and Figure 3-3). Soil size and surface roughness can affect satellite data dry regions. Results of the Kendal Rank correlation for the averaged pixel

values of SSM show Experiment 2 having the strongest correlation coefficients with satellite observations (correlation coefficient=0.63). The lowest correlation coefficient was between satellite observations and Experiment 5 (correlation coefficient=0.62) but the differences between the correlation coefficient was small (0.01).

The third objective of this study is to examine the changes in energy, moisture and momentum on the land-surface over time. Least square regression was used to achieve this objective. SSM responds to changes in precipitation and this was reflected in changes in precipitation in the 1980s and 1990s resulting in an increase in SSM as shown in the least square regression. Latent heat flux also increased in response to SSM and sensible heat steadily reduced. Modelled GPP was able to recover from the drought years of the 1980s and steadily increased in the 1990s.

Finally, the study was able to introduce heterogeneity in model output for SSM and to a certain degree on runoff as reflected in the t test and Kolmogorov-Smirnov test. However, the improvement in overall output cannot be ascertained because the correlation between the satellite observations and precipitation is higher with Experiment 2 than with the four other experiments in which the new soil data set was introduced. The model was able to successfully simulate changes in land-surface conditions in the region during the drought years of the 1980s and the ecosystems recovery as a result of the increased precipitation in the 1990s.

### **3.5 Discussions on modelling past land surface conditions**

#### **3.5.1 Testing the Land models sensitivity to changes in scale and non-linearity in the calculation of soil input parameters**

In the first stage of modelling land surface conditions in North-eastern Nigeria the study tested the sensitivity of the JULES model to changes in scale and soil input data. The reason for this was to identify the best means to improve model output. Comparing model output with observations and conducting sensitivity analysis are part of the model evaluation process (Smith and Smith, 2007; Hamby, 1994). The first step used to analyse the experiments described in Chapter 3 was to compare the relationship, the percentage error and differences among the modelled variables. Despite significant correlations between the 4 experiments and Experiment 2, variations between the experiments exist as can be seen in the plots of SSM and soil temperature in Figures 3-4, 3-5, 3-6, and 3-7. These variations reflect the heterogeneity introduced by the soil data used for simulating Experiments 1, 3, 4, and 5. Exploring the percentage error between the 4 Experiments and experiment 2 (Figure 3-8) indicates a seasonal variation where the differences increase during the summer when the moisture content in the soil is lowest and soil temperature is much higher but then reduces in the wet season when the soil moisture values are higher and soil temperature is low. This presupposes a moderating effect of SSM on soil temperature. Soil temperature in JULES is soil moisture dependent. The temperature of a layer of soil in the model is dependent on heat transfer and moisture fluxes into and out of the layer (Cox *et al.*, 1999; Essery *et al.*, 2001; Best *et al.*, 2011). In these experiments differences between predicted soil moisture and soil temperature for Experiment 2 and the other 4 experiments was much larger in the five layers (10 cm, 25 cm, 50 cm, 1 meter and 2 meters respectively) below the topmost 5 cm layer of the soil. The reason for the smaller differences in soil moisture and soil temperature at the top

5 cm layer could be that moisture and heat at the layer is partitioned into fluxes of heat and evapotranspiration. While, excess moisture on the surface is turned into run-off.

Differences in predicted SSM between the experiments contributed to changes in surface energy fluxes of latent and sensible heat flux. The difference in predicted energy fluxes between the experiments is similar to those obtained by Xue *et al.* (1996) after comparing two experiments conducted using the Simplified Simple Biosphere Model (SSiB) with each experiment using a different input data. They attributed the differences in predicted surface temperature of 2°K and latent heat flux of 25W m<sup>-2</sup> between the two experiments to the influence of soil parameters and leaf area index. Differences in predicted SSM between the 5 experiments in this study are an indication of the importance of “high-quality” soil input data for producing land surface conditions in modelling land surface-atmosphere interaction (Koster *et al.*, 2004).

### **3.5.2 Comparing model output of surface soil moisture with ERS satellite product**

The model is evaluated using satellite observations of SSM and precipitation. Direct correlation between satellite observation and the 5 model experiments was strong despite slight variations over space. There was also a strong correlation between the direct correlation between predicted SSM with precipitation and satellite SSM observation with precipitation.

However, this direct correlation between model soil moisture and a similar data set could be misleading as pointed out by Koster *et al.* (2009) and suggested a more appropriate means by comparing the time series of their normal standard deviates or the anomaly indices. In this study correlation between predicted and satellite SSM anomaly indices was strong for the months of June-October when all parts of the study area was under the influence of the West

African Monsoon with the exception of July which has a lower correlation. The strength of the correlation between predicted SSM and precipitation anomaly indices in most part of the study area especially in the semi-arid parts is similar to results obtained by Koster *et al.* (2004) suggesting that North-eastern Nigeria is an area of strong coupling between soil moisture and precipitation.

Previous studies of the relationship between precipitation and soil in areas with similar conditions within the West African sub region have recorded a strong correlation existing between the two phenomena (Wagner and Scipal, 2000; Zribi *et al.*, 2008). Precipitation has a strong influence on moisture in the region which is controlled by the West African Monsoon. It is responsible for the seasonal and spatial variation in SSM in the region and producing a latitudinal gradient. This may also explain the reason why correlation between precipitation and SSM is strongest in the Northern part of the area where moisture is limited the soil is only recharged with moisture during periods of short precipitation and quickly dries off afterwards (Figure 3-15 and Figure 3-16).

### **3.5.3 Trends in Land-Surface conditions in the study area 1980-2000**

Two decades (1980-2000) of changes to three land-surface conditions significant for terrestrial productivity were analysed using least squares regression. Regression for annual total SSM within this period indicates an increase for the whole study area (Figure 3-18). The increase in predicted latent heat flux and the reduction in sensible heat flux (Figure 3-17) seem to be a response to the changes in soil moisture since it is largely responsible for the partitioning of energy from the surface into latent and sensible heat. The Bowen ratio and the Evaporative Fraction were derived from the predicted energy fluxes. Increasing trends in the Evaporative Fraction is an indication of an increased contribution of moisture from the land

surface into the lower atmosphere, further increasing chances of convection and instability. The region experienced a drought in the early 1980s with below average rainfall for most of the decade. This was followed by decade of above average rainfall in the 1990s. The model was, therefore, successful in replicating this trend. Plants were also able to recover after the period of drought as there is an increase in total annual GPP (Figure 3-17). Variation in predicted GPP during the drought years from 1980-1990 was similar to the variations in remote sensed vegetative index observed by Tucker *et al.*, (1991) in the Sahel during the same period. These findings further strengthen the argument that the West African Sahel is able to recover from periods of drought whenever these years are accompanied by periods of relatively higher precipitation (Los *et al.*, 2006; Anyamba and Tucker, 2005).

## Chapter 4. Modelling land cover change in North-eastern

### Nigeria

#### 4.1 Introduction

Continuous monitoring and assessment of land cover change is an important prerequisite in the on-going study of the problems of global environmental change. Land use and land cover change (LUCC) is having a direct impact on biotic diversity, contributing to regional and global climate change, a source of soil degradation and by altering the ecosystem affects the productivity of the ecological system to support human needs (Lambin *et al.*, 2001). Changes to the surface albedo as a result of LUCC postulated by Charney *et al.* (1977) created an awareness of the link between LUCC and climate change. The driving forces related to LUCC are numerous and vary in time and space but there is a general adoption of two broad categories social and biophysical (Dolman *et al.*, 2003). Social drivers relate LUCC to economic factors of demand for particular land uses, population changes and land holding systems, including culture and administrative policies. Biophysical driving forces include climatic, soil and topographic factors. These factors vary in time and space and work together to determine changes in the land cover. Mortimore *et al.* (2005) puts a global and regional dimension to the social driver of LUCC; further explaining that while regional drivers are affected by local administration and social organizations global drivers are controlled by global markets and international corporations. Land cover modification is often driven by climate change while land use change is driven by a combination of factors such as resource scarcity which increases the pressure on resources through increase in production, markets created by increasing opportunities, changes in social organisation and attitudes, and policy interventions (Lambin *et al.*, 2003).

Land use (LU) and land cover (LC) are two distinctive terms that are closely related (Riebsane *et al.*, 1994). A simple meaning of land use is put forward by Dolman *et al.* (2003) “a purpose for which land is put to use”. While, Ellis and Pontius (2007) defined land cover as “the biological and physical cover over the earth surface”. The earth surface in many parts is covered by vegetation of various types, water bodies, and the human built environment or in some parts exposed bare surfaces. Land is transformed by man and put to use for various purposes such as agricultural, residential, lumbering or industrial. Changes in LU affect LC and changes in LC also affects LU but the changes in either of these may not necessarily be the product of the other (Riebsane *et al.*, 1994).

In West Africa LUCC in the last 50 years has been primarily a result of cropland expansion driven by an increasing demand for food to satisfy the rapidly growing population (Ramankutty, 2004) but within a global context these changes are also a response by the population to economic opportunities mediated by international markets (Lambin *et al.*, 2001). This explains the increase in plantations and croplands in the region at the expense of the forest and savannas. In North-eastern Nigeria the rapid agricultural expansion in the last century was accompanied by the transformation of many parts of the savanna woodlands into naturally regenerating fallows (Mortimore *et al.*, 1999). The significant LUCCs in recent years have been attributed by some authors like Charney (1975) as responsible for the changes in the climate and the re-occurrence of drought in the West African Region although this assertion is contentious. Taylor *et al.* (2002) assessed the impact of LUCC on the climate of the region using a general circulation model driven by results of land cover change obtained from a land use model. Their findings indicate that changes in LC causes a later onset of the wet season as a result of a reduction in rainfall for the month of July.

Despite the availability of global LUC data there have been only been two attempts made within Nigeria to produce an inventory and asses the changes in North-eastern Nigeria. The

Nigerian Radar (NIRAD) project 1976 was the first attempt undertaken to produce a land cover map of Nigeria. The project used images obtained from the Side Looking Airborne Radar (SLAR) for a cloud free and dust free coverage (Parry and Trevett, 1979). This was followed by the Forestry Management Evaluation and Coordinating Unit (FORMECU) project undertaken by GEOMATICS International Canada in 1996 to assess the Vegetation and LU changes in Nigeria between 1976/78 and 1993/95. This project used a combination of remote sensing images obtained from Landsat multispectral, SPOT multispectral, Land TM, ERS-1 Radar, AVHRR, and JERS-1 Radar (Ademiluyi *et al.*, 2008). Subsequently, other studies have focussed on assessing small segments within the North-east region such as the works of Garba (2007). Most of these studies only attempted to provide an assessment of the LUCC using two or more images of different time periods without attempting to carry out a projection of future changes. This study attempts to bridge this gap. In addition to analysing the trends in LUCC in the region over a period of three decades this study also attempts to produce a spatially explicit projection of land cover for 2046 using the Cellular-Automata Markov Model. The projected LC map was used as forcing data to simulate future land surface conditions of the study area based on the A2 IPCC climate scenario using the Met Office Land surface model JULES (Joint UK Land Environment Simulator).

#### **4.1.1 Limitations**

Because the study intended to cover the entire area of North-eastern Nigeria a decision was made to use readily available LU and LC data from the FORMECU and GLOBCOVER data sets . This may prove to be a short coming of the study but it also enables the objectives to be achieved within the available time and resources.

## **4.2 Methodology**

The study aims to achieve its objectives by acquiring secondary data and making analysis within a GIS environment. Since the data sets to be used were in a spatial format it became a preference for the study to source all the data required in a digital format. The stages of developing the methodology and executing the study are presented in Figure 4-01.

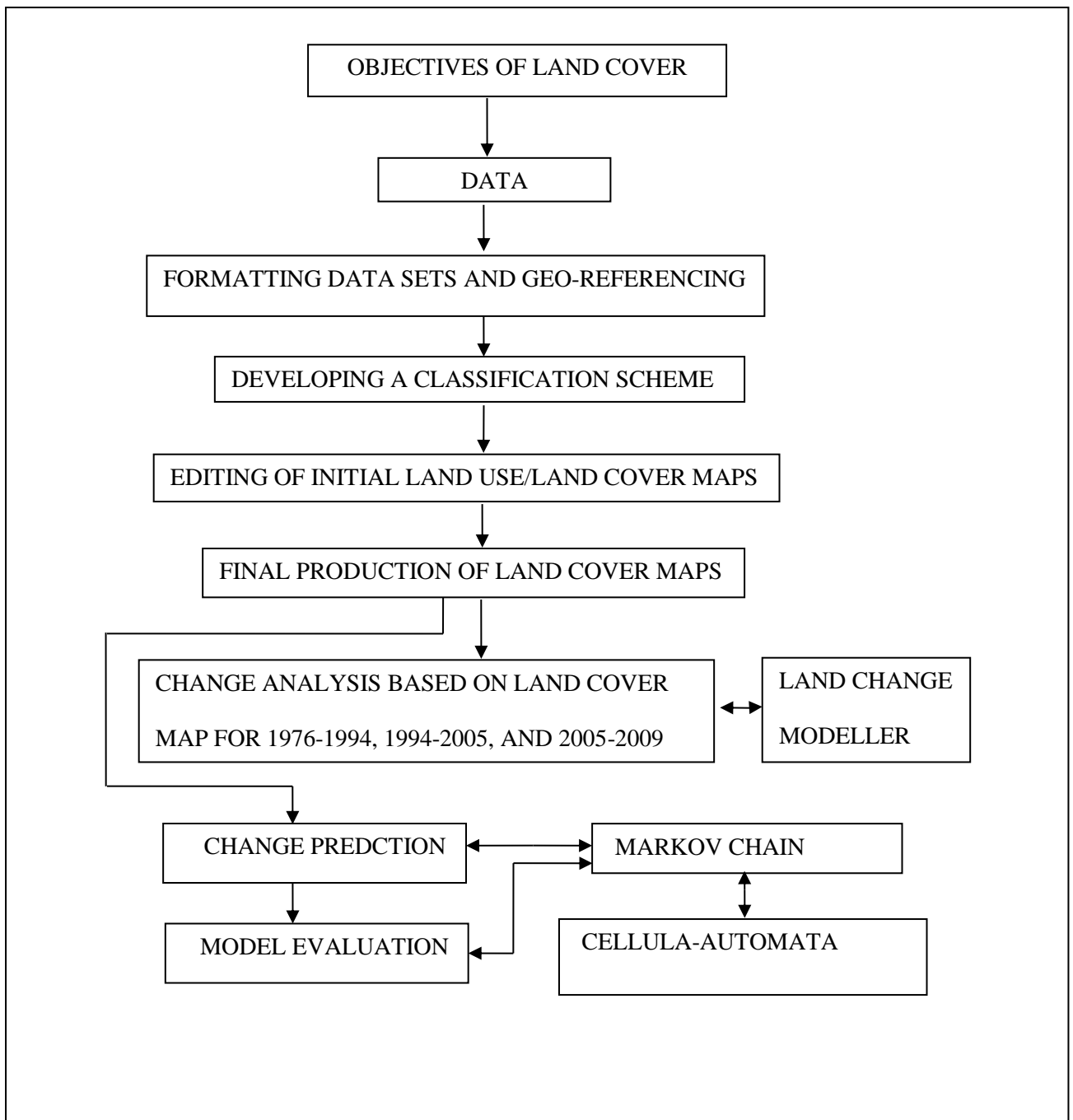


**Figure 4-1: Research flow chart for Chapter 4**

#### **4.2.1 Data Acquisition**

The data used for the study was sourced from the Nigeria FORMECU project of 1996 and the GLOBCOVER 2006 and 2009 projects. These include LUCC polygons for 1976/78 and

1993/95 from the FORMECU project and the 2004/06 and 2009 land cover images from the GLOBCOVER Projects in the form of tagged image file format (TIFF) files accompanied by land cover legends in an Arc GIS layer file format. A description of the FORMECU project was provided earlier at the Introduction section of this chapter and details of the shortcomings of the project is provided by Ademiluyi *et al.* (2008). The GLOBCOVER project uses MERIS multi spectral imager on board the ENVISAT satellite launched in 2002 to produce 300 meter resolution global land cover maps for 2004/2006 and 2009 (Bicheron *et al.*, 2005; Bontemps *et al.*, 2011). Land cover classification is based on the United Nations classification scheme consisting of 22 classes representing the entire global land cover types. These data sets can be downloaded from the European Space Agency (ESA) website including the “read me” files and validation report. Other data sets used include a shape file of North-eastern Nigeria digitized from a geo-referenced political boundary map of Nigeria.

#### **4.2.2 Data Analysis Techniques**

The platforms used for data processing and analysis include Arc Map and Arc Catalogue, ERDAS Imagine and IDRISI Taiga version 16.

The main analysis techniques used for the study is The Markov Chain Analysis and Cellular Automata (CA) –Markov model. The CA-Markov model is a simple method of predicting future changes in land cover by comparing changes in the past (Garcia-Frapoli *et al.*, 2007). Given two maps the Markov model outputs a transition probability matrix, transition area matrix, and a set of conditional probability images. The probability of one pixel changing from one class to another over a projected period is provided by the transition probability matrix. The transition area matrix gives the number of pixels that could change from one class to another over a projected period while, the conditional probability images indicate the

probability of a given class being in each of the pixels. The CA-Markov Model uses the contiguity rule where the nearest cell to LC type A is more likely to change to LC type A. The proximity of the a cell to LC type A is user defined and can be assigned using a 3 x 3, 5 x 5, and 7x 7 filter. However, this rule largely depends on the number cells containing LC type A. The more the number of cells containing A the more likely that a neighbouring cell will be converted to LC type A. The method used on the model in this study is solely based on past trends of LCC and does not to account for either anthropogenic or physical disturbances that may alter this trend. Despite these short comings CA-Markov model is useful where the data concerning the process causing the changes is limited or not existent.

Percentage difference of a LC type based on two images at different times was calculated using the following equation:

$$LCA\% = \left( \frac{PLCA - RLCA}{PLCA} \right) 100 \quad \text{Eq. [4-1]}$$

where LCA% is the percentage change in area for LC type X, PLCA is the previous area for LC type X and RLCA is the most recent area for LC type X.

### **4.3 Results**

The shape file of North-east Nigeria was used to delineate the area of interest in the 1976/78 and 1993/95 FORMCU LUC shape files of Nigeria on the Arc Map platform to produce the LUC of North-east Nigeria for the two periods. In view of the format and size of the GLOBCOVER data sets the area of interest was delineated on the ERDAS Imagine version 10 classic interface platform using the subset tool in the data preparation menu. The FORMECU data set and GLOBCOVER have different classification schemes. In order to consolidate the two different classifications the JULES classification scheme was adopted. This was in line with one of the two objectives of the study that is producing a projected land cover map of the study area for 2046 to be subsequently used as forcing data to simulate

future land surface processes in JULES. Therefore, the 32 classes in the FORMECU LUC maps and the 14 classes identified in the study area out of the 22 classes in the GLOBCOVER land cover maps were reclassified into 7 classes. The JULES land cover classes consist of five vegetation tiles and four non-vegetation types. Within the study area there are 7 land cover types including four vegetation cover types and three non-vegetation types. Codes and values used for the classification are provided in Table 4-1, Table 4-2 and Table 4-3. The reclassified maps for the four separate years (1977, 1994, 2005, and 2009) are presented in Figure 4-2.

**Table 4-1: LC classes and the JULES LC code assigned to each class**

<b>Value</b>	<b>LC type</b>	<b>Code</b>	<b>New Value</b>
<b>1</b>	Broad leaf evergreen, deciduous Trees	BT	1
<b>2</b>	Needle Leaf evergreen , deciduous Trees	NT	
<b>3</b>	Carbon 3 Grass	C3G	2
<b>4</b>	Carbon 4 Grass/Crops	C4G	3
<b>5</b>	Shrub lands, bush land, and transitional areas	Shrubs	4
<b>6</b>	Urban/Artificial	Urban	5
<b>7</b>	Lakes and other water bodies	Lake	6
<b>8</b>	Soil/bare surfaces	Soil	7
<b>9</b>	Ice	Ice	

**Table 4-2: Reclassification of the 32 FORMECU LC classes for the 1977 and 1994 LUC maps into 7 LC classes**

<i>Code</i>	<i>Description</i>	<i>JULES Code</i>	<i>New Value</i>
11	Major Urban	Urban	5
12	Minor Urban	Urban	5
22	Rainfed arable Crop Plantation	C4G	3
23	Floodplain Agriculture	C4G	3
24	Irrigation Project	C4G	3
25	Agricultural Tree Crop Plantation	BT	1
26	Livestock Project	Urban	5
31	Grassland	C3G	2
32	Discontinuous grassland dominated by grasses and bare surface	Shrub	4
33	Montane grassland	C3G	2
41	Dominantly trees/woodlands/shrubs with a subdominant grass component	BT	1
42	Dominantly shrubs and dense grasses with a minor tree component	Shrub	4
43	Dominantly grasses with discontinuous shrubs and scattered trees	C3G	2
51	Disturbed Forest	BT	1
52	Undisturbed Forest	BT	1
53	Riparian Forest	BT	1
54	Forest Plantation	BT	1
55	Montane Forest	BT	1
62	Graminoid/Sedge Freshwater Marsh	Lake	6
63	Shrub/Sedge/Graminoid Freshwater Marsh/Swamp	Shrub	4
71	Natural Waterbodies: Ocean,River,Lake	Lake	6
73	Canal	Lake	6
74	Reservoir	Lake	6
81	Rock Outcrop	Soil	7
82	Sand Dunes/Aeolian	Soil	7
83	Alluvial	Soil	7
84	Gullies	Soil	7
85	Mining Areas	Soil	7
211	Intensive (row crops, minor grazing) Small Holder Rainfed Agriculture	C4G	3
212	Extensive (grazing, minor row crops) Small Holder Rainfed Agriculture	C3G	2
213	Extensive Small Holder Rainfed Agriculture with Denuded Areas	C4G	3

541	Teak/Gmelina Plantation	BT	1
-----	-------------------------	----	---

**Table 4-3: Reclassification of the 15 GLOBCOVER LC classes for the 2005 and 2009**

**LUC maps into 7 new classes**

<i>Code</i>	<i>Description</i>	<i>JULES Code</i>	<i>New Value</i>
0	No data		0
14	Rainfed croplands	C4G	3
20	Mosaic croplands/Vegetation	C4G	3
30	Mosaic Vegetation/croplands	C3G	2
40	Closed/open broadleaved evergreen semi deciduous forest	BT	1
60	Open broadleaved deciduous forest	BT	1
110	Mosaic forest/shrub land/grassland	BT	1
120	Mosaic grassland/forest/shrub land	C3G	2
130	Closed/open shrub land	Shrub	4
140	closed/open grasslands	C3G	2
150	sparse vegetation	Shrub	4
180	closed/open vegetation regularly flooded	Lake	6
190	Artificial areas	Urban	5
200	Bare areas	Soil	7
210	Water bodies	Lake	6

Editing of the classes was carried in Arc GIS and the final land cover maps transferred into Idrisi Taiga and geo-referenced using the UTM 33 coordinate system. Change analysis was carried out using the Idrisi land change modeller (LCM) in order to determine the trends in land cover change between 1976 and 2009. This was achieved by comparing the land cover maps of 1976 and 1994 and between 1994 and 2005 and 2005 and 2009.

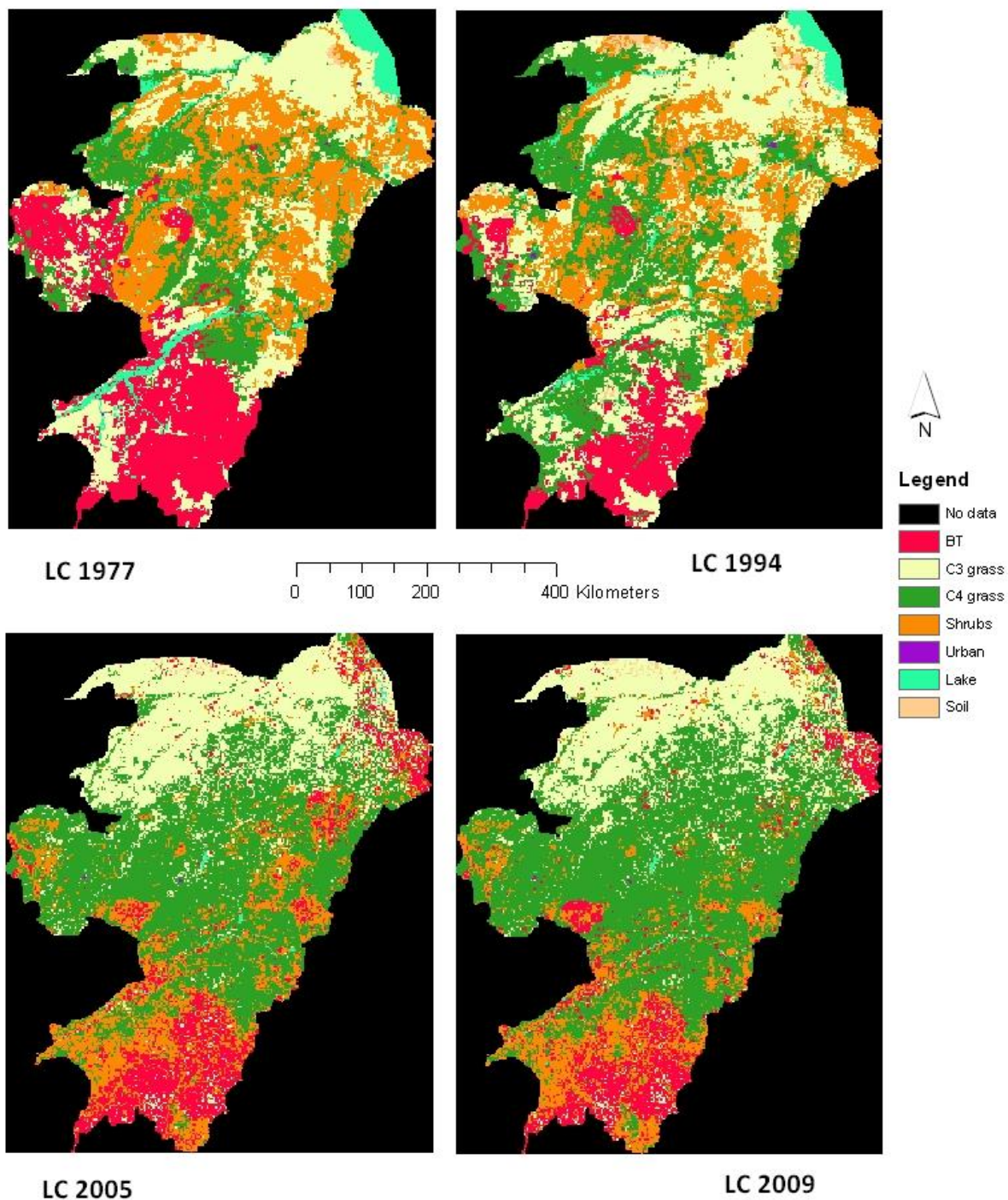


**Figure 4-2: Reclassified LC for 1977, 1994, 2005 and 2009 using the JULES LC classification scheme**

Over the period between 1977 and 1994 (Figure 4-3 and Table 4-4) croplands classified as C4 Grass in this study increased by 26719.11 km<sup>2</sup> or by 51.3% of its previous size, grasslands increased by (C3 grass) 15792.12 km<sup>2</sup> (20.8%) and soil (bare surfaces) increased by

5497.81km<sup>2</sup> (438.4%). Urban areas represent only 0.085% of the study area, had the largest increase rate of 106.3%. During the same period broad leaf trees (BT) representing forest and deciduous woodlands lost an area of 28975.6km<sup>2</sup> (or 48% of its previous size). Lakes and other water bodies lost 4908.75km<sup>2</sup> (-36.9%).

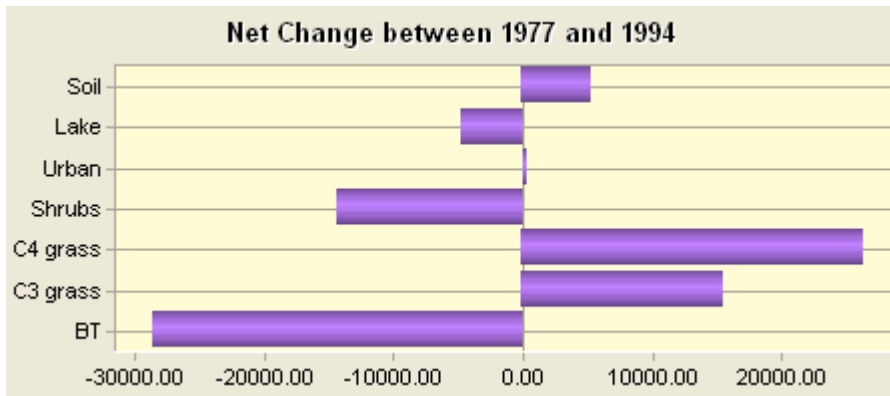


**Figure 4-3: Changes in LC 1977 to 1994 gains and losses for each class in km<sup>2</sup>**

Between 1994 and 2005 (Figure 4-5) C4 grass cover increased by 40422.7km<sup>2</sup> (51.3%) and broad leaf trees (BT) by 4639.89 km<sup>2</sup> (14.9%). The size of other classes decreased during this period especially C3 grass which decreased by 20689.8km<sup>2</sup> (22.5%) and Urban areas decreased by 390.4km<sup>2</sup> (80%).

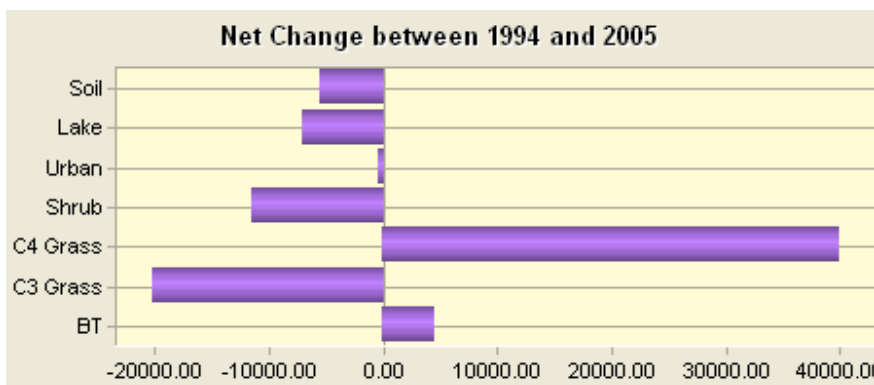


**Figure 4-4: Changes in LC 1994 to 2005 gains and losses for each class in km<sup>2</sup>**

**Table 4-4: Magnitude of LCC between the year 1977 to 1994**

	<b>LC 1977 Area in km<sup>2</sup></b>	<b>Area in percentage</b>	<b>LC 1994 Area in km<sup>2</sup></b>	<b>Area in percentage</b>	<b>Difference in km<sup>2</sup></b>	<b>Percentage difference</b>
<b>BT</b>	60191.19	21.69598	31215.57	11.25169	-28975.6	-48.1393
<b>C3</b>	75997.71	27.39345	91789.83	33.08574	15792.12	20.77974
<b>C4</b>	52053.68	18.76281	78772.8	28.39374	26719.11	51.32992
<b>Shrubs</b>	74393.18	26.8151	60017.14	21.63324	-14376	-19.3244
<b>Urban</b>	236.5689	0.085271	487.927	0.175874	251.3582	106.2516
<b>Lake</b>	13303.72	4.79534	8394.968	3.025975	-4908.75	-36.8976
<b>Soil</b>	1254.125	0.452051	6751.936	2.433743	5497.811	438.3782

**Table 4-5: Magnitude of LCC between the year 2005 and 2009**

	<b>LC 2005 Area in km<sup>2</sup></b>	<b>Area in percentage</b>	<b>LC 2009 Area in km<sup>2</sup></b>	<b>Area in percentage</b>	<b>Difference in km<sup>2</sup></b>	<b>Percentage difference</b>
<b>BT</b>	35855.47	12.92	30999.83	11.17	-4855.64	-13.54
<b>C3</b>	71100.03	25.63	68160.81	24.57	-2939.21	-4.13
<b>C4</b>	119195.5	42.97	135573.5	48.87	16378.01	13.74
<b>Shrubs</b>	48737.38	17.57	40480.84	14.59	-8256.54	-16.94
<b>Urban</b>	97.56	0.04	104.50	0.038	6.95	7.12
<b>Lake</b>	1238.87	0.45	1023.74	0.37	-215.13	-17.37
<b>Soil</b>	1198.38	0.43	1079.95	0.39	-118.44	-9.88

The magnitude of changes in land cover between 2005 and 2009 (Table 4-5, and Figure 4-5) is dominated by an increase in the C4 grass class by 16378.0 km<sup>2</sup> (13%) and Urban areas by 6.9km<sup>2</sup> (7%). Shrubs and areas of transition decreased by 8256.5 km<sup>2</sup> (17%) and the BT class decreased by 4855.64 km<sup>2</sup> (13.5%).

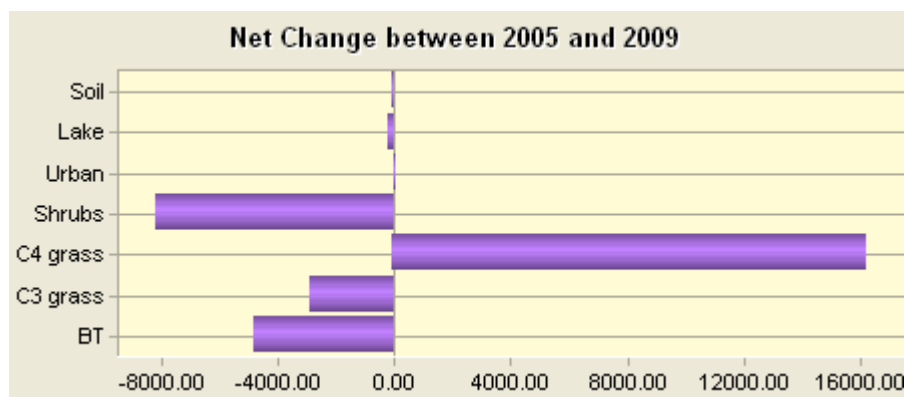


**Figure 4-5: Changes in LC 2005 to 2009 gains and losses for each class in km<sup>2</sup>**

In the 1976 LUC map grasslands (C3 grass) were the most dominant land cover type (27.4%) then shrub lands (26.8%) followed by forest and wood lands (21.7%). Croplands classified as C4 Grass in this study is the major recipient of LCC. In 1977, 18.8% of the area was covered by croplands. However, this increased to 28.4% in 1994, 42.9% in 2005 and 48.9% in 2009 (Table 4-5) more than doubling in size within the period of 32 years. In 2009 forest and woodlands (BT) represented only 11% of the LC, 10% less than in 1977 and lakes and water bodies covered only 0.4% compared to 4.8% in 1977.

Conversion between the LC classes was analysed using the LCM in order determine the nature of the changes and the transition that has taken place between 1977 -1994 and 2005-2009 (Figures 4-6 and 4-7). Between 1977 and 1994 the major conversion in LC was the transition from shrubs to C3 grass and the transition from C3 grass to C4 grass accounting for 17% and 15% of the LCC during the period. There was also an 8% transition from C4 grass

to C3 grass. Conversion of the BT (forest and woodlands) LC class included the transition into C3 grass class (13%), C4 grass (7%) and shrubs (6%). Major loss of lake cover was a result of the transition to C4 grass (4%). The transition from other LC classes into C3 and C4 grass accounted for over 80% of all land conversion. Between 2005 and 2009 the major LCC included the conversion of shrubs to C4 grass (20%), BT to shrub (17%), C3 grass to C4 grass and shrubs to BT (12%). Conversion of other LC classes to C4 grass accounted for more than 38% of the total LCC, shrubs 24%, and conversion to BT accounted for 18%.

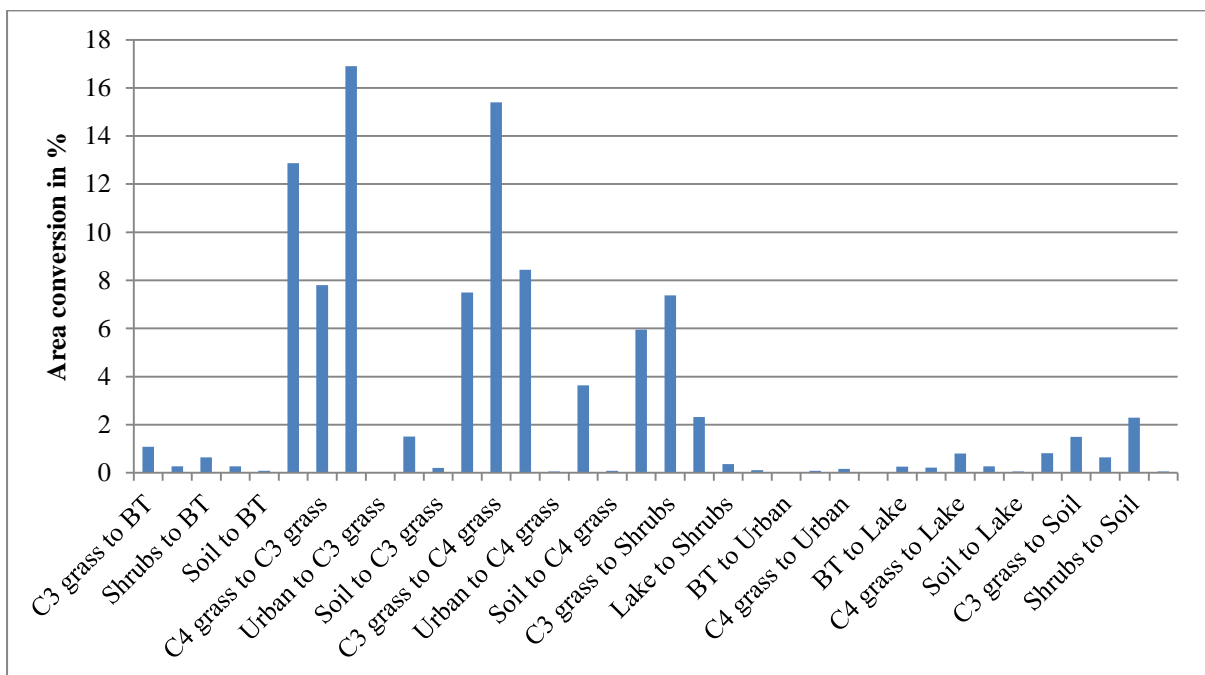


**Figure 4-6: Bar chart of LC conversion from 1977 to 1994**

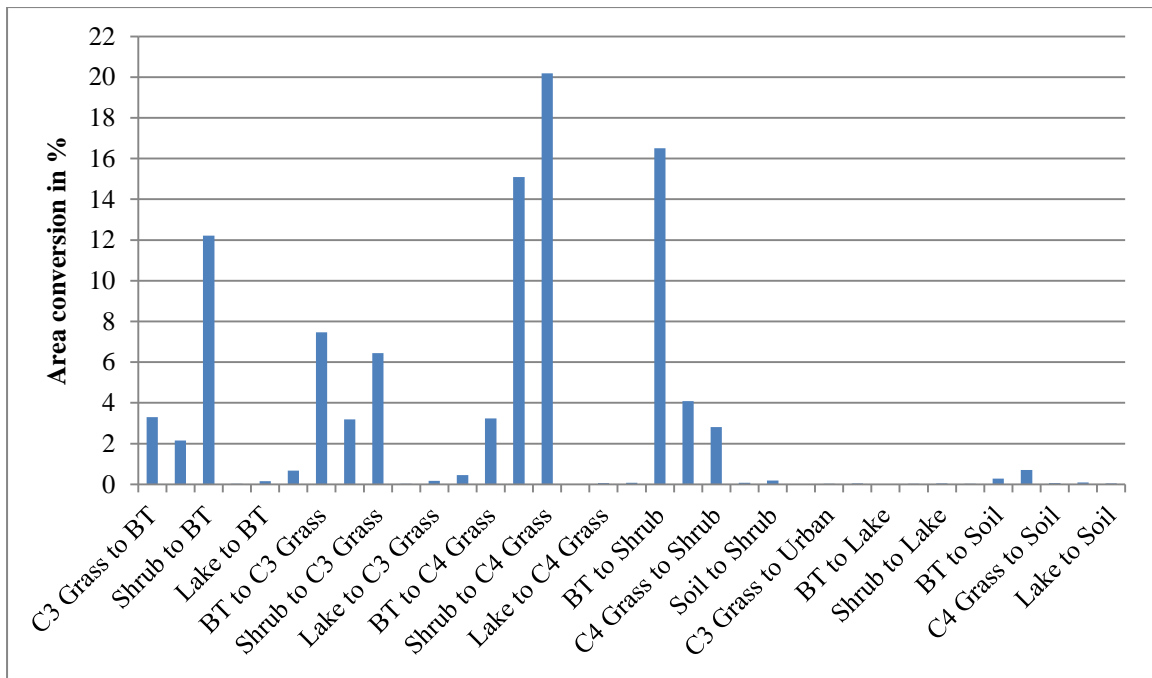


**Figure 4-7: Bar chart of LC conversion from 2005 to 2009**

To produce a projected LC map for 2046 the Markov chain analysis was adopted in producing a transition area matrix, transition probability matrix and conditional probability image for each LC class using the LC maps of 2005 and 2009. These three inputs were used in running the CA-Markov model using the 5 x 5 contiguity filter (explained earlier in the methodology section), where conditional probability images served as the transitional suitability image collection (Figures 4-8 and 4-9). The LC projection for 2046 presented in Figure 4-11). It shows C4 grass covering an area of 200450.4km<sup>2</sup> (72.3%) and C3 grass covering an area of 42018.65km<sup>2</sup> (15.2%). In order to validate the model, the same process was repeated using the LC maps of 1994 and 2005 to simulate LC of 2009 (Figure 4-12). The differences in the LC classes between the 2009 map and the projected map is less than 17% or more than 83% in similarity for six of the seven LC classes except for the Lake cover class which has a 33.2% difference (Table 4-7).

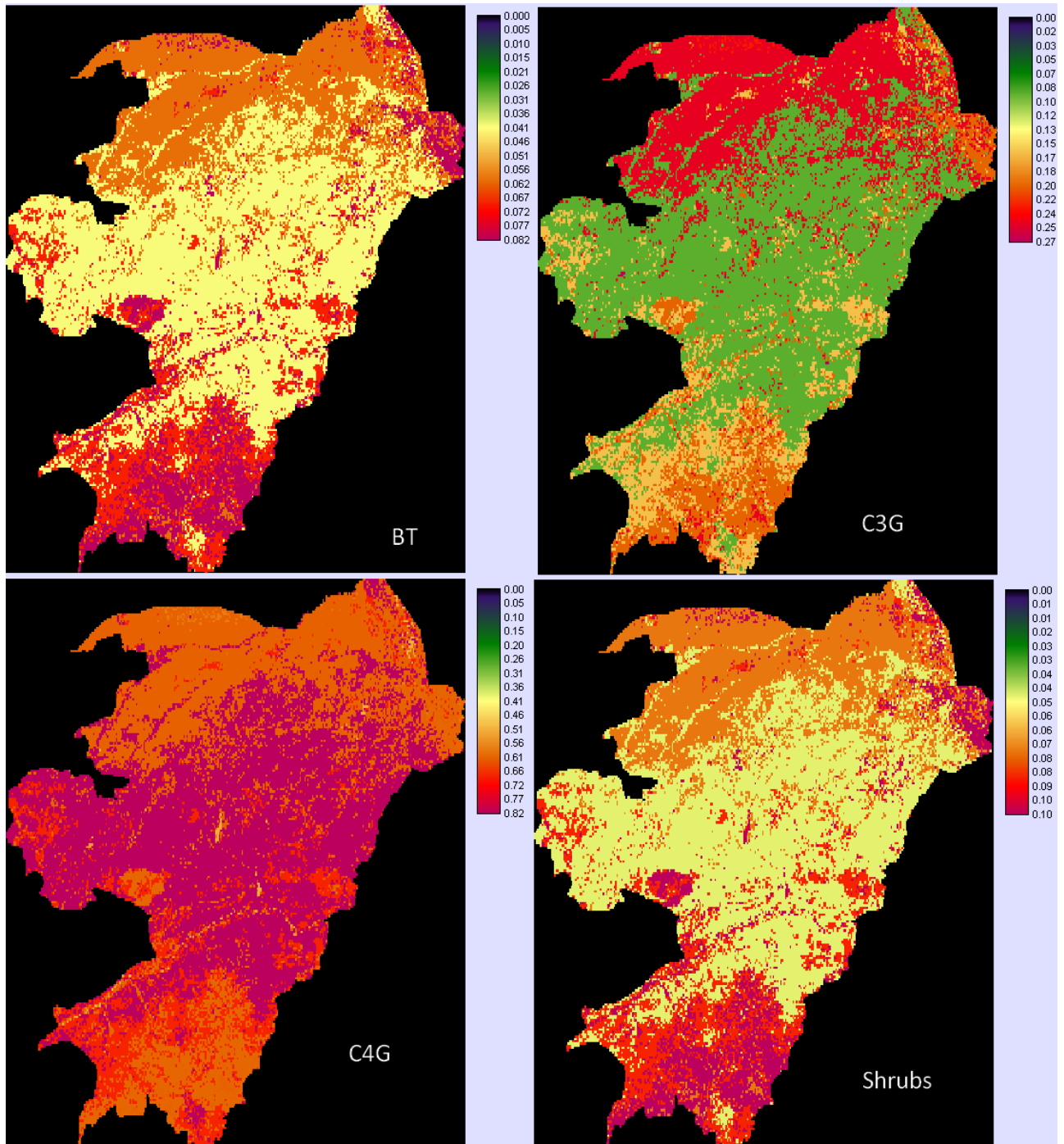


**Figure 4-8: Markov chain analysis conditional probability of being one the seven LC classes**

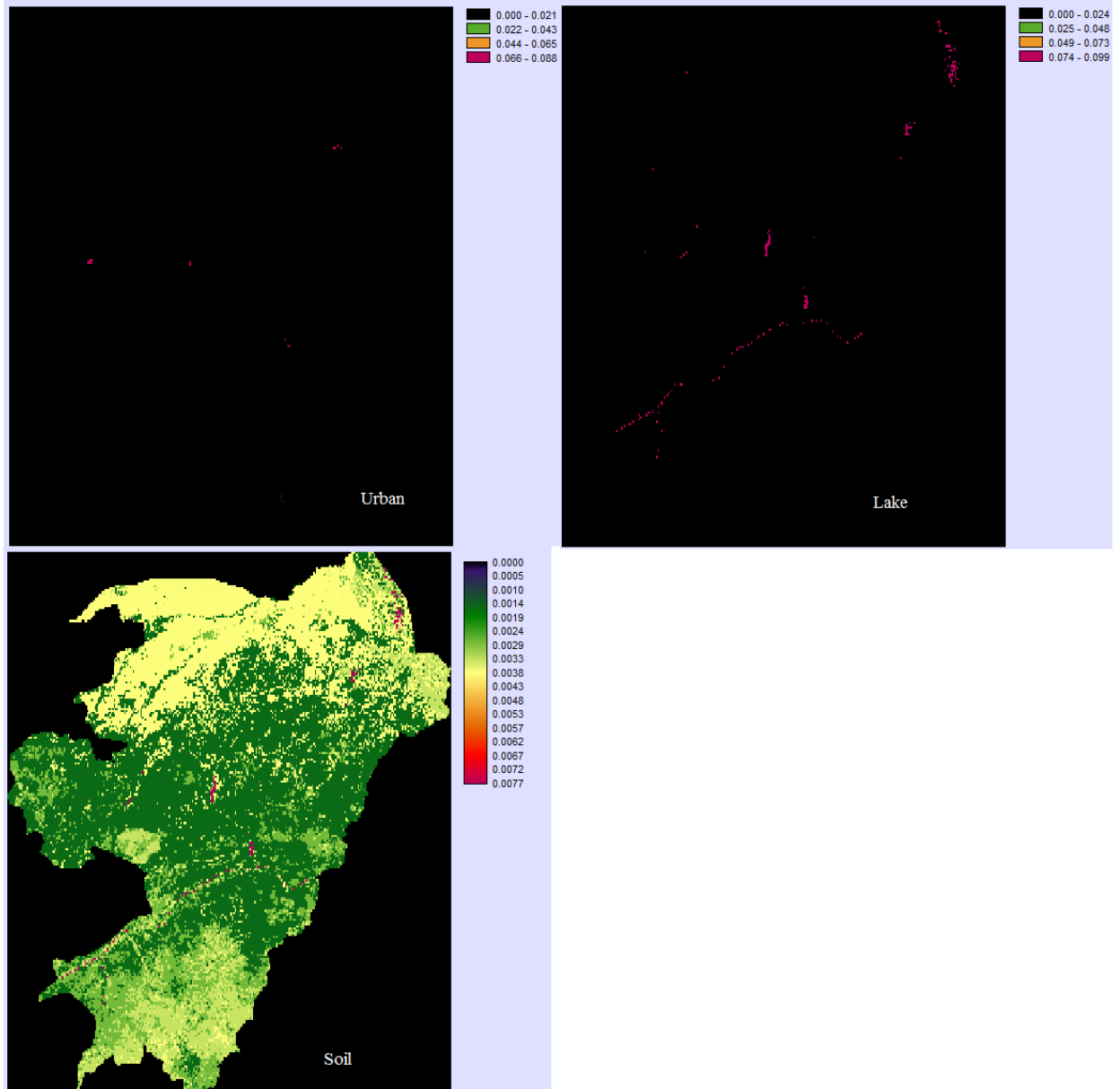


**Figure 4-9: Markov chain analysis conditional probability of being one the seven LC classes**

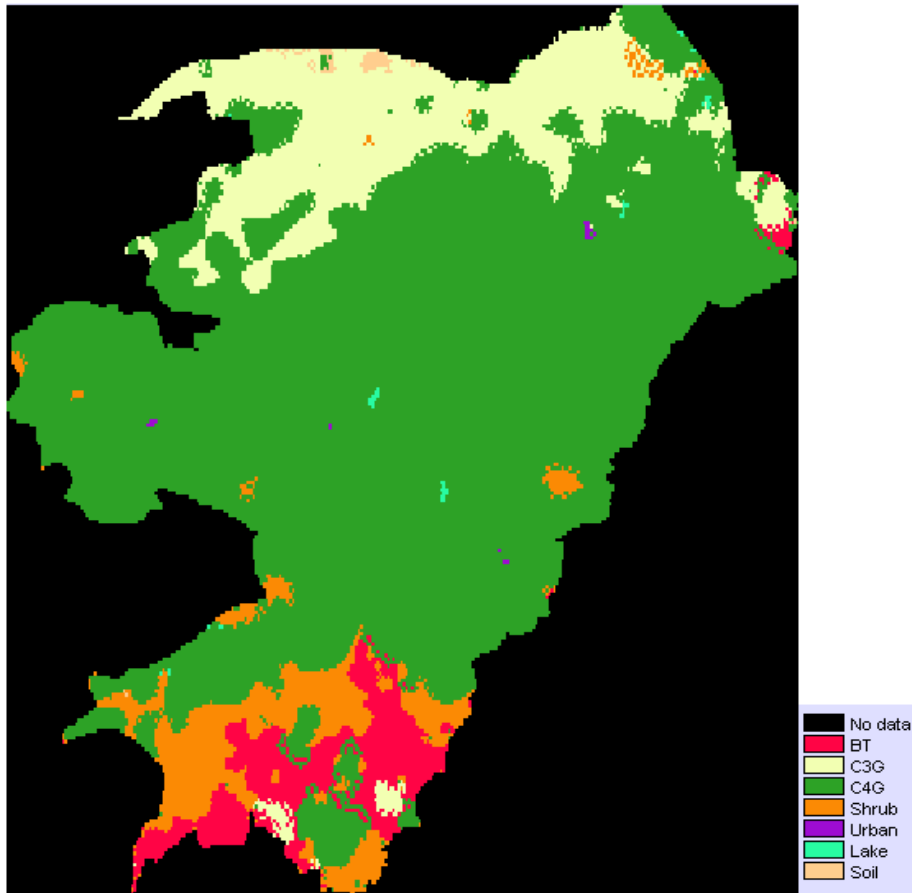


Figure 4-10: LC Projection 2046

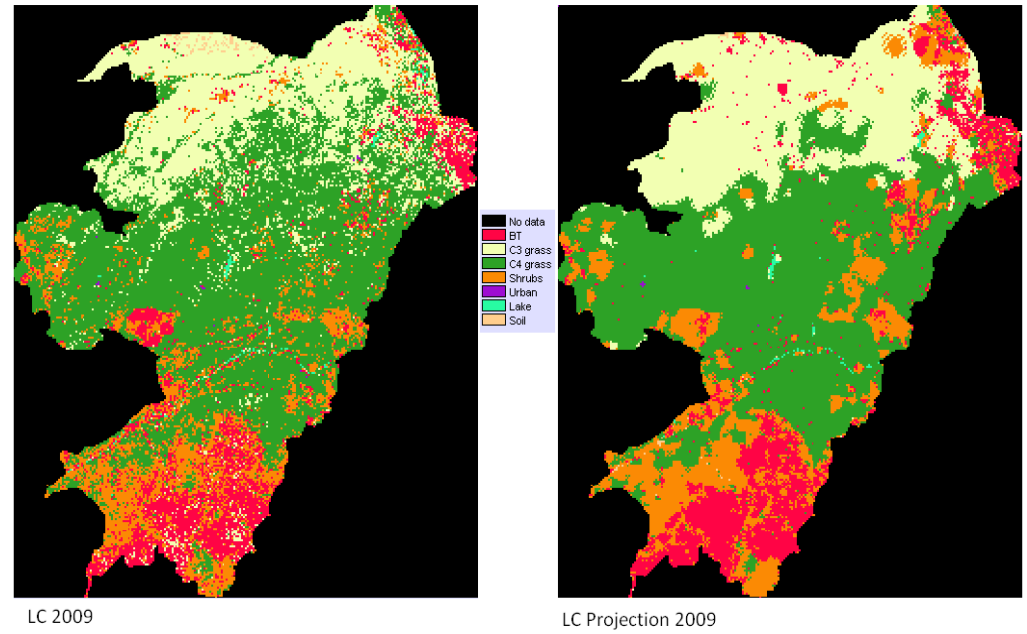


Figure 4-11: comparison between LC 2009 and predicted LC for 2009 using the CA-Markov model

**Table 4-6: Projected LC 2046 in km<sup>2</sup> from trends in LCC between 2005 and 2009**

<b>LC code</b>	<b>Area in km<sup>2</sup></b>	<b>Area in percentage</b>
<b>BT</b>	15023.02	5.417256
<b>C3G</b>	42018.65	15.15179
<b>C4G</b>	200450.4	72.28179
<b>Shrub</b>	18523.83	6.679636
<b>Urban</b>	173.94	0.062723
<b>Lake</b>	389.36	0.140403
<b>Soil</b>	738.78	0.266401

**Table 4-7: Differences between the 2009 LC and the 2009 projected LC**

<b>Code</b>	<b>LC 2009</b>	<b>Area in percentage</b>	<b>Projected LC 2009</b>	<b>Area in percentage</b>	<b>Percentage difference</b>
<b>BT</b>	36254.86	13.07	30999.83	11.17	-16.95
<b>C3</b>	69110.07	24.91	68160.81	24.57	-1.39
<b>grass</b>					
<b>C4</b>	124440.1	44.85	135573.5	48.87	8.21
<b>grass</b>					
<b>Shrubs</b>	45927.77	16.55	40480.84	14.59	-13.46
<b>Urban</b>	97.44	0.04	104.50	0.038	6.75
<b>Lake</b>	683.47	0.25	1023.74	0.37	33.24
<b>Soil</b>	923.31	0.33	1079.95	0.39	14.51

#### **4.4 Summary**

This Chapter highlighted the significance of LUCC in global environmental change and attempted to assess the changes in LC in North-eastern Nigeria. The study intended to achieve this by assessing the changes that has taken within the last three decades (1977-2009) and use the CA-Markov model to project LC for 2046. This projection was used subsequently as forcing data to simulate future land surface conditions in the area based on the A2 IPCC climate scenario using

JULES (see Chapter 5). Results of the LC analysis using the LCM in the IDRISI Taiga GIS software suggest that changes in LC are strongly influenced by LU because of the continuous increase in the size of croplands and grasslands at the expense of other LC classes.

Between 1977 and 2009 croplands (represented as the C4 grass class in the study) increased in size from 18% of the total area to 48.9% while forest and woodlands (represented as BT) reduced in size from 21.7% to 11%, thereby representing a loss 48% of its previous size, therefore, the largest loser of LC. Changes in LC involve the conversion from one cover type to another. The study revealed that the main LC conversion between 1977 and 1994 was the conversion of shrub lands into grasslands (C3 grass) [17%] and grasslands into croplands [15%]. Between 2005 and 2009 the major LC conversion was the transition from shrubs to croplands [20%] and forest/woodlands into shrub [17%]. Because of the differences in location of these conversions (either north or south of the study area) the results suggest that the dominant driver were: deforestation; the gradual expansion of croplands southwards and shifting cultivation as the reason for the transition. In the north, grasslands replaced the savanna woodlands and in the south the forest was replaced by scrub lands and bush lands.

Based on the 2005 and 2009 trends in LCC, the projected LC for 2046 suggest an increasing dominance of croplands in the study area constituting 72% of the total LC and grasslands [15%]. Forest and woodlands are projected to reduce to 5.4% of the total LC. The study attempted to validate the performance of the model in predicting future LC in the study area by using the 1994 and 2005 LC maps to

project LC for 2009. A comparison of the two LC maps indicate similarities above 83% (or less than 17% difference) in area for six out of the seven LC classes, with the exclusion of the Lake class (representing lakes, rivers and all water bodies) having a similarity of 66.8% (or difference of 33.2%).

These results show, to a certain degree, that the model can be satisfactorily used in projecting future LC in the area.

#### **4.5 Discussion on modelling land cover change**

After analysing trends in land surface conditions in the study area in Chapter 3 an attempt is made to analyse and predict changes in land cover in chapter 4. Results from this study suggest that changes in LC between 1977 and 2009 are strongly influenced by LU which explains the transition of other LC types into croplands. This LC type has increased in size at the expense of other land cover types in the study area presumably due to increase in demand for food and cash crops to satisfy the growing population and emerging markets similar to the assertions made by Ramankutty (2004) and Lambin (2001). The broad leaf tree (BT) LC class representing woodlands lost most of its area between 1977 and 2009. Most of the area of the land cover type was converted to C3 grass and shrubs. Likely causes of this conversion could be deforestation for reasons other than cropland expansion probably the demand for wood used in building and domestic energy requirements like fire wood. Since most of the conversion occurred in the central and northern parts of the study area cut tress will be replaced by grasslands.

Visual observations of the LCC maps show most of the changes during the 2005-2009 period took place in the southern part of the study area. This means a gradual encroachment into the forest cover in the south. During the same period transition from shrubs to C4 grass accounted for 20% (Figure 4-7) of LCC. A bush fallow pattern can be established from this, where wood lands and forest are cleared after exploiting the wood products, land is converted into croplands and then left to fallow when productivity diminishes. After a second regeneration and some years of fallow the bushlands are reconverted to croplands. This system of shifting cultivation is very common in tropical and sub-tropical regions (Dvořák, 1992) and a common practice in the forested and woodland regions of the study area (Akobundu *et al.*, 1999).

Another change noticed in the study is the continuous reduction in the Lake LC class by 36% (Table 4-4) between 1977 and 1994 by 17% (Table 4-5) between the 2004 and 2005. This trend may be linked to the diminishing area covered by Lake Chad in the north of the study area. In recent years the lake has considerably reduced in size and the water body has mostly been replaced by aquatic vegetation (Lemoalle *et al.*, 2012, Leblanc *et al.*, 2011). The urban LC class did not show any (Table 4-4) clear trend during the period. It increasing by 106% (Table 4-4) in the 17 years from 1977 to 1994 but reduced in size by 80% from 1994 to 2005 and increased by 7% (Table 4-5) from 2005 to 2009. This is attributed to the representation of the LC type in the different data used for this study with more settlements covered by the FORMECU LUC maps of 1977 and 1994 (Table 4-4).

The GLOBCOVER LC maps of 2005 and 2009 cover only the largest urban centres in the study area (Table 4-5).

Based on current trends in LCC the projected LC map of 2046 shows a LC dominated by croplands (Table 4-6) and grasslands while, the forest and woodlands reduce to only 5.4% of their area in 2009. This may have a large impact on the surface hydrology, possibly increasing surface runoff and reducing soil moisture retention, biological diversity, biomass carbon concentrations, and increasing the surface albedo. Results obtained in the process of validating the model indicate that, based on the comparison made between the 2009 LC map and the 2009 projected LC map, the CA-Markov model can successfully simulate future LCC in the study area. The strength of the prediction based on the length of the period predicted is not, however, be confirmed.

# Chapter 5. **Modelling future land surface conditions in North-eastern Nigeria from 2046-2065 based on the IPCC special report on emission scenario (SRES) A2**

## **5.1 Introduction**

Never have human induced changes to the environment been more apparent than in the last 300 years (Bengtsson *et al.*, 2006). Since the industrial revolution in the 18<sup>th</sup> century atmospheric pollution and land use has increased significantly with possible lasting effect on the global climate and regional hydrologic systems (Mahmood *et al.*, 2010). There is already evidence of an increase in temperatures and extreme weather events across the globe (Mahmood *et al.*, 2010; IPCC 2007). There are many views on the future impact of these changes with different scenarios developed to predict the impacts based on future global economic and social structures, and changes in demography and technology. The level of future consumption of fossil fuels and land use change are dependent on these changes together with the resulting greenhouse gas emissions. Parts of Africa where local economies are dependent on rain fed agriculture may be affected by global warming especially areas already vulnerable to climatic perturbations (Vigaud *et al.*, 2009).

This chapter highlights these issues and attempts to simulate future land surface conditions and associated fluxes in energy and momentum in the North-eastern

region of Nigeria, as part of the land surface-atmosphere feedback mechanism. This is in view of current trends in climate change where short and medium term projections are required, especially, between the years 2020-2050 for developing adaptation strategies for local societies (Vigaud *et al.*, 2009). For this reason the study chose to focus on the period between the years 2046-2065 for examining the impact of global warming and land use/cover change (LUCC). The objective was to study the impact of the major cause of global warming-that is anthropogenic emissions of greenhouse gasses in one experiment and the impact of both anthropogenic emissions of greenhouse gasses and LUCC in a second experiment. This study draws from the works of Taylor *et al.* (2002), Vigaud *et al.* (2009), Mariotti *et al.* (2011), Bounoua *et al.* (2002), and Hulme *et al.* (2001). These previous studies are more general in the context of attempting to use general circulation models (GCMs) to examine the trends in climate change and the influence of global warming in Africa or in the West African sub region. The most notable of these studies is the work of Taylor *et al.* (2002) that considered the impact of LUCC on the changes in the climate of the West African Sahel. In this study, we use a “standalone” mode of JULES (version 3.0) i.e. not coupled in a GCM to observe changes in fluxes of momentum, and energy in the form of sensible and latent heat. The area of study is localised and limited to the North-eastern region of Nigeria in West Africa.

Subsequent pages in this section explain: how greenhouse gasses cause global warming; the role of LUCC on modifying surface albedo and fluxes in energy, moisture and momentum; and the role of soil organic carbon in contributing to

atmospheric carbon concentrations in the process of LUCC. Section 5.2 explains the methodology and analysis techniques used for the study. The results are presented in Section 5.3, comparison between the results from predicted future land surface conditions (2046-2065) and past land surface conditions (1980-2000) are presented in section 5.4. Finally, a summary of this chapter is presented in Section 5.4.

### **5.1.1 Climate scenarios**

Anthropogenic causes of climate change may continue well into the future as a result of greenhouse gas emissions. However, there is uncertainty as to the extent of future greenhouse gas emissions emanating from very complex and dynamic systems (IPCC, 2000). At the forefront of the global awareness campaign on global warming and climate change is the Intergovernmental Panel on Climate Change (IPCC). The IPCC has identified demographic, socio-economic, and technological changes as the 3 major driving forces of future greenhouse gas emissions. Thus, the business as usual and five other scenarios published in 1992 (Houghton *et al.*, 1992) were replaced by a set of new scenarios formulated to reflect the likely changes to these driving forces in the future. The new scenarios introduced by the IPCC to replace the earlier ones are grouped into 4 families and are classified into six broad categories. These scenarios are the A1FI, A1B, and A1T from the A1 family, the A2, B1 and B2 (IPCC, 2000).

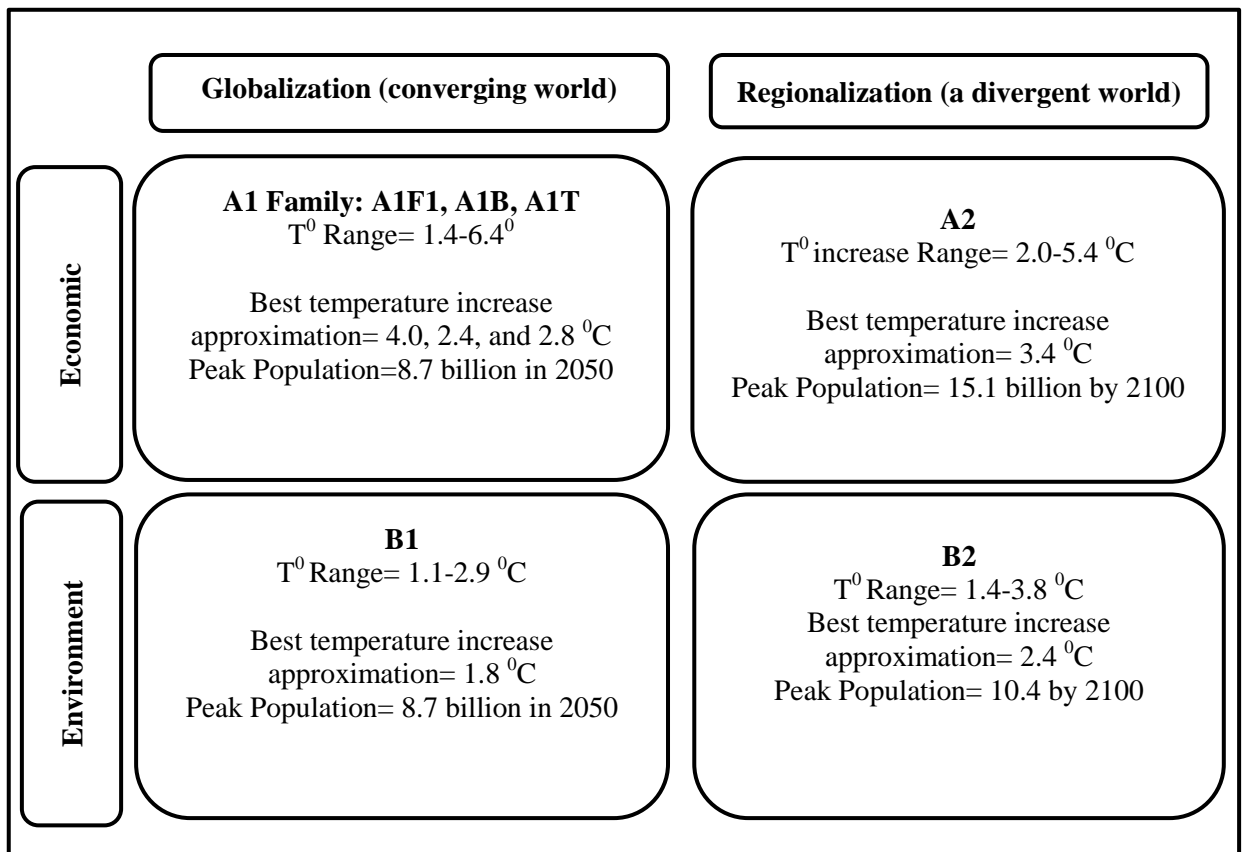


**Figure 5-1: General description of the IPCC SRES highlighting how they are related and their differences based on environmental issues and the level of global integration**

The six climate scenarios are presented in Figure 5-1. The A1 family group presupposes a world with rapid economic and population growth in the near future with the global population reaching a peak level of 8.7 billion by 2050 and decreasing thereafter. Rapid technological change is predicted as efficient technologies are introduced and spread globally in a more homogenous world. Technology is the main factor differentiating the three major groups in this family. The A1FI is fossil fuel intensive, while the A1T scenario has an emphasis on non-fossil fuel energy supply and the A1B is a balance between the two.

The A2 scenario envisages a divergent world with very slow economic growth and technological change, which is highly fragmented and regionalised. As a result of this, the global population increases continuously. The major theme of the scenario is “self-reliance and the preservation of local identities”.

In the B1 climate scenario the population reaches a peak by 2050 and then declines due to changes in demography and the birth rate. In a converging world, the emphasis is on global solutions to socio-economic and environmental issues so there is a rapid change towards the use of efficient technologies.

Similarly, the B2 climate scenario describes a world which is conscious of environmental issues but efforts towards sustainability are made at local and regional levels. The main emphasis is on local solutions to social and economic problems. Economic and technological change is projected to be slow and diverse.

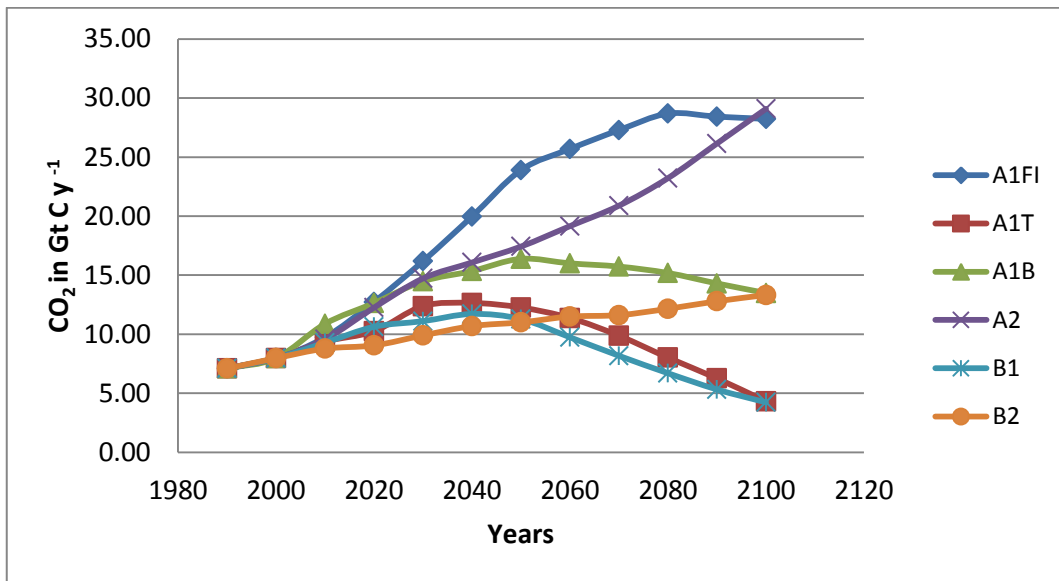


**Figure 5-2: Global carbon dioxide emissions from the six IPCC special emission scenarios for the years 1990 to 2100**

Data source: IPCC (2000)

### **5.1.2 The impact of Land use and land cover change on the global and regional climate**

Land cover change is the second source of greenhouse gas emissions after fossil fuel combustion. Lucc has the potential to change the climate by changes to the surface albedo, modifying the fluxes of energy and momentum and contributing directly to changes in greenhouse gas concentrations and aerosol loadings (Forster *et al.*, 2007). In addition Lucc can change the efficiency of the land to sequester carbon dioxide (Solomon *et al.*, 2007). In recent years land cover conversion to agriculture has reduced considerably in North America, Europe and China with a subsequent increase in forest cover over the last 50 years. However, there has

been a rapid increase in LUCC in Africa, South America, South and South-east Asia (Foster *et al.*, 2007).

LUCC has an impact on hydrology and atmospheric conditions at a regional level and can even influence rainfall regimes. Charney (1975) was the first to suggest that a reduction in vegetation from LUCC can increase the albedo on the surface causing a sinking motion in the lower atmosphere, additional drying and enhanced arid conditions. While a lot of uncertainty exists on the degree and time scale of the changes in surface albedo essential to cause an effect on the climate, it is widely acknowledged that changes to the vegetation can have an effect on the radiative properties of the surface especially in the partitioning of surface energy fluxes into latent and sensible heat (Fuller and Ottke, 2002). The fluxes in energy, moisture and momentum have a considerable effect on the lower atmosphere especially on the Bowen ratio, evaporative fraction, and the creation of convection currents favourable for precipitation. Significant changes in the land cover are acknowledged by many researchers as responsible for the recent droughts in the West African Sahel. On this notion Taylor *et al.* (2002) studied the influence of LUCC on the climate of the West African Sahel using a General Circulation Model (GCM) and noticed a significant reduction in rainfall in the month of July. LUCC has the potential to affect the amount, structural composition, and stability of soil organic carbon (SOC), the largest store of terrestrial organic carbon (1500 PgC) more than that contained in the biosphere (560 PgC) and the atmosphere (760 PgC) (Solomon *et al.*, 2007). Despite having a low SOC the total organic pool of dryland ecosystems is about 15.5% of the world's total contained by the

soil surface up to 1 meter depth (Lai, 2003). A significant proportion of dry land ecosystems comprising of dry sub-humid and semi-arid regions are found in Africa and play an important role in the loss of SOC. Although Africa has a low fossil fuel emission and a terrestrial productivity that in most cases compensates for respiration, LUCC is the continents main source of net carbon emission (Williams *et al.*, 2007).

Despite the significance of LUCC on climate change there has been little attention to the notion that regional changes in LC can have significant influences on the global climate (Chase *et al.*, 2000). It is certain that floods, drought and other climatic perturbations are mostly a response to regional changes rather than global changes but LUCC also has a regional impact on atmospheric temperature that may have tele-connections with global atmospheric circulations (Mahmood *et al.*, 2010).

## **5.2 *Materials and Methods***

The study uses the Met Office Joint UK Land Environment Simulator (JULES) to model future land surface processes in North-eastern Nigeria. The types of data and analysis techniques are explained in this section.

### **5.2.1 *Methods***

The main tool used in this study is the “stand alone” mode of JULES version 3.0. Details of the land surface model are provided in Chapter 3. The study was intended to run a set of experiments with JULES using atmospheric forcing data from the A2 climate scenario and a projected land cover map for 2046. The reason

for choosing this climate scenario is because, apart from the A2 and A1FI SRES, anthropogenic emission of carbon dioxide is projected to stabilise by the year 2050 and then gradually decrease. In these two emission scenarios (A2 and A1FI) atmospheric CO<sub>2</sub> concentrations are projected to continue to increase to the year 2100 and exceptionally, in the A2 SRES, emissions from LUCC remain positive.

### **5.2.1 Data types**

The study used atmospheric forcing data from the IPCC A2 SRES to conduct two separate experiments. Land cover fraction was derived from a land cover projection of the study area for 2046 derived using Cellular-Automata Markov chain model on an Idrisi Taiga GIS platform (see Chapter 4). Other data sets used as forcing data for the model include soil hydraulic parameters developed from the dominant soil maps of Nigeria Sonneveld (1997).

### **5.2.2 Experiments and analysis techniques**

In this study we conduct two experiments using the JULES land surface model that differ from each other only by the fractional land cover used as a forcing. As the main objective of the study is to simulate future land surface conditions under certain changes in climate and land cover changes the first experiment used the present fractional land cover and SRES A2 atmospheric drivers for the years 2046 to 2065. The second experiment used the same atmospheric drivers and a projected fractional land cover for the year 2046 (Figure 5-3). Initial conditions for running the model in both experiments were obtained by a “spin up” run of the

first two years (2046-2047) 100 times. Subsequently, the output from the “spin up” was used as initial conditions. The reason for the “spin up” was to obtain stable soil conditions when running the model in each of the experiments.

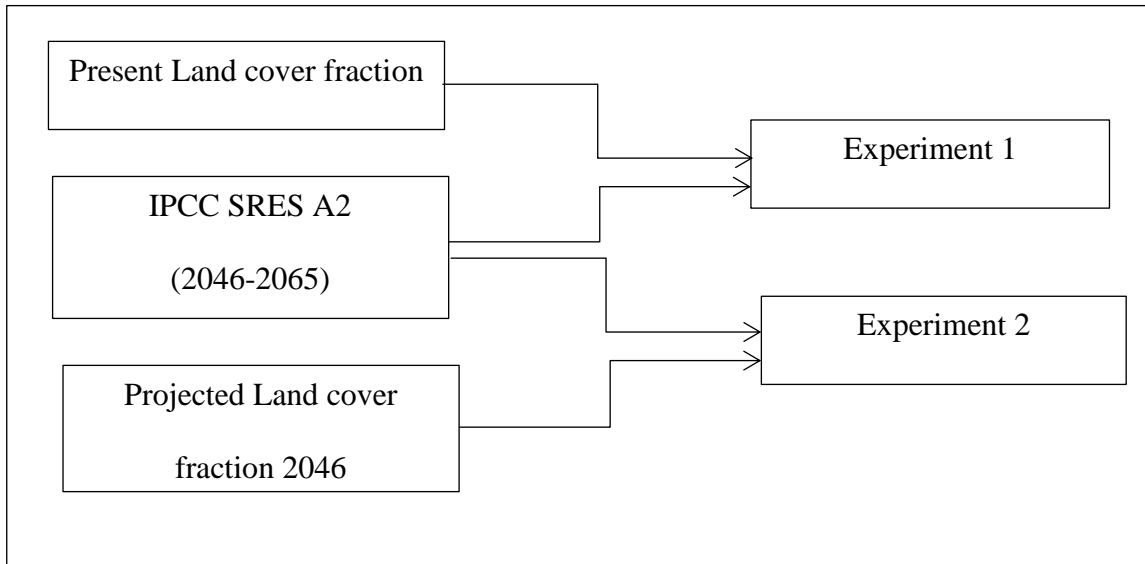


**Figure 5-3: A schematic of the two experiments. In both cases the IPCC SRES A2 was used as forcing data**

\*However 2 separate fractional land cover data sets were used for the two experiments.

The projected fractional land cover for 2046 at  $\frac{1}{2}^\circ \times \frac{1}{2}^\circ$  degree spatial resolution used in the second experiment was produced from a  $0.024^\circ \times 0.024^\circ$  resolution projected land cover of North-eastern Nigeria for 2046. This was derived for each of the 9 fractional land cover types by adding the total number of  $0.024^\circ \times 0.024^\circ$  grids covered by a land cover type divided by the total number of  $0.024^\circ \times 0.024^\circ$  grid cells contained in a  $\frac{1}{2}^\circ \times \frac{1}{2}^\circ$  grid.

$$lcf(a)b = \frac{\sum lt(a)}{\sum T} \quad \text{Eq. [5-1]}$$

Where  $lcf(a)$  is the land cover fraction for land cover type  $a$  in a  $\frac{1}{2}^0 \times \frac{1}{2}^0$  grid box  $b$ ,  $\sum lt(a)$  is the summation of all  $0.024^0 \times 0.024^0$  covered by land cover type  $a$  in  $b$ , and  $\sum T$  is the summation of all  $0.024^0 \times 0.024^0$  grids in a  $\frac{1}{2}^0 \times \frac{1}{2}^0$  grid cell  $b$ .

Results from the experiment were analysed using the percentage difference, Student's t test, and Kolmogorov Smirnov test for making comparisons, and least square regression for analysing temporal trends. All of the analysis techniques have been used and elaborated in Chapter 3.

The percentage difference in this chapter is calculated as the differences between Experiment 1 subtracted from that obtained in Experiment 2. Other methods used in this chapter and previously discussed in Chapter 3 are the equations for driving the Bowen Ratio and Evaporative Fraction using latent and sensible heat fluxes. Box plots are also used here for comparisons.

### **5.3 Results**

The differences between the vegetative land cover fractions used for driving the two experiments are shown in Figure 5-4. JULES covers the entire land surface using a grid and each grid cell is made up of fractions of nine land cover tiles five are vegetative (Broad leaf, needle leaf, C3 grass, C4 grass, and shrubs) and four are non-vegetative (Urban, Water bodies, soils, and snow). Based on this, there are four dominant vegetative fractional land cover types for the entire study area. These are broadleaf woodlands, C3 grass, C4 grass, and shrubs. The study made a comparison between the fractional land cover data sets used in each of the two experiments. Between the two fractional land cover data used for the two

experiments there is a grid box difference ranging between -55%-105% in the Broad leaf woodlands, -25%-105% in the C3 grass, -95%-100% in the C4 grass and -4%-92% in the shrub land cover fraction. Grid boxes previously dominated by the Broad leaf woodlands in the forcing data for Experiment 1 are mostly replaced by C4 grass in Experiment 2.

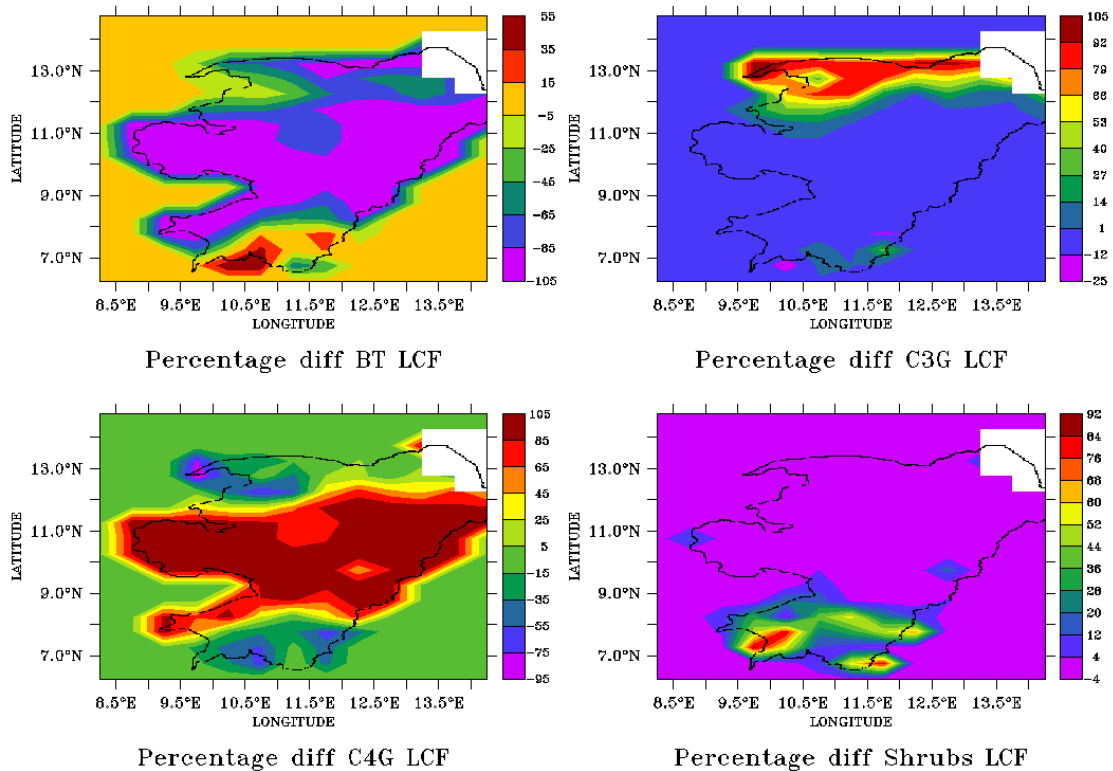


**Figure 5-4: Percentage difference in the four vegetative fractional land cover types in the area represented by acronyms BT (Broad leaf trees), C3G (C3 grass), and C4G (C4 grass)**

Results of the two experiments are compared for grid box differences in the evaporative fraction, surface runoff, soil moisture as a fraction of saturation and GPP (Figures 5-5). These four were selected for the following reasons:

evaporative fraction is selected for better understanding the changes in energy fluxes on the land surface; changes in land cover normally has impacts on the surface run off; soil moisture was selected for its relevance in the availability of moisture at the root zone and the partitioning of incoming radiation into sensible and latent heat fluxes; GPP was selected as proxy for studying the carbon status of the area. It is a good indicator of the scale of net ecosystem productivity, respiration and carbon fluxes and the productivity of each grid box especially, in this case, under different land cover types.

The pixel averaged percentage differences between the two experiment range between -42%-38% for the evaporative fraction, -30%-150% for surface runoff, -9%-5% for top surface soil moisture, and -0.06%-0.6% GPP.

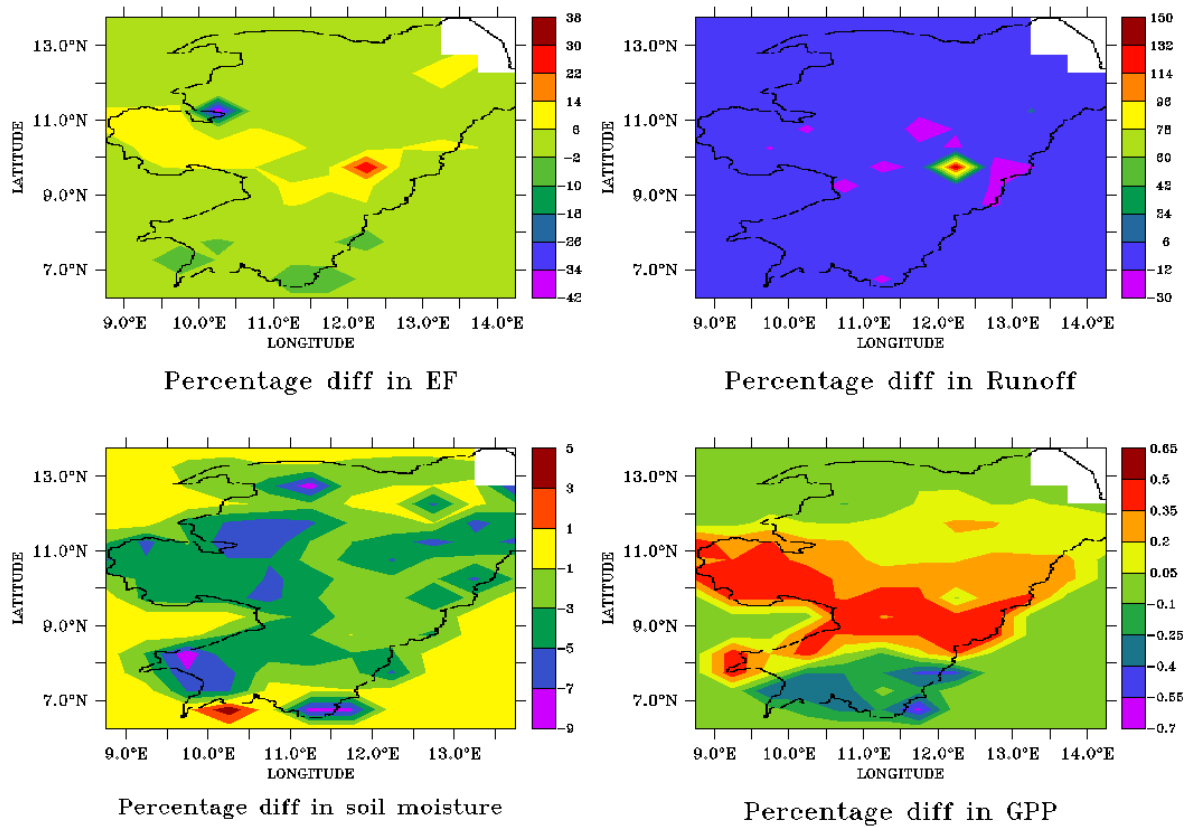
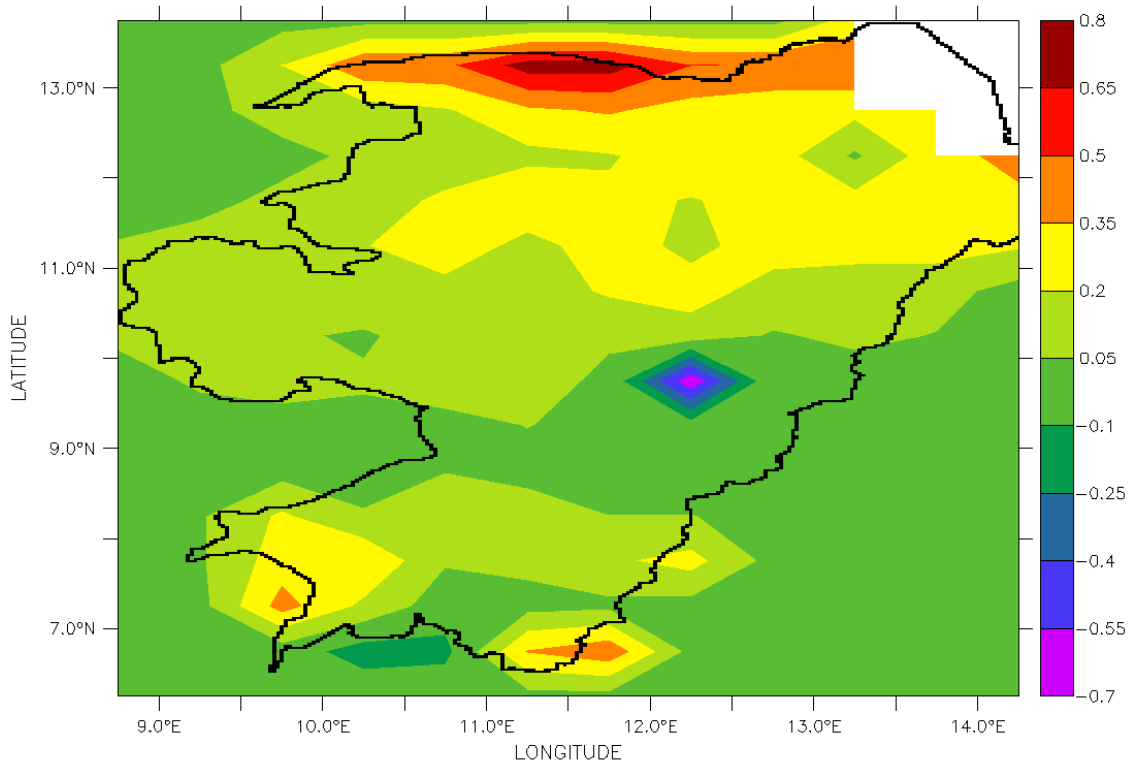


**Figure 5-5: Temporally averaged percentage differences of Evaporative Fraction (EF), surface runoff (top right), soil moisture as a fraction of saturation, and GPP (expressed in  $\text{kg C m}^{-2}$ ) averaged for the period 2046-2065.**

Differences in predicted surface temperature between the two experiments averaged for the 20 year period (5-6) has a range between  $-0.7$ - $0.8^{\circ}\text{C}$ .



Differences in surface Temperature in °C between Exp. 2 and Exp. 1

**Figure 5-6: Temporally averaged differences in predicted land surface temperature in °C between Experiment 2 and Experiment 1**

Differences from the outputs between the two experiments were compared on grid cell bases and the grid cells that have the highest variability were further examined. For instance the fractional land cover for a grid cell (latitude 9.5-10.00 N, longitude 12-12.50 E) with the highest percentage difference in Evaporative Fraction (38%) and surface runoff (150%) between the two experiments for the period of study was compared. The differences between the two fractional land cover data set are provided in Table 5-2. In this grid cell broad leaf trees with a fraction of 0.96 are replaced by C4 grass (0.5) and water bodies (with a land cover fraction of 0.5 but previously 0.026). This may explain the large variability in

evaporative fraction and surface runoff between the two experiments in that particular grid box.

**Table 5-1: Fractional land cover types of a grid cell (latitude 9.5-10.00 N, longitude 12-12.50 E)**

<i>Land cover types</i>	<i>Fractional Land cover</i>	
	Experiment 1	Experiment 2
Broad leaf trees	0.96	0.0
C3 grass	0.0	0.0
C4 grass	0.002	0.5
Shrub	0.0	0.0
Urban	0.0	0.0
Water bodies	0.028	0.5
Soil	0.01	0.0
Total	1.0	1.0

The grid box is having an Evaporative fraction and surface runoff increase by 38% and 150% in Experiment 2 respectively.

The large variation in percentage differences especially in Evaporative Fraction and surface run off between the two experiments is greatly narrowed when the pixels were averaged to produce a time series plot (Figure 5-6). Finally these land surface conditions were paired (i.e. GPP in Experiment 1 to GPP in Experiment 2) and tested for differences in means and distribution of their variables. Just like in Chapter 3, an attempt was made to test whether there are no differences in both the means and the distribution of the land surface condition under different experimental set up. All the tests yielded no significant difference ( $p > 0.05$ ).

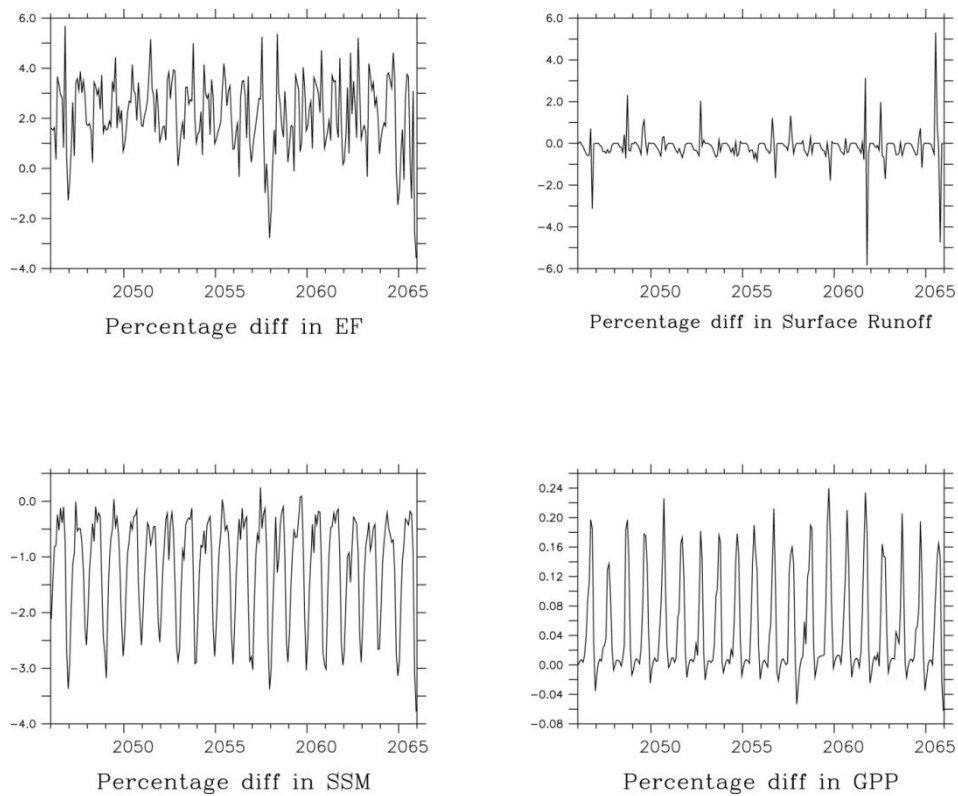


**Figure 5-7: Pixel averaged percentage differences in Evaporative Fraction, predicted surface run off, surface soil moisture, and GPP obtained between the two experiments**

Differences in predicted soil moisture content vary with depth (Figure 5-7). However, significant differences in predicted soil moisture content between the two experiments was only statistically significant at the 2 meter depth layer. The root mean square error for the predicted soil moisture content between the two experiments was  $16.6 \text{ kg m}^{-2} \text{ month}^{-1}$ .

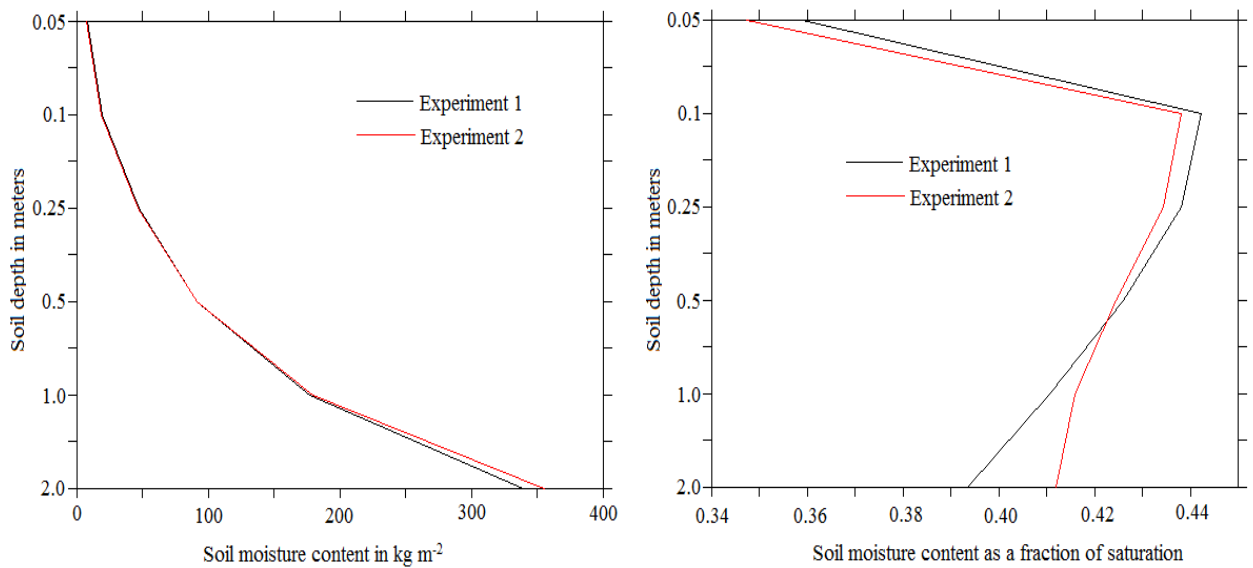


**Figure 5-8: Predicted soil moisture content (left) and soil moisture content as a fraction of saturation (right) at different depth plotted for Experiment 1 and Experiment 2**

The impact of land cover conversion from broadleaf trees (BT) to croplands on land surface conditions of Evaporative Fraction, predicted runoff, SSM, and GPP was examined. This was achieved by identifying and comparing grid cells of the same coordinate that have BT as the dominant land cover fraction in Experiment 1 and C4 grass as the dominant in Experiment 2.

Two separate grid cells with a BT land cover fractions of 0.99 in the first cell (Latitude 10-10.5 North, Longitude 11-11.5 East) and 0.88 in the second cell (Latitude 8-8.5 North, Longitude 12-12.5 East) for Experiment 1 but have a C4 grass land cover fraction of 0.99 in the first cell and 0.87 in the second cell for Experiment 2 are presented here to show the significance of this conversion (Figure 5-7 and 5-8). Differences in the fractional land cover types in these grid

cells suggest an increase in the surface run off and GPP in Experiment 2. The study further tested for differences in these results by testing the differences in the means and distribution of the result between Experiment 1 using the present fractional land cover and Experiment 2 using the projected fractional land cover for 2046 in each of the selected grid cells using the Student's t test and the Kolmogorov-Smirnov test. In the first selection (Latitude 10-10.5 North, Longitude 11-11.5 East) results of the Student's t test and Kolmogorov-Smirnov test between the two experiments yielded no significant difference ( $p=1$ ) in the Evaporative Fraction, significant difference ( $p<0.05$ ) in predicted surface soil moisture, and significant difference ( $p<0.01$ ) in predicted surface runoff and GPP, respectively. In the second selected grid cell (Latitude 8-8.5 North, Longitude 12-12.5 East), results of the Student's t test and Kolmogorov-Smirnov test between the two experiments suggest no significant difference ( $p=1$ ) in Evaporative Fraction, significant difference ( $p<0.05$ ) in predicted surface runoff and significant difference ( $p<0.01$ ) in GPP. The Student's t test for predicted runoff between the two experiment suggest significant differences ( $p<0.05$ ) between the two but the Kolmogorov-Smirnov test suggest no difference ( $p>0.05$ ) in their distribution.

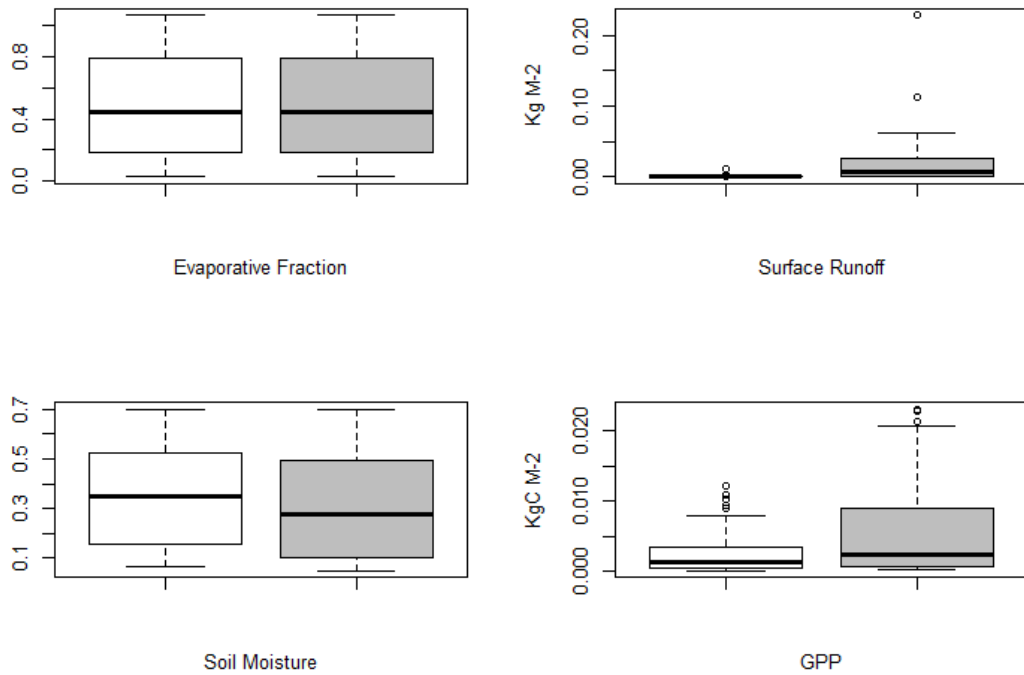


**Figure 5-9: Box plots of Evaporative Fraction, predicted surface soil moisture, surface runoff and GPP (Latitude 10-10.5 North, Longitude 11-11.5 East). The first (white) box represents Experiment 1 while the second (grey) box represents Experiment 2.**

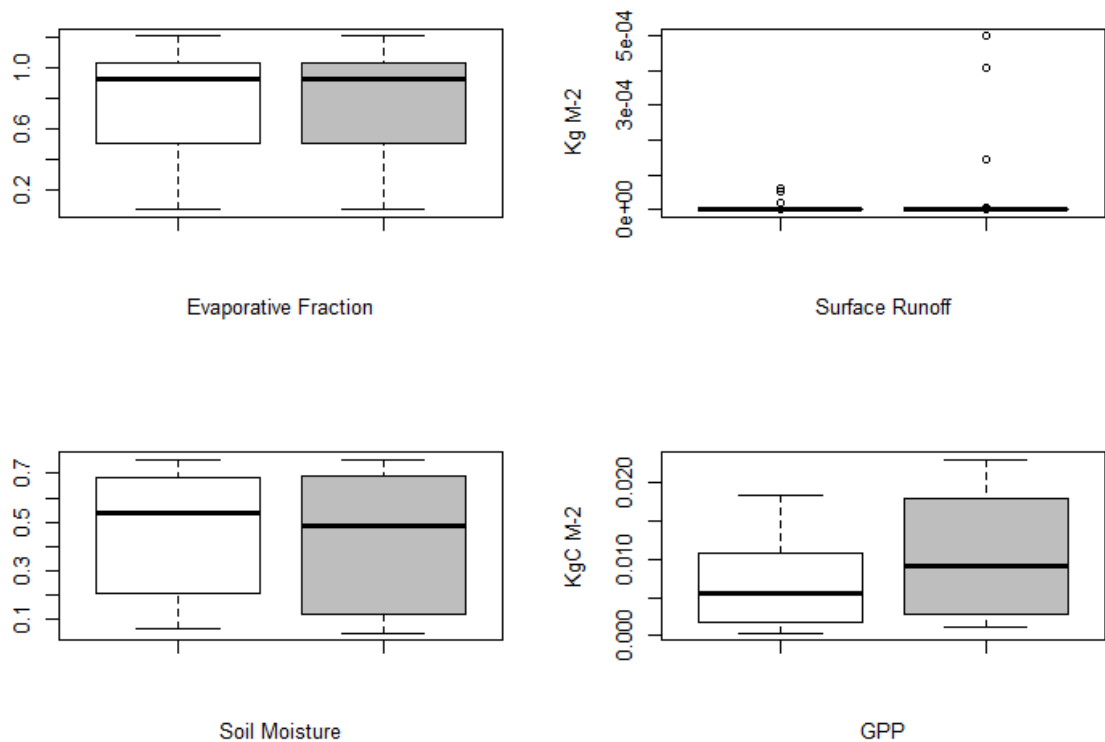


**Figure 5-10: Box plots of Evaporative Fraction, predicted surface soil moisture, surface runoff and GPP (Latitude 8-8.5 North, Longitude 12-12.5 East)**

\*Of the two boxes in each case the first (white) represents Experiment 1 while the second (grey) represents Experiment 2.

Monthly trends in the Bowen ratio (slope=-1.7e-03,  $p>0.05$ ), Evaporative Fraction (slope=2.0e-03,  $p>0.05$ ), predicted surface soil moisture (slope=0.5e-03,  $p>0.05$ ) and GPP (slope=4.3e-05 kgC m<sup>2</sup>,  $p>0.05$ ) were examined over the 20 year period using the output from Experiment 2(Figure 5-9). An annual increase in GPP of

0.38e-03 kgC m<sup>-2</sup> (p>0.05) was predicted suggesting an insignificant increase during the period.

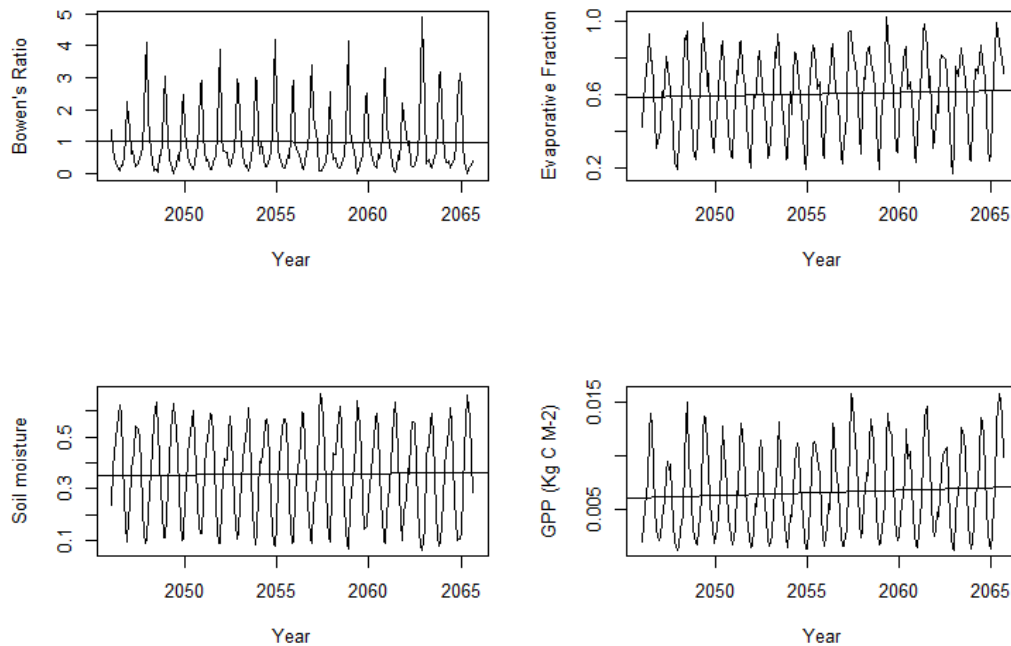


**Figure 5-11: Pixel averaged trends in the Bowen ratio (upper left), predicted Evaporative Fraction (upper right), top surface soil moisture (lower left), and GPP (lower right) from Experiment 2.**

\*The straight lines across each plot are least regression lines giving an insight of either a decreasing or increasing trend.

#### **5.4 Differences in past (1980-2000) and future (2046-2065) land surface condition**

In this section prediction of past land surface conditions are compared with future conditions in order to ascertain the level of changes between the two. The study used the Student's t-test and Kolmogorov-Smirnov test to determine the level of

significance of change in the land surface conditions. The study assumes that any significant differences in the mean and distribution of a land surface condition can be interpreted as a significant change between the two time periods. The results of the two statistical tests are provided in Table 6-1. In Figure 6-2 mean monthly rainfall and atmospheric temperature data used for driving the model are compared. There is a significant difference in the temperature used to drive the model between 1980-2000 and 2046-2065. The difference in mean temperature is  $2.04^{\circ}\text{C}$  with the month of June having as much as  $3.02^{\circ}\text{C}$ . However, the difference between the rainfall data set had no significant statistical difference.

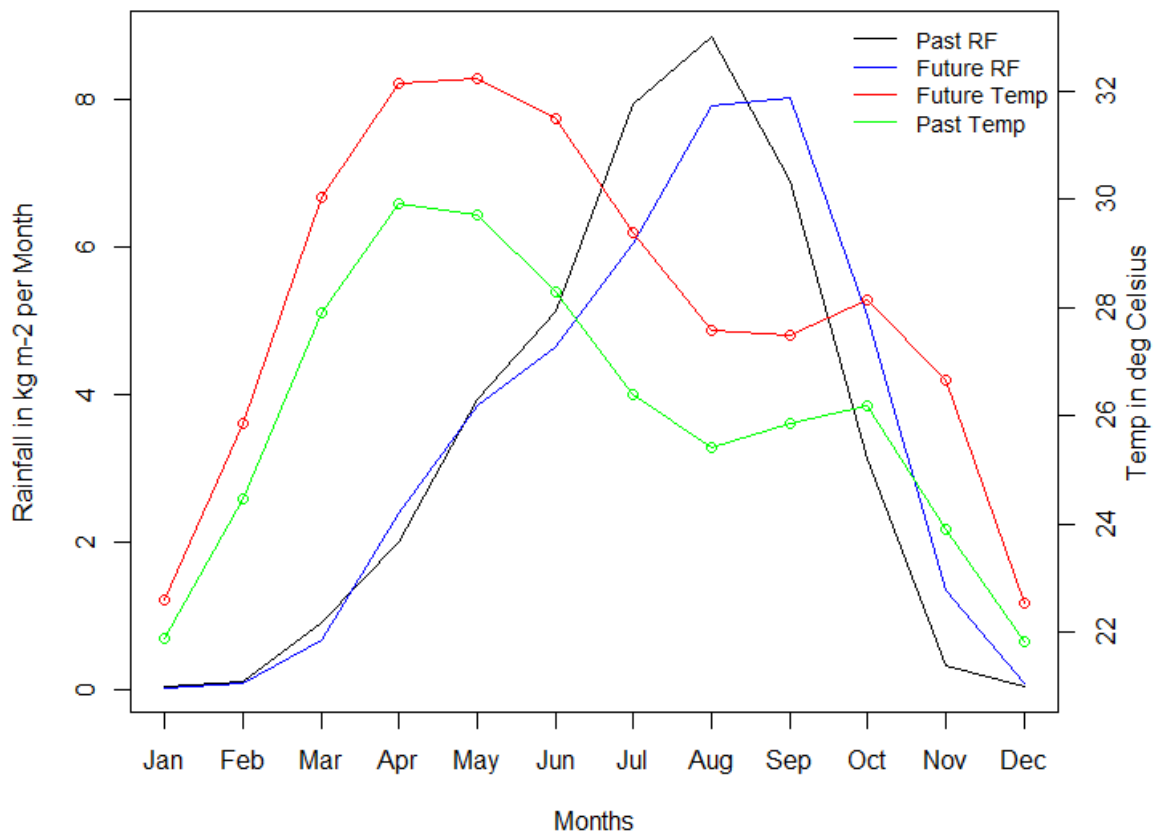


**Figure 5-12: Mean monthly rainfall (RF) and temperature (Temp) used in driving the model to simulate past and future land surface conditions**

Differences between land surface conditions of latent heat flux suggest no change in the mean but a significant change in the distribution (Figure 6-3). Significant changes in the sensible heat flux, soil temperature, GPP and the Evaporative Fraction were, however, apparent. Sensible heat flux is lower in the 2046-2065 experiments than in the 1980-2000 experiment especially during the monsoon season (May-September) and this may be the reason for the higher Evaporative Fraction.

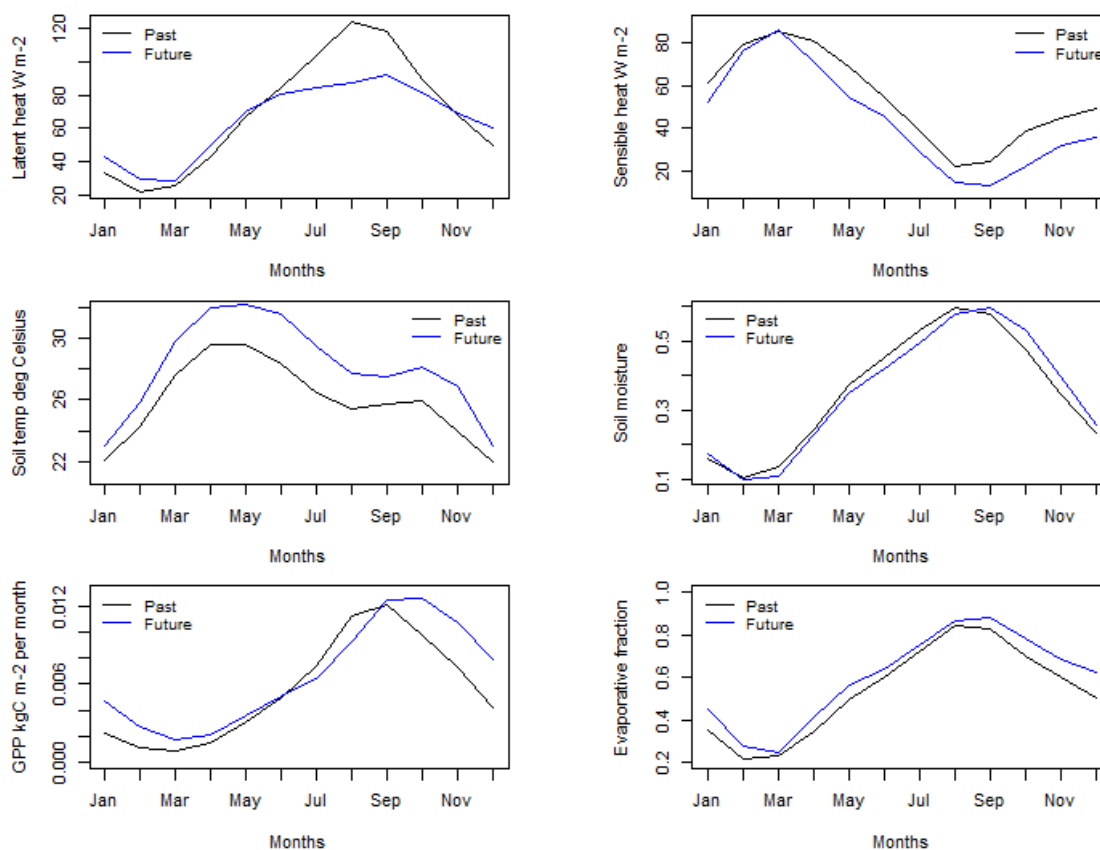


**Figure 5-13: Mean monthly differences in simulated past (1980-2000) and future (2046-2065) land surface conditions**

**Table 5-2: Results of p-values of a Student's t-test and Kolmogorov-Smirnov test for differences in means and distribution between past and future land surface conditions**

Statistical Test	Rain	Air T <sup>0</sup>	Latent heat	Sensible heat	Soil T <sup>0</sup>	Soil Moisture	GPP	Evaporative fraction
Student's t-test	0.798	<0.01*	0.11	<0.01*	<0.01*	0.98	<0.01*	<0.01*
Kolmogorov-Smirnov test	0.6	<0.01*	<0.01*	<0.01*	<0.01*	0.88	<0.01*	<0.01*

The \* indicate statistical significance

## 5.5 Summary

As a result of the current trends in human, induced climate change short and medium term predictions of possible impacts of changes is necessary for informed decision. This study was conceived based on this notion and, therefore, attempted to predict the impact of climate and land cover change in the future on land surface conditions in North-eastern Nigeria. For this purpose the IPCC SRES A2 atmospheric forcing data was used to conduct two experiments using the UK Met Office land surface model JULES. The first twenty year experiment (2046-2065) used existing fractional land cover data. Predicted energy fluxes, soil moisture, surface run off and GPP were compared with those from a second experiment conducted for the same period using a projected fractional land cover for 2046. Results suggest that on average there is a smaller range in difference between the experiments in the long term as expressed in Figure 5-6. While there is an increase in the Evaporative Fraction during the wet season in Experiment 2 with an increase in GPP (maximum of 0.24%) over the same period, there is a reduction in the surface soil moisture by as much as 3.6% during the wet season. Differences in surface soil moisture between the two experiments, almost levelling out during the dry season. The test for differences in the means and distribution of the land surface conditions between the two experimental set ups using the Student's t test and the Kolmogorov Smirnov test yielded  $p > 0.05$  suggesting no differences in both the means and distribution of the variables or no significant differences between the land surface conditions obtained in the two

experiments. However, the grid box that had the highest degree of conversion from a predominantly BT vegetation to a predominantly C4 grass between the two experiments recorded a significant difference in the predicted surface soil moisture, surface runoff, and GPP with the Evaporative Fraction remaining the same.

Experiment 2 was used to study the monthly trends in the land surface conditions over the 20 year period since both atmospheric forcing and fractional land cover projected for that period is used to drive the model. Monthly trends in the Bowen ratio decreased by  $-1.7e-03$  ( $p>0.05$ ) and other land surface conditions of Evaporative Fraction, predicted surface soil moisture and GPP increased by  $2.0e-03$  ( $p>0.05$ ),  $0.5e-03$  ( $p>0.05$ ), and  $4.3e-05$   $\text{kgC m}^{-2}$  ( $p>0.05$ ) respectively. An annual increase in predicted GPP of  $0.38e-03$   $\text{kgC m}^{-2}$  ( $p>0.05$ ) suggests that monthly, and annual trends in the land surface conditions have no statistical significance.

## **5.6 Discussions**

This chapter described how two experiments were conducted to examine the impact of land cover change and climate change under the IPCC A2 climate scenario on land surface conditions of soil moisture, surface run-off, soil temperature, GPP and latent and sensible heat flux in North-eastern Nigeria from the year 2046 to 2065. Each of the two experiments differs from the other by the fractional land cover data set used in running the JULES land surface model. All other input parameters remained the same. While, in Experiment 1 fractional land

cover input based on the present land cover of the study area was used to run the model, in Experiment 2 a fractional land cover input based on a projected land cover of the study area for 2046 was used to run the model.

The two experiments were conducted based on the assumption that changes to land cover is driven by climatological conditions and no changes to land use during the period of the experiment (2046-2065). However, it was expected that different land cover data used in the two experiments would influence how the model calculates the surface energy budget, moisture and respiration. Supposedly, this may produce a significant difference in the outputs between the two experiments. For this reason the model outputs of soil moisture, surface runoff, GPP and latent and sensible heat flux were compared between the two experiments. These surface properties are important in studying the fluxes in energy, moisture and momentum in the area.

While, differences in predicted soil moisture averaged for the 6 layers (5 cm, 10 cm, 25cm, 50 cm, 1 meter and 2 meter) were statistically insignificant between the two experiments, there was a significant difference in the lower bottom layer at 2 meter depth. Differences in fractional land cover with a larger percentage broadleaf trees used in Experiment 1 and mostly C4 grass and C3 grass dominant fractional land cover used in Experiment 2 may be responsible for this. Since, in the JULES model, soil loss from a layer of soil is dependent on root uptakes that is dependent on the plant phenological type and loss from the layers above and below the soil layer (see methodology section in Chapter 3).

Overall, the differences in the land surface properties between the two experiments are statistically insignificant based on the Student's t-test and Kolmogorov-Smirnov test. This insignificant statistical difference between the two experiments suggest that, generally, the magnitude of changes in land cover had little effect on predicted land surface conditions of soil moisture, surface runoff, GPP and latent and sensible heat flux. Although, these differences were significant in areas where there is over 80% change in the fractional land cover from broadleaf trees to croplands. In these areas, there was a significant increase in surface run off, GPP but a significant decrease in soil moisture with no significant changes to the Evaporative Fraction. Unlike the study by Clark and Gedney (2008) this study had little success in introducing heterogeneity in the averaged surface runoff. In their study they compared the impact of using the TOP MODEL or the Probability Distributed Moisture model (PDM) on surface runoff and soil moisture heterogeneity. JULES has the option to use either of the two models. However, in this study none of the two models were used. This may be responsible for the insignificant average changes in the surface runoff obtained in the study.

Differences in predicted GPP between the two experiments in those areas where there is over 80% difference in fractional land cover (between broadleaf trees and C4 grass) is a clear representation of the models configuration on how plant respiration and productivity is calculated based on different plant phenological types. A similar study by Taylor *et al.*, (2002), while, examining the impact of land use and land cover on rainfall in the West African Sahel noticed an

insignificant contribution of land use and land cover change on seasonal rainfall in the region. However, they noticed a reduction in rainfall in the months at the start of the wet season.

Difference in predicted surface temperature between Experiment 1 and Experiment 2 suggest an increase in most parts. This increase by as much as  $0.8^{\circ}\text{C}$  in some parts is similar to the findings of Bounoua *et al.* (2002). They suggested that potential surface warming from land conversion in the tropics and sub-tropics is caused by both physiological and morphological changes in vegetation leading to a reduction in latent heat flux.

In order to observe the trends in energy, moisture and carbon flux over the 20 year period (2046-2065) a time series plot of the Bowen ratio, predicted Evaporative Fraction, soil moisture, and GPP was fitted to a least square regression line (Figure 5-9). While, there was an insignificant decreasing trend in the Bowen ratio (slope= $-1.7\text{e-}03$ ,  $p>0.05$ ) but an insignificant increasing trend in the Evaporative Fraction (slope= $2.0\text{e-}03$ ,  $p>0.05$ ), soil moisture (slope= $0.5\text{e-}03$ ,  $p>0.05$ ) and GPP (slope= $4.3\text{e-}05$   $\text{KgC m}^2$ ,  $p>0.05$ ).

The significant increase in predicted soil temperature in the future (2046-2056) compared to predicted soil temperature in the past (1980-2000) may have implications in agriculture since germination and growth in certain crops are influenced by soil conditions including temperature. There is no significant change to the average predicted soil moisture condition between the two periods which does not explain the significant increase in the Evaporative Fraction. Soil moisture is responsible for the partitioning of incident energy into sensible and

latent heat flux. However this increase may be related to the increase in the GPP. The increase in GPP is related to the increase in atmospheric temperature since plant respiration initially responds positively to increase in temperature and atmospheric carbon concentrations. This finding is similar to the revelations made by Henderson-Sellers *et al.* (1995) on the effects of increasing atmospheric carbon dioxide concentrations and stomatal resistance of different vegetation groups. In JULES, flux of moisture and carbon dioxide uptake is linked through stomatal resistance of the vegetation (Clark *et al.*, 2011) and is clearly reflected in the predicted GPP.

## **5.7 Acknowledgment**

The Author wish to express his appreciation to the FORMECU unit and the GLOBCOVER project for providing access to the land cover data used for this study.

## Chapter 6. **General Discussion**

### **6.1 Introduction**

In the preceding chapters of this thesis an attempt was made to analyse and predict; rainfall as a driver of land surface processes in North-eastern Nigeria, and past and future conditions of land surface conditions under changing climatic and LUC conditions. A general discussion of the results is presented in this chapter linking all of the results provided in each of the chapters.

### **6.2 Overview and general discussion**

The west African Sahel has experienced consistent droughts in the 1960s, 1970s, and 1980s with a talk of recovery in the 1990s (Nicholson 1979; 1997,). As a result two contending views developed from the scientific research community to explain the causes of this re-occurring natural disaster. The first view to evolve emphasized on the rapid changes in land cover in the region and associated changes in land surface-atmosphere feedback mechanism. The second view focussed on the ocean-atmosphere interaction mechanism with emphasis on the relationship between sea surface temperatures (SSTs) and the West African Monsoon (WAM), the strength of the African Easterly Jet and the influence of atmospheric dust on rainfall.

An attempt was made to study the strength of the recovery in rainfall from the severe drought years of the 1980s by analysing past records of monthly rainfall in North-eastern Nigeria described in Chapter 2. A notable finding presented in

Chapter 2 was that, despite the recovery in rainfall in the 1990s evidenced in previous studies using rainfall data (Nicholson, 1997; 2013) and satellite based vegetative index data (Anyamba and Tucker, 2005) the strength of the recovery of monthly rainfall in the months following the onset of the wet season was very weak in the southern savannah regions. This result is very consistent with the reports of increasing episodes of dry-spells in the region (Jury *et al.*, 2002; Odekunle, 2006; Hess 1995). Dry spells or dry episodes in the onset of the wet season increases the risk of crop failure and is a threat to agricultural production and food security in the region (Jury *et al.*, 2002).

Also in Chapter 2 the ARIMA model was shown to be a satisfactory method of forecasting short term monthly rainfall. In the study, it was proven that the ARIMA model was not merely repeating the long term means of monthly rainfall used to make the prediction. This is an indication of a memory in the models prediction. Possibly, the model can be used by climatologist, agriculturalist, hydrologist and other researchers in the study area for predicting monthly rainfall over a short time period and forecasting droughts.

An insignificant change in monthly rainfall and number of rainy days in the months marking the commencement of the wet season in the months of May, June, and July was very similar to the findings of Taylor *et al.* (2002) on the impact of land use, land cover change on the climate of the Sahelian West Africa. They refer to changes in the land surface conditions during the period as the major cause of the weakening in rainfall at the onset of the wet season. This finding

raises a question “how do land surface conditions in the study area respond to climate variability and land cover change?”

Chapter 3 presents a detailed description of predicted land surface conditions in the past (1980-200) using the Joint UK Land Environment Simulator (JULES). During the 1980s the study area experienced the worst prolonged period of drought since the beginning of modern day record keeping. While, the 1990s was marked as period when there was a recovery in rainfall. The study described in Chapter 3 was meant to capture this transition from dry years to wet years and how this change influence the land surface conditions of soil moisture, soil temperature, surface runoff, GPP and latent and sensible heat flux.

In Chapter 3, it was established that the JULES model is more sensitive to scale used for soil input data than non-linearity in the calculation of soil hydraulic parameters. However, the differences in predicted SSM between the Experiment 2 and the other 4 experiments indicate a strong influence of soil texture on the models output in line with earlier studies conducted by Wilson *et al.* (1987), Xue *et al.* (1996) both using a different land surface schemes and more recent work by Ellis *et al.* (2009) using the JULES model. The difference introduced by the soil texture is further amplified by the scale used in each of the experiments. Thus, the JULES model produce similar outputs for experiments using soil input data of the same scale.

Land cover change in JULES is driven by the atmospheric forcing data (i.e. climatic variability) and, therefore, does not take into account changes due to land use. During a model run changes in land use is assumed to be static. And this

raises some degree of uncertainty in the model results since land cover change in West Africa are driven by land use largely the conversion of other land uses to croplands (Ramankutty, 2004). Therefore, any future prediction of land surface condition in Africa needs to take into consideration land use and land cover change (LUCC).

Changes to land cover from 1976 to 2009 were analysed using the land change modeller (LCM) in IDRISI Taiga and presented in Chapter 4. The Cellular-Automata Markov model which uses trends in past changes in land cover to predict future change was used to produce a projected land cover of the area for 2046. The model was evaluated by using the land cover of 1994 and 2005 to predict the land cover (LC) of 2009. Based on evaluation the CA-Markov model was successful in predicting LC for 2009. It was established that changes in the LC was dominated by land use which is similar to the generalised statements made by Ramankutty (2004) and Lambin (2001) on West Africa. However, the process of harmonising land cover types from two different data sets, the FORMECU land use and land cover (LULC) maps ( 1977 and 1994) and the GLOBCOVER data (2005 and 2009) may have introduced discrepancies and effect the final results of the study. Also, the method of CA-Markov model employed in this study where the future land cover is based on past trends in land cover change produces a linear trend in land cover change which may not be the same as in reality. Despite these uncertainties, the study was a first combined attempt to asses and project land cover change in North-eastern Nigeria as a whole.

In order to predict future land surface conditions (2046-2065) under changing climatic conditions and land cover two sets of experiments were carried out. Both experiments used the JULES model with the A2 atmospheric forcing but differ in the fractional land cover used to generate boundary conditions. The results were presented in Chapter 5. Experiment 1 used existing land cover and Experiment 2 used a projected land cover fraction for 2046 derived from the projected land cover map produced earlier using the CA-Markov model. There were no statistically significant changes in predicted soil moisture, surface runoff, soil temperature, GPP, latent and sensible heat averaged across the study area between the two experiments. There were no significant changes in Evaporative Fraction and the Bowen ratio between the two experiments. But there were significant changes in areas where broadleaf fractional land cover was replaced with C4 grass by over 80%. In those areas there were significant increases in surface runoff, GPP and Evaporative Fraction. Also, predicted soil moisture content averaged across the six soil layers decreased. The reason for these changes was related to the water efficiency usage by C4 grass compared to broadleaf trees. In some areas predicted surface temperature increased by as much 0.8 °C as a result of the difference in fractional land between the two experiments. These changes in surface temperature were in the same areas where broadleaf trees dominant fractional land cover type was replaced by either C3 or C4 grass. These findings were similar to another study conducted by Bounoua *et al.* (2002).

It is notable that the assumption on land use change when running JULES explained earlier in Chapter 3 still remains the same while conducting the two

experiments into the future. The influence of fires and its influence on the climate and the carbon dioxide cycle were not considered.

Still on Chapter 5, the predicted land surface conditions of soil moisture, soil temperature, GPP, Evaporative Fraction and latent and sensible heat flux were compared between the past (1980-2000) and the future (2046-2065) predictions. The reason for the comparison was to determine the level of significance of the differences between the two periods. There were significant changes in the soil temperature, GPP, Evaporative Fraction and sensible heat and latent heat. There were no significant changes in soil moisture content averaged across the 6 soil layers between the two periods. There were also no significant changes in monthly rainfall between the two periods and this may explain the reason for the insignificant changes in the soil moisture content. Significant increase in predicted GPP and latent heat flux in the future (2046-2065) were in response to changes in atmospheric carbon concentration and temperature which is similar to the findings of Henderson-Sellers *et al.* (1995).

## Chapter 7. **Conclusions**

Based on results discussed in Chapter 6 the following conclusions were made:

- Despite a recovery from the droughts years of 1960s, 70s and 80s in the sub-humid part of the study area there appears to have been no significant recovery of rainfall in the months signalling the commencement of the Wet Season (June and July) with potential repercussions for rain fed agriculture.
- Based on the evaluations made on the ARIMA model, the model was successful in forecasting monthly rainfall in the study area over a short period.
- The JULES land surface model was more sensitive to scale than non-linearity in the calculation of soil hydraulic parameters used as input data.
- A strong correlation was found between the model surface soil moisture content and observations retrieved from the ERS satellite data with corresponding similarities in the anomaly pattern. These suggest a positive evaluation of the model.
- There was an increasing trend in land surface condition of near surface soil moisture content, energy fluxes and GPP between 1980 and 2000 suggesting that the model was able to replicate the recovery in this part of the West African Sahel from droughts after 1990 as widely publicised by other literature.

- There is an indication that land cover change in the area is mainly driven by land use since analysed land cover change is mainly the conversion of forest and wood lands to croplands.
- Land cover conversions had little impact on the land surface conditions in the area on average, although there were significant changes in predicted soil moisture content, and GPP but no significant change in the Evaporative Fraction in areas where there is a conversion from mainly broadleaf trees to C4 grass (croplands).
- Future land cover change and climate variability based on the IPCC A2 climate scenario suggest a higher level of GPP, soil temperature and evaporative fraction between the periods of 2046-2065 than in the 1980-2000 period. But there is no significantly increasing trend in land surface conditions during the period.
- Overall, it has been established that climate variability has the major influence on land surface conditions with land cover change having a minor influence. However, the influence of land cover change is very strong in areas where there is complete conversion of tree cover to croplands or grasslands.

## 7.1 Further work

Most of the uncertainties and limitations of this study were already mentioned in Chapter 6 and previous chapters. Proposal for future work is laid down in this section based on those limitations, uncertainties and some of the novel findings in this research.

The study suggests that future predictions of monthly rainfall should consider comparing the performance of the ARIMA model with other models such as artificial neural networks (ANN) that will take into account conditions favourable for rainfall in the area. These conditions may include SST, the AEJ, land surface conditions and the position of the ITCZ.

One of the limitations of the study noted in Chapter 3 is the availability of ground observations. Future studies may consider evaluating the model output using observations data. Presently, observations of soil moisture and energy fluxes are scanty. Another consideration may be the use of meteorological station data to drive the model.

The experiments carried out to predict past (1980-2000) and future (2046-2065) land surface conditions described in Chapter 3 and Chapter 5 were conducted using JULES without the TOP MODEL or the PDM model, and therefore, the influence of topography on soil moisture heterogeneity and surface runoff were ignored. Future studies may consider using one of the options which are already available on JULES in order to reduce uncertainties.

The results of the land surface predictions presented in the preceding chapters of this thesis were conducted using the JULES model on a  $1^{\circ} \times 1^{\circ}$  and  $\frac{1}{2}^{\circ} \times \frac{1}{2}^{\circ}$

scale. Future studies may use a finer scale for further improving the representation of the land surface.

Further studies involving projecting future land cover in the area should consider the use of more realistic probability maps for running the CA\_Markov model instead of using the Markov chain model that produces probability maps based on past trends in land cover change. A multi criteria evaluation (MCE) method may be applied in producing land suitability maps based on land use, demographic changes, soils, slope and elevation data.

It could be appropriate in the future to consider running experiments on the impact of land cover and climate variability in a coupled land surface, atmospheric, and land use model similar to the work of Taylor *et al.* (2002) and compare this with results from an “offline mode” of JULES. This is in view of the availability of more detailed data sets for running climate models and land surface models. Another reason for this is that while there have been studies of this nature that used a coupled model there is little information on how these models perform under different circumstances. For instance in this study the impact of land cover change is insignificant probably because of the lack of feedback and could have been more significant if the land surface model has been coupled to an atmospheric model.

In Africa LUCC and bush fires have a strong influence on the continents carbon cycle (Cias *et al.*, 2011). The effect of bush fires was not considered in this study and this provides an avenue for future work.

## **Bibliography**

Abdi, H., 2007 Kendall rank correlation. In: Salkind, N.J. ed. *Encyclopedia of Measurement and Statistics*.

Adefolalu, D.O., 1986 Rainfall Trends in Nigeria *Theoretical and Applied Climatology* 37, 205-219

Ademiluyi, I.A., Okude A.S. and Akanni C.O., 2008 An appraisal of land use and land cover mapping in Nigeria *African Journal of Agricultural Research* 3:9, 581-586

Akobundu, I.O., Ekeleme, F. and Chikoye, D., 1999 Influence of fallow management systems and frequency of cropping on weed growth and crop yield *Weed Research* 39,241-256 Blackwell Science

Amissar-Arthur, A., and Jagtap S.S., 1999 Geographic Variation in Growing season rainfall during three decades in Nigeria using principal component and cluster analysis *Theoretical and Applied Climatology* 63, 107-116 Springer-Verlag

Anyamba, A. and Tucker, C. J., 2005 Analysis of Sahelian vegetation dynamics using the NOAA-AVHRR NDVI data from 1981-2003 *Journal of Arid Environments* 63 596–614

Ati, O.F., Stigter, C.J., Iguisi, E.O. and Afolayan J.O., 2009 Profile of rainfall change and variability in the Northern Nigeria, 1953-2002 *Research Journal of Environmental and Earth Sciences* 1:2, 58-63

Barbour, K. M., 1971 North-eastern Nigeria-A case study of state formation *The Journal of African studies* 9:1, 49-71 <http://www.jstor.org/stable/159251>

Bengtsson, L., Hodges, K.I., Roeckner, E., Brokopf, R., 2006 On the natural variability of the pre-industrial European climate *Climate Dynamics* 27:7-8, 743-760

Best, M.J., Pryor, M., Clark, D.B., Rooney, G.G., Essery, R.L.H., Ménard, C.B., Edwards, J.M., Hendry, M.A., Porson, A., Gedney, N., Mercado, L.M., Sitch, S., Blyth, E., Boucher, O., Cox, P.M., Grimmond, C.S.B. and Harding R.J., 2011 The Joint UK Land Environment Simulator (JULES), Model description-Part 1: Energy and water fluxes *Geoscientific Model Development Discussion* 4, 595-640

Betts R., 2006 *JULES as a framework for Impacts modelling* JULES Workshop 2<sup>nd</sup> October 2006

Betts A.K., and Silva Dias M.A.F., 2010 Progress in Understanding land-surface-atmosphere coupling over the Amazon: a review *Journal of Advances in Modelling Earth Systems JAMES* 2, 1-20

Betts, A.K., Beljaars, A.C.M., Miller, M.J. and Viterbo P.A., 1996 The land surface-atmosphere interaction: A review based on observational and global modelling perspectives. *Journal of Geophysical Research* 101:3, 7209-7225

Bicheron, P., Leroy, M., Brockmann, C., Krämer, U., Miras, B., Huc, M., Ninõ, F., Defourny, P., Vancutsem, C., Arino, O., Ranéra, F., Petit, D., Amberg, V., Berthelot, B. and Gross, D., 2005 *GLOBCOVER: A 300m global land cover product for 2005 using ENVISAT MERI time series* Proceedings of the Recent Advances in Quantitative Remote Sensing Symposium, Valencia September 2006

Bontemps, S., Defourny, P., Van Bogaert, E., Arino, O., Kalogirou, V., Perez, J.R. 2011 *GLOBCOVER 2009: Products description and validation report* European Space Agency (ESA)/ Université Catholique de Louvain (UCL) Pp 1-53

Borokini, T.I., Babalola, F. D., Amusa, T. O., Ivande, S. T., Wala, Z. J., Jegede, O. O., Tanko, D. and Ihuma J. O., 2012 Tropical Montane Forest Biodiversity in Nigeria – Case Study of Ngel Nyaki Forest Reserve, Mambilla Plateau  
*International Journal of Environmental Sciences* 1: 2, 95-104

Bounoua, L., Defries, R., Collatz, G. J., Sellers, P., and Khan, H., 2002 Effects of land cover conversion on surface climate *Climate Change* 52: 29-64

Box, G.E.P, and Jenkins, G.M. 1976 *Time series analysis forecasting control*  
Holden-Day San-Francisco

Bovill, E.W., 1921 The Encroachment of the Sahara on the Sudan *Journal of the Royal African Society* 20: 79, 174-185

Brocca, L., Melon, F., Maramarco, T. and Morbidelli, R., 2010 Saptial-temporal variability of soil moisture and its estimation across scales *Water Resources Research*, 46, W02516, doi:10.1029/2009WR008016, 2010

Brooks, R.H., Corey and A.T., 1964 *Hydraulic properties of porous media*  
Hydrology Paper No. 3, Colorado State University, Fort Collins, CO, 27 pp.

Carlson, T.N. and Prospero, J.M., 1972 The large-scale movement of Saharan air outbreaks over the Northern Equatorial Atlantic *Journal of Applied Meteorology* 11, 283-297

Cias, P., Bombelli, A., Williams, M., Piao, S.L., Chave, J., Ryan, C.M., Henry, M., Brender, P. and Valentini, R., 2011 The carbon balance of Africa: synthesis of recent research studies *Philosophical Transactions of the Royal Society* 369, 1-20

Charney, J., Quirk, W., Chow, S. and Kornfield, J., 1977 A comparative study of the effects of albedo change on drought in Semi-arid Regions *Journal of the Atmospheric Science* 34, 1366-1385

Charney, J.G., 1975 Dynamics of deserts and drought in the Sahel *Quarterly Journal of the Royal Meteorological Society* 101, 193-202

Chase, T.N., Pielke, R.A.S., Kittel, T.G.F, Nemani, R.R. and Running, S.W., 2000 Simulated impacts of historical land cover changes on global climate in northern winter *Climate Dynamics* 16, 93-105

Clark, D. and Gedney N., 2008 Representing the effects of subgrid variability of soil moisture on runoff generation in a land surface model *Journal of Geophysical Research* 113 (D10111). Doi:1029/2007/JD 008940

Clark D., Harris P. (2007) *Joint UK Land Environment Simulator (JULES) Version 2.0 User Manual* None, 100pp. (Unpublished)

Clark D., Harris P., Pryor M, Hendry M (2011) *Joint UK Land Environment Simulator (JULES) Version 3.0 User Manual* (Unpublished)

Cook, K.H., 1999 Generation of African Easterly Jet and its role in determining West African Precipitation *Journal of Climate* 12, 1165-1184

Cosby, B.j., Hornberger G.M., Clapp, R.B. and Ginn, T.R, 1984 A statistical exploration of the relationships of soil moisture characteristics to the physical properties of soils *Water Resources Research* 20:6, 682-690

Cox, P.M., Betts, R., Jones, C.D., Spaal, S.A. and Totterdell, I., 2000 Acceleration of Global warming due to carbon-cycle feedbacks in a coupled climate model *Letters to Nature* 408, 184-187

Cox, P.M, Betts, R.A., Bunton, C.B. Essery, R.L.H., Rowntree, P.R. and Smith J., 1999 The impact of new land surface physics on the GCM simulation of climate and Climate Sensitivity *Climate Dynamics* 15:183-203

Decharne, B., Boone, A. and Noilhan J., 2011 Local evaluation of the interaction between soil biosphere atmosphere soil multilayer diffusion scheme using four pedotransfer functions *Journal of Biophysical Research* 116, D20126, doi:10.1029/2011JD016002, 2011

DeMott, P. J., Sassen, K., Poellot, M. R., Baumgardner, D., Rogers, D. C.,  
Brooks, S. D., Prenni, A. J. and Kreidenweis, S. M., 2003 African dust aerosols  
as atmospheric ice nuclei, *Geophys. Res. Lett.* 30, 1732,  
doi:10.1029/2003GL017410, 14.

Dirmeyer, P.A., Schlosser, C.A. and Brubaker K.L. 2009 Precipitation, recycling,  
and land memory: An integrated analysis *Journal of Hydrometeorology* 10,278-  
288

Dolman, A.J., Verhagen, A. and Rovers, C.A., 2003 *Global environmental change  
and land use* Kluwer Academic Publishers Netherlands

Dvořák, K.A., 1992 Resource Management by West African farmers and the  
economics of shifting cultivation *American Journal of Agricultural Economics*  
74:3, 809-815

Ellis, E. and Pontius, R., 2007 Land-use and land-cover change; In: *Encyclopedia  
of Earth*. Eds. Cutler J. Cleveland (Washington, D.C.: Environmental Information  
Coalition, National Council for Science and the Environment)

Ellis, R. J., Taylor, C.M., Weedon, G.P., Gedney, N., Clark, D.B. and Los, S.,  
2009 Evaluating the Simulated Seasonality of Soil Moisture with Earth

Observation Data. *J. Hydrometeor* 10, 1548–1560. doi:

<http://dx.doi.org/10.1175/2009JHM1147.1>

Ellis, S. and Mellor, A., 1995 *Soils and Environment* Routledge London and Newyork.

Essery, R., Best, M. and Cox P., 2001 MOSES 2.2 Technical Documentation

Flanagan, L.B. and Johnson, B. G., 2005 Interacting effects of temperature, soil moisture and plant biomass production on ecosystem respiration in a northern temperate grassland, *Agricultural and Forest Meteorology* 130:3–4, 237-253, ISSN 0168-1923, 10.1016/j.agrformet.2005.04.002.

<http://www.sciencedirect.com/science/article/pii/S016819230500081X>

Folland, C.K., Palmer, T.N and Parker, D.E., 1986 Sahel rainfall and worldwide sea temperatures, 1901-1985 *Nature* 320, 602-607

Fontaine, B., Janicot, S. and Moron, V., 1995 Rainfall anomaly patterns and wind field signals over West Africa in August (1958–1989) *J. Climate*, 8, 1503–1510

Forster, P., Ramaswamy, V., Artaxo, P., Berntsen, T., Betts, R., Fahey, D.W., Haywood, J., Lean, J., Lowe, D.C., Myhre, G., Nganga, J., Prinn, R., Raga, G., Schulz, M. and Van Dorland, R., 2007: Changes in Atmospheric Constituents and

in Radiative Forcing. In: [Solomon, S., Qin, D., Manning, M., Chen, Z., Marquis, M., Averyt, K.B., Tignor, M. and Miller, H.L., (eds.)] *Climate Change 2007: The Physical Science Basis*. Contribution of Working Group I to the Fourth Assessment Report of the Intergovernmental Panel on Climate Change. Cambridge University Press, Cambridge, United Kingdom and New York, NY, USA.

Fuller, D.O. and Ottke, C., 2002 Land cover, rainfall and land-surface albedo in West Africa *Climate Change* 54 181-204

Garba, S. S., 2008 *Assessment of land cover change in North-eastern Nigeria* PhD Cranfield University

Garcia-Frapoli, E., Ayala-Orozco, B., Bonilla-Moheno, M., Espadas-Manrique, C. and Ramos-Fernández, G. 2007 Biodiversity conservation, traditional agriculture and ecotourism: Land cover/use change projections for a natural protected area in the northeastern Yucatan Peninsula, Mexico *Landscape and Urban planning* 83,137-153

Gedney, N. and Cox, P.M., 2003 the sensitivity of global climate model simulations to the representation of soil moisture heterogeneity. *Journal of Hydrometeorology* 4:1265-1275

Ghent, D., Kaduk, J., Remedios, J., Ardö, J. and Balzter H., 2010 Assimilation of land surface temperature into the land surface model JULES with an ensemble Kalman filter *J. Geophys. Res.* 115, D19112, doi:10.1029/2010JD014392.

Giannini, A., Saravan, R. and Cheng, P., 2003 Oceanic forcing of Sahel rainfall on interannual to interdecadal time scales *Science* 302, 1027-1030

Global Carbon Project 2012 *Carbon Budget and Trends 2012*

[[www.globalcarbonproject.org/carbonbudget](http://www.globalcarbonproject.org/carbonbudget)] released on 3 December 2012

Goddard Institute for space studies GISS NASA 2012 Surface temperature anomalies 1880-2012 Anomaly text data

Guo, Z., Dirmeyer, P.A., Koster, R.D., Bonan, G., Chan, E., Cox, P., Gordon, C.T., Kanae, S., Kowalczyk, E., Lawrence, D., Liu, P., Lu, C., Malyshev, S., McAveney, B., McGregor, J.L., Mitchell, K., Mocko, D., Oki, T., Oleson, K.W., Pitman, A., Sud, Y.C., Taylor, C.M., Verseghy, D., Vasic, R., Xue, Y. and Yamada, T., 2006 GLACE: the global land-atmosphere coupling experiment. Part II: Analysis. *Journal of Hydrometeorology* 7:611-625

Hamby, D.M., 1994 A review of techniques for parameter sensitivity analysis of environmental models *Environmental Monitoring and Assessment* 32:135-154

Hardisty, J., Taylor D.M., and Metcalfe, S.E 1993 *Computational Environmental Modelling: A practical approach using Excel* John Wiley and sons West Essex England

Hankin, S., Callahan, J., Manke, A., O'Brien K. and Li J., 2007 *Ferret User's Guide: Version 6.02* Pp 1-12 NOAA/PMEL/TMAP

Hastings, D. A., Dunbar, P. K., Elphinstone, G. M., Bootz, M., Murakami, H., Maruyama, H., Masaharu, H., Holland, P., Payne, J., Bryant, N. A., Logan, T. L., Muller, J.-P., Schreier, G., and MacDonald, J. S., eds., 1999 *The Global Land One-kilometer Base Elevation (GLOBE) Digital Elevation Model, Version 1.0*. National Oceanic and Atmospheric Administration, National Geophysical Data Center, 325 Broadway, Boulder, Colorado 80305-3328, U.S.A. Digital data base on the World Wide Web URL: <http://www.ngdc.noaa.gov/mgg/topo/globe.html>

Helldén, U., 1988. Desertification monitoring: Is the desert encroaching? *Desertification Control Bulletin* 17, 8-12.

Henderson-Sellers, A., McGuffie, K. and Gross, C., 1995 Sensitivity of global climate model simulations to increased stomatal resistance and CO<sub>2</sub> increases *Journal of Climate* 8, 1738-1756

Hess, T.M., Stephens W., Maryah U.M., 1995 Rainfall trends in the North East Arid Zone of Nigeria 1961-1990 *Agricultural and Forest Meteorology* 74, 87-97

Houghton, J.T., Callander, B.A. and Varney, S.K., 1992 *Climate change 1992: The supplementary report to the IPCC scientific assessment* Cambridge publishers

Huang, J., Zhang, C. and Prospero J.M., 2009 African aerosol and large-scale precipitation variability over West Africa *Environ. Res. Lett.* 4 015006  
[doi:10.1088/1748-9326/4/1/015006](https://doi.org/10.1088/1748-9326/4/1/015006)

Hubert, H., 1917 Progression du dessèchement dans les Régions Sénégalaises *Annales de Géographie.* 26:143, 376-385

Hulme, M., Doherty, R., Ngara, T., New M. and Lister, D., 2001 African climate change: 1900-2100 *Climate Research* 17: 145-168

IPCC (Intergovernmental Panel on Climate Change), 2000 IPCC Special Report on Emissions Scenarios (SRES) Emissions Scenarios Dataset Version 1.1.

Palisades, NY: NASA Socioeconomic Data and Applications Center (SEDAC).

<http://sedac.ciesin.columbia.edu/data/set/ipcc-emissions-v1-1>

IPCC, 2001 *Climate Change 2001: The Scientific Basis. Contribution of Working Group I to the Third Assessment Report of the Intergovernmental Panel on Climate Change* [Houghton, J.T., Y. Ding, Griggs, D.J., Noguer, M., Van der Linden, P.J., Dai, X., Maskell, K., and C.A. Johnson (eds.)] Cambridge University Press, Cambridge, United Kingdom and New York, NY, USA, 881pp.

IPCC, 2007: Summary for Policymakers. In: *Climate Change 2007: The Physical Science Basis. Contribution of Working Group I to the Fourth Assessment Report of the Intergovernmental Panel on Climate Change* [Solomon, S., Qin, D., Manning, M., Chen, Z., Marquis, M., Averyt, K.B., Tignor, M., and Miller, H.L., (eds.)]. Cambridge University Press, Cambridge, United Kingdom and New York, NY, USA.

Jalloh, A., Roy-Macauley, H. and Sereme, P., 2011 Major agro-ecosystems of West and Central Africa: Brief descriptions, species richness, management, environmental limitations and concerns *Agriculture, Ecosystems and Environment* (2011), doi:10.1016/j.agee.2011.11.019

Jury, M.R., Enfield, D.B., and Mélice, J.L., 2002 Tropical Monsoons around Africa: Stability of El Niño-Southern Oscillation associations and links with continental climate *Journal of Geophysical Research* 107, NO. 0, 10.1029/2000JC000507, 2002

Karl, T.R. and Trenberth, K.E., 2003 Modern global climate change *Science* 302, 1719-1723

Khan, S., Gabriel, H.F. and Rana, T., 2008 Standard precipitation index to track drought and assess impact of rainfall on water tables in irrigation areas *Irrigation Drainage Systems* 22:159-177

Koster, R.D., Dirmeyer, P.A., Guo, Z., Bonan, G., Chan, E., Cox, P., Gordon, C.T., Kanae, S., Kowalczyk, E., Lawrence, D., Liu, P., Lu, C., Malyshev, S., MaAvaney, B., Mitchell, K., Mocko, D., Oki, T., Oleson, K., Pitman, A., Sud Y.C., Taylor, C.M., Verseghy, D., Vasic, R., Xue, Y. and Yamada, T., 2004 Regions of strong coupling between soil moisture and Precipitation *Science* 305, 1138-1140

Koster, D.R., Guo, Z., Yang, R., Dirmeyer, P.A., Mitchell, K. and Puma, M.J., 2009 On the nature of soil moisture in land surface models *Journal of Climate* 22; 4322- 4335

Koster, R.D., Suarez, M.J., Higgins, W., and Van den Dool 2003 Observational evidence that soil moisture variations affect precipitation *Geophysical Research Letters* 30, 5, 1241, doi:10.1029/2002GL016571, 2003

Kurnik, B., Barbosa, P. and Vogt, J., 2011 Testing two different precipitation datasets to compute the standardized precipitation index over the Horn of Africa *International Journal of Remote Sensing* 32:21,5947-5964

Lai R., 2003 Carbon sequestration in dryland ecosystems *Environmental Management* 33:4, 528-544

Lamb, P.J., 1978 Large-scale Tropical Atlantic surface circulation patterns associated with Subsaharan weather anomalies *Tellus* 30, 240-251

Lamb, P.J., 1983 West African water vapour variations between recent contrasting Sub-Saharan rainy seasons *Tellus* 35A, 198-212

Lambin, E.F., Geist, H.J. and Lepers, E., 2003 Dynamics of Land-use and land-cover change in tropical regions *Annual Reviews in Environmental Resources* 28:205-41

Lambin, E.F., Turner, B.L., Geist, H.J., Agbola, S.B., Angelsen, A., Bruce, J.W., Coomes, O.T., Dirzo, R., Fischer, G., Folke, C., George, P.S., Homewood, K., Imbernon, J., Leemans, R., Li, X., Moran, E.F., Mortimore, M., Ramakrishnan, P.S., John, F.R., Skanes, H., Steffen, W., Stone, G.D., Sveden, U., Veldkamp, T.A., Vogel, C. and Xu, J., 2001 The causes of land-use and land-cover change: moving beyond the myths *Global Environmental Change* 11, 261-269

Lamprey, H.F., 1975 Report on the desert encroachment reconnaissance in Northern Sudan, 21 Oct. to 10 Nov., 1975. *Unesco/UNEP (mimeo.)*, 16 Pp

Leblanc, M., Lemoalle, J., Bader, J.-C., Tweed, S. and Mofor, L., 2011 Thermal remote sensing of water under flooded vegetation: New observations of inundation patterns for the 'small' Lake Chad *Journal of Hydrology* 404, 87-98

Lemoalle, J., Bader, J.-C., Leblanc, M. and Sedick, A., 2012 Recent changes in Lake Chad: Observations, simulations and management options 1973-2011 *Global Planetary Change* 80-81; 247-254

Li, H., Robock, A., and Wild, M., 2007 Evaluation of intergovernmental panel on climate change fourth assessment soil moisture simulations for the second half of the century *Journal of Geophysical Research*, 112, D06106, doi:10.1029/2006JD007455, 2007

Li, S., Liu, S. and Liu, H., 2010 Influences of climate change and its interannual variability on the surface energy fluxes from 1948 to 2000 *Adv. Atmos. Sci.* 27 1438-1452

Los, S.O., Weedon, G.P., North, P.R.J, Kaduk, J.D., Taylor, C.M. and Cox, P.M., 2006 An observation-based estimate of the strength of rainfall-vegetation

interactions in the Sahel *Geophysical Research Letters* 33, L16402,

doi:10.1029/2006GL027065

Lykke, A.M., Barford, A.S., Svendsen, G.T., Greve, M. and Svenning, J-C., 2009

Climate change mitigation and carbon stock-the case of semi-arid West Africa

*IOP Conf. Series: Earth and Environmental Sciences* 8 (2009) 012004

(<http://iopscience.iop.org/1755-1315/8/1/012004>)

Mahmood, R., Pielke, R.A., Hubbard, K.G., Niyogi, D., Bonan, G., Lawrence, P.,

McNider, R., McAlpine, C., Etter, A., Gameda, S., Qian, B., Carleton, A.,

Beltran-Prezekurat, A., Chase, T., Quintanar, A.I., Adegoke, J.O.,

Vezhapparambu, S., Coner G., Asefi, S., Sertel, E., Legates, D.R., Wu, Y., Hale,

R., Frauenfeld, O.W., Watts, A., Shepherd, M., Mitra, C., Anantharaj, V.G., Fall,

S., Lund, R., Treviño, A., Blanken, P., Du, J., Chang, H., Leeper, R., Nair, U.S.,

Dobler, S., Deo, R. and Syktus, J. 2010 Impacts of land use/land cover change on

climate and future research priorities *Bulletin of the American Meteorological*

*Society BAMS* 91: 1, 37-46 DOI:10.1175/2009BAMS2769.1

Mahmood, R., Leeper, R., and Quintanar, A.I., 2011 Sensitivity of planetary

boundary layer atmosphere to historical and future changes in land use/land cover,

vegetation fraction, and soil moisture in Western Kentucky, USA *Global and*

*Planetary Change* 78:36-53

Mariotti, L., Coppola, E., Sylla, M.B., Giorgi, F., and Piani C., 2011 Regional climate model simulation of projected 21<sup>st</sup> century climate change over an all-Africa domain: Comparison analysis of nested and driving model results *Journal of Geophysical Research* 116, D15111, doi:10.1029/2010JD015068, 2011

Mbourou-N'Tchayi, G., Bertrand, J. J. and Nicholson, S. E., 1997: The Diurnal and Seasonal Cycles of Wind-Borne Dust over Africa North of the Equator. *J. Appl. Meteor.* 36, 868–882.

Mortimore, M. and Adams, W.M., 1999 *Working the Sahel: Environment and Society in Northern Nigeria* Routledge Publishers London 1:1-14

Mortimore, M., Ba, M., Mahamane, A., Rostom, R.S., Pozo ,P.S. and Turner, B. 2005 Changing systems and changing landscapes: Measuring and interpreting land use transformation in African drylands *Geografisk Tidsskrift, Danish Journal of Geography* 105(1), 101-118

Mortimore, M., Harris, F.M.A. and Turner, B., 1999 Implications of land use change for the production of plant biomass in densely populated Sahelo-Sudanian shrub-grasslands in North-east Nigeria *Global Ecology and Biogeography* 8, 243-256

Manabe S., 1969 Climate and the ocean circulation: The atmospheric circulation and the hydrology of the Earth surface *Monthly Weather Review* 97:11,739-774

Meng, L., and Quiring, S.M., 2010 Observational relationship of sea surface temperature and precedent soil moisture with summer precipitation in the US Great Plains *International Journal of Climatology* 30, 884-893

Nicholson, S., 1979 Sub-Saharan rainfall in the years 1976-80: Evidence of continued drought *Monthly Weather Review* 111, 1646-1654

Nicholson, S. E., 2013 The West African Sahel: A Review of Recent Studies on the Rainfall Regime and Its Interannual Variability, *ISRN Meteorology*, 2013, Article ID 453521, 32 pages, 2013. <http://dx.doi.org/10.1155/2013/453521>  
[Accessed 14th May 2013]

Nicholson, E. and Kim, J., 1997 The relationship of the El Niño-southern oscillation to African rainfall *International Journal of Climatology* 17, 117-135

Nicholson, S.E., Some, B. and Kone, B., 1998 An analysis of recent rainfall conditions in West Africa, including the rainy seasons of the 1997 El Niño and the 1998 La Niña years *Journal of climate* 13:2628-2640

Njoku, E.G., Jackson, T.J., Lakshmi, V., Chan, T.K. and Nghiem, S.V., 2003 Soil moisture retrieval from AMSR-E *IEEE Transactions on Geoscience and Remote Sensing* 41:2,215-229

Obaje, N. G., 2009 *Geology and Mineral Resources of Nigeria* Pp 57-6 Springer Publishers

Obaje, N. G., Attah, D. O., Opeloye, S. A. and Moumouni, A., 2006 Geochemical evaluation of the hydrocarbon prospects of sedimentary basins in Northern Nigeria *Geochemical Journal* 40, 227-243

Oladipo, E. O., 1993 A Comprehensive Approach to Drought and Desertification in Northern Nigeria. *Natural Hazards Journal* 8, 235-261

Olugbemi, R.O., Ligouis, B. and Abaa, S.I., 1997 The cretaceous series in the Chad Basin, NE Nigeria: Source rock potential and thermal maturity *Journal of Petroleum Geology* 20(1), 51-68

Odekunle, T.O., 2006 Determining rainy season onset and retreat over Nigeria from precipitation amount and number of rainy days *Theoretical and Applied Climatology* 83, 193-201

Oguntude, P.G., Abiodun, B.J. and Lischeid, G., 2011 Rainfall trends in Nigeria, 1901-2000 *Journal of hydrology* 411, 207-218

Oreskes, N., 2003 The role of quantitative models in science. In: Canham C.D., Cole J.J. and Lauenroth W.K., ed. 2003. *Models in ecosystem science* Princeton University Press

Otterman, J., 1974 Baring high-albedo soils by overgrazing: A hypothesized desertification mechanism *Science* 186, 531- 533

Peel, M.C., Finlayson, B.L, and Mc Mahon, T.A., 2007 Updated world map of the Köppen-Geiger climatic classification *Hydrol. Earth Syst. Sci.* 11, 1633-1644

Parry, D.E., and Trevett, J.W. 1979 Mapping Nigeria's Vegetation from Radar *The Geographical Journal* 145, 2: 265-274

Pidwirny, M., 2006. Climate Classification and Climatic Regions of the World *Fundamentals of Physical Geography, 2nd Edition*. [Online] Available at: <http://www.physicalgeography.net/fundamentals/7v.html> [Accessed 11 February, 2011]

Pitman, A.J., 2003 Review: the evolution of, and revolution in land surface schemes designed for climate models. *International Journal of Climatology* 23:479-510

Prince, S.D., BrownDe Colstoun, E. and Kravitz, L. L., 1998 Evidence from rain-use efficiencies does not indicate extensive Sahelian desertification *Global Change Biology* 4:4, 359– 374

Ramankutty, N., 2004 Croplands in West Africa: A geographically explicit data set for use in models *Earth Interactions* 8: 23, 1-22

Raupach, M. R., Marland, G., Cias, P., Quere, C., Candell, J. G., Klepper, G. and Field, C.B., 2007 Global and regional drivers of accelerating CO<sub>2</sub> emissions, *Journal of the Proceedings of the National Academy of Sciences of the USA (PNAS)* 104:24, 10288-10288

Rawls, W. J., Brakensiek, D. L., and Saxton, K.E., 1982 Estimation of soil water properties *Transactions of the ASAE* 25(5), 1316-1320

Riebsane, W.E., Meyer, W.B. and Turner II, B.L., 1994 Modelling Land use and cover as part of global environmental change *Climatic Change* 28, 45-64

Ripley, E. A., 1976 Drought in the Sahara: Insufficient Biogeophysical Feedback?

*Science* 191: 4222, 100 DOI: 10.1126/science.191.4222.100

Robock A., Vinikov K. Y., Srinivasan G., Entin J., Hollinger S. E., Speranskaya

N. A., Liu S., and Namkhai A. (2000) The global soil moisture data bank.

*American Meteorological society* 8:61,1281-1299

Rowell, D. P., 2001 Teleconnections between the tropical Pacific and the Sahel

*Q.J.R. Meteorol. Soc.* 127, 1683–1706. doi: 10.1002/qj.49712757512

Rowell, D.P., Folland, C.K., Maskell, K. and Ward, M.N., 1995. Variability of

summer rainfall over tropical North Africa (1906-92): observations and

modelling. *Quarterly Journal of the Royal Meteorological Society* 121, 669}704

Sankaran, M., Niall, P. H., Scholes, R. J., Ratnam, J., Augustine, D.J., Cade, B.S.,

Gignoux, J., Higgins, S.I., Le Roux, X., Ludwig, F., Ardö, J., Banyikwa, F.,

Bronn, A., Buccini, G., Caylor, K., Coughenour, M.B., Diouf, A., Ekaya, W.,

Feral, C.J., February, C.E., Frost, P.G., Hiernaux, P., Hrabar, H., Metzger, K.L.,

Prins, H.T., Ringrose, S., Sea, W., Tews, J., Worden, J. and Zambatis N., 2005

Determinants of woody cover in African savannas. *Nature* 438/8,846-849

- Saxton, K. E., Rawles, W.J., Romberger, J.S. and Papendick, R.I., 1986  
Estimating generalized soil-water characteristics from texture. *Soil Sci. Soc. Am. J.* 50,1031-1036
- Schmidli, J. and Frei, C., 2005 Trends of heavy precipitation and wet and dry spells in Switzerland during the 20<sup>th</sup> Century *International Journal of Climatology* 25, 753-771
- Schüttemeyer, D. 2005 *The surface energy balance over drying semi-arid terrain in West Africa*. PhD University of Wageningen Netherlands
- Solomon, S., D. Qin, M. Manning, R.B. Alley, T. Berntsen, N.L. Bindoff, Z. Chen, A. Chidthaisong, J.M. Gregory, G.C. Hegerl, M. Heimann, B. Hewitson, B.J. Hoskins, F. Joos, J. Jouzel, V. Kattsov, U. Lohmann, T. Matsuno, M. Molina, N. Nicholls, J. Overpeck, G. Raga, V. Ramaswamy, J. Ren, M. Rusticucci, R. Somerville, T.F. Stocker, P. Whetton, R.A. Wood and D. Wratt, 2007: Technical Summary. In: *Climate Change 2007: The Physical Science Basis. Contribution of Working Group I to the Fourth Assessment Report of the Intergovernmental Panel on Climate Change* [Solomon, S., D. Qin, M. Manning, Z. Chen, M. Marquis, K.B. Averyt, M. Tignor and H.L. Miller (eds.)]. Cambridge University Press, Cambridge, United Kingdom and New York, NY, USA.

Sonneveld, B.G.J.S., 1997 *Dominant Soils of Nigeria Map* Stichting Onderzoek Wereldvoedselvoorziening van de Vrije Universiteit (SOWVU), Amsterdam

Steiner, A. L., Pal, J.S., Rauscher, S.A., Bell, J.L., Diffenbaugh, N.S., Boone, A., Sloan, L.S. and Giorgi, F., 2009 Land surface coupling in regional climate simulations of the West Africa monsoon, *Climate Dynamics* 33:6, 869-892 DOI 10.1007/s00382-009-0543-6

Taylor, C.M., Lambin, E.F., Stephenne, N., Harding, R.J. and Essery, R. L.H., 2002 The influence of land use change on climate in the Sahel *Journal of Climate* 14, 3615-3629

The Land Surface Process Representation in JULES, 2007. *JULES website* [online] Available at <https://jules.jchmr.org/> [Accessed 17 March 2010].

Tietje, O. and Hennings, V., 1996 Accuracy of the saturated hydraulic conductivity prediction by pedo-transfer functions compared to the variability within FAO textural classes. *Geoderma* 69, 71-84

Tischler, M., Garcia, M., Peters-Lidard, C., Moran, M.S., Miller, S., Thoma, D., Kumar, S. and Geiger, J., 2007 A GIS framework for surface-layer soil moisture estimation combining satellite radar measurements and land surface modelling

with soil physical property estimation *Environmental Modelling and Software* 22,  
891-8

Tucker, C.J., Dregne, H.E. and Newcomb, W.W., 1991 Expansion and  
Contraction of the Sahara Desert from 1980 to 1990 *Science* 253, 299-300  
[DOI:10.1126/science.253.5017.299]

Van Minnen, J. G., Goldewijk, K.K., Stefast, E., Eickhout, B., Drecht, G. and  
Leemans, R., 2009 The Importance of three centuries of land-use change for the  
global and regional terrestrial carbon cycle *Climate Change* 97, 123-144

Venables, V.N., Smith, D.M. and The R Core Team, 2013 *An Introduction to R*.  
[Online] Available at: <http://www.cran.r-project.org/doc/manuals/R-intro.pdf>

Vigaud, N., Roucou, P., Fontaine, B., Sijikumar, S. and Tyteca S., 2009  
WRF/ARPEGE-CLIMAT simulated trends over West Africa *Climate Dynamics*  
36, 926-944

Viterbo P., 2002 *A review of parameterization schemes for land surface processes*  
Meteorological training course lecture series ECMWF 2002

Wagner W., 1998 *Soil moisture retrieval from the ERS scatterometer data* PhD  
Technisch-naturwissenschaftliche Fakultät Vienna University of Technology  
Wien Austria

Wagner, W. and Scipal K., 2000 Large-scale soil moisture mapping in Western  
Africa using the ERS scatterometer *IEEE transactions on geosciences and  
remote sensing*, 38:4, 1777-1782

Wagner, W., Blösch, G., Pampaloni, P., Calvet, J., Bizarri B., Wigneron, J., Kerr  
Y., 2007 Operational readiness of microwave remote sensing of soil moisture for  
hydrological applications *Nordic Hydrology* 38:1,1-20

Wagner, W., Lemoine, G. and Rott H., 1999 A Method for Estimating Soil  
Moisture from ERS Scatterometer and Soil Data, *Remote Sensing of Environment*  
70, 191-207. doi:10.1016/S0034-4257(99)00036-X

Wagner, W., Scipal, K., Pathe, C., Gerten, D., Lucht, W. and Rudolf B., 2003  
Evaluation of the agreement between the first global remotely sensed soil  
moisture data with model and precipitation data *Journal of Geophysical  
Research*, 108, NO. D19, 4611, doi:10.1029/2003JD003663, 2003

Western, A.W., Grayson, R.B. and Blöschl, G., 2002 Scaling of soil moisture: A  
hydrologic perspective *Annual Reviews Earth Planet Science* 30, 149-80

Williams, C.A, Hanan, N.P., Neff, J.C., Scholes, R.J., Berry, J.A., Denning, A. S. and Baker, D.F., 2007 Africa and the global carbon cycle *Carbon Balance and Management* 2:3, 2-13

Williams, C.A., Hanan, N., Scholes, R.J. and Kutsch, W., 2009 complexity in water and carbon dioxide fluxes following rain pulses in African Savanna *Oecologia* 161, 469-480

Wittig, R., König, K., Schmidt, M. and Szarzynski J., 2007 A Study of Climate Change and Anthropogenic Impacts in West Africa *Env. Sci. Pollut. Res.* 14:3, 182–189

Xue, Y., Bastable, H.G., Dirmeyer, P. A. and Sellers, P.J., 1996 Sensitivity of simulated surface fluxes to changes in land surface parameterization -- a study using ABRACOS data. *J. Appl. Meteor.* 35, 386-400

Xue, Y.X. and Shukla, J.S., 1993 The Influence of land surface properties on Sahel climate Part 1: Desertification *Journal of Climate* 6:12, 2232-2245

Yang, Z. -L., 2003 Modelling land surface processes in short-term weather and climate studies. In: X. Zhu, X. Li, M. Cai, S. Zhou, Y. Zhu, F.-F. Jin, X. Zou, and M. Zhang ed., 2003 *Observation, Theory and Modeling of Atmospheric*

*Variability*, World Scientific Series on Meteorology of East Asia, World Scientific, New Jersey, pp. 288-313

Yoshioka, M., Mahowald, N.M., Conley, A.J., Collins, W.D., Fillmore, D.W., Zender C.S., Coleman, D.B., 2007: Impact of desert dust radiative forcing on sahel precipitation: relative importance of dust compared to sea surface temperature variations, vegetation changes, and greenhouse gas warming. *J. Climate*, 20, 1445–1467. doi: <http://dx.doi.org/10.1175/JCLI4056>

Yurekli, K. and Kurunc A., 2006 Simulating agricultural drought periods based on daily rainfall and crop water consumption *Journal of Arid Environments* 67 629-640

Zao Z., Chow T.L., Rees H.W., Yang Q., Xing Z., and Meng F. (2009) Predict soil texture distributions using artificial neural network model. *Computers and Electronics in Agriculture* 65:1, 36-48 Elsevier publishers

Zhang, Y. and Shihua, L, 2001 The sensitivity of a land surface model to the physical properties of different soils *Bingchuan Dongtu = Journal of Glaciology and Geocryology* 23:3, 270-275

Zribi M., André C., and Decharme B., (2008) A method for soil moisture estimation in Western Africa based on the ERS Scatterometer. *IEEE Transactions on Geoscience and Remote Sensing* 46:2,438-448

Zulkafli, Z., Buytaert, W., Onof, C., Lavado, W. and Guyot, J.L., 2012 A critical assessment of the JULES land surface model hydrology for humid tropical environments *Hydrology and Earth Science Systems Sciences Discussion* 9, 12523-12561

## Appendix

1. Jules input file used in one of the five experiments for predicting past land surface conditions:

```
# File used to control a run of the JULES code.

# The format of this file is described in the documentation.

#

# This example is for a global GSWP2 run.

# This is intended to serve as an example of how to set up a common type of run.

# It is not necessarily the best set up for a particular application.

#####

#####

## Model options.

>INIT_OPTS

5,4    ! npft,nnvg

F      ! l_aggregate

'BT', 'NT', 'C3G', 'C4G','shrub' ! pftName

'urban', 'lake', 'soil', 'ice'    ! nvgName
```

```

62481,1 ! nxIn,nyIn

6      ! sm_levels

0      ! nsmax

2      ! can_model

3,10   ! can_rad_mod,ilayers

F,F    ! l_cosz,l_spec_albedo

F,F,F,F ! l_phenol,l_triffid,l_veg_compete, l_trif_eq

F,F    ! l_top,l_pdm

F,F    ! l_anthrop_heat_src,l_moruses

F      ! l_o3_damage

F      ! l_imogen

F,F    ! l_epot_corr, l_snowdep_surf

0      ! i_scrn_t_diag

F      ! yrevIn

'watch' ! ncType

T      ! echo

48     ! print_step

#####

#####

## Date and time information

```

>INIT\_TIME

1800 ! timestep

19800101,'09:00:00' ! start date and time (dateMainRun,timeRun)

20001231,'09:00:00' ! end date and time

F ! 1\_360

1,1 ! phenol\_period,triffid\_period

19800101,19801231,0 ! dateSpin,nspin

F ! terminate run if spin-up fails (T,F)

>VARS

smcl F 1.0 ! variable name,spinTolPercent,spinTol

t\_soil F 0.1

>ENDVARS

#####

#####

## Model grid and points to use.

>INIT\_GRID

```

F,F,F      ! pointsList,coord,coordLL
T          ! landOnly
T,T        ! subArea,subAreaLatLon
7,15,5,15  ! xcoord(1:2),ycoord(1:2) 6,16,4,16 7,15,5,15
1          ! npoints
F          ! readFilePoints
 ! fileNamePoints

#####
#####

# Land fraction.
>INIT_LAND

T          ! readFileLand
'nc'       ! fileFormatLand
'/home/JULES/data/cruncep/baseline/xlfracCNJ1.1w.nc' ! fileNameLand
>ASCBIN

0,0        ! nheaderFileLand,nheaderFieldLand
1          ! fieldLand

>NC

'lfrac'    ! varNameLand

```

```
#####
```

```
#####
```

```
# Latitude and longitude of points.
```

```
>INIT_LATLON
```

```
F          ! regLatLon
```

```
-89.75,-179.75      ! regLat1,regLon1
```

```
0.5,0.5           ! regDlat,regDlon
```

```
T              ! readFile
```

```
'nc'           ! fileFormat
```

```
'/home/JULES/data/cruncep/baseline/llonlatCNJ1.1w.nc' ! fileNameLand
```

```
>ASCBIN
```

```
0,0           ! nheaderFile,nheaderField
```

```
1,2           ! fieldLat,fieldLon
```

```
>NC
```

```
'xlat','xlon'     ! varNameLat,varNameLon
```

```
#####
```

```
#####
```

# Data for points, land fraction and lat/lon.

>DATA\_POINTS

1 ! mapIn

>DATA\_LAND

1.0 ! flandg

>DATA\_LATLON

52.168 ! lat

5.744 ! lon

#####

#####

## Fractional cover.

>INIT\_FRAC

T ! readFracIC

T ! readFile

'nc' ! fileFormat

'/home/JULES/data/cruncep/baseline/PARAM/xlfracCNJ1.1w.nc' ! fileName

>ASCBIN

0,0 ! nheaderFile,nheaderField

1 ! fieldNum

>NC

'lfrac' ! varName

# Data fields to be read from this file should appear below here.

>DATA

0.355, 0.355, 0.208, 0.0, 0.0, 0.0, 0.0, 0.082, 0.0 ! frac(:, :)

#####

#####

## Soil layer details, including hydraulic and thermal characteristics, and albedo.

>INIT\_SOIL

F ! l\_vg\_soil

F ! l\_soil\_sat\_down

T ! l\_q10

1 ! soilhc\_method

F ! useSoilType

T,F ! constZ,zrev

T ! readFile

'nc' ! fileFormat (quoted)

'/home/JULES/data/cruncep/baseline/PARAM/soilparAlbCNJ1.1NIGw.nc' !

soilparAlbCNJ1.1w.nc soilparAlbCNJ1.1NIGw.nc

soilparAlbCNJ1.1NIGHiresPint1w.nc fileName (quoted)

'input/soil\_lut.txt' ! soilLUTfile (look-up table file)

>ASCBIN

0,0 ! nheaderFile,nheaderField

>VARS

b 1 ! name,field number

sathh 2

satcon 3

sm\_sat 4

sm\_crit 5

sm\_wilt 6

hcap 7

hcon 8

albsoil 9

>ENDVARS

>NC

>VARS ! name,name of SDF variable

b B2

sathh SATHH2

satcon SATCON2

```

sm_sat  SMVCST2

sm_crit SMVCCL2

sm_wilt SMVCWT2

hcap    HCAP2

hcon    HCON2

albsoil ALBSOIL2

>ENDVARS

>DATA_DZSOIL

0.05,0.1, 0.25, 0.50,1.0, 2.0 ! 0.1, 0.25, 0.65, 2.0 ! dzsoil(1:sm_levels)

0.15          ! albSoilConst

# Data fields to be read from this file should appear below here.

>DATA

    6.63,   6.63,   6.63,   6.63 ! b or 1/(n-1)

0.049460, 0.049460, 0.049460, 0.049460 ! sathh

0.004715, 0.004715, 0.004715, 0.004715 ! satcon

0.458150, 0.458150, 0.458150, 0.458150 ! smvcst

0.242433, 0.242433, 0.242433, 0.242433 ! smvccl

0.136328, 0.136328, 0.136328, 0.136328 ! smvcwt

1185676., 1185676., 1185676., 1185676. ! hcap

0.226873, 0.226873, 0.226873, 0.226873 ! hcon

0.110000          ! albsoil

```

```

#####

#####

## TOPMODEL parameters

>INIT_TOP

5.0      ! zw_max

10.0     ! ti_max

2.0      ! ti_wetl

F        ! readFile

'asc'    ! fileFormat

'input/top.dat' ! fileName

>ASCBIN

0,0      ! nheaderFile,nheaderField

>VARS

fexp    -1 3.0 ! varName,varFlag,constVal

ti_mean  1 0.0

ti_sig   2 0.0

>ENDVARS

>NC

>VARS

fexp    1 0.0 fexp ! varName,varFlag,constVal,SDF varname

ti_mean  1 0.0 ti_mean

ti_sig   1 0.0 ti_sig

>ENDVARS

```

```

>DATA

10.0 ! ti_mean

1.0 ! ti_sig

#####

#####

## PDM parameters

>INIT_PDM

1.0 ! dz_pdm

1.0 ! b_pdm

#####

#####

## Tile surface heights (relative to gridbox average).

>INIT_HGT

T          ! zeroHeight

F          ! readFile

'asc'      ! fileFormat

'input/surf_hgt.dat' ! fileName

>ASCBIN

0,0        ! nheaderFile,nheaderField

1          ! fieldHgt

>NC

```

```

'surf_hgt'      ! varName

>DATA

9*0.0 ! surf_hgt

#####

#####

# PFT parameters

>INIT_VEG_PFT

F              ! readFile

'/home/JULES/data/gswp/baseline/PARAM/standard_pft_param.dat' !

fileName (quoted)

5              ! npftInFile

# Data fields to be read from this file should appear below here.

>DATA

  'BT', 'NT','C3G', 'C4G','shrub' ! pftName

  1,  1,  1,  0,  1 ! c3

19.01, 16.38, 0.79, 1.26, 1.00 ! canht_ft

  5.0,  4.0,  2.0,  4.0,  1.0 ! lai

0.50, 0.50, 0.50, 0.50, 0.50 ! catch0

0.05, 0.05, 0.05, 0.05, 0.05 ! dcatch_dlai

0.05, 0.05, 0.10, 0.10, 0.10 ! dz0v_dh

  0.1,  0.1,  0.1,  0.1,  0.1 ! z0h_z0m

4.00, 4.00, 2.00, 2.00, 2.00 ! infil_f

```

3.00, 1.00, 0.50, 0.50, 0.50 ! rootd\_ft  
0, 1, 0, 0, 0 ! snowCanPFT  
0.15, 0.15, 0.60, 0.60, 0.40 ! albsnc\_max  
0.30, 0.30, 0.80, 0.80, 0.80 ! albsnc\_min  
0.10, 0.10, 0.20, 0.20, 0.20 ! albsnf\_max  
0.50, 0.50, 0.50, 0.50, 0.50 ! kext  
0.50, 0.50, 0.50, 0.50, 0.50 ! kpar  
0, 0, 0, 0, 0 ! orient  
0.08, 0.08, 0.12, 0.060, 0.08 ! alpha  
0.45, 0.35, 0.58, 0.58, 0.58 ! alnir  
0.10, 0.07, 0.10, 0.10, 0.10 ! alpar  
0.15, 0.15, 0.15, 0.17, 0.15 ! omega  
0.70, 0.45, 0.83, 0.83, 0.83 ! omnir  
0.65, 0.65, 0.005, 0.005, 0.10 ! a\_wl  
10.00, 10.00, 1.00, 1.00, 10.00 ! a\_ws  
1.667, 1.667, 1.667, 1.667, 1.667 ! b\_wl  
0.01, 0.01, 0.01, 0.01, 0.01 ! eta\_sl  
0.25, 0.25, 0.25, 0.25, 0.25 ! g\_leaf\_0  
0.0, 0.0, 0.0, 0.0, 0.0 ! dgl\_dm  
9.0, 9.0, 9.0, 9.0, 9.0 ! dgl\_dt  
1.0E-6, 1.0E-6, 1.0E-6, 1.0E-6, 1.0E-6 ! glmin  
0.090, 0.060, 0.100, 0.075, 0.100 ! dqcrit  
0.015, 0.015, 0.015, 0.025, 0.015 ! fd

```

0.875, 0.875, 0.900, 0.800, 0.900 ! f0
0.00, 0.00, 0.00, 0.00, 0.00 ! fsmc_of
0.8e-3,0.8e-3,0.8e-3,0.4e-3,0.8e-3 ! neff
0.046, 0.033, 0.073, 0.060, 0.060 ! nI0
1.00, 1.00, 1.00, 1.00, 1.00 ! nr_nl
0.10, 0.10, 1.00, 1.00, 0.10 ! ns_nl
0.25, 0.25, 0.25, 0.25, 0.25 ! r_grow
0.0375,0.1000,0.0250,0.0500,0.0500 ! sigI
278.15,233.15,278.15,278.15,233.15 ! tleaf_of
0.0, -10.0, 0.0, 13.0, 0.0 ! tlow
36.0, 26.0, 36.0, 45.0, 36.0 ! tupp
1.00, 1.00, 1.00, 1.00, 1.00 ! emis_pft
1.6, 1.6, 5., 5., 1.6 ! fl_o3_ct
0.04, 0.02, 0.25, 0.13, 0.03 ! dfp_dcuo

#####

#####

# Vegetation (PFT) parameters that vary with time and/or location.
>INIT_VEG_VARY
0 ! nvegVar
-1,86400 ! vegDataPer, vegUpdatePer
1,-2 ! nvegFileTime, vegFilePer
T ! vegClim
F ! readList

```

```

/home/JULES/data/cruncep/baseline/PARAM/xlglcCNJ1.1w.nc' ! file name
(quoted)
19800115,'00:00:00' ! vegFileDate(1),vegFileTime(1)
F ! vegEndTime
'nc' ! fileFormat
>ASCBIN
0 ! nfieldVegFile
0,0,0 ! nvegHeaderFile,nvegHeaderTime,nvegHeaderField
T ! noNewLineVeg
'lai','tx', 1, 'i', " ! name,flag,field number,interpolation type, name used in
file name
>NC
'lai','tx','i','LAIECGLC','laifile' ! name,flag,interpolation type,name of netCDF
variable,name used in file name
#####
#####
# Non-veg parameters
>INIT_NONVEG
F ! readFile
'/home/JULES/data/gswp/baseline/PARAM/standard_nonveg_param.dat'
!'PARAM/standard_nonveg_param.dat' ! fileName
4 ! nnvgInFile

```

# Data fields to be read from this file should appear below here.

>DATA

'urban', 'lake', 'soil', 'ice' ! nvgName

0.40, 0.80, 0.80, 0.80 ! albsnc\_nvg

0.18, 0.06, -1.00, 0.75 ! albsnf\_nvg

0.50, 0.00, 0.00, 0.00 ! catch\_nvg

0.00, 0.00, 1E-2, 1E6 ! gs\_nvg

0.10, 0.00, 0.50, 0.00 ! infil\_nvg

1.00, 3E-4, 3E-4, 1E-4 ! z0\_nvg

0.1, 0.1, 0.1, 0.1 ! z0h\_z0m

0.28E6, 2.11e7, 0.00, 0.00 ! ch\_nvg

1.00, 1.00, 0.00, 0.00 ! vf\_nvg

1.00, 1.00, 1.00, 1.00 ! emis\_nvg

#####

#####

# Urban parameters

>INIT\_URBAN

F,T ! l\_urban\_empirical,l\_moruses\_macdonald

T,T,T ! l\_moruses\_albedo,l\_moruses\_emissivity,l\_moruses\_rough

T,T ! l\_moruses\_storage,l\_moruses\_storage\_thin

1.0 ! anthrop\_heat\_scale

```

F          ! readFile

'asc'      ! fileFormat

'moruses_example_2d.dat' ! fileName

>ASCBIN

0,0        ! nheaderFile,nheaderField

>VARS

wrr  1  0.5    ! varName,varFlag,constVal

hwr  2  1.0

hgt  3  10.0

ztm  4  1.0

disp 5  5.0

albwl 6  0.375

albrd 7  0.08

emisw 8  0.875

emisr 9  0.95

>ENDVARS

>NC

>VARS

wrr  -1  0.5  wrr ! varName,varFlag,constVal,SDF varname

hwr  -1  1.0  hwr

hgt  -1  10.0 hgt

ztm  -1  1.0  ztm

```

```

disp -1 5.0 disp
albwl -1 0.375 albwl
albrd -1 0.08 albrd
emisw -1 0.875 emisw
emisr -1 0.95 emisr
>ENDVARS

# Data fields for MORUSES to be read from this file should appear below here.
# This will always be read, but overwritten if using parametrisation

>DATA

15238*0.5 ! wr: Width ratio/ canyon fraction (also used by URBAN-2T)
15238*1.0 ! hwr: Height-to-width ratio
15238*10.0 ! hgt: Building height
15238*1.0 ! ztm: Roughness length
15238*5.0 ! disp: Displacement height
15238*0.375 ! albwl: Albedo wall
15238*0.08 ! albrd: Albedo road
15238*0.875 ! emisw: Emissivity wall
15238*0.95 ! emisr: Emissivity road

#####

#####

## Snow parameters

>INIT_SNOW

0.1, 0.2, 0.2 ! dzsnow

```

```

250.0,          ! rho_snow
0.63e6, 0.265   ! snow_hcap,snow_hcon
0.05           ! snowliqcap
50.0, 2000.0    ! r0,rmax
0.6, 0.06, 0.23e6 ! snow_ggr(1:3)
0.98, 0.7      ! amax(1:2)
2.0, 0.3       ! dtland,kland (incl. dtland in denominator)
50.0           ! maskd
4.4, 0.7, 0.4   ! snowLoadLAI,snowInterceptFact,snowUnloadFact
#####
#####
## TRIFFID parameters.
>INIT_TRIF
F              ! readfile
'/home/JULES/data/gswp/baseline/PARAM/standard_trif_param.dat'
!'PARAM/standard_trif_param.dat' ! fileName
5             ! npftInFile
# Data fields to be read from this file should appear below here.
>DATA
  'BT', 'NT','C3G', 'C4G','shrub' ! trifName
  0, 0, 1, 1, 0 ! crop
0.005, 0.007, 0.20, 0.20, 0.05 ! g_area
15.00, 20.00, 20.00, 20.00, 20.00 ! g_grow

```

```

0.25, 0.15, 0.25, 0.25, 0.25 ! g_root
0.005, 0.005, 0.20, 0.20, 0.05 ! g_wood
9.00, 5.00, 4.00, 4.00, 3.00 ! lai_max
1.00, 1.00, 1.00, 1.00, 1.00 ! lai_min

#####

#####

## Agricultural fraction.

>INIT_AGRIC

F ! readFile
'asc' ! fileFormat
'input/agr.dat' ! fileName

>ASCBIN

0,0 ! nheaderFile,nheaderField
1 ! fieldNum

>NC

'frac_agr' ! varName

# Data fields to be read from this file should appear below here.

>DATA

10000*0.0 ! frac_agr

#####

#####

## Miscellaneous surface and carbon/veg parameters.

```

```

>INIT_MISC

5.7E4, 1.1E4    ! hleaf,hwood

0.83, 0.93     ! beta1,beta2

0.5, 2.0e4     ! fwe_c3, fwe_c4

2.0            ! q10_leaf

0.5e-8         ! kaps

3.22e-7,9.65e-9,2.12e-8,6.43e-10 ! kaps_roth(1:4)

2.0           ! q10_soil

1.0e-6        ! cs_min

5.24100e-04   ! co2_mmr

1.0e-6, 0.01  ! frac_min, frac_seed

20.0         ! pow (for SIGM)

#####

#####

## Miscellaneous surface and carbon/veg parameters.

>INIT_IMOGEN

'/path/to/imogen_order.dat' ! IMOGEN points order

'/path/to/imogen.nlst' ! IMOGEN namelist file

#####

#####

## Details of driving data.

>INIT_DRIVE

21600         ! driveDataPer

```

```

27,-2      ! ndriveFileTime,driveFilePer
T          ! readList

'/home/JULES/data/cruncep/baseline/drivefile.txt' ! file name
19800101,'06:00:00' ! driveFileDate(1),driveFileTime(1)

F          ! driveEndTime

'nc'      ! driveFormat

1,F       ! ioPrecipType,l_point_data
274.0     ! tForSnow
373.15,0.3 ! tForCRain,conFrac
1,F       ! io_rad_type,ioWindSpeed
F,0.0     ! useDiffRad,diffFracConst
10.0, 2.0 ! z1_uv, z1_tq

0         ! ndriveExtra

>ASCBIN

F         ! byteSwapDrive
9         ! nfieldDriveFile
0,0,0    ! ndriveHeaderFile,ndriveHeaderTime,ndriveHeaderField
T         ! noNewLineDrive

>VARS

pstar    8 i  psfc ! name,field number, interpolation type, name as in file
name

```

```

t      5 i t
q      9 i q
u      6 i u
v      7 i v

lw_down  2 nb lw
sw_down  1 nb sw
precipTR 3 nb liqp
precipTS 4 nb solp
>ENDVARS

>NC

'gswp2'      ! ncTypeDrive

>VARS

pstar    PSurf  PSurf  i ! name,name of SDF variable, name as in file name,
interpolation type

t      Tair  Tair  i
q      Qair  Qair  i
u      uwind uwind i
v      vwind vwind i

lw_down  LWdown LWdown nb
sw_down  SWdown SWdown nb
precip   Rainf  Rainf  nb
>ENDVARS

```

```

#####

#####

## The initial state.

>INIT_IC

T          ! readfile

'nc'       ! fileFormat

T,T        ! dumpFile,allDump

'/home/umb2/JULESv3/OUTPUT/hispin05_19800101_090000_spunup_dump.nc'

! fileName  data/init_ic_file.dat

F,F       ! zrevSoil,zrevSnow

T         ! totalWetness

T         ! totalSnow

>ASCBIN

0,0        ! nheaderFile,nheaderField

>VARS

canopy    -1  0.0

tstar_tile -1 275.0

gs        -1  0.0

t_soil    -1 278.0

sthuf     -1  0.75 ! varName,varFlag,constVal

snow_tile -1  0.0

rgrain    -1  0.0

cs        -1 10.0

```

>ENDVARS

>NC

>VARS

sthuf 1 0.9 sthuf ! varName,varFlag, constVal,SDF varname

canopy 1 0.0 canopy

snow\_tile 1 0.0 snow\_tile

rgrain 1 50.0 rgrain

tstar\_tile 1 275.0 tstar\_t

t\_soil 1 278.0 t\_soil

cs 1 10.0 cs

gs 1 0.0 gs

>ENDVARS

# Data fields to be read from this file should appear below here.

>DATA

0.749, 0.743, 0.754, 0.759 ! sthu+sthf(1:sm\_levels)(top to bottom)

9\*0.0 ! canopy(1:ntiles)

9\*0.46 ! snow\_tile(1:ntiles)

9\*50.0 ! rgrain(1:ntiles)

9\*276.78 ! tstar\_tile(1:ntiles)

276.78,277.46,278.99,282.48 ! t\_soil(1:sm\_levels)(top to bottom)

12.100 ! cs

0.0 ! gs

```

#####

#####

#####

#####

## Output selection.

>INIT_OUT

'case1' ! run_id xxpin105

'./OUTPUT' ! directory for output

4 ! dumpFreq

'nc' ! dumpFormat

'replace' ! dumpStatus

2 ! number of output profiles

'nc' ! outFormat

T ! gradsNc

'replace' ! outStatus

F ! yrevOut

T,T ! zrevOutSoil,zrevOutSnow

T ! numMonth

T ! useTemplate

-1.0e33 ! missing/undefined data value for output (undefOut)

```

1.0, 1.0 ! zsmc,zst

'big\_endian' ! outEndian

#####

#####

# Each output 'profile' should appear below here.

# A profile starts with >NEWPROF.

# Within each profile, the list of variables appears between >VARS and  
>ENDVARS.

#####

#####

>NEWPROF

'p1' ! outName

-1,-8 ! outPer,outFilePer

0 ! outSamPer

0,'00:30:00' ! outDate(1),outTime(1) (hh:mm:ss, quoted)

19980101,'00:00:00' ! outDate(2),outTime(2) (hh:mm:ss, quoted)

0,3 ! pointsFlag(1:2)

T | outAreaLL

10,20,10,50 ! outRangeX(1:2),outRangeY(1:2)

F,T ! outCompress,outLLorder

```
F          ! readFile

```

M longitude  
M albedoLand  
M fsat  
M tstar  
M latentHeat  
M bSoil  
M hCapSoil  
M hConSoil  
M satCon  
M sathh  
M vsmcCrit  
M vsmcSat  
M vsmcWilt  
M sthu  
M sthf  
M runoff  
M surfRoff  
M ftl  
M smcl  
M soilWet  
M swetTot  
M tSoil  
M npp

```

M fsmc

M fwetl

M gpp

M respP

M respS

M ecan

M esoil

M fqw

M frac

>ENDVARS

>NEWPROF

'p2'  ! outName

43200,-8  ! outPer,outFilePer

0      ! outSamPer

19800101,'10:00:00' ! outDate(1),outTime(1) (hh:mm:ss, quoted)

20061231,'22:00:00' ! outDate(2),outTime(2) (hh:mm:ss, quoted)

0,3      ! pointsFlag(1:2)

T        | outAreaLL

10,20,10,50  ! outRangeX(1:2),outRangeY(1:2)

F,T       ! outCompress,outLLorder

F         ! readFile

```

```
'input/outgrid1.dat' ! fileName
```

```
1 ! pointsOut
```

```
1 ! mapOut(1:pointsOut,1)
```

```
1 ! mapOut(1:pointsOut,2)
```

```
>GRID
```

```
1,1 ! outNx,outNy
```

```
>VARS
```

```
S sthu
```

```
S sthf
```

```
S runoff
```

```
S soilWet
```

```
S tSoil
```

```
S surfRoff
```

```
S fwetl
```

```
>ENDVARS
```

```
#####
```

```
#####
```

```
M bSoil
```

```
M hCapSoil
```

```
M hConSoil
```

M satCon

M sathh

M vsmcCrit

M vsmcSat

M vsmcWilt

M sthu

M sthf

## End of file.

2. JULES Input file used to run future land surface conditions (2046-2065)

# File used to control a run of the JULES code.

# The format of this file is described in the documentation.

#

# This example is for a global GSWP2 run.

# This is intended to serve as an example of how to set up a common type of run.

# It is not necessarily the best set up for a particular application.

#####

#####

## Model options.

>INIT\_OPTS

5,4 ! npft,nnvg

F ! L\_aggregate

'BT', 'NT', 'C3G', 'C4G', 'shrub' ! pftName

'urban', 'lake', 'soil', 'ice' ! nvgName

```

62481,1 ! nxIn,nyIn

6    ! sm_levels

0    ! nsmax

2    ! can_model

3,10 ! can_rad_mod,ilayers

F,F  ! l_cosz,l_spec_albedo

F,F,F,F ! l_phenol,l_triffid,l_veg_compete, l_trif_eq

F,F  ! l_top,l_pdm

F,F  ! l_anthrop_heat_src,l_moruses

F    ! l_o3_damage

F    ! l_imogen

F,F  ! l_epot_corr, l_snowdep_surf

0    ! i_scrn_t_diag

F    ! yrevIn

'watch' ! ncType

T    ! echo

48   ! print_step

#####

#####

## Date and time information

>INIT_TIME

```

```

1800          ! timestep

20460101,'09:00:00' ! start date and time (dateMainRun,timeRun)

20651231,'09:00:00' ! end date and time

F            ! 1_360

1,1         ! phenol_period,triffid_period

20460101,20471231,0 ! dateSpin,nspin

F            ! terminate run if spin-up fails (T,F)

>VARS

smcl  F 1.0   ! variable name,spinTolPercent,spinTol

t_soil F 0.1

>ENDVARS

#####

#####

## Model grid and points to use.

>INIT_GRID

F,F,F       ! pointsList,coord,coordLL

T           ! landOnly

T,T        ! subArea,subAreaLatLon

7,15,5,15   ! xcoord(1:2),ycoord(1:2) 6,16,4,16 7,15,5,15; 7,15,5,15

2,16,4,16

```

```

1          ! npoints

F          ! readFilePoints



```

-89.75,-179.75 ! regLat1,regLon1

0.5,0.5 ! regDlat,regDlon

T ! readFile

'nc' ! fileFormat

'llonlatCNJ1.1w.nc' ! fileNameLand

>ASCBIN

0,0 ! nheaderFile,nheaderField

1,2 ! fieldLat,fieldLon

>NC

'xlat','xlon' ! varNameLat,varNameLon

#####

#####

# Data for points, land fraction and lat/lon.

>DATA\_POINTS

1 ! mapIn

>DATA\_LAND

1.0 ! flandg

>DATA\_LATLON

52.168 ! lat

5.744 ! lon

```

#####

#####

## Fractional cover.

>INIT_FRAC

T          ! readFracIC

T          ! readFile

'nc'       ! fileFormat

'xlfracCNJ1.1w.nc' ! fileName /scratch/landmod/shared/PARAM/!uses prj lcf

>ASCBIN

0,0        ! nheaderFile,nheaderField

1          ! fieldNum

>NC

'lfrac'    ! varName

# Data fields to be read from this file should appear below here.

>DATA

0.355, 0.355, 0.208, 0.0, 0.0, 0.0, 0.0, 0.082, 0.0 ! frac(:, :)

#####

#####

## Soil layer details, including hydraulic and thermal characteristics, and albedo.

>INIT_SOIL

F          ! l_vg_soil

F          ! l_soil_sat_down

```

```

T    ! l_q10

1    ! soilhc_method

F    ! useSoilType

T,F  ! constZ,zrev

T            ! readFile

'nc'        ! fileFormat (quoted)

'PARAM/soilparAlbCNJ1.1NIGw.nc' ! case1 soilparAlbCNJ1.1w.nc

soilparAlbCNJ1.1w.nc soilparAlbCNJ1.1NIGHiresPint1w.nc fileName (quoted)

'input/soil_lut.txt' ! soilLUTfile (look-up table file)

>ASCBIN

0,0        ! nheaderFile,nheaderField

>VARS

b    1    ! name,field number

sathh    2

satcon    3

sm_sat    4

sm_crit    5

sm_wilt    6

hcap    7

hcon    8

albsoil    9

>ENDVARS

>NC

```

```

>VARS   ! name,name of SDF variable

b       B2

sathh   SATHH2

satcon  SATCON2

sm_sat  SMVCST2

sm_crit SMVCCL2

sm_wilt SMVCWT2

hcap    HCAP2

hcon    HCON2

albsoil ALBSOIL2

>ENDVARS

>DATA_DZSOIL

0.05, 0.1, 0.25, 0.50, 1.0, 2.0 ! dzsoil(1:sm_levels) 0.1, 0.25, 0.65, 2.0

0.15           ! albSoilConst

# Data fields to be read from this file should appear below here.

>DATA

    6.63,  6.63,  6.63,  6.63 ! b or 1/(n-1)

0.049460, 0.049460, 0.049460, 0.049460 ! sathh

0.004715, 0.004715, 0.004715, 0.004715 ! satcon

0.458150, 0.458150, 0.458150, 0.458150 ! smvcst

0.242433, 0.242433, 0.242433, 0.242433 ! smvccl

0.136328, 0.136328, 0.136328, 0.136328 ! smvcwt

```

```

1185676., 1185676., 1185676., 1185676. ! hcap
0.226873, 0.226873, 0.226873, 0.226873 ! hcon
0.110000          ! albsoil

#####

#####

## TOPMODEL parameters

>INIT_TOP

5.0          ! zw_max

10.0         ! ti_max

2.0          ! ti_wetl

F            ! readFile

'asc'        ! fileFormat

'input/top.dat' ! fileName

>ASCBIN

0,0          ! nheaderFile,nheaderField

>VARS

fexp   -1 3.0 ! varName,varFlag,constVal

ti_mean  1 0.0

ti_sig   2 0.0

>ENDVARS

>NC

>VARS

```

```

fexp      1 0.0 fexp  ! varName,varFlag,constVal,SDF varname
ti_mean   1 0.0 ti_mean
ti_sig    1 0.0 ti_sig
>ENDVARS

>DATA

10.0 ! ti_mean

1.0 ! ti_sig

#####

#####

## PDM parameters

>INIT_PDM

1.0 ! dz_pdm

1.0 ! b_pdm

#####

#####

## Tile surface heights (relative to gridbox average).

>INIT_HGT

T          ! zeroHeight

F          ! readFile

'asc'      ! fileFormat

'input/surf_hgt.dat' ! fileName

```

>ASCBIN

0,0 ! nheaderFile,nheaderField

1 ! fieldHgt

>NC

'surf\_hgt' ! varName

>DATA

9\*0.0 ! surf\_hgt

#####

#####

# PFT parameters

>INIT\_VEG\_PFT

F ! readFile

'PARAM/standard\_pft\_param.dat' ! fileName (quoted)

5 ! npftInFile

# Data fields to be read from this file should appear below here.

>DATA

'BT', 'NT','C3G', 'C4G','shrub' ! pftName

1, 1, 1, 0, 1 ! c3

19.01, 16.38, 0.79, 1.26, 1.00 ! canht\_ft  
5.0, 4.0, 2.0, 4.0, 1.0 ! lai  
0.50, 0.50, 0.50, 0.50, 0.50 ! catch0  
0.05, 0.05, 0.05, 0.05, 0.05 ! dcatch\_dlai  
0.05, 0.05, 0.10, 0.10, 0.10 ! dz0v\_dh  
0.1, 0.1, 0.1, 0.1, 0.1 ! z0h\_z0m  
4.00, 4.00, 2.00, 2.00, 2.00 ! infil\_f  
3.00, 1.00, 0.50, 0.50, 0.50 ! rootd\_ft  
0, 1, 0, 0, 0 ! snowCanPFT  
0.15, 0.15, 0.60, 0.60, 0.40 ! albsnc\_max  
0.30, 0.30, 0.80, 0.80, 0.80 ! albsnc\_min  
0.10, 0.10, 0.20, 0.20, 0.20 ! albsnf\_max  
0.50, 0.50, 0.50, 0.50, 0.50 ! kext  
0.50, 0.50, 0.50, 0.50, 0.50 ! kpar  
0, 0, 0, 0, 0 ! orient  
0.08, 0.08, 0.12, 0.060, 0.08 ! alpha  
0.45, 0.35, 0.58, 0.58, 0.58 ! alnir  
0.10, 0.07, 0.10, 0.10, 0.10 ! alpar  
0.15, 0.15, 0.15, 0.17, 0.15 ! omega  
0.70, 0.45, 0.83, 0.83, 0.83 ! omnir  
0.65, 0.65, 0.005, 0.005, 0.10 ! a\_wl  
10.00, 10.00, 1.00, 1.00, 10.00 ! a\_ws  
1.667, 1.667, 1.667, 1.667, 1.667 ! b\_wl

```

0.01, 0.01, 0.01, 0.01, 0.01 ! eta_sl
0.25, 0.25, 0.25, 0.25, 0.25 ! g_leaf_0
0.0, 0.0, 0.0, 0.0, 0.0 ! dgl_dm
9.0, 9.0, 9.0, 9.0, 9.0 ! dgl_dt
1.0E-6,1.0E-6,1.0E-6,1.0E-6,1.0E-6 ! glmin
0.090,0.060,0.100,0.075,0.100 ! dqcrit
0.015,0.015,0.015,0.025,0.015 ! fd
0.875,0.875,0.900,0.800,0.900 ! f0
0.00, 0.00, 0.00, 0.00, 0.00 ! fsmc_of
0.8e-3,0.8e-3,0.8e-3,0.4e-3,0.8e-3 ! neff
0.046,0.033,0.073,0.060,0.060 ! nl0
1.00, 1.00, 1.00, 1.00, 1.00 ! nr_nl
0.10, 0.10, 1.00, 1.00, 0.10 ! ns_nl
0.25, 0.25, 0.25, 0.25, 0.25 ! r_grow
0.0375,0.1000,0.0250,0.0500,0.0500 ! sigl
278.15,233.15,278.15,278.15,233.15 ! tleaf_of
0.0, -10.0, 0.0, 13.0, 0.0 ! tlow
36.0, 26.0, 36.0, 45.0, 36.0 ! tupp
1.00, 1.00, 1.00, 1.00, 1.00 ! emis_pft
1.6, 1.6, 5., 5., 1.6 ! fl_o3_ct
0.04, 0.02, 0.25, 0.13, 0.03 ! dfp_dcuo
#####
#####

```

```

# Vegetation (PFT) parameters that vary with time and/or location.

>INIT_VEG_VARY

0          ! nvegVar

-1,86400   ! vegDataPer, vegUpdatePer

1,-2      ! nvegFileTime, vegFilePer

T          ! vegClim

F          ! readList

'PARAM/xIFASIRCNJ1.1int2w.nc' ! file name (quoted)

19800115,'00:00:00'      ! vegFileDate(1),vegFileTime(1)

F          ! vegEndTime

'nc'       ! fileFormat

>ASCBIN

0          ! nfieldVegFile

0,0,0     ! nvegHeaderFile,nvegHeaderTime,nvegHeaderField

T          ! noNewLineVeg

'lai','tx', 1, 'i', "      ! name,flag,field number,interpolation type, name used in
file name

>NC

'lai','tx','i','LAIECGLC','laifile' ! name,flag,interpolation type,name of netCDF
variable,name used in file name

#####

#####

# Non-veg parameters

```

```

>INIT_NONVEG

F                ! readFile

'PARAM/standard_nonveg_param.dat'

!'PARAM/standard_nonveg_param.dat' ! fileName

4                ! nnvgInFile

# Data fields to be read from this file should appear below here.

>DATA

'urban', 'lake', 'soil', 'ice' ! nvgName

    0.40,  0.80,  0.80,  0.80 ! albsnc_nvg
    0.18,  0.06, -1.00,  0.75 ! albsnf_nvg
    0.50,  0.00,  0.00,  0.00 ! catch_nvg
    0.00,  0.00,  1E-2,  1E6 ! gs_nvg
    0.10,  0.00,  0.50,  0.00 ! infil_nvg
    1.00,  3E-4,  3E-4,  1E-4 ! z0_nvg
    0.1,   0.1,   0.1,   0.1 ! z0h_z0m
    0.28E6, 2.11e7,  0.00,  0.00 ! ch_nvg
    1.00,  1.00,  0.00,  0.00 ! vf_nvg
    1.00,  1.00,  1.00,  1.00 ! emis_nvg

#####

#####

# Urban parameters

>INIT_URBAN

```

```

F,T      ! l_urban_empirical,l_moruses_macdonald
T,T,T    ! l_moruses_albedo,l_moruses_emissivity,l_moruses_rough
T,T      ! l_moruses_storage,l_moruses_storage_thin
1.0      ! anthrop_heat_scale

F        ! readFile
'asc'    ! fileFormat
'moruses_example_2d.dat' ! fileName

>ASCBIN

0,0      ! nheaderFile,nheaderField

>VARS

wrr  1  0.5    ! varName,varFlag,constVal
hwr  2  1.0
hgt  3  10.0
ztm  4  1.0
disp 5  5.0
albwl 6  0.375
albrd 7  0.08
emisw 8  0.875
emisr 9  0.95

>ENDVARS

>NC

>VARS

```

```

wrr -1 0.5 wrr ! varName,varFlag,constVal,SDF varname
hwr -1 1.0 hwr
hgt -1 10.0 hgt
ztm -1 1.0 ztm
disp -1 5.0 disp
albwl -1 0.375 albwl
albrd -1 0.08 albrd
emisw -1 0.875 emisw
emisr -1 0.95 emisr
>ENDVARS

# Data fields for MORUSES to be read from this file should appear below here.
# This will always be read, but overwritten if using parametrisation

>DATA

15238*0.5 ! wrr: Width ratio/ canyon fraction (also used by URBAN-2T)
15238*1.0 ! hwr: Height-to-width ratio
15238*10.0 ! hgt: Building height
15238*1.0 ! ztm: Roughness length
15238*5.0 ! disp: Displacement height
15238*0.375 ! albwl: Albedo wall
15238*0.08 ! albrd: Albedo road
15238*0.875 ! emisw: Emissivity wall
15238*0.95 ! emisr: Emissivity road

```

```

#####

#####

## Snow parameters

>INIT_SNOW

0.1, 0.2, 0.2    ! dzsnow

250.0,          ! rho_snow

0.63e6, 0.265   ! snow_hcap,snow_hcon

0.05           ! snowliqcap

50.0, 2000.0    ! r0,rmax

0.6, 0.06, 0.23e6 ! snow_ggr(1:3)

0.98, 0.7      ! amax(1:2)

2.0, 0.3       ! dtland,kland (incl. dtland in denominator)

50.0           ! maskd

4.4, 0.7, 0.4   ! snowLoadLAI,snowInterceptFact,snowUnloadFact

#####

#####

## TRIFFID parameters.

>INIT_TRIF

F                ! readfile

'PARAM/standard_trif_param.dat'      !'PARAM/standard_trif_param.dat'

! filename

5                ! npftinfile

# Data fields to be read from this file should appear below here.

```

```

>DATA

  'BT', 'NT','C3G', 'C4G','shrub' ! trifName

    0,  0,  1,  1,  0 ! crop

0.005,0.007, 0.20, 0.20, 0.05 ! g_area

15.00,20.00,20.00,20.00,20.00 ! g_grow

  0.25, 0.15, 0.25, 0.25, 0.25 ! g_root

0.005,0.005, 0.20, 0.20, 0.05 ! g_wood

  9.00, 5.00, 4.00, 4.00, 3.00 ! lai_max

  1.00, 1.00, 1.00, 1.00, 1.00 ! lai_min

#####

#####

## Agricultural fraction.

>INIT_AGRIC

F           ! readfile

'asc'       ! fileFormat

'input/agr.dat' ! fileName

>ASCBIN

0,0         ! nheaderFile,nheaderField

1           ! fieldNum

>NC

'frac_agr'  ! varName

# Data fields to be read from this file should appear below here.

```

```

>DATA

10000*0.0      ! frac_agr

#####

#####

## Miscellaneous surface and carbon/veg parameters.

>INIT_MISC

5.7E4, 1.1E4   ! hleaf,hwood

0.83, 0.93    ! beta1,beta2

0.5, 2.0e4    ! fwe_c3, fwe_c4

2.0           ! q10_leaf

0.5e-8        ! kaps

3.22e-7,9.65e-9,2.12e-8,6.43e-10 ! kaps_roth(1:4)

2.0           ! q10_soil

1.0e-6        ! cs_min

8.09965e-04   ! co2_mmr 5.24100e-04

1.0e-6, 0.01  ! frac_min, frac_seed

20.0         ! pow (for SIGM)

#####

#####

## Miscellaneous surface and carbon/veg parameters.

>INIT_IMOGEN

'/path/to/imogen_order.dat' ! IMOGEN points order

```

```

'/path/to/imogen.nlst' ! IMOGEN namelist file

#####

#####

## Details of driving data.

>INIT_DRIVE

21600      ! driveDataPer

20,-2      ! ndriveFileTime,driveFilePer

T          ! readList

'drivefile2046.txt' ! file name

20460101,'06:00:00' ! driveFileDate(1),driveFileTime(1)

F          ! driveEndTime

'nc'      ! driveFormatjules-v3.0

1,F       ! ioPrecipType,l_point_data

274.0     ! tForSnow

373.15,0.3 ! tForCRain,conFrac

1,F       ! io_rad_type,ioWindSpeed

F,0.0     ! useDiffRad,diffFracConst

10.0, 2.0 ! z1_uv, z1_tq

0         ! ndriveExtra

>ASCBIN

```

```

F          ! byteSwapDrive
9          ! nfieldDriveFile
0,0,0     ! ndriveHeaderFile,ndriveHeaderTime,ndriveHeaderField
T          ! noNewLineDrive

>VARS

pstar     8 i  psfc ! name,field number, interpolation type, name as in file
name

t         5 i  t

q         9 i  q

u         6 i  u

v         7 i  v

lw_down   2 nb  lw

sw_down   1 nb  sw

precipTR  3 nb  liqp

precipTS  4 nb  solp

>ENDVARS

>NC

'gswp2'    ! ncTypeDrive

>VARS

pstar     psl  psl   i ! name,name of SDF variable, name as in file name,
interpolation type

t         tas  tas   i

q         hus_xy hus  i

```

u ua\_xy ua i

v va\_xy va i

lw\_down rlds rlds nb

sw\_down rsds rsds nb

precip pr pr nb

>ENDVARS

#####

#####

## The initial state.

>INIT\_IC

T ! readFile

'nc' ! fileFormat

T,T ! dumpFile,allDump

'a201sp2\_20460101\_090000\_spunup\_dump.nc' ! fileName

F,F ! zrevSoil,zrevSnow

T ! totalWetness

T ! totalSnow

>ASCBIN

0,0 ! nheaderFile,nheaderField

>VARS

canopy -1 0.0

tstar\_tile -1 275.0

```

gs      -1  0.0
t_soil  -1 278.0
sthuf   -1  0.75 ! varName,varFlag, constVal
snow_tile -1  0.0
rgrain  -1  0.0
cs      -1 10.0

>ENDVARS

>NC

>VARS

sthuf    1  0.9  sthuf    ! varName,varFlag, constVal,SDF varname
canopy   1  0.0  canopy
snow_tile 1  0.0  snow_tile
rgrain   1 50.0  rgrain
tstar_tile 1 275.0 tstar_t
t_soil   1 278.0  t_soil
cs       1 10.0  cs
gs       1  0.0  gs

>ENDVARS

# Data fields to be read from this file should appear below here.

>DATA

0.749, 0.743, 0.754, 0.759 ! sthu+sthf(1:sm_levels)(top to bottom)
9*0.0                      ! canopy(1:ntiles)
9*0.46                      ! snow_tile(1:ntiles)

```

```

9*50.0          ! rgrain(1:ntiles)

9*276.78       ! tstar_tile(1:ntiles)

276.78,277.46,278.99,282.48 ! t_soil(1:sm_levels)(top to bottom)

12.100        ! cs

0.0           ! gs

#####

#####

#####

#####

## Output selection.

>INIT_OUT

'a2_exp1'     ! run_id xxpin105

'./OUTPUT'   ! directory for output

4            ! dumpFreq

'nc'         ! dumpFormat

'replace'    ! dumpStatus

1           ! number of output profiles

'nc'        ! outFormat

T          ! gradsNc

'replace'  ! outStatus

F         ! yrevOut

```

```

T,T      ! zrevOutSoil,zrevOutSnow

T        ! numMonth

T        ! useTemplate

-1.0e33  ! missing/undefined data value for output (undefOut)

1.0, 1.0 ! zsmc,zst

'big_endian' ! outEndian

#####

#####

# Each output 'profile' should appear below here.

# A profile starts with >NEWPROF.

# Within each profile, the list of variables appears between >VARS and

>ENDVARS.

#####

#####

#####

#####

>NEWPROF

'p1'    ! outName

-1,-8   ! outPer,outFilePer

0       ! outSamPer

0,'00:30:00' ! outDate(1),outTime(1) (hh:mm:ss, quoted)

20460101,'00:00:00' ! outDate(2),outTime(2) (hh:mm:ss, quoted)

```

```

0,3      ! pointsFlag(1:2)
T        | outAreaLL
10,20,10,50 ! outRangeX(1:2),outRangeY(1:2)
F,T      ! outCompress,outLLorder

F        ! readFile


```

M u1  
M v1  
M pstar  
M latitude  
M longitude  
M albedoLand  
M fsat  
M tstar  
M latentHeat  
M bSoil  
M hCapSoil  
M hConSoil  
M satCon  
M sathh  
M vsmcCrit  
M vsmcSat  
M vsmcWilt  
M sthu  
M sthf  
M runoff  
M surfRoff  
M ftl  
M smcl

M soilWet

M swetTot

M tSoil

M gpp

M npp

M sat\_excess\_roff

M fwetl

M gppP

M nppP

>ENDVARS

#####

#####

M bSoil

M hCapSoil

M hConSoil

M satCon

M sathh

M vsmcCrit

M vsmcSat

M vsmcWilt

M sthu

M sthf

## End of file.

### 3. R codes used for the ARIMA model

```
setwd("E:/NE_rain")

rata<-read.table("NE_rain.txt",skip=6)

rata[1:3,]

sa<-rata[,4]#semi-arid

sh<-rata[,5] #sub-humid

sa1=ts(sa[1:300],start=1980,freq=12) # 25 yr time series semi-arid part

sa2=ts(sa[301:324],start=2005,freq=12) #24 months observation

plot(sa1)

sa1.fit<-arima(sa1,order=c(1,1,0),seasonal=list(order=c(1,1,0),period=12))

sa1.pred<-predict(sa1.fit,n.ahead=24)

cor(sa2,sa1.pred$pred)

reg1<-lm(sa2~sa1.pred$pred)

summary(reg1)

plot(sa1,xlim=c(2002,2007), ylim=c(0,300),ylab="Rainfall in mm",xlab="Year")

lines(sa1.pred$pred,col="blue",type="l") #24 months prediction

lines(sa2,type="l",col="black") # 24 months observation

legend("topleft",c("Obs", "Pred"),lty=c(1,1),lwd=c(1.0),col=c("black", "blue"))

#RMSE

rmse <- function(obs, pred) sqrt(mean((obs-pred)^2))

rmse(sa2,sa1.pred$pred)

# include monthly mean function called rsum
```

```

rsum<-function (x) {
  e1<-length(x)
  e2<-e1/12
  e3<-matrix(x,ncol=12,nrow=e2,byrow=TRUE)
  e5<-colMeans(e3,na.rm=TRUE)
  return (e5)
}
o1<-rsum(sa1)
o11<-rsum(sa2)
p1<-rsum(sa1.pred$pred)
mon<-
c("Jan", "Feb", "Mar", "Apr", "May", "Jun", "Jul", "Aug", "Sep", "Oct", "Nov", "Dec")
plot(p1,type="o",pch=3,ylim=c(0,300),xaxt="n",xlab="Months",ylab="Rainfall in
mm")
axis(1, at=1:12, labels=mon)
lines(o1,type="o",pch=7 ) #col="blue"
lines(o11,type="o",pch=8) # col="red"
legend("topright",c("Previous Obs","24 Months Obs"," 24 Months
Pred"),pch=c(3,7,8),lty=c(1,1),lwd=c(1.5),col=("black" )
boxplot(o1,o11,p1)
#####
sh1=ts(sh[1:300],start=1980,freq=12) # 25 yr time series semi-arid part
sh2=ts(sh[301:324],start=2005,freq=12) #24 months observation

```

```

plot(sh1)

sh1.fit<-arima(sh1,order=c(1,1,0),seasonal=list(order=c(1,1,0),period=12))

sh1.pred<-predict(sh1.fit,n.ahead=24)

cor(sh2,sh1.pred$pred)

reg2<-lm(sh2~sh1.pred$pred)

summary(reg2)

plot(sh1,xlim=c(2002,2007), ylim=c(0,300), ylab="Rainfall in mm",xlab="Year")

lines(sh1.pred$pred,col="blue",type="l")      #24 months prediction

lines(sh2,type="l",col="black")              # 24 months observation

legend("topleft",c("Obs","Pred"),lty=c(1,1),lwd=c(1.0),col=c("black","blue"))

rmse(sh2,sh1.pred$pred)

# include monthly mean function rsum

ob1<-rsum(sh1)

ob11<-rsum(sh2)

pb1<-rsum(sh1.pred$pred)

plot(pb1,type="o",pch=3,ylim=c(0,300),xaxt="n",xlab="Months",ylab="Rainfall
in mm")

axis(1, at=1:12, labels=mon)

lines(ob1,type="o",pch=7) #col="blue"

lines(ob11,type="o",pch=8) # col="red"

```

```

legend("topright",c("Previous Obs","24 Months Obs"," 24 Months
Pred"),pch=c(3,7,8),lty=c(1,1),lwd=c(1.5),col=("black" )
boxplot(ob1,ob11,pb1)
#
p1<-as.vector(sa1.pred$pred)
p2<-as.vector(sh1.pred$pred)
sa22<-as.vector(sa2)
sh22<-as.vector(sh2)
# means s-arid and s-humid
mn1<-c(o1,o1)
mn2<-c(ob1,ob1)
a1<-(sa22-mn1)
a2<-(p1-mn1) # diff pred
b1<-(sh22-mn2)
b2<-(p2-mn2) # diff pred
#plotting diff between 25 yr mean obs, 24 month obs, 24 months prediction
#marg<-par()$mar
par(mar=c(4.5,4.0,1.5,0.5))
par(mfrow=c(2,1))
ex<-1:24
plot(a1,type="o",pch=7,ylim=c(-80,50),xlab="Months",ylab="Ranfall in
mm",xaxt="n")
lines(a2,type="o",pch=8)

```

```

axis(1, at=1:24, labels=ex)

legend("bottomright",c("OA","PA"),pch=c(7,8),lty=c(1,1),lwd=c(1.5),col=("black
"))

#

plot(b1,type="o",pch=7,ylim=c(-80,50),xlab="Months",ylab="Ranfall in
mm",xaxt="n")

lines(b2,type="o",pch=8)

axis(1, at=1:24, labels=ex)

legend("bottomright",c("OA","PA"),pch=c(7,8),lty=c(1,1),lwd=c(1.5),col=("black
"))

ex1<-c("Mean diff A1","Mean diff A2","Mean diff B1","Mean diff B2")

plot(c(mean(a1),mean(a2),mean(b1),mean(b2)),col=c("red","blue","green","black
"),type="p",pch=7,lwd=2,xaxt="n",xlab="",ylab="Rainfall in mm")

axis(1, at=1:4, labels=ex1)

t.test(a1,a2)

t.test(b1,b2)

ks.test(a1,a2)

ks.test(b1,b2)

```